UNIVERSITY OF SOUTHAMPTON

FACULTY OF NATURAL AND ENVIRONMENTAL SCIENCES

School of Ocean and Earth Science

A Model Study of Decadal Climate Variability and Predictability associated with the Atlantic Meridional Overturning Circulation

by

Aurélie S.A. Persechino

Thesis for the degree of Doctor of Philosophy

December 2012

UNIVERSITY OF SOUTHAMPTON

ABSTRACT

FACULTY OF NATURAL AND ENVIRONMENTAL SCIENCES
School of Ocean and Earth Science

Doctor of Philosophy

A MODEL STUDY OF DECADAL CLIMATE VARIABILITY AND PREDICTABILITY ASSOCIATED WITH THE ATLANTIC MERIDIONAL OVERTURNING CIRCULATION

by Aurélie S.A. Persechino

This study addresses the decadal variability and predictability of the Atlantic Meridional Overturning Circulation (AMOC), and associated key variables, in two IPCC-class climate models. The AMOC variability is analyzed in a new climate model CHIME, which features a novel (largely isopycnic) ocean component. Power Spectral analysis reveals enhanced variability for periods in the range 15-30 years. The primary mode of variability is associated with decadal changes in the Labrador and the Greenland-Iceland-Norwegian (GIN) seas, in both cases linked to the tropical activity about 15 years earlier. These decadal changes are controlled by the low-frequency North Atlantic Oscillation (NAO), associated with a tropical-extratropical teleconnection. Poleward advection of salinity anomalies in the mixed layer also leads to AMOC changes that are linked to convective processes in the Labrador Sea. A secondary mode of variability is associated with interannual changes in the Labrador and GIN Seas, through the impact of the NAO on local surface density. The decadal potential predictability of the AMOC and climate as represented in the non-isopycnic IPSL-CM5A model and CHIME is explored using prognostic and diagnostic approaches. The modelled AMOC has an average predictive skill of 8 and 6 years, respectively. Over the ocean, surface temperature has the highest skill up to 2 decades in the far north of the North Atlantic, in both models. Additional oceanic areas of predictability are identified in IPSL-CM5A in the tropics and subtropics. The spatio-temporal predictability of both surface temperature over land and precipitation differs somewhat between the two models, but is of limited extent compared to that of ocean variables. Predictability of climate arises from the mechanisms controlling the decadal AMOC fluctuations. Predictive skills of AMOC and climate are favoured by extreme AMOC events but the role of minimum versus maximum states remains to be clarified. The expected better predictive skills of CHIME over non-isopycnic models (due to its better preservation of water masses and more coherent internal structure to the anomalies) are not borne out.

Contents

List of Figures

List of Tables

Declaration of Authorship

I, Aurélie S.A. Persechino , declare that the thesis entitled *A Model Study of Decadal Climate Variability and Predictability associated with the Atlantic Meridional Overturning Circulation* and the work presented in the thesis are both my own, and have been generated by me as the result of my own original research. I confirm that:

- this work was done wholly or mainly while in candidature for a research degree at this University;
- where any part of this thesis has previously been submitted for a degree or any other qualification at this University or any other institution, this has been clearly stated;
- where I have consulted the published work of others, this is always clearly attributed;
- where I have quoted from the work of others, the source is always given. With the exception of such quotations, this thesis is entirely my own work;
- I have acknowledged all main sources of help;
- where the thesis is based on work done by myself jointly with others, I have made clear exactly what was done by others and what I have contributed myself;
- parts of this work have been published as: (Persechino et al., 2012a), and (Persechino et al., 2012b)

Signed:.....

Date:.....

Acknowledgements

Many people contributed directly and indirectly to this work, and I hope I am not forgetting anyone. My first thanks go to my main supervisor, Bob Marsh, whose guidance and support have been of great value to me. He has always encouraged me to explore new horizons and gave me the freedom to develop new collaborations. My next thanks go to my two other supervisors, Bablu Sinha and Alex Megann. Bablu, thanks for always keeping your door open and answering my questions. Alex, thanks for your help in familiarizing myself with coupled climate models, and for helping me tackling some of the temperamental behaviour of CHIME. A particular thanks also goes to Adam Blaker, for his uncountable sound advice, for sharing his wide knowledge, and for his remarkable patience in helping me fixing my many computing bugs. I am also grateful to my panel chair, Adrian New, for his important role in my PhD process, and his constructive comments. I sincerely believe that this thesis would not have seen the light of day without the invaluable support of the "LOCEAN predictability team" at the Université Pierre et Marie Curie (in Paris). I am deeply grateful to Juliette Mignot, Didier Swingedouw and Eric Guilyardi, for welcoming me there for three months, and for their continuous support beyond that. My sincere thanks for your precious guidance, for providing me with great ideas and (most importantly) motivation to accomplish this work! I would also like to thank the ANDREX project team, and more particularly Alberto Naveira Garabato, for giving me the opportunity to participate to two cruises in the Antarctic and for giving me a taste of working at sea. A HUGE thanks to some amazing people met during my PhD, and more particularly, the Southampton French, Canadian and Japanese teams, and my two "Hungarian Parisian" girls, for all the happy times we had together, for being so supportive, and becoming such good friends! Even though we are now all spread worldwide, I would like to warmly thank my longstanding friends wherever they are, for having been so present and supportive despite the distance that separates us, for more than 10 years for some of them. Finally, I would like to particularly thank my family for their continuous support and love. Thank you to my parents for raising me, loving me and always encouraging me! At last, but not least, I would like to thank my husband, Loïc, who has always been there for me, especially in the difficult moments. Thank you for always supporting me, believing in me, and for choosing me to share your life. Without their encouragements and understanding it would have been impossible for me to finish this work. So to my husband and my parents, I want to dedicate this thesis ...

Abbreviations

AABW	AntArctic Bottom Water
ACC	Antarctic Circumpolar Current
AAIW	AntArctic Intermediate Water
AMO	Atlantic Multi-decadal Oscillation
AMOC	Atlantic Meridional Overturning Circulation
AOGCM	Atmosphere-Ocean General Circulation Model
CMIP	Coupled Model Intercomparison Project
DPP	Diagnostic Potential Predictability
DWBC	Deep Western Boundary Currents
EC	Ensemble Correlation
EGC	East Greenland Current
ENSO	El-Niño Southern Oscillation
EOF	Empirical Orthogonal Functions
ES	Ensemble Spread
FCT	Flux Corrected Transport
GIN	Greenland-Iceland-Norwegian
GSW	Greenland Sea Water
IPCC	Intergovernmental Panel on Climate Change
ITCZ	InterTropical Convergence Zone
KPP	K-Profile Parameterization
LSW	Labrador Sea Water
MLD	Mixed Layer Depth
MOC	Meridional Overturning Circulation
NAC	North Atlantic Current
NADW	North Atlantic Deep Water
NAO	North Atlantic Oscillation
PDF	Probability Density Function
PPP	Prognostic Potential Predictability
ppvf	Potential Predictability Variance Fraction
SAMW	SubAntarctic Mode Water
SAT	Surface Air Temperature
SLP	Sea Level Pressure

SSS	Sea Surface Salinity
SST	Sea Surface Temperature
TA	Tropical Activity
TKE	Turbulent Kinetic Energy
TOA	Top Of Atmosphere
WBC	Western Boundary Currents
ZWCL	Zero Wind stress Curl Line

Chapter 1

Introduction

1.1 The Ocean as a component of the climate system

In recent years, both natural and anthropogenic climate change have become a topic of growing interest and concern for scientists, as shown by the increasing number of international conferences held on the subject (e.g. United Nations Climate Change Conferences in Copenhagen 2009, Cancun 2010, Durban 2011, Bonn 2012). The roles of the atmosphere and greenhouse gases as well as the role of deforestation have been widely acknowledged in the media. However, although the ocean covers 70% of the global surface of our planet (hence the "blue planet"), the ocean's importance for climate is somewhat neglected. Yet, like the atmosphere, the ocean redistributes the solar heating from the equatorial regions (where there is a surplus of incoming over outgoing radiations) toward the icy poles (where there is a deficit of incoming over outgoing radiations), and therefore significantly contributes to the heat budget of the Earth.

One of the primary reasons for the strong influence of the ocean on the climate is due to its great heat capacity. Indeed, the ocean stores more heat in the uppermost 3 m than the entire atmosphere. It absorbs much of the solar energy that reaches earth, and thanks to the high heat capacity of water, the ocean slowly releases heat over months or years. The ocean's vital role in the climate system results also from its great transport capability. The ocean can transport heat, freshwater and other material properties, mainly achieved by boundary currents, large gyres and by the large-scale ocean circulation known as the thermohaline circulation. By both its storage and transport capacities, the ocean can therefore be seen as a great reservoir, which continuously exchanges heat, moisture and carbon with the atmosphere, driving our weather patterns and influencing the slow, subtle changes in our climate.

In the context of climate change, the ocean also plays a major role. First, because of its great heat capacity, it delays the warming of the atmosphere. Second, the ocean also

represents a major sink for anthropogenic carbon dioxide (e.g. Le Quéré et al. 2009). Third, its associated regional pattern of heat transport and absorption lead to significant changes in regional rainfall and temperature distribution (e.g. causing droughts such as in West Africa in the 1970's, Conway et al. 2009). Fourth, the ocean heat absorption leads to sea level rise through thermal expansion leading to coastal erosion and flooding (e.g. Nicholls and Cazenave 2010). Fifth, changes in formation of deep-water masses at high latitudes could lead to abrupt changes in the global ocean thermohaline circulation that could result in a major rearrangement of global climate in the space of a few decades (e.g. Clark et al. 2002; Rahmstorf 2002).

This latter point constitutes the basis of the present study. This large-scale thermohaline circulation is considered as the "Achilles heel of the climate system" (Broecker 1997). It is primarily (but not exclusively) meridional, and is often characterised as the Meridional Overturning Circulation (MOC). Because the Atlantic MOC (AMOC) is thought to play an important role in maintaining the European and North Atlantic climate by transporting heat from low to high latitudes (e.g. Hall and Bryden 1982; Trenberth and Caron 2001; Gordon et al. 1992; Winton 2003; Knight et al. 2005; Sutton and Hodson 2005; Pohlmann et al. 2006; Sinha et al. 2012), the AMOC has been a major research focus for many years.

1.2 The importance of decadal AMOC prediction to understand future climates

Because anthropogenic climate impacts are likely to be expressed on decadal timescales (IPCC 1996), understanding processes behind naturally occurring decadal variability in the climate system, is of primary importance. At multiyear to decadal timescales, the memory (and hence the potential for predictability of the climate system) are thought to reside in the ocean. The ocean indeed has a larger thermal inertia than land areas, and observations suggest that it has enhanced variability at the decadal time scales (e.g. Deser and Blackmon 2010; Czaja and Marshall 2001; Frankcombe et al. 2010). Most studies thus point to oceanic mechanisms as central to climate memory, particularly those related to reservoirs of ocean heat or slowly evolving circulation and their interaction with the atmosphere. For instance, sea surface temperatures in mid-latitudes are well described by the stochastic climate model paradigm (Frankignoul and Hasselmann 1977), where random atmospheric surface forcing with "white noise" is integrated by the ocean mixed layer to produce a "red noise" spectrum, in which power is amplified at lower frequencies (Deser et al. 1993). In addition, a number of ocean processes (e.g. overturning and gyre circulations, the triggering of Rossby waves) are potential candidates that may provide additional predictability by influencing atmospheric and thus terrestrial variability. A potentially large source of predictability of natural climate

variability on decadal timescales is thought to come from fluctuations in the AMOC (e.g. Delworth and Mann 2000; Dijkstra et al. 2006; Zhang and Delworth 2006).

Due to a lack of AMOC observations, the impact of AMOC changes have been studied using climate models. The most direct impact of changes in the AMOC is on the ocean heat transport, with decreases in the AMOC leading to decreases in northward heat transport (e.g. Stouffer et al. 2006; Vellinga and Wood 2008). If the AMOC transports less heat northward this will impact sea surface temperatures and near-surface air temperatures. Several modelling studies have indeed linked the leading pattern of SST variability over the North Atlantic (known as the Atlantic Multidecadal Oscillation or AMO, Schlesinger and Ramankutty 1994) to changes in the AMOC (e.g. Delworth and Mann 2000; Knight et al. 2005), though models differ considerably in the timescale of the AMO they reproduce (Knight 2009). Sutton and Hodson (2005) showed evidence from observations that the AMO modulates the North American and European boreal summer climate on multidecadal timescales. The presence of feedbacks linking AMOC, SST, and the atmospheric circulation therefore open opportunities for predictability of decadal climate variability over land associated with predictability of AMOC variations (Knight et al. 2006). Because the AMOC influences many aspects of climate, it can be considered as an important potential carrier of climate predictability.

Wunsch and Heimbach (2012) showed some observational evidence for the AMOC to exhibit a stationary Gaussian red noise behaviour which is not particularly surprising since the system is subject to continuous stochastic disturbances by external processes (winds, precipitations, etc.), and to internal instabilities of a wide assortment. The Gaussian behaviour is consistent with the central limit theorem for a process arising from numerous independent disturbances (Wunsch and Heimbach 2012). However, it is somewhat surprising that the frequency spectrum is not more "red" given the long-time scales of ocean memory. This underlines the dominance of the known white noise behaviour of the wind field, which is only slightly reddened by the longer oceanic timescales. A simple model for red noise is the univariate AR(1) process. In the mathematical formulation of the slow processes, atmospheric variability (weather) is treated as "noise", which is integrated by the ocean resulting in low-frequency variability (Hasselmann 1976). The differential equation describing this AR(1) process for the oceanic mixed layer temperature is given by:

$$\frac{\partial T}{\partial t} = -\gamma T + \epsilon \tag{1.1}$$

where γ is the damping coefficient and ϵ is a random variable with Gaussian characteristics. The latter term refers to the fact that as the correlation increases the equation approximates more and more closely persistence with some added noise; it represents a stochastic process with some memory. The mixed layer temperature is forced by white (weather) noise ϵ and is damped about its equilibrium temperature by feedback processes represented by a damping time scale $\frac{1}{\gamma}$. If the long time scale variability of the coupled system is a consequence of the damping of the weather noise forcing in the

manner discussed by Hasselmann (1976) and Frankignoul and Hasselmann (1977), then skilful forecasting is limited by the damping timescale.

Although there is several evidence for the power spectrum of modelled AMOC indexes to show power resembling a theoretical red noise spectrum, the acquisition of long time series with climate models (up to thousand years) also allowed identification of energy peaks that are significantly above the red noise (e.g. Delworth et al. 1993; Jungclaus et al. 2005; Medhaug et al. 2011) with periods ranging from 10 to 100 years. Modelling studies therefore show evidence that AMOC prediction is promising for potential predictability of climate at multi-decadal timescales.

1.3 Potential for abrupt changes in the AMOC

Because of its long timescale, the AMOC is thought to provide a stabilizing effect on climate, but is also suspected (from paleoclimatic and modeling evidence) to cause abrupt climatic change in the space of a few decades if it is disturbed in certain ways. Before reviewing some of its past shifts and its possible future behaviour, a general description of the AMOC is first given.

1.3.1 Overview of the AMOC

The AMOC is described as the zonally averaged meridional flow forced by winds and buoyancy fluxes, transporting ∼15 Sv of water and 1 PW of heat poleward (estimation at 40°N, Ganachaud and Wunsch 2000). It is usually defined as the basin-wide circulation in the latitude-depth plane, as typically quantified by a meridional transport streamfunction. Thus, at any given latitude, the maximum value of this streamfunction, and the depth at which it occurs specified the total amount of water moving meridionally above this depth (and below it, in the reverse direction).

A schematic representation of the global MOC (which can be seen as the mean large-scale circulation in the ocean) is shown in Figure 1.1. Essentially, cold, dense water is formed in the Nordic Seas, Labrador Sea, and Weddell Sea through vertical mixing, which sinks and flows out into the oceans. The North Atlantic Deep Water (NADW) flows southward along Deep Western Boundary Currents (DWBCs) to the Southern Ocean. The deep water joins the Antarctic Circumpolar Current (ACC), which mixes and redistributes it to all ocean basins. Deep water is upwelled around Antarctica, along the equator and along eastern coastlines (Gordon 1986). This cool water is warmed in the tropics, and most of it is transported poleward along Western Boundary Currents (WBCs), completing the circulation loop.

More specifically, in the North Atlantic (Figure 1.2), the warm and saline waters of the Gulf Stream (originating from the Gulf of Mexico) are transported northward by

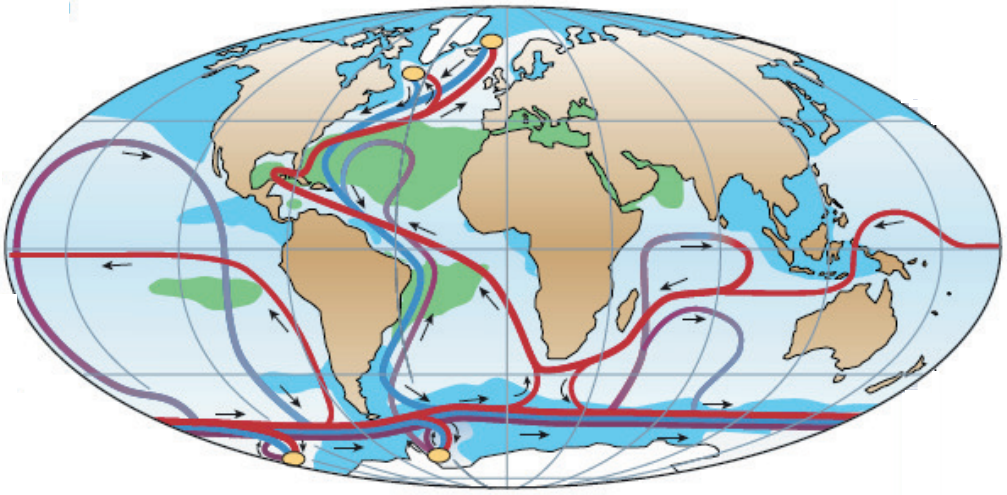

Figure 1.1: Schematic representation of the global Meridional Overturning Circulation. Surface currents are shown in red, deep waters in light blue and bottom waters in dark blue. The main deep-water formation sites are shown in yellow. (From Rahmstorf 2002).

the North Atlantic Current (NAC). On its way to the Nordic and Labrador Seas, the warm saline surface water loses heat to the cold atmosphere (warming it) whereas its salt content remains relatively constant (as salt cannot be exchanged in more than trace quantities at the air-sea interface). The increase in density resulting from the strong heat loss renders the surface water unstable and it overturns, sinking in quite specific areas to reach a depth where waters have the same density: NADW is ultimately formed. Note that open ocean deep convection is more frequently observed in the Labrador Sea than in the Greenland Sea (Marshall and Schott 1999). The newly formed NADW flows southward as a deep western boundary current along the continental slope of America to about 35°S (Stommel and Arons 1960), to counter-balance the northward export of surface water (in accordance with mass conservation). In summary, the underpinning concept for the Atlantic MOC (hereinafter AMOC) consists of four main components: (i) upwelling mixing processes that transport volume from depth to near the ocean surface, (ii) surface currents that transport relatively light water toward high latitudes, (iii) deep-water regions where water become denser and sinks, (iv) deep currents closing the loop.

1.3.2 Past AMOC shifts

Analysis of sediment cores and corals provides a wealth of information on past ocean circulation and show that it has undergone major changes during the past 120,000 years (Rahmstorf 2002). For example, time slice compilations suggest that at different times, latitude shift of convection sites (between the Nordic Seas and the regions south of Iceland) have occurred (e.g. Alley and Clark 1999), and that at certain times NADW formation was even interrupted (Keigwin et al. 1994). Clark et al. (2002) and Rahmstorf

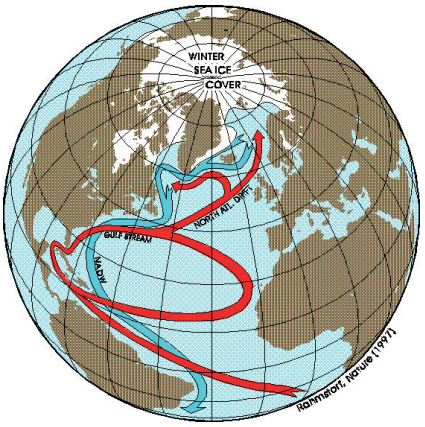

Figure 1.2: Simplified representation of the present-day Atlantic Meridional Overturning Circulation. Warm surface currents are shown in red, North Atlantic Deep Water is shown in blue. (From Rahmstorf 1997).

(2002) also suggested that past reorganizations of the AMOC were involved in climatic temperature changes of several degrees in a few decades.

The most dramatic abrupt climate changes are the Dansgaard-Oeschger warm events (observed quasi-periodically during the last glacial period), with a warming that can exceed 10°C within a decade (Severinghaus et al. 2003). Another type of abrupt change is the Heinrich events (also observed during the last glacial period); sediment data indicate a large discharge of icebergs into the northern Atlantic (Heinrich 1988), decreasing the density of surface water in the North Atlantic to such an extent that the NADW circulation essentially shuts down in the course of a few decades, cooling the North Atlantic dramatically (Keigwin et al. 1994). At the end of the last glacial period, rapid warming occurred, as the AMOC restarted. As the climate warmed and ice sheets melted, the ocean circulation went through a number of oscillations that may be explained by meltwater input as the great northern ice sheets further disintegrated. The effect may have been rapid cooling of up to 10°C in a matter of decades (causing the Younger Dryas and 8.2 kyr cold events). The variability of the AMOC during the Holocene after the 8.2 kyr event is discussed by Keigwin and Boyle (2000). Variations are clearly much smaller than during glacial times, but the evidence for them is still controversial and not very strong. In the last decade or so, Bryden et al. (2005) reported that the AMOC seems to have weakened by about 30% from 1957 to 2004. This work was followed by an intense debate suggesting that the five snapshots used in this study might have subsampled intense high-frequency variability. Indeed, there are at present no observations indicating a sustained weakening of the AMOC during the last few decades (e.g. Knight et al. 2005; Cunningham et al. 2007; Cunningham and Marsh 2010). On the contrary, high-resolution modelling (Biastoch et al. 2008), and combined satellite altimetry and in situ observations (Willis 2010) even hint at a weak upward trend in the AMOC during the last decades. Evidence from both observational and modelling studies of a weakening/strengthening of the AMOC during the last decades is still controversial.

For the present-day climate system, the AMOC has been associated with a large northward heat flux which transports about 1.2 PW of heat poleward of 25°N, or 20-30% of the total heat flux carried by the atmosphere-ocean system at this latitude (Hall and Bryden 1982; Trenberth and Caron 2001). Consequently, changes in the AMOC have the potential to change the climate in this region (e.g. Manabe and Stouffer 1994; Vellinga and Wood 2002), and to lead to a major rearrangement of global climate (e.g. Manabe and Stouffer 1999) as already seen in the geological past. Abrupt changes in the AMOC are considered as one of the major challenges in climate change (Broecker 1997; O'Neill and Oppenheimer 2002).

1.3.3 Future behaviour of AMOC in a changing climate

In the future, there is a risk that substantial changes in the AMOC could occur as a result of global warming from increasing levels of atmospheric greenhouse gases (Manabe and Stouffer 1994; Rahmstorf and Ganapolski 1999; Zickfeld et al. 2007). However, there is still much uncertainty as to how it will respond. Indeed, even when forced by the same scenario, climate models show a wide range of AMOC responses to global warming (IPCC 2001, Figure 1.3). Nevertheless, although some projections of greenhouse gases-induced climate change show little or no weakening of the AMOC, the majority of the state-of-the-art climate models show a weakening in the AMOC throughout the 21^{st} century (e.g. Gregory et al. 2005; IPCC 2007; Medhaug and Furevik 2011). Most of them assessed "very likely" that the AMOC would weaken (with an average predicted slowdown of 25%, IPCC 2007) by 2100, in response to increase freshening and warming in the subpolar seas (Rahmstorf 1999; Rahmstorf and Ganapolski 1999; Delworth and Dixon 2000). Since the overflow and descent of cold, dense waters across the Greenland-Scotland Ridge (i.e. NADW) is a principal mean by which the deep ocean is ventilated and renewed, the suggestion is that a reduction in upper-ocean density at high northern latitudes will weaken the AMOC. If this were to occur, northern Europe and the north-eastern American continent would correspondingly cool. The climatic impacts would not be restricted to the Atlantic regions but extend globally through atmospheric teleconnections (e.g. Dong and Sutton 2002; Zhang and Delworth 2005) and through global oceanic wave mediated adjustment (Goodman 2001; Johnson and Marshal 2004; Blaker et al. 2006). Note that, although a transient weakening is the most common response of the AMOC to greenhouse forcing, to date there is no published climate scenario run that simulates a collapse of the AMOC before the year 2100 (Gregory et al. 2005).

For the Atlantic sector, the fate of the AMOC will be important in shaping both regional and global climate change. However the fact that the climate exhibits strong internal decadal to multidecadal variability in this sector (e.g. Latif et al. 2006) makes the prediction of the AMOC challenging because of its likelihood to mask the anthropogenic climate signal during the next few decades (e.g. Knight et al. 2005; Sutton 2003). This

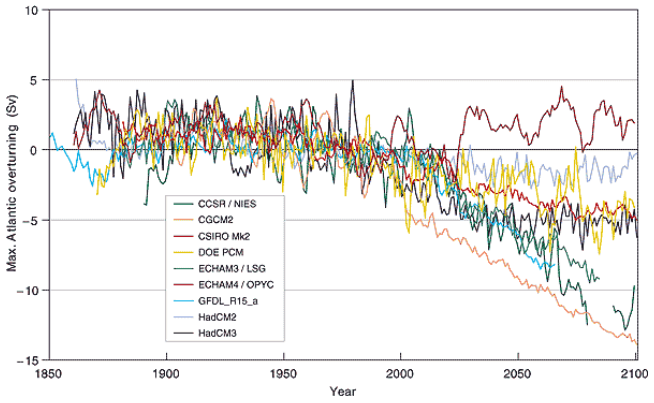

Figure 1.3: Evolution of the AMOC in greenhouse warming simulations with different coupled ocean-atmosphere global climate models. All models were driven with a "Business as Usual" scenario. (From IPCC 2001).

is clearly illustrated in Figure 1.4, which shows four different greenhouse gas simulations (with a CO_2 increase of 1% per year) initialized from different states of a control run (Sutton 2003). Although the global mean temperature exhibits a rather monotonic increase (left panel), the AMOC evolution closely follows of the control run for some decades (right panel).

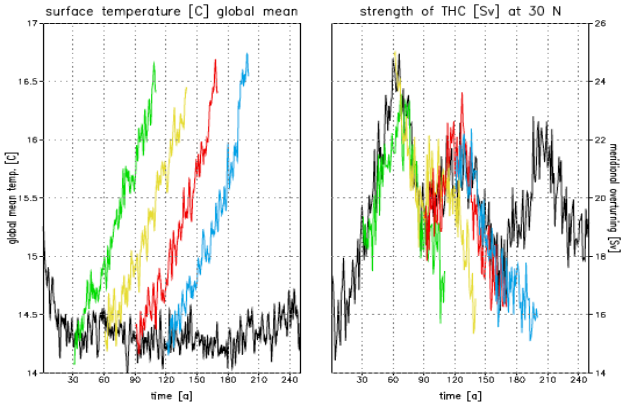

Figure 1.4: Global mean surface air temperature (left panel) and meridional overturning index (right panel) from the control run (black) and four greenhouse gas experiments (colored lines) with the ECHAM5/MPI-OM climate model. (From Sutton 2003).

Because of the economic and socio-economic consequences (e.g. for fisheries, agriculture, infrastructure), the ability to predict anthropogenic climate change therefore demands a good understanding of the natural decadal variability associated with the AMOC, as it is precisely on this timescale that anthropogenic impacts are likely to be expressed (IPCC 1996). Although a large body of literature exists on the processes that potentially give rise to decadal climate variability, the subject is still under debate.

1.4 Characteristics and mechanisms of decadal climate variability associated with the AMOC

In search of the origin of decadal variability in the climate system, the AMOC has long been regarded as one of the best candidates. Indeed, both observational and modelling studies support the idea that the decadal climate variability in the North Atlantic has been closely related to the AMOC (e.g. Gordon et al. 1992; Winton 2003; Herweijer et al. 2005; Latif et al. 2004). The question of how changes in the AMOC develop and whether there are general modes describing the global overturning circulation have been addressed by a large variety of numerical experiments and with models of varying complexity. However, the nature and mechanism of the decadal variability of the AMOC is still controversial.

In the existing literature, there are two leading mechanisms for the decadal AMOC variability. The first idea is that it is part of a coupled ocean-atmosphere mode (e.g. Timmerman et al. 1998; Vellinga and Wu 2004; Danabasoglu 2008), and the second argument is that it is simply an oceanic response to low-frequency atmospheric forcing (e.g. Delworth et al. 1993; Delworth and Greatbatch 2000; Dong and Sutton 2005; Born and Mignot 2011).
Timmerman et al. (1998) illustrate the first idea by showing evidence for a coupled air-sea mode with a 35-year period, in a multi-century integration of the ECHAM3/LSG climate model. The mechanism for this mode is as follows. When the AMOC is anomalously weak, the North Atlantic Ocean is dominated by negative sea surface temperature (SST) anomalies. The atmospheric response to these SST anomalies involves a weakened North Atlantic Oscillation (NAO, Hurrell 1995a), which then induces positive sea surface salinity (SSS) anomalies in the convection site through anomalous freshwater fluxes and Ekman transport. This in turn, enhanced deep convection and leads to an intensified AMOC and an increased northward heat transport. As a result the North Atlantic Ocean is dominated by positive SST anomalies, which completes the phase reversal of the oscillation. An active air-sea coupling is also found by Danabasoglu (2008) in the CCSM3 model where a strong 21-year oscillation is seen in the AMOC time series. This study suggests a prominent role of the NAO, in particular, in modulating the subpolar gyre strength and contributing to the formation of temperature and salinity anomalies that lead to positive/negative density anomalies at the deep-water formation site. Vellinga and Wu (2004) also agree with the idea of a coupled ocean-atmosphere mode. Using the HadCM3 climate model, they presented a mechanism to explain the multi-decadal AMOC variations through slow advection of salinity anomalies from the tropical Atlantic to the high latitudes. They argued that the salinity anomalies are generated by AMOC induced shifts in the location of the InterTropical Convergence Zone (ITCZ) and that, in the North Atlantic, these anomalies act to reverse the phase of the oscillation by changing the upper ocean density.

In contrast, Delworth et al. (1993) support the second idea by showing evidence for a pure damped oceanic mode excited by atmospheric forcing in the GFDL model. They associated this mode with a 50-year period, which relates to changes of the subpolar gyre strength. The mechanism is summarised as follows. A weak overturning reduces the northward heat transport, which leads to a cooling of the North Atlantic Ocean and an acceleration of the subpolar gyre (caused by the increase in density gradient). The strengthening of the subpolar gyre increases the advection of salty water into the sinking regions, enhancing deep-water formation, which intensifies the AMOC (phase reversal of the oscillation). This is turn, enhances the northward heat transport, leading to the transport of warmer, less dense water into the sinking area. As a result, the AMOC weakens again, accompanied with reduced heat transport. This variability is interpreted as a damped ocean-only mode excited by low-frequency atmospheric noise. Dong and Sutton (2005) reached the same conclusions in the HadCM3 climate model. Although the timescale is shorter in HadCM3 ($\sim$ 25 years), the mechanisms that they identified are very similar to those of Delworth et al. (1993), which are related to changes in the strength of the subpolar gyre that therefore modulate the transport of saline water into the Nordic Seas. In good agreement with these two studies, Delworth and Greatbatch (2000) found no conclusive evidence, in their analysis of a series of coupled and uncoupled global climate model integrations, that the AMOC variability is part of a dynamically coupled atmosphere-ocean mode. Recent results from Born and Mignot (2011) with the IPSL-CM4 model, and Kwon and Frankignoul (2011) with the CCSM3 model, also support the interpretation of the AMOC oscillating in response to stochastic forcing of the atmosphere proposed by Delworth et al. (1993), and later confirmed by Delworth and Greatbatch (2000) and Dong and Sutton (2005).
The conflict between these two viewpoints (truly coupled mode or not) arises mainly because of the uncertainties in the atmospheric response to the mid-latitude SST anomalies. Indeed, the extent to which North Atlantic SST contributes to the variation in the main mode of atmospheric circulation (and climate variability) in the North Atlantic/European sector, that is the NAO, is still questionable. Although several studies indicate a strong impact of the leading pattern of SST variability over the North Atlantic (or AMO) on the NAO (e.g. Rodwell et al. 1999; Sutton et al. 2001; Peng et al. 2003), others suggest that this latter is rather impacted by tropical Pacific or Indo-Pacific SST anomalies (e.g. Fraedrich and Müller 1992; Hoerling et al. 2001; Merkel and Latif 2002; Bader and Latif 2003). There are also several lines of evidence for the AMO to be a direct response of the AMOC to the anomalous air-sea fluxes associated with the NAO (e.g. Delworth et al. 1993; Curry et al. 1998; Marshall et al. 2001; Knight et al. 2005; Collins et al. 2006a). Although these relationships between the NAO, AMOC and AMO on decadal to multidecadal timescales are widely accepted, it is not clear to what extent the NAO-induced multidecadal changes in the AMOC and AMO will feed back onto the NAO itself.

In the existing literature, there are also two different viewpoints about the relative role

of freshwater export from the Arctic (e.g. Delworth et al. 1997; Jungclaus et al. 2005; Hawkins and Sutton 2007) and tropical processes (e.g. Vellinga and Wu 2004; Mignot and Frankignoul 2005) in the decadal AMOC fluctuations.
For example, Hawkins and Sutton (2007) support the idea of a link with the Arctic. They characterized low frequency AMOC variability (70-80 year period) as an internal mode, dominated by changes in convection in the Nordic Seas, which lead the changes in the AMOC after a few years. In this study, variations in salinity transports from the Arctic and from the North Atlantic are the main feedbacks which control the oscillation. A similar low-frequency ocean mode to Hawkins and Sutton (2007), also excited by the atmosphere, was found in the ECHAM5/MPI-OM model (Jungclaus et al. 2005). In this model, which has a relatively high resolution at high latitudes, they found that variations in the Atlantic salt and heat transport drive circulation changes in the Nordic Seas. These circulation changes modulate the storage and release of freshwater from the Arctic. In agreement with the idea of a link with the Arctic, Delworth et al. (1997) described a 40 to 80-year oscillation of the AMOC in the GFDL model which is found to be associated with fluctuations in the Arctic, Greenland Sea and in the intensity of the East Greenland Current (EGC); a similar mechanism has been found in the recent study of Escudier et al. (2012) in the IPSL-CM5 model.
These above studies suggest a link with the Arctic different from the mechanism suggested by Vellinga and Wu (2004). Indeed, as mentioned earlier, they presented a mechanism to explain multidecadal AMOC variations through slow advection of salinity anomalies from the tropical Atlantic to the high latitudes, in which there was no role for the Arctic. Mignot and Frankignoul (2005) also identified a similar link with the tropics in the Bergen Climate Model. They claimed that part of the salinity anomaly in the tropical Atlantic (induced by El-Niño events) is advected in the ocean interior along the NAC, reaching the Irminger and Labrador Seas after about 35 years, where it destabilizes the water column and favors deep convection.

In summary, the mechanisms responsible for the AMOC variability in the models have been partially understood, but there appear to be significant differences of details between the different models (see Table 1.1). Although some modelling studies found that mechanisms responsible for decadal variability of the AMOC are associated with a pure damped oceanic mode excited by atmospheric forcing (which is e.g. related to changes in the strength of the subpolar gyre, Delworth et al. 1993; Dong and Sutton 2005), others found clear evidence of an active coupling between the ocean and the atmosphere (either NAO or ITCZ-related, Timmerman et al. 1998; Danabasoglu 2008; Vellinga and Wu 2004). In addition, while some studies suggest that the reversal of these AMOC oscillations is triggered by an anomalous advection of salinity from the tropics (e.g. Vellinga and Wu 2004; Mignot and Frankignoul 2005), others argue that the main salinity feedback comes from the Arctic (e.g. Jungclaus et al. 2005; Hawkins and Sutton 2007). The driving mechanism(s) of the decadal AMOC fluctuations, known to strongly influence climate in the North Atlantic (e.g. Latif et al. 2004), remain largely unresolved,

Table 1.1: Summary of some proposed mechanisms for decadal to multidecadal AMOC variability from modelling studies (non-exhaustive list).

Reference	Model	AMOC cycle	Mechanism(s)	Process(es) involved
Delworth et al. (1993)	GFDL R15	40-80 years	Internal ocean-only model excited by atmosphere noise (NAO)	A weak AMOC state is associated with a reduced northward heat transport, cooling the dense pool in central North Atlantic. Temperature anomaly generates cyclonic anomaly in subpolar gyre circulation, which transports salt into convection site, strengthening the AMOC.
Delworth et al. (1997)	GFDL R15	40-80 years	Internal ocean-only model excited by atmosphere noise. Link with the Arctic	Enhanced transport of freshwater and sea ice from the Arctic via the East Greenland Current and Denmark Strait. These anomalies propagate around the subpolar gyre into the Labrador Sea, capping the convection. Greenland Sea oscillations are implicated, but how they are generated is unknown.
Timmerman et al. (1998)	ECHAM3/ LSG	35 years	Coupled ocean-atmosphere mode	An anomalous strong AMOC state tends to warm the North Atlantic. The atmospheric response involves a strengthened NAO, leading to weak evaporation and Ekman transport off Newfoundland and in the Greenland Sea. This decreases SSS, weakening deep convection in sinking regions, weakening the AMOC.
Delworth and Greatbatch (2000)	GFDL R15	70-100 years	Damped ocean-only mode, excited by low-frequency atmospheric forcing (NAO)	Same as Delworth et al. (1993).
Vellinga and Wu (2004)	HadCM3	70-200 years	Coupled ocean-atmosphere mode. Link with Tropics	A strong AMOC state is associated with an enhanced northward heat transport, generating cross-equatorial SST gradient. As a consequence, ITCZ is shifted northward, increasing precipitation (hence decreasing SSS) in northern tropical Atlantic. Northward advection of SSS into sinking regions, weakening the AMOC.
Dai et al. (2005)	PCM	25 years	Internal ocean-only model excited by atmosphere noise (NAO)	Same as Delworth et al. (1993). It however suggests stronger ties to the NAO.
Dong and Sutton (2005)	HadCM3	25 years	Internal ocean-only model excited by atmosphere noise (NAO)	Same as Delworth et al. (1993). It however suggests stronger ties to the NAO.
Mignot and Frankignoul (2005)	BCM	<50 years	Coupled ocean-atmosphere mode. Link with Tropics	Part of the salinity anomaly in the tropical Atlantic (induced by El-Niño events) is advected in the ocean interior along the NAC, reaching the Irminger and Labrador Sea after about 35 years, where they destabilize the water column and favour deep convection.
Jungclaus et al. (2005)	ECHAM5/ MPI-OM	70-80 years	Damped ocean-mode excited by atmosphere noise. Link with the Arctic	Storage and release of freshwater from the central Arctic to the Labrador Sea convection site along with circulation changes in the Nordic Seas due to Atlantic heat and salt transports.
Hawkins and Sutton (2007)	HadCM3	centennial	Damped ocean mode excited by atmosphere noise. Link with the Arctic	Changes in the Nordic Seas convection lead to AMOC changes. Variations in salinity transports from the Arctic and from the North Atlantic are the main controlling feedbacks. Similar to Delworth et al. (1997) and Jungclaus et al. (2005), but convection regions are different.

Danabasoglu (2008)	CCSM3	21 years	Coupled ocean-atmosphere mode	Prominent role of the NAO in modulating the subpolar gyre strength and contributing to the formation of temperature and salinity anomalies that lead to positive/negative density anomalies at the deep-water formation site.
Msadek and Frankignoul (2009)	IPSL-CM4	∼100 years	Coupled ocean-atmosphere mode	Convection is primarily influenced by the anomalous advection of salinity due to changes in the East Atlantic Pattern.
Medhaug et al. (2011)	BCM	40-70 years	Coupled ocean-atmosphere mode	The variability in the Labrador Sea and the Nordic Seas convection is driven by decadal scale air-sea fluxes in the convective region that can be related to opposite phases of the NAO. The Labrador Sea convection is directly linked to the variability in AMOC. Linkages between convection and water mass transformation in the Nordic Seas are more indirect; the Scandinavian Pattern drives the ocean's poleward heat transport (PHT) affecting sea ice coverage there. Increased PHT is both associated with an increased water mass exchange across the Greenland-Scotland Ridge, and a stronger AMOC.
Kwon and Frankignoul (2011)	CCSM3	20 years	Internal ocean-only model excited by atmosphere noise (NAO)	The NAO plays a major role in AMOC variability through setting the surface flux anomalies in the Labrador Sea and affecting the subpolar gyre circulation strength.
Escudier et al. (2012)	IPSL-CM5	20 years	Coupled ocean-atmosphere mode. Link with Arctic	Positive temperature and salinity anomalies in the Labrador Sea are advected eastward (along the subpolar gyre), favouring deep convection south of Greenland and Iceland, and strengthening the AMOC. These anomalies eventually reach the Nordic Seas inducing sea ice melting and anomalous cyclonic circulation there. This strengthens the East Greenland Current, creating negative temperature and salinity anomalies in the Labrador Sea.

showing differences among various climate models (Latif et al. 2006). As a consequence, the inherent decadal predictability of the climate system is also not well established. From the perspective of developing operational decadal prediction schemes, improving our understanding of such variability is therefore pre-requisite.

1.5 Prospects for decadal climate prediction in the North Atlantic sector

1.5.1 Why is climate predictable?

In the 1960's Edward Lorenz made an "accidental" discovery in trying to model the weather: the chaotic phenomenon known as the "butterfly effect". This concept implies that small deviations in the initial conditions affect the weather for regions thousands of miles away some days later. Thus, for both the atmosphere and ocean being chaotic systems, detail of their state at a given time is strongly dependent on their previous state.

Because of this "butterfly effect", detailed day-to-day weather forecasting is effectively impossible more than a couple of weeks ahead, and knowledge of initial conditions (or states) is fundamental. But how could climate predictions be possible when weather forecasts are limited to a couple of weeks in advance? The answer is actually in the question: because climate and weather are fundamentally different. Weather forecasting aims to predict how the weather will evolve over a few days, while climate prediction aims to predict the weather we expect to have on average at both a given year and place. In a narrow sense, climate is usually defined as the statistical description of weather elements over a period of time, and describes the "macroscopic" weather characteristics like the mean or the variance, not the "microscopic" single weather phenomenon. Thus for climate prediction, accurate knowledge of initial conditions is not as crucial as for weather forecasting. In contrast, knowledge of average modifications (e.g. variation in atmospheric greenhouse gas concentrations), although weak, is more important because the associated signals, undetectable at a couple of weeks, accumulate with time. Therefore, in certain circumstances "macroscopic" weather characteristics (climate) are predictable although the forecast of "microscopic" characteristics (weather) are not. However, the system being chaotic in both cases, it is important to make several ensemble experiments to ensure the statistical robustness of the prediction.

1.5.2 Why is decadal climate prediction challenging?

Reliable predictions of the future climate mainly depend on sustained observations of changes in the ocean. The lack of subsurface ocean observations (Cunningham et al. 2007) has been a limiting factor for realizing the full skill potential of such predictions (Smith et al. 2007). Although the Atlantic Ocean has historically been the best observed of the world's oceans, the lack of sufficient subsurface data remains a limitation for the initialization of hindcasts used to develop and test coupled prediction systems. In addition, many observational gaps remain and the supply of data for the tropical Atlantic is limited relative to, for instance, the tropical Pacific. There is also a need for more atmospheric observations. Observations and the assimilation of salinity, which plays a more important role in Atlantic than in Pacific climate, also remains a particular challenge. For modelers, the climate timescale presents different challenges as compared to weather forecasting. Models tend to accumulate errors as computational time is extended, and errors of no consequence for weather timescales can dominate the calculation of the climate state. However, while ocean models are still not reproducing many observed ocean signals well, these models have reached a level of realism sufficient for serious experiment design and optimization studies to be usefully undertaken.

1.5.3 Evidence for decadal climate predictability in the North Atlantic

Decadal climate prediction is a relatively new field in climate science with a number of modelling groups performing near-term experiments for CMIP5 (Taylor et al. 2009) to be assessed as part of the IPCC Fifth Assessment Report. The prospect of providing climate change information regarding the next several decades highlights the strong need for assessing the potential predictability of climate on decadal timescales. Three methods, which heavily rely on models, are commonly used to estimate potential predictability. First, in the"Diagnostic Potential Predictability" (DPP) approach, the predictability is analysed by decomposing the variance of a climate variable into a long timescale component considered as potentially predictable, and an unpredictable noise component. Previous studies using such an approach for both real and modelled systems include those of Rowell (1998), Boer (2001, 2004, 2011), Boer and Lambert (2008), and Hawkins et al. (2011). Second, in the"Prognostic Potential Predictability" (PPP) approach, the predictability is estimated prognostically, by re-running a climate simulation with slightly perturbed initial conditions. This approach does not compare to observations directly, and only assesses the ability of the modelled climate to reproduce itself given a certain uncertainty on initial conditions, representing for example the atmospheric noise. These experiments are thus often called "perfect ensemble" experiments. Predictability studies using such an approach began with Griffies and Bryan (1997a,b), and have been followed by e.g. Grötzner et al. (1999), Boer (2000), Collins and Sinha (2003), Pohlmann et al. (2004), Collins et al. (2006a), Hermanson and Sutton (2009), Hurrell et al. (2009), Msadek et al. (2010). Third, in the ocean dynamics approach, the predictability is quantified by comparing the variability simulated with and without the inclusion of active ocean dynamics; it is likely that the regions in which ocean dynamics are important in generating the variability, are also those of high potential predictability (Pavan and Doblas-Reyes 2000).

All three methods (the DPP, PPP, and ocean dynamics approaches) indicate four regions where predictability may exist at decadal timescales: the North Atlantic, the Southern Ocean, the North Pacific, and the tropical Pacific. These regions are shown to be largely model independent by Boer (2001), where the potential predictability of decadal means of surface air temperature (SAT) from an ensemble of eleven state-of-art coupled climate models was calculated (Figure 1.5). The most prominent regions are the North Atlantic and the Southern Ocean, where more than 50% of the variance exists in the decadal band. Because eddies are of primary importance in controlling the momentum and buoyancy budget in the Southern Ocean (e.g. Hallberg and Gnanadesikan 2006), we can however question the reliability of results from climate models for the Southern Ocean since eddies are parametrized. Note that the oceans are a priori assumed to be among the most predictable component of the climate system on the decadal timescale as they provide long-term climatic memory due to their large thermal inertia.

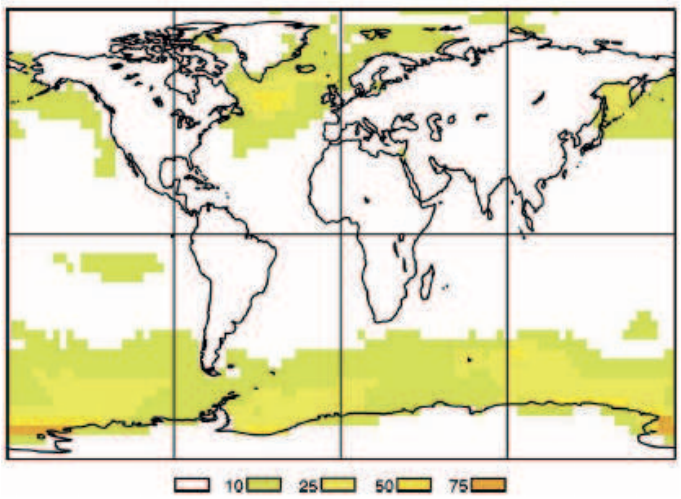

Figure 1.5: Potential predictability for decadal mean surface air temperatures from a model ensemble of 11 coupled models. (From Boer 2001).

For the North Atlantic and the Southern Ocean, the results of the Collins and Sinha (2003) and Pohlmann et al. (2004) PPP studies (with the HadCM3 and ECHAM5/MPI-OM models, respectively) are in good agreement with Boer (2001)'s study, showing that these regions are predictable out to 10 years or longer. The North Atlantic has received the largest amount of attention since it shows the largest potential for decadal predictability and because of its potential influence on Western Europe and the Eastern United States. Decadal variations of SST in the North Atlantic region (referred to as the AMO) are thought to influence important climatic features, including rainfall over the African Sahel, India and Brazil, Atlantic hurricanes and summer climate over Europe and America (e.g. Pohlmann et al. 2004; Sutton and Hodson 2005; Zhang and Delworth 2006; Knight et al. 2006; Dunstone et al. 2011). Because of the evidence that the AMO is linked to the AMOC (Knight et al. 2005), the latter has been considered as an ideal candidate for the study of decadal potential predictability (e.g. Delworth and Mann 2000; Curry et al. 2003; Latif et al. 2004; Collins et al. 2006a).

There have been several studies investigating the predictability of the AMOC in coupled models using the "perfect model" experiment approach (e.g. Griffies and Bryan 1997a,b; Sutton 2003; Collins and Sinha 2003; Collins et al. 2006a; Hermanson and Sutton 2009; Msadek et al. 2010). Most of them indicate that the AMOC variations are predictable out to a decade or more (see Table 1.2). For instance, in the PREDICATE project (Sutton 2003), a systematic comparison of the predictability of five state-of-the-art climate models (HadCM3, ECHAM/MMPI-OM, ARPEGE3/ORCA, BCM, ECHAM4/ORCA) is made. The results indicate that in general the strength of the AMOC is potentially predictable at least a decade in advance and, in some situations, multidecadal predictions of the AMOC may be possible. Consistent with earlier model comparisons of AMOC predictability made by Collins et al. (2006a), Msadek et al. (2010) recently found the leading mode of AMOC variability to have predictability for nearly two decades in the GFDL

model. There are even some hints of potential predictability for more than 50 years into the future in the HadCM3 model according to Collins and Sinha (2003). Although all the above predictability studies agree to some extent on the level of predictability of the AMOC, there are some disagreements on the level and extent of predictability of AMOC-related variation in North Atlantic SST. Results from Griffies and Bryan (1997b) with the GFDL model suggest the variations in North Atlantic SST to be predictable up to one to two decades, in good agreement with results from Pohlmann et al. (2004) with the ECHAM5/MPI-OM model. In contrast, Grötzner et al. (1999) found the North Atlantic SST to be predictable only about one year in advance, although they found a potential predictability of the AMOC up to one decade.

Table 1.2: Summary of AMOC predictive skills from modelling studies (non-exhaustive list).

Reference	Model(s)	Experimental set-up [ensemble(s), members, integration-length]	AMOC predictability skills
Griffies and Bryan (1997a)	GFDL	[2, 8, 30]	$\sim$ 20 years
Griffies and Bryan (1997b)	GFDL	[1, 12, 30]	20 years
Collins and Sinha (2003)	HadCM3	[3, 9, 20] ([1, 3, 70])	$\sim$ 15-20 (50) years; Better predictive skills when anomalously stronger overturning
Collins et al. (2006a)	(i) ARPEGE3-ORCALIM; (ii) BCM; (iii) ECHAM5/MPI-OM; (iv) HadCM3; (v) INVG	(i) [2, 6, 25]; (ii) [2, 3, 20]; (iii) [3 ,6 , 20]; (iv) [3, 8, 20]; (v) [2, 2, 20]	$\sim$ 10-20 years; Better predictive skills when anomalously stronger overturning
Hermanson and Sutton (2009)	HadCM3	[4, 10, 10]	From 3 to 8 years or 5 years on average
Msadek et al. (2010)	GFDL CM2.1	[6, 10, 20]	$\sim$ 10-20 years; Evidence for sensitivity to AMOC initial states

Predictions of AMOC variability and related oceanic fields may be of interest to scientists, but they would be of little relevance to society unless they are accompanied by predictions of surface climate variables. However, as for the North Atlantic SST, there are major disagreements on the level and extent of predictability of atmospheric quantities such as SAT and precipitation (mainly over land). Although previous studies (Griffies and Bryan 1997b; Grötzner et al. 1999) found little predictability of societally relevant surface quantities associated with AMOC variations, more up-to-date studies found evidence for potentially predictable variation in SATs on decadal timescales. Collins et al. (2006a) indeed found that the North Atlantic Ocean is a region in all the models in which there is significant relationship between decadal variations in SAT (and underlying SST) and the AMOC. In their study, the potential predictable surface climate variations associated with variations in the AMOC appear consistent. However potential predictive skill in surface climate variations appears to be less than those seen

for AMOC variations. In addition, following Boer (2001) and using nine models participating in the first Coupled Model Intercomparison Project (CMIP1), Boer (2004) predominantly found potential predictability of SAT over the high latitude oceans, with appreciable values on multidecadal timescales, especially in the North Atlantic. On shorter timescales, he also found some hints of potential predictability in the tropical Atlantic. Boer (2011) extended this study to simulations taking into account different climate change scenarios and trying to distinguish between internal and externally forced potential predictability. Using two different coupled climate models (HadCM3 and HadGEM1), Hawkins et al. (2011) identified the far North Atlantic in general, and the NAC region in particular, as regions with high potential predictability. For climate variables over land the evidence is much less clear. Grötzner et al. (1999) found that predictability for land-surface variables was less than a year. Boer (2000, 2004) and Collins (2002) also found no consistent evidence for predictability of surface temperatures beyond seasonal timescales. Boer and Lambert (2008) showed evidence of some predictability beyond seasonal timescales for surface temperature over land. In contrast, Collins and Sinha (2003), Sutton and Hodson (2005) and Pohlmann et al. (2006) have shown that the multidecadal AMOC predictability in HadCM3 and ECHAM3/MPI-OM models can lead to some predictability of European climate on decadal timescales. Pohlmann et al. (2004), Boer and Lambert (2008), and Boer (2011) all find that potential predictability is largely absent for precipitation.

Many studies in decadal climate predictability have considered only average levels of predictability. However, there is also evidence that decadal predictability of the AMOC and associated impacts on climate may be sensitive to the initial oceanic conditions with transitions around extreme states appearing as the most predictable events (e.g. Griffies and Bryan 1997b; Collins and Sinha 2003; Collins et al. 2006a). For instance, the latter study suggested that experiments initiated from stronger than normal AMOC states show more potential predictability than those initiated from weaker than average states. The possibility of predictability-dependence on initial oceanic state should be no surprise in view of the considerable evidence that the skill of weather forecasts is state dependent, and that the skill of seasonal forecasts varies with season and decade (Balmaseda et al. 1995; Pavan and Doblas-Reyes 2000). In the decadal case, however, there has been much less research to explore and understand the degree to which predictability, for different variables of interest, is sensitive to the initial oceanic state. Yet this is a very important matter in view of the increasing attention that is being paid to initialised decadal climate predictions.

In summary, there is a growing body of evidence from a variety of modelling studies that, in general, the strength of the AMOC could be predicted at least a decade in advance (e.g. Griffies and Bryan 1997b; Collins and Sinha 2003; Pohlmann et al. 2004; Sutton and Hodson 2005; Collins et al. 2006a). However there are major disagreements on the level and extent to which these AMOC variations lead to useful predictability of SST and

any atmospheric quantities (such as SAT and precipitation). Most of the recent studies would, nevertheless, tend to indicate that variations of SAT in the North Atlantic and over Europe exhibits useful decadal predictability (e.g. Collins and Sinha 2003; Sutton and Hodson 2005; Pohlmann et al. 2006), albeit with potential skill levels that are less than those seen for AMOC variations. Although there has been an increasing number of studies on decadal predictability of the climate system in the last few years due to the impetus of the "near term" CMIP5 protocol (Taylor et al. 2009), the realism of decadal climate predictability studies remains unclear as the level of predictability differs from one study to another (e.g. Meehl et al. 2009). This may be subject to model differences and uncertainties, as well as differences in the experimental protocol and metrics used. Considerable technical and scientific issues remain unresolved.

1.6 Aim of the study

1.6.1 Overall presentation of the project

With all the current focus on rapid changes in the AMOC due to global warming, it is important to understand its natural variability on decadal timescales, as this is precisely on this timescale that anthropogenic impacts in climate are likely to be expressed (IPCC 1996). However, as mentioned earlier, the mechanisms behind this variability have only been partially understood so far. As understanding the variability is an integral part of understanding the predictability, the inherent decadal predictability of the climate system is, by consequence, also not well established. Improving our understanding of this variability is therefore pre-requisite for an accurate prediction of future (anthropogenic) climate changes. The overall objective of the project is therefore **to assess the predictability of decadal fluctuations in the AMOC (and associated climate impacts) by investigating processes that drive its decadal variability**.

Given the lack of AMOC observations, numerical models need to be used to help with the understanding of such processes. There are, indeed, indications that the current generation of climate models can simulate aspects of decadal to multidecadal climate variability, as seen in the instrumental record (Knight et al. 2005) and proxy data (Delworth and Mann 2000). However, the projections of such models for climate-related variables (such as the AMOC strength, SAT) are widely different (IPCC 2001, 2007), as are the mechanisms involved. Spread in climate projections may be associated with differences in model resolution, parameter choice, the representation of physical and dynamic processes, and in the representation of the vertical coordinate of the ocean components. Hawkins and Sutton (2009) underline the importance of model uncertainty in decadal climate projections (Figure 1.6). By comparing models with different vertical representation of the ocean component, the present project also addresses, to

some extent, **the dependence of simulated AMOC variability and predictability on ocean model type**.

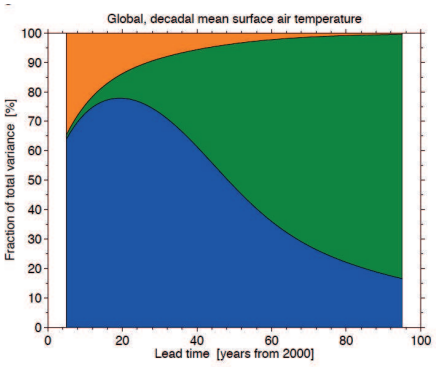

Figure 1.6: The fraction of total variance in global, decadal mean SAT predictions explained by three components of total uncertainty is shown. Green regions represent scenario uncertainty, blue regions represent model uncertainty and orange regions represent the internal variability component. (From Hawkins and Sutton 2009).

1.6.2 Specific objectives

More specifically, the present study aims at:

(1) Improving our understanding of the potential mechanisms responsible for the natural decadal variability of the AMOC.
The following questions mainly guide our investigation: (i) What is the spatial and temporal variability of the AMOC? (ii) What are the oceanic and atmospheric impacts of such variability? (iii) What are the mechanisms and key variables governing that variability? For this purpose, a new coupled climate model CHIME (Coupled Hadley-Isopycnic Model Experiment, Megann et al. 2010) developed at the National Oceanography Centre in Southampton (UK) is used. CHIME is as similar as possible to the widely used IPCC-class model HadCM3 (Gordon et al. 2000), with the important exception that the hybrid-coordinate ocean model HYCOM (Bleck 2002) has replaced the ocean component of this latter. The pre-industrial control simulation has been used to isolate the internal variability of the model under constant external forcing.

(2) Determining the extent to which decadal climate fluctuations associated with the AMOC are predictable and the processes involved.
The following questions mainly guide our investigation: (i) Where do climate-related fields exhibit the strongest sensitivity to decadal AMOC fluctuations? (ii) Are changes in the AMOC potentially predictable and which observations of the ocean state are likely to be of greatest value to constrain predictions? (iii) What is the spatio-temporal predictability of the Atlantic climate and how does this link to low-frequency AMOC variability? Because the CHIME model was made available late during my PhD allocated

time, this objective has first been addressed using the latest version of the Institut Pierre-Simon Laplace model (IPSL-CM5A, Dufresne et al. 2012), developed as part of the 5^{th} phase of the Coupled Model Intercomparison Project (CMIP5, Taylor et al. 2009).This model allowed us to develop an efficient experimental design prior to a similar such study with the CHIME model. Pre-industrial control simulations of both the IPSL-CM5A and CHIME models have been used to quantify their inherent predictive skills of internal fluctuations under constant external forcing. Both diagnostic and prognostic predictability approaches have been employed for this purpose.

(3) Better understanding of how the vertical representation of the ocean component can affect mechanisms governing AMOC variability and the predictability skills of the model.
By comparing experiments with models featuring ocean components with two different types of vertical coordinates, the dependence of simulated AMOC variability on ocean model type has also been provisionally addressed in this study. Indeed, as CHIME and HadCM3 differ only by their ocean components (hybrid and z-coordinates, respectively), an assessment of the extent to which the structural biases inherent in the vertical representation of the ocean model affect the decadal variability could be made. To do so, the natural decadal variability in CHIME will be evaluated alongside corresponding variability found in previous studies with the HadCM3 model (e.g. Vellinga and Wu 2004; Dong and Sutton 2005). However such a comparison with existing studies to evaluate the impact of the vertical representation on predictive skills is more difficult, first because of the limited number of such studies with HadCM3 and second because of the many differences in the experimental protocol for predictability studies. Since, here, a near-identical experimental protocol has been used for CHIME and IPSL-CM5A, a comparison of the results between these two models can still be useful considering that this latter model belongs to the new generation of z-coordinate models, and could therefore be seen as a more up to date z-coordinate model than HadCM3. Nevertheless, it has to be kept in mind that CHIME and IPSL-CM5A differ in more than the vertical representation of their ocean components.

1.6.3 Anticipated achievements of the project

By improving our understanding of the mechanisms driving the decadal AMOC fluctuations and associated impacts on the North Atlantic climate, this project contributes to the improvement of our ability to predict climate on decadal timescales. Such decadal climate forecasts may provide important information to decision makers since they have application to strategic planning in many areas (e.g. energy, fisheries, financial services and infrastructure). Decision makers in these sectors and European Union policy makers, will increasingly have to face up to the challenge of adaptation to anthropogenic climate change and will therefore require access to the best possible decadal climate

forecasts. In addition, by investigating the possible impact of using a different ocean component on the mechanisms, frequencies and predictability of decadal variability in climate models, this project contributes, to some extent, to a better understanding of the sources of uncertainty in climate models, which is of primary importance in decadal climate projections (Hawkins and Sutton 2009). Finally by comparing different approaches to quantify predictability and testing different measures of skill, this project also contributes to the coordinated effort of determining a common skill evaluation framework to evaluate decadal predictions; this is highly desirable to allow a comparison of decadal prediction systems across different modelling centres (Meehl et al. 2012).

The structure of this thesis is as follows. An overview of the main characteristics of both the CHIME and IPSL-CM5A models is presented in **Chapter 2**, followed in **Chapter 3**, by a description of the data and methods used here in both variability and predictability studies. **Chapter 4** addresses *objective (1)*, by analysing the natural variability of the AMOC (along with the variability of associated oceanic and atmospheric fields) on the shorter decadal timescale (i.e. 15-30 years) as seen in CHIME. Both **Chapter 5** and **Chapter 6** address *objective (2)* by analysing the decadal potential predictability of the North Atlantic climate associated with AMOC fluctuations as represented in both the IPSL-CM5A and CHIME models. **Chapter 7** briefly addresses *objective (3)* along with a discussion and summary of the main results of the thesis.

Chapter 2

Description of Models

In this chapter, we present the two models used in the framework of this thesis. Firstly, a full description of the new coupled climate model CHIME is given. This model is used here to investigate both the mechanisms and predictability of decadal AMOC fluctuations and climate in the Atlantic sector. Secondly, the IPSL-CM5A model is briefly described. The use of this model here is restricted to the study of the potential predictability of decadal AMOC fluctuations and climate; it allowed us to develop an efficient experimental design prior to a similar study with CHIME.

2.1 Coupled Hadley-Isopycnic Model Experiment (CHIME)

2.1.1 Model description

CHIME (Megann et al. 2010) is a new coupled climate model that features an innovative hybrid coordinate in the ocean, but is otherwise identical to the widely used IPCC-class model HadCM3 (Gordon et al. 2000). This has therefore the same atmosphere and ice models as HadCM3 (with the same ocean resolution over most of the globe), but uses the hybrid-coordinate ocean model HYCOM (Bleck 2002) instead of the conventional constant-depth vertical coordinate system used in HadCM3.

2.1.1.1 The ocean model (HYCOM) in CHIME

The oceanic component of CHIME is version 2.1.34 of HYCOM, which has been fully described by Bleck (2002). HYCOM is a primitive equation ocean general circulation model that evolved from MICOM, the Miami Isopycnic-Coordinate Ocean Model (Bleck et al. 1992). Although this latter has been validated (Chassignet et al. 1996; Roberts et al. 1996) and used in numerous ocean climate studies (New et al. 1995; Halliwell 1998;

Paiva et al. 2000), MICOM has a major weakness in the inadequate vertical resolution of weakly stratified regions. The HYCOM's hybrid coordinate algorithm was developed to ameliorate this limitation of MICOM by assigning different vertical coordinates types in those regions where they are quasi-optimum. HYCOM has become one of the primary ocean models in use today (e.g. Chassignet et al. 2003; Halliwell 2004; Kara et al. 2008), and has been adopted by the United States Navy as its main operational model. Development of the data assimilative system as well as ocean prediction through HYCOM have also been discussed by Chassignet et al. (2006, 2007). In this section, the salient features of the oceanic component of CHIME are described.

Governing Equations

Like MICOM, HYCOM contains five prognostic equations, comprising two horizontal velocity component equations (Equation 2.1); a mass continuity equation (Equation 2.2) and two other conservation equations (Equation 2.3) for a pair of thermodynamic variables (chosen from density, salinity and temperature). Following Bleck et al. (2002), the model equations are listed below:

Momentum:

$$\frac{\partial \vec{v}}{\partial t_s}+\nabla_s\frac{\vec{v}^2}{2}+(\xi+f)\vec{k}\times\vec{v}+(\dot{s}\frac{\partial p}{\partial s})\frac{\partial \vec{v}}{\partial p}+\nabla_s M-p\nabla_s\alpha=-g\frac{\partial \tau}{\partial p}+(\frac{\partial p}{\partial s})^{-1}\nabla_s\cdot(\upsilon\frac{\partial p}{\partial s}\nabla_s\vec{v}) \quad (2.1)$$

Continuity:

$$\frac{\partial(\frac{\partial p}{\partial s})}{\partial t_s}+\nabla_s\cdot(\vec{v}\frac{\partial p}{\partial s})+\frac{\partial(\dot{s}\frac{\partial p}{\partial s})}{\partial s}=0 \quad (2.2)$$

Tracers:

$$\frac{\partial(\frac{\partial p}{\partial s}\theta)}{\partial t_s}+\nabla_s\cdot(\vec{v}\frac{\partial p}{\partial s}\theta)+\frac{\partial(\dot{s}\frac{\partial p}{\partial s}\theta)}{\partial s}=\nabla_s\cdot(\nu\frac{\partial p}{\partial s}\nabla_s\theta)+H_\theta \quad (2.3)$$

where s is the vertical coordinate of HYCOM, $\dot{s}$ is the time derivative of s, $\vec{v}=(u,v)$ is the horizontal velocity vector, p is the pressure, θ represents any one of the model's thermodynamic variables, $\alpha=\rho_{pot}^{-1}$ is the potential specific volume, $\xi=\frac{\partial v}{\partial x_s}-\frac{\partial u}{\partial y_s}$ is the relative vorticity, $M=gz+p\alpha$ is the Montgomery potential, $gz=\Phi$ is the geopotential, f is the Coriolis parameter, $\vec{k}$ is the vertical unit vector, υ is the eddy viscosity, ν is the diffusivity coefficient, and τ is the wind and bottom drag induced shear stress vector. H_θ represents the sum of diabatic source terms, including diapycnal mixing, acting on θ. Subscripts indicate which variable is held constant during partial differentiation. The above prognostic equations are complemented by three diagnostic equations, including the hydrostatic equation ($\frac{\partial M}{\partial \alpha}=p$); the equation of state and an equation prescribing the vertical mas flux $\dot{s}\frac{\partial p}{\partial s}$ through a s surface. The last equation controls both spacing and movement of layer interfaces and this comprises the essence of hybrid modelling.

Transport and mixing processes

All prognostic equations are time-integrated using the split-explicit treatment of barotropic

and baroclinic modes developed by Bleck and Smith (1990). The horizontal mass fluxes are computed using the Flux Corrected Transport (FCT) scheme (Zalesak 1979) while horizontal tracer transport is treated in flux form and handled by a variant of the MP-DATA scheme (Drange and Bleck 1997). The K-profile parameterization (KPP) diapycnal mixing scheme (Large et al. 1994) is used in CHIME, which was found by Halliwell (2004) to afford superior performance to the Kraus-Turner bulk mixed layer scheme when used with HYCOM. This is significantly different from the bulk mixed layer scheme and the Pacanowski and Philander internal mixing parameterization used in HadCM3, and we note that this introduces an additional difference between the two models besides the vertical coordinate. The HYCOM parameter values used for this scheme in CHIME are background internal wave viscosity $difmiw = 1 \times 10^{-4} m^2 s^{-1}$, background internal wave diffusivity $difsiw = 1 \times 10^{-5} m^2 s^{-1}$, and the critical bulk Richardson number $ricr = 0.45$.

Vertical coordinate system

The oceanic component HYCOM uses 25 vertical layers combining potential density layers in the ocean interior with constant depth layers near the surface. In the interior, which in the present model configuration constitutes more than 93% of the ocean domain by volume, the vertical coordinate is close to isopycnic over the whole annual cycle. However, layers smoothly transition to z-coordinates in the weakly stratified upper-ocean mixed layer. Therefore HYCOM allows coordinate surfaces to locally deviate from isopycnals wherever the latter may fold, outcrop, or generally provide inadequate vertical resolution in portions of the model domain. The freedom to adjust the vertical spacing of the coordinate surfaces in HYCOM simplifies the numerical implementation of several physical processes (e.g. mixed layer detrainment, convective adjustment, etc.) without robbing the model of the basic and numerically efficient resolution of the vertical structure that is characteristic of isopycnic models throughout most of the ocean's volume. In the near-surface waters (or wherever layer density is not used), the layers that would be unused in a purely isopycnic model are constrained to have a minimum thickness and their density is allow to vary. In the present implementation, the surface layer thickness is 5 m, and the minimum thickness of subsurface layers increases to a maximum of 15 m by layer 15. The vertical coordinate is potential density referred to a pressure of 2000 dbar, and the thermobaric correction to the pressure gradient of Sun et al. (1999) is applied. If the density in a given grid cell changes as a result of mixing, HYCOM adjusts the depth of the upper or lower interface of each layer to return the density toward the reference density of that layer; this regridding process is carried out using a piecewise linear mapping algorithm. In the mixed layer, grid points are placed vertically so that a smooth transition of each layer interface from an isopycnic to a constant-depth surface occurs where the interface outcrops into the mixed layer. The reference densities for the 25 layers (Table 2.1) were chosen to resolve the major water masses of the global ocean, with enhanced resolution at low densities to improve the accuracy of the mixing scheme in the mixed layer. HYCOM therefore behaves like a

z-level coordinate model in the mixed layer or other unstratified regions, and like an isopycnic-coordinate model in stratified regions. In doing so, the model is thought to combine the advantages of the different types of coordinates.

Table 2.1: Layer target density, density resolution and minimum thickness in CHIME (From Megann et al. 2010).

k	σ_k	$\triangle\sigma_k$ (m)	$\triangle z_k^0$ (m)
1	29.60	0.6	5.0
2	30.20	0.6	7.0
3	30.80	0.6	9.8
4	31.40	0.6	13.7
5	32.00	0.6	15.0
6	32.60	0.6	15.0
7	33.20	0.6	15.0
8	33.80	0.6	15.0
9	34.40	0.6	15.0
10	35.00	0.3	15.0
11	35.30	0.3	15.0
12	35.60	0.25	15.0
13	35.85	0.2	15.0
14	36.05	0.2	15.0
15	36.25	0.2	15.0
16	36.45	0.15	15.0
17	36.60	0.15	15.0
18	36.75	0.11	15.0
19	36.86	0.10	15.0
20	36.96	0.08	15.0
21	37.04	0.08	15.0
22	37.12	0.08	15.0
23	37.20	0.12	15.0
24	37.32	0.12	15.0
25	37.44	0.12	15.0

Spherical grid

The east-west filtering procedure used in HadCM3 to prevent violations of the Courant-Friedrich-Lewy (CFL) stability criterion (Courant et al. 1967) at latitudes poleward of 75°N is inappropriate in a layer model such as HYCOM, where layer thickness is required to be positive definite, so the spherical grid used throughout HadCM3 is not useable in the Arctic in CHIME. The ocean model therefore uses a spherical-bipolar grid similar to that described by Sun and Bleck (2001), which is composed of two regions: (i) from 55°N to 78°S it has a constant angular resolution of $1.25° \times 1.25°$ (where the mass points are exactly coincident with those of the HadCM3 ocean model grid), and (ii) north of 55°N the spherical grid is matched smoothly to a bipolar grid (avoiding problems caused by the convergence of the meridians toward the North Pole). The poles of the bipolar grid are situated at (55°N, 110°W) and (55°N, 70°E), with resolution at ocean points (north

of 55°N) between 40 and 140 km. All HYCOM variables are stored on an Arakawa C-grid.

2.1.1.2 The atmosphere model (HadAM3) in CHIME

The atmospheric component is described in detail in Gordon et al. (2000). The basic features are as follows. HadAM3 is a version of the UK Met Office Unified climate model run with a horizontal grid spacing of 3.75° east-west and 2.5° north-south, and 19 vertical levels using a hybrid vertical coordinate. The timestep is 30 min, and it uses an Arakawa B-grid. HadAM3 uses a prognostic cloud scheme, described by Smith (1990) and modified by Gregory and Morris (1996), which diagnoses cloud ice, cloud water and cloud amount from the primary model variables (total moisture) and liquid water potential temperature. It also uses the precipitation scheme described by Senior and Mitchell (1993). Moist and dry convection are modelled using the mass-flux scheme of Gregory and Rowntree (1990) with the addition of convective downdrafts (Gregory and Allen 1991). The parameterization of sub-grid scale orographic gravity-wave drag is that of Gregory et al. (1998). The model uses the boundary layer scheme developed by Smith (1990, 1993). It also uses the radiation scheme developed by Edwards and Slingo (1996) and modified by Cusack et al. (1999). This has six shortwave bands and eight longwave bands. As well as including the effects of CO_2, H_2O, and O_3 it also includes the effects of O_2, N_2O, CH_4, CFC_{11} and CFC_{12}. The model uses trace gas values appropriate for the AMIP I period, i.e. 1979-1988. It also includes the developments made by Cusack et al. (1998) to include the effects of background aerosols. The direct impact of convection on momentum is included in HadAM3 using the scheme developed by Gregory et al. (1997). HadAM3 includes MOSES, the land surface scheme developed by Cox et al. (1999). It includes a representation of the freezing and melting of soil moisture, and a formulation of evaporation which includes the dependence of stomatal resistance on temperature, vapour pressure deficit and CO_2. In the model, the critical relative humidity is setup to 0.7 above level 3 (Pope et al. 2000). This value was chosen to maintain a global mean radiation balance close to zero at the top of the atmosphere in pre-industrial simulations. The coefficient known as Cw, which controls the rate at which cloud liquid water is converted to large-scale precipitation, takes different values over land ($Cw = 2.0 \times 10^{-4}$) to those over the sea ($Cw = 0.5 \times 10^{-4}$) in an attempt to take account of the differences in cloud condensation nuclei.

2.1.1.3 The ice model in CHIME

A key feature of high-latitude climate is its snow and ice cover, which therefore has to be well represented. The sea ice model (Cattle and Crossley 1995) is taken from HadCM3. It is a simple thermodynamic model, plus ice drift with the ocean surface current, and with partial ice coverage to allow representation of leads. The three scalar prognostic

fields of the sea ice model are ice thickness, fractional ice cover, and snow depth. A simple ice thickness advection scheme is used following Bryan et al. (1975). The formulation of fractional ice cover is based on that of Hibler (1979), which assumes the ice-covered area to have a uniform thickness distribution of mean thickness. The sea ice thermodynamics formulation used in the model follows the zero-layer model of Semtner (1986) in which the ice-snow layer is treated as single slab. For surface temperatures below -10°C, the snow/ice surface albedo is taken to have constant value of 0.8. Above this temperature, ice albedo decreases linearly to a value of 0.5 at the melting point (0°C) to allow for the lowering of albedo caused by the presence of melt ponds on the ice surface. The albedo of leads is assumed to be a constant 0.06. Any heat flux entering (or leaving) the leads is partitioned between ice melt (or ice formation) and warming (or cooling) of the upper layer of the ocean. The partitioning between ice melt/formation and ocean warming/cooling is chosen to be directly proportional to the ice area. The advection and diffusion scheme in the sea ice model are recoded for consistency with the Arakawa C-grid used for the CHIME ocean model, the HadCM3 ocean being defined on a B-grid.

2.1.1.4 Bathymetry and coastlines

The bathymetry and coastlines used in CHIME are shown in Figure 2.1. The bathymetry is derived from Sandwell and Smith (1997), interpolated onto the HYCOM mass grid points. A minimum depth of 100 m is then imposed everywhere to prevent numerical barotropic instabilities in shallow water (HadCM3, by comparison, has a minimum depth of 139 m). Use of the bipolar grid in the Arctic means that the locations of grid points (and hence of the coastlines) in this region cannot be identical to those in HadCM3, so in CHIME the coastlines are defined everywhere at the ocean resolution, where in HadCM3 coastlines are at the coarser resolution. The coastlines are at first defined to be the zero-depth contour after interpolation, and are then adjusted to ensure critical straits remain open to a realistic depth. The bathymetry was excavated in the North Atlantic so that the sills between Greenland and Scotland have a minimum depth of 800 m, resulting in comparable sill depths to those in HadCM3. The Bering and Gibraltar straits are both open in CHIME, and are represented by channels a single grid cell wide. The continuity of the computational grid across Bering Strait is ensured by explicitly copying all prognostic fields into “shadow zones” on each side of the strait. This is in contrast to HadCM3, in which the numerical B grid of the ocean model prohibits flow through single-grid point channels. Because the coastlines in CHIME do not correspond exactly to the atmospheric grid north of 55°N, a coastal tiling and interpolation scheme identical to that used by Sun and Bleck (2001) is employed to conserve fluxes passed between the atmosphere and ocean.

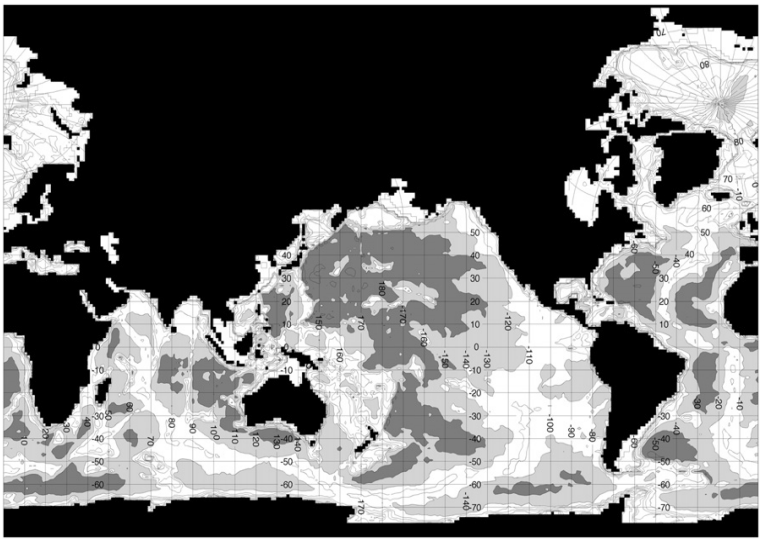

Figure 2.1: CHIME bathymetry and coastlines: gray shading denotes depths > 3000 m; dark gray denotes depths > 5000 m. (From Megann et al. 2010).

2.1.1.5 Atmosphere-ocean coupling

The ocean and ice fields are coupled daily to the atmosphere using the OASIS v2.4 coupler (Valcke et al. 2000). To avoid spurious maxima in the wind stress curl, the wind stress passed from the atmosphere to the ocean is linearly interpolated between the centres of each atmospheric cell. As is the case in HadCM3, no flux adjustment is applied to the air-sea coupling.

2.1.2 Initial conditions and control runs

Both variability and predictability studies carried out with CHIME have been done using two different control integrations, arbitrarily named as *cD* and *E*3.

2.1.2.1 Control integration for climate variability study: *cD*

The core of the variability study with CHIME is *cD*, its first 200-year control integration (obtained prior to its port to a new operating system) which has been fully described and analysed in Megann et al. (2010). *cD* was obtained by initializing the model from the full-depth Levitus et al. (1998) autumn climatology, projected onto the model density layers. Atmospheric forcing was with pre-industrial levels of greenhouse gases and aerosols, therefore enabling us to isolate the internal variability of the model under constant external forcing. The atmospheric initial state was identical to that in the HadCM3 control run described in Gordon et al. (2000). Initial sea ice cover was taken from estimates of Gloersen et al. (1993), and the initial thickness of sea ice in all ice-covered grid cells was set to 2 m. CHIME is run in fully coupled mode for 200 years from rest, and

output is stored at monthly-mean time resolution. A spin-up time is clearly identified up to year 80 as seen in the time series of the AMOC index (defined as the maximum of the annual mean Atlantic meridional mass transport streamfunction at 30°N, Figure 2.2), further described in *Sect. 4.2.1.* After year 80, the AMOC has nearly stabilized; we will therefore restrict our variability analyses starting from this year (despite a decreasing trend of about 1.5 Sv century^{-1} thereafter).

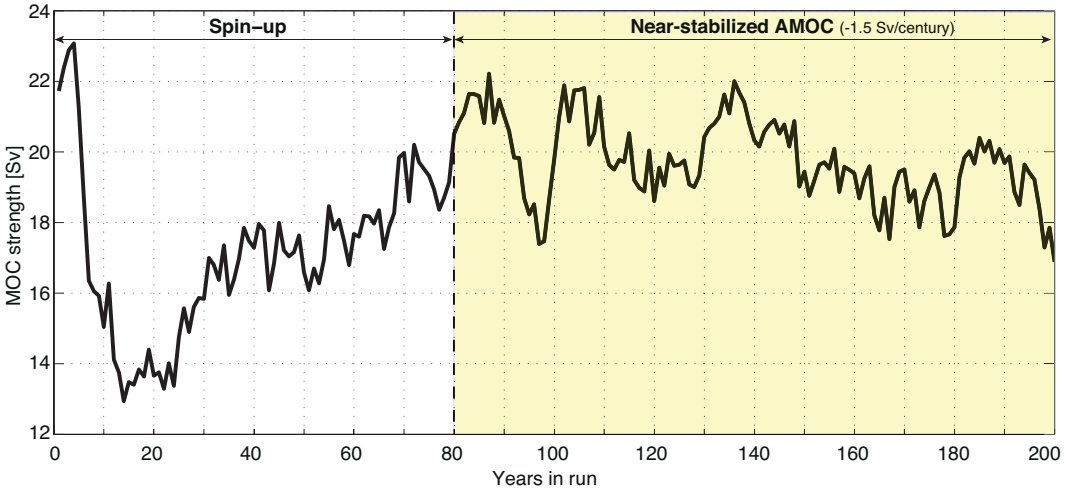

Figure 2.2: Time series of annual AMOC index for the whole 200-year simulation *cD*. Yellow shading corresponds to the time-period (80-200) analysed in the variability study with CHIME.

2.1.2.2 Control integration for climate predictability study: *E3*

The core of the predictability study with CHIME is *E*3, a 445-year control integration that is part of a set of trial runs obtained once CHIME has been ported to the new operating system. For *E*3, the model has been initialized similarly to *cD*. Note, however, that *E*3 uses a slightly different version of HYCOM (v2.2.18, against v2.1.34 in *cD*), and a higher-order vertical regridding scheme. For technical reasons, the Bering Strait is also closed in *E*3 in contrast to *cD*. It is run in fully coupled mode for 445 years from rest, and output is stored at monthly mean time resolution. As seen in Figure 2.3, the AMOC index in *E*3 has the most stabilized state between year 105 and 305 (with a slight decreasing trend of about 0.24 Sv century^{-1}); prior to this period, a spin-up time is clearly identified, after which a continuous decreasing trend is apparent. This subsequent weakening of the AMOC is probably a consequence of the continuous warming (freshening) of global mean SST (SSS) during the near-stabilized time-period of the AMOC index (Figure 2.4), leading to an increase in the global SAT. In contrast to *E*3, the decreasing trend also observed in *cD* during the near-stabilized time-period of the AMOC was not accompanied by such continuous increasing (decreasing) trends of temperature (salinity) fields. Although the worldwide warming (freshening) of SST (SSS) appears to be problematic in *E*3, we could not wait for a more acceptable control

integration to be run because of time constraints. In order to limit the impact of such trends on our predictability study, we will therefore restrict our analyses to years 105-305, that is when the AMOC has not been yet affected by the global warming and freshening trends. Note also, that for all atmospheric output, the January months have been accidentally lost. To settle this problem, we interpolated the values of December and February to obtain the missing data. Such problems (i.e. climate drift and missing data) have to be borne in mind when interpreting results obtained from $E3$.

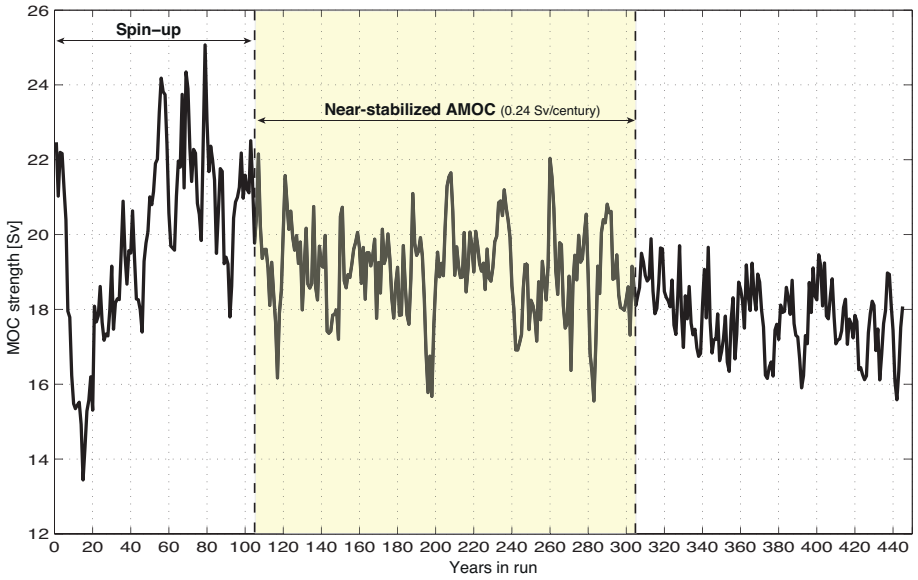

Figure 2.3: Time series of annual AMOC index for the whole 445-year simulation $E3$. Yellow shading corresponds to the time-period (105-305) in the variability study with CHIME.

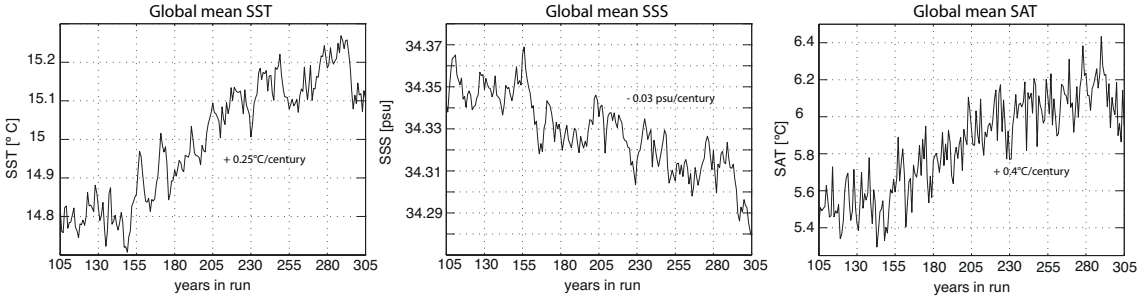

Figure 2.4: Time series of global mean SST, SSS, and SAT in $E3$ during the analysed time-period (105-305).

2.1.3 How faithful is CHIME to the real climate system?

2.1.3.1 Control integration *cD*

Megann et al. (2010) analyzed cD, and showed that it has a generally realistic climate. However some discrepancies with the real climate system have been identified, which are

worth pointing out. Here is a summary of the main findings of Megann et al. (2010) on model realism.

Surface temperature errors

Figure 2.5 shows SST anomalies with respect to the annual NOCS (1999) climatology in CHIME. There are warm errors off the western coasts of South America and South Africa most likely resulting from the unrealistically low cloud cover, as in HadCM3 (Gordon et al. 2000). In the Pacific, there is a significant cold bias of up to 1.5°C in the equatorial band. In the North Pacific, there is also a moderate cold error of 0-1°C south of 30°N and a warm error of similar magnitude in the subpolar gyre. The North Atlantic is generally too warm in CHIME. The whole subpolar gyre is significantly warmer than climatology, with an error of 6°C centered at (50°N,45°W). CHIME is also too warm throughout the Southern Ocean, with errors of up to 3°C. This is at least partially due to the use of the KPP mixing scheme in this model, which has been shown to produce unrealistically shallow summer mixed layers in the Southern Ocean in HadCM3, leading to warm errors (Gordon et al. 2000). Excluding the Southern Ocean and the region affected by shortcomings in the cloud scheme, the overall impression, however, is that the CHIME has a surface warm bias. As for the global mean SAT in CHIME, it is about 1°C warmer than that in the NOCS climatology.

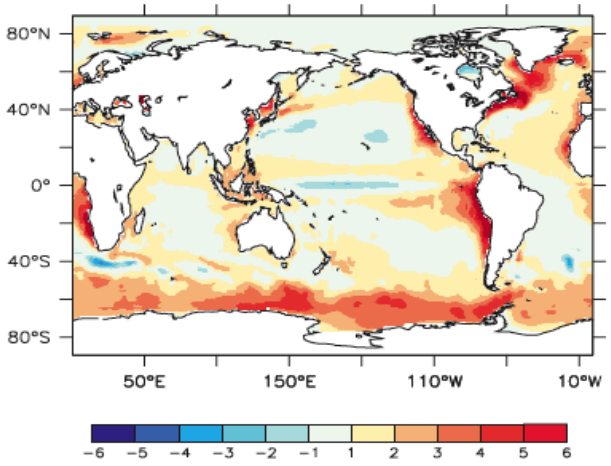

Figure 2.5: CHIME ocean surface temperature anomalies (°C) with respect to the annual NOCS (1999) climatology, averaged over years 80-119 of *cD*. (After Megann et al. 2010).

Sea surface salinity errors

Figure 2.6 shows SSS anomalies from the annual Levitus et al. (1998) climatology. In the Pacific, there is a tripolar error pattern; the surface is too fresh north of 30°N, too salty between the equator and 30°N and in the Western Warm Pool on the equator west of 180°, and too fresh in the Southern Hemisphere. CHIME is too fresh in the South Atlantic, and too salty in both the subtropical and the subpolar North Atlantic. The surface salinity is also too high over the whole Arctic, with an error of over 1 psu nearly everywhere.

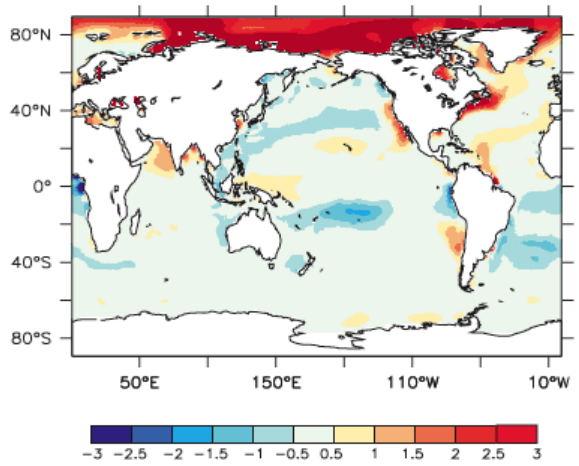

Figure 2.6: CHIME ocean surface salinity anomalies (psu) with respect to the annual Levitus et al. (1998) climatology, averaged over years 80-119 of *cD*. (After Megann et al. 2010).

Precipitation/Inter-Tropical Convergence Zone (ITCZ)

Figure 2.7 shows the global annual mean precipitation in CHIME and the Global Precipitation Climatology Project climatology (GPCP, Huffman et al. 2001). CHIME generally simulates the main precipitation patterns as seen in the observations, except for the double-ITCZ pattern in the Pacific sector similar to that produced by most of the current state-of-the-art CGCMs (Lin 2007). This double-ITCZ problem has been a long-standing tropical bias which is characterized by excessive precipitation off the equator but insufficient precipitation on the equator. Schneider (2002) showed that the problem is mainly caused by the atmosphere models rather than the ocean models; the fact that HadCM3 also has this double-ITCZ structure (Harvey 2003) is in good agreement with this statement given that CHIME and HadCM3 only differ from their ocean components. In addition, although the CHIME model has generally slightly stronger (weaker) precipitation in the tropical Pacific (tropical Atlantic) than in the observations, it at least reasonably well simulates the correct placement of the precipitation maxima.

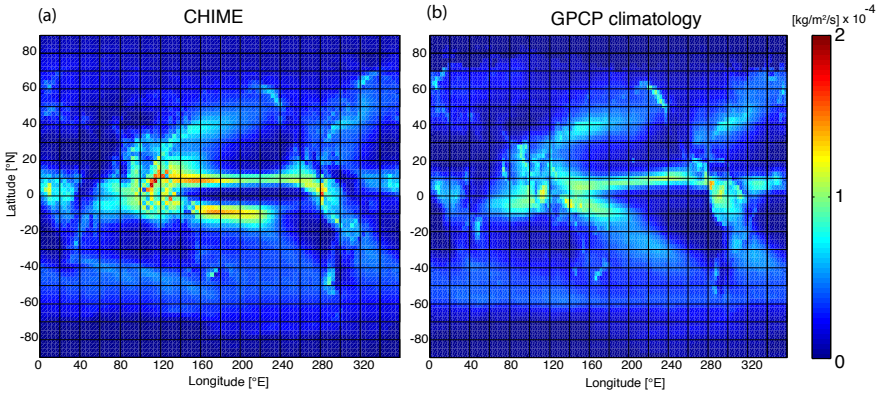

Figure 2.7: Global annual mean precipitation in (a) CHIME and (b) GPCP climatology (Huffman et al. 2001).

Oceanic heat transport

The global northward oceanic heat transport in CHIME is in good agreement with the observational estimates at 32°S, 19°S, and 48°N, but carries less heat at 24°N than that estimates by Ganachaud and Wunsch (2000) and more heat north of 40°N (Figure 2.8). In the North Atlantic (not shown), CHIME heat transport lies within observational bounds at 48°N and does not at 24°N, whereas in the North Pacific (not shown) it lies within observational estimates at 24°N and does not at 48°N. Overall, however, the global heat transport in CHIME is generally within the error bars of the observational estimates.

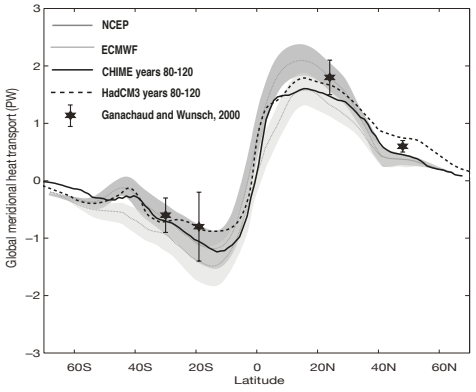

Figure 2.8: Global mean ocean heat transport in PW in CHIME (solid curve) and HadCM3 (dashed curve). The stars show the estimates of Ganachaud and Wunsch (2000). The dotted lines are from the reanalysis of Trenberth and Caron (2001): the darker grey shading denotes the confidence limits of estimates based on NCEP fluxes, while the light gray shading corresponds to estimates based on ECMWF fluxes. (After Megann et al. 2010).

March Mixed layer depth

Figure 2.9 shows the average March Mixed Layer Depth (MLD) in both CHIME and observations. Shallow biases are obvious in the Southern Hemisphere summer in CHIME; the MLD is nowhere deeper than 50 m across the whole Southern Ocean, where in the climatology there is a band of mixing to around 100 m between 40°S and 60°S spanning the whole circumpolar region. This overly shallow MLD in the austral summer is the principal reason for the SST being too warm in CHIME in this region. In the Northern Hemisphere, the overall pattern of winter mixing in CHIME is similar to that in the Levitus climatology. In the North Pacific, the tongue of mixing to 300-400 m in the Kuroshio separation region, and the 100-200 m depth of the wintertime MLD north of 20°N are well represented. In the North Atlantic, the mode-water formation region extending northeastward from the Sargasso Sea to 30°W is also well represented by CHIME, with realistic MLDs of 300-450 m. However the convection is too deep from the Labrador Sea in the west to northwest of Scotland in the east. In the Nordic Seas, the convection is also too deep (up to 4000 m) and extends not only across most of the Nordic Seas but through Fram Strait and as far as the Canadian Basin. This excessive

mixing is consistent with the anomalously high surface salinity that develops in CHIME in the North Atlantic subtropical gyre and the Arctic. Overall, CHIME has mixed layer depths that are too shallow in the summer but too deep in the winter; this is attributed to the use of the KPP mixing scheme in this model (Megann et al. 2010).

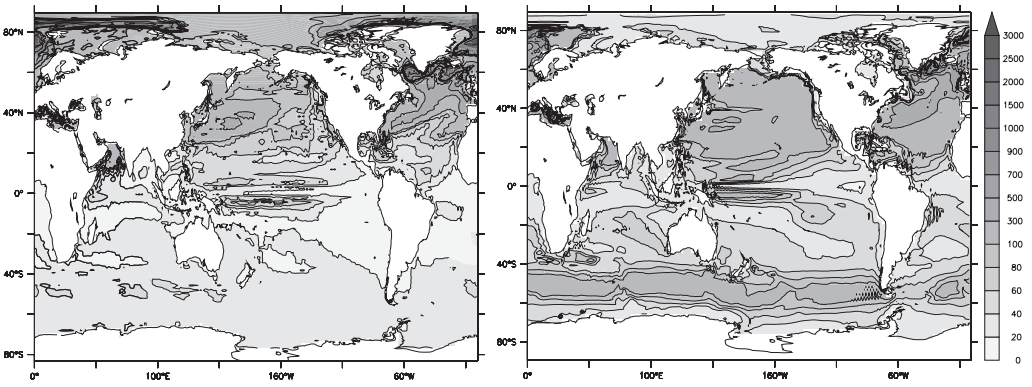

Figure 2.9: The mean mixed layer depth (m) in CHIME in March averaged over years 80-119 (left panel) and the March mixed layer depth diagnosed from the Levitus et al. (1998) climatology (right panel). (After Megann et al. 2010).

Ice cover

The annual range of ice cover in both hemispheres is rather larger than those in observations (Figure 2.10). The maximum Arctic (Antarctic) winter ice cover is over 40% (50%) higher in CHIME than observed; this is likely to reduce the amount of winter heat loss, and hence potentially the production of dense bottom water. CHIME tends, however, to have rather less ice in the summer than in observations.

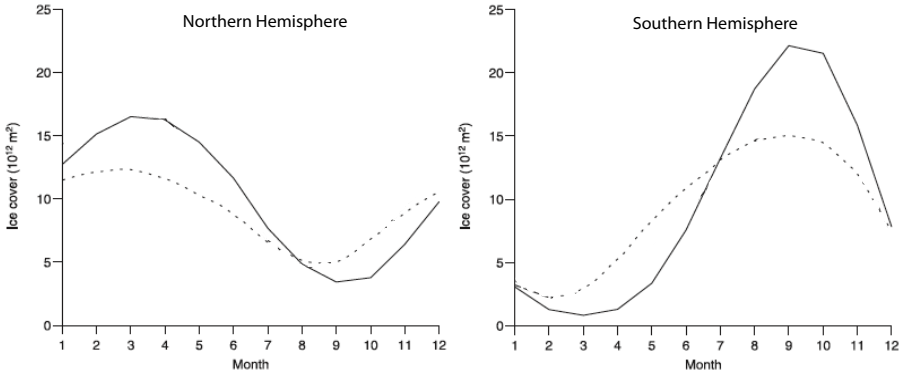

Figure 2.10: Mean annual cycle of total ice area in the Northern Hemisphere and the Southern Hemisphere. The ice cover in CHIME (the observations from Special Sensor Microwave Imager) is shown by the solid line (dotted line). (Adapted from Megann et al. 2010).

Wind stress

The large-scale structure of the wind stress field in CHIME is generally in good agreement with observations (not shown). The mean wind stress is substantially weaker in the North Atlantic than in the NOCS climatology (Josey et al. 1998), with a maximum eastward stress at 40°W of around 0.06 Nm^{-2}, as compared with 0.10 Nm^{-2} in the

climatology, and this is more likely to influence the strength and path of the ocean circulation than the variability itself. Differences in the zero wind stress curl line (ZWCL) off the eastern seaboard of the United States are clearly visible at about 37°N at 70°W, while the position of the observed ZWCL (estimated from the NOCS climatology) at this longitude is at 33°N.

North Atlantic Oscillation (NAO)

Figure 2.11 shows the NAO index time series (defined as the normalized pressure difference between Iceland and the Azores during the winter season) in CHIME and the observations (Hurrell 1995b), together with their corresponding power spectrum. The NAO oscillation in CHIME seems to have a weaker amplitude than in the observations, with a standard deviation of 1.6 and 1.9, respectively. The power spectrum of the observed NAO shows most energy at a period of about 70 years (above the 95% confidence limit) and then at about 8-9 years and 1-3 years (above the 80% confidence limit). Because of the short time series available, CHIME does not capture the 70-year peak. However, both peaks at 8-9 years and 1-3 years are well captured by the model (although periods in the range 1-3 years are slightly below the 80% confidence limit). Although the NAO in CHIME is slightly too weak than in the observations in term of amplitude, it is reasonably well represented in term of variability.

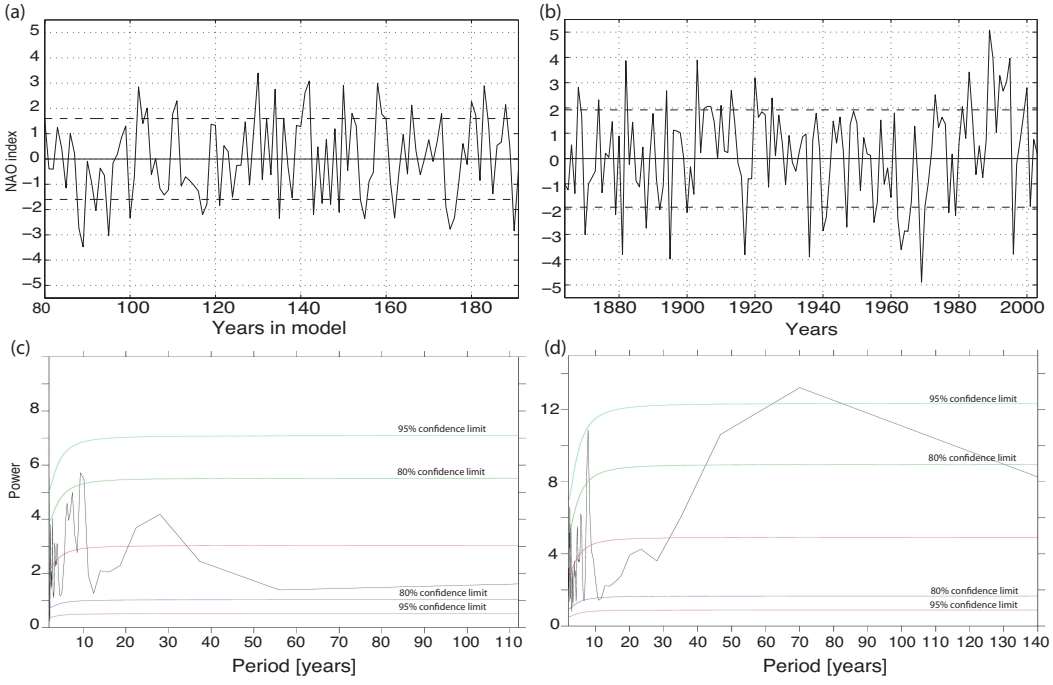

Figure 2.11: Time series of the NAO index in (a) CHIME and (b) the observations (Hurrell 1995b); the standard deviations are shown as the dashed lines. Corresponding power spectrum in (c) CHIME and (d) the observations. The smooth red line is the power of a red noise spectrum with the same AR(1) coefficient fitted from the NAO time series.

Ocean surface circulation

In CHIME, the Gulf Stream separates at about 39°N, while observations suggest it separates at Cape Hatteras at about 36°N. The more northerly separation of the Gulf Stream in CHIME is therefore broadly consistent with the northerly position of the ZWCL. At 65°W, the Gulf Stream transport at 15 Sv is considerably less than the 80 Sv or so observed at this longitude (e.g. Johns et al. 1995). As in the North Atlantic, both the ZWCL and separation of the western boundary current in the northwest subtropical Pacific are farther north in CHIME than in observations. In the real ocean, the Kuroshio separates from the coast of Japan at around 35°N (e.g. Qu et al. 2001), whereas in CHIME it separates at 37-40°N. The separation in CHIME is therefore 3-4° too far to the north. The observed transport in the Drake Passage is around 135 Sv (Cunningham et al. 2003). The Drake Passage transport in CHIME has a realistic value of 140 Sv in the first decade, but spins down to 60 Sv by year 200. Because Subantarctic Mode Water (SAMW) and Antarctic Intermediate Water (AAIW) are well preserved (see next paragraph), we suspect that the AMOC is relatively unaffected by this transport drop in the Drake Passage. The flow through the Bering Strait into the Arctic, rather variable, lies between 0 and +1 Sv, and compared reasonably well with an observed barotropic flow of around 0.83 ± 0.66 Sv (Roach et al. 1995). The flow through the Canadian Archipelago has a transport of about 2 Sv through Davis Strait, which is in good agreement with observations (e.g. Cuny et al. 2005). The southward export of dense water through the Denmark Strait into the North Atlantic is about 3 Sv, with an additional southward flow of about 3 Sv of dense water over the Iceland-Scotland ridge system; this is in broad agreement with observations (e.g. Cuny et al. 2005).

Interior water mass preservation and structure

AAIW is formed through surface mixing around the Southern Ocean between 45°S and 55°S, and is characterized by a surface salinity minimum. Overall, the fresh signature of AAIW is well maintained in CHIME. The ability of HYCOM to preserve water mass characteristics is similarly evident in the North Pacific, where the fresh tongue of North Pacific Intermediate Water is mainained with little variation over the 200-year run of CHIME. SAMW is formed along the northern side of the ACC. In the real ocean it has a clear minimum in stratification and hence potential vorticity, which is traceable for thousand of kilometers. After 80 years, the low stratification of SAMW in the formation region is well preserved, as is the subduction route. While the Antarctic Bottom Water (AABW) cell (below 4000 m) is weaker than that observed, the region between 1500 m and 4000 m with low vertical shear associated with the North Atlantic Deep Water (NADW) is well simulated.

Although the substantial warming and increasing salinity in the North Atlantic subpolar gyre in *cD* are clearly not realistic, CHIME has overall a realistic climate and is therefore considered as a useful tool for the study of climate variability in the real climate system.

2.1.3.2 How is *E3* different from *cD*?

Because *cD* is examined for investigating variability while *E*3 is used for investigating predictability, the main differences between these two runs are highlighted, as these have to be kept in mind as analogies are drawn between the mechanisms of AMOC variability and predictability.

Sea surface temperature differences

Figure 2.12 shows differences in SST between *E*3 and *cD*. In *E*3, the Southern Ocean is, overall, colder (up to 4°C) and the tropical regions warmer (up to 6°C). The colder (and more realistic, see *Sect. 2.1.3.1*) Southern Ocean is possibly due to the use of a higher-order regridding scheme in *E*3, consistent with a more stable Drake Passage transport. The reason for warmer tropical regions still remains unclear. Note that the strongest temperature differences are in the deep tropical Pacific, suggesting that *E*3 does not represent the main features of the typical El-Niño event. More specifically, in the Atlantic Ocean (region of interest here), the strongest difference appears in the tropics where *E*3 is warmer by about 1-2°C.

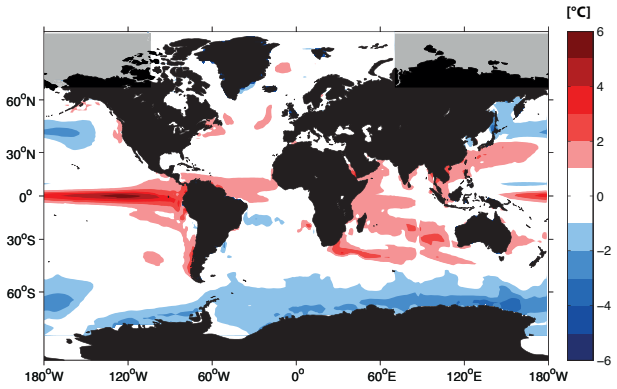

Figure 2.12: Difference of annual SST mean averaged over the period of analysis between *E*3 and *cD*. Positive values are for $\mathrm{SST}_{E3} > \mathrm{SST}_{cD}$.

Sea surface salinity differences

Figure 2.13 shows differences in SSS between *E*3 and *cD*. Overall, *E*3 is fresher than *cD*. The main differences in SSS are localized in the tropical regions, especially in the Pacific Ocean where *E*3 is fresher by up to 3 psu. This suggests again, some problems related to the representation of the El-Niño phenomenon in *E*3. Concerning the Atlantic Ocean, there are few differences compared to the other ocean basins although some significant differences are identified in the southern tropics. The western Coast of Africa is generally saltier (up to 3 psu), and the South Atlantic subtropical gyre fresher (up to 1.5 psu). Higher salinity off the western coast of Southern Africa and lower salinity in the western Indian Ocean suggest a difference in interbasin salt exchange between the two runs, probably linked to the Agulhas leakage.

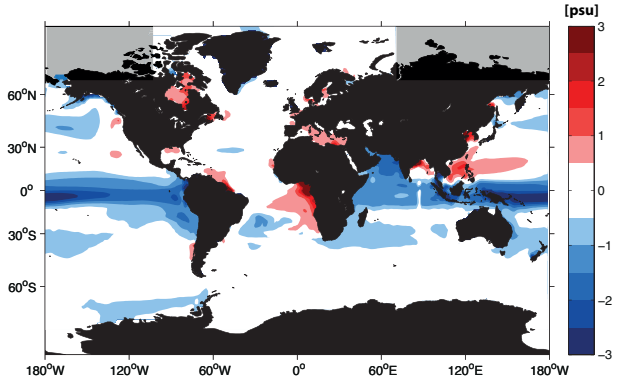

Figure 2.13: Difference of annual SSS mean averaged over the period of analysis between $E3$ and cD. Positive values are for $\mathrm{SSS}_{E3} > \mathrm{SSS}_{cD}$.

Surface air temperature differences

Figure 2.14 shows differences in SAT between $E3$ and cD. The SAT pattern is very similar to the SST pattern (Figure 2.12) with generally colder temperatures over the polar regions and most of the Eurasian continent, and warmer temperatures over the tropics. We suspect that the difference over land is at least partly due to a bug in cD, which removed all of the snow cover everyday making the land in cD warmer than it should be. Once again, the strongest differences are situated in the tropical Pacific where SAT is warmer by up to 5°C. Although the colder (and more realistic) Southern Ocean has been associated with the use of a higher-order regridding scheme in $E3$, the cooler (and less realistic, see *Sect. 2.1.3.1*) Arctic Ocean may be partly a consequence of the Bering Strait being closed in that run. Similar to SST, the main differences in the Atlantic Ocean are in the tropics where SAT is warmer by about 1-2°C in $E3$.

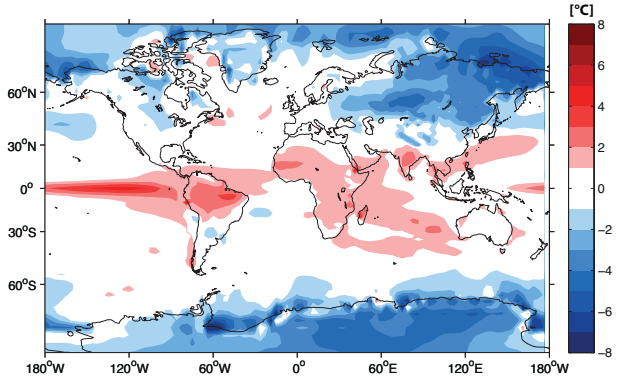

Figure 2.14: Difference of annual SAT mean averaged over the period of analysis between $E3$ and cD. Positive values are for $\mathrm{SAT}_{E3} > \mathrm{SAT}_{cD}$.

Oceanic heat transport difference

Figure 2.15 shows differences in the Atlantic mean ocean heat transport between $E3$ and cD. Although the ocean heat transport is slightly larger in $E3$ (up to 0.15 PW in the northern tropics), they are overall very similar. This slight difference is probably the consequence of the larger equator-to-pole SST difference in $E3$.

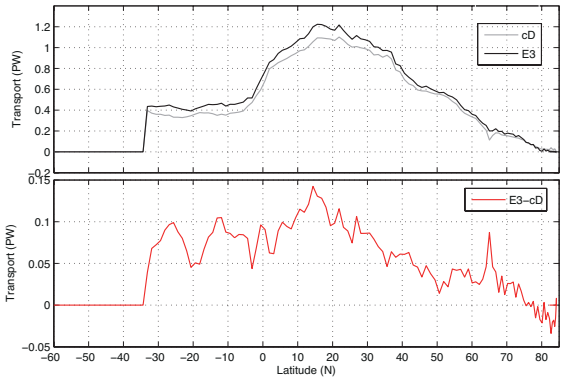

Figure 2.15: Upper-panel: Atlantic mean ocean heat transport in PW in cD (grey curve) and $E3$ (black curve) averaged over the common period from years 105 to 199. Lower-panel: difference in Atlantic heat transport; positive (negative) values are for $E3$ stronger (weaker) than cD.

March Mixed Layer Depth differences

Figure 2.16 shows differences in March MLD between $E3$ and cD. The convection site in the Labrador Sea is shallower in $E3$ by about 400-600 m. There are also significant differences in the Greenland Sea where west of the Mid-Atlantic ridge, MLD is shallower up to ∼1000 m while it is ∼600-800 m deeper east of the ridge. Note that although $E3$ and cD sometimes differ in their MLD depths in the high-latitude North Atlantic, similar convection sites have been identified there in both runs. Because the Bering Strait appears to exert some influence on the formation of deep water masses (by affecting the freshwater budget of the Greenland and Norwegian Seas, Reason and Power 1994; Goose et al. 1997), and a closed Bering Strait has been associated with a reduction of the intensity of the Atlantic deep circulation of about 17% (Hasumi 2002), we suspect the shallower MLD in the Northern high-latitude regions in $E3$ to be partly caused by the closure of the Bering Strait. Note that there are no notable differences in MLD in the Southern Ocean.

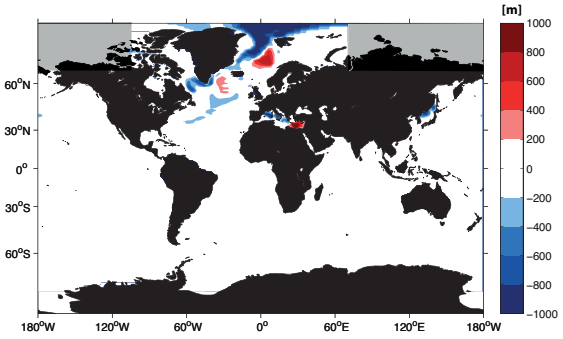

Figure 2.16: Difference of March MLD mean averaged over the period of analysis between $E3$ and cD. Positive values are for $\mathrm{MLD}_{E3} > \mathrm{MLD}_{cD}$.

In summary, $E3$ is generally warmer and fresher in the tropical regions and colder in the polar regions than cD. These discrepancies have to be kept in mind when analogies

are sought between the mechanisms behind the AMOC variability and predictability. Predictability results from $E3$ can be used as benchmark for future experiments once a more reliable and control integration of CHIME will be available.

2.1.4 CHIME: an improved version of HadCM3?

The fact that CHIME shares its atmosphere and ice components with HadCM3 means that comparison between the two models should allow a clear assessment to be made of the extent to which structural biases inherent in the vertical representation of the ocean model affect the mean state of the simulated climate system. But why has the ocean component of HadCM3 been replaced by the hybrid-coordinate ocean model HYCOM? The main advantages and disadvantages of the different vertical coordinates of ocean models are first summarized here. The well-known systematic errors inherent to HadCM3 are then briefly described before summarizing the main findings of Megann et al. (2010) concerning comparison of the CHIME and HadCM3 control simulations.

2.1.4.1 Advantages/disadvantages of the different coordinates for ocean models

As with any model, important decisions are made early in the development stage regarding the coordinate system that determines how the model will be implemented and how it will perform. Figure 2.17 shows traditional vertical coordinate choices (z-coordinates, σ-coordinates, ρ-coordinates), which are not by themselves optimal everywhere in the ocean, as pointed out by model comparison exercises performed in Europe (DYnamics of North Atlantic MOdels - DYNAMO, Willebrand et al. 2001) and in the United States (Data Assimilation and Model Evaluation Experiment - DAMEE, Chassignet et al. 2000). These and earlier comparison studies (Chassignet et al. 1996; Roberts et al. 1996; Marsh et al. 1996) have shown that different models are able to simulate the large-scale characteristics of the oceanic circulation reasonably well, but that the interior water mass distribution and associated thermohaline circulation are strongly influenced by localized processes that are not represented equally by each model's vertical discretization.

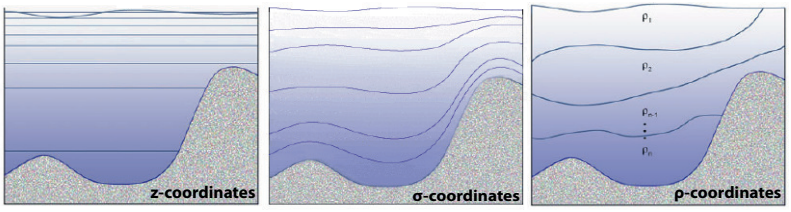

Figure 2.17: The three main vertical coordinate systems of ocean models: z-coordinates (left panel), terrain-following (middle panel), isopycnic (right panel).

Ideally, an ocean general circulation model should (i) retain its water mass characteristics for centuries (a characteristic of ρ-coordinates), (ii) have adequate vertical resolution in the surface mixed layer for proper representation of thermodynamic and biogeochemical processes (a characteristic of z-coordinates), (iii) maintain sufficient vertical resolution in unstratified or weakly-stratified regions of the ocean, and (iv) have high vertical resolution in coastal regions (a characteristic of σ-coordinates). z-coordinates are therefore best used to provide high vertical resolution near the surface within the mixed layer, isopycnal layers are best in the deep stratified ocean, and σ-levels are often the best choice in shallow coastal regions. Hence, many developers have been motivated to pursue research into hybrid approaches, and the hybrid-coordinate models in which interior isopycnal layers transition to z-levels in near-surface waters, should in principle combine the advantages of both model types without the weakness of either. A brief description of the two main vertical coordinates inherent to the hybrid coordinate system (i.e. z-coordinates and ρ-coordinates) in CHIME is given below.

The z-coordinate system (Figure 2.17, left-panel) is the simplest and best established, primarily because it was adopted in the first models and valuable experience has been built up over the years with this type of model. Examples of z-coordinate models are CNRM-CM3 (Deque et al. 1994), MOM (Pacanowski 1995), HadCM3 (Gordon et al. 2000), and CCSM3 (Collins et al. 2006b). The fields at each water column are defined at a set of constant depth levels, and the ocean is thus split into a 3-D array of points. The levels are unevenly spaced in the vertical, to allow for more detail near the upper (and sometimes lower) boundaries. This allows the ocean to have high resolution near the surface, but generally leads to excessive diapycnal mixing (Sun and Bleck 2006). In response to this and other problems with the z-coordinate formulation, models using the isopycnal coordinate system have been developed.

Models with ρ-coordinates (Figure 2.17, right-panel) have the equations of motion formulated on constant potential density surfaces. Examples of isopycnal models are MICOM (Bleck et al. 1992), OPYC (Oberhuber 1993), HIM (Hallberg 1995, 1997), and NLOM (Wallcraft et al. 2003). In the real ocean, mixing processes are believed to be predominantly along constant density surfaces. The isopycnal coordinate system therefore mimics, as much as possible, real structures within the ocean. It has the advantage of formulating the model in a manner that rigorously preserves the structure of water masses faithfully over long time and length scales (Marsh et al. 1996). On the other hand, problems arise when thickness of isopycnal layers drops to near zero or when they intersect with the surface. Hybrid coordinate systems and model schemes have been developed to overcome some of these problems.

The theoretical foundation for implementing hybrid coordinate systems was set forth by Bleck and Boudra (1981) and Bleck and Benjamin (1993). The term "hybrid vertical coordinate" can mean different things to different people: it can be a linear combination of two or more conventional coordinates (Song and Haidvogel 1994; Ezer and Mellor 2004;

Barron et al. 2006) or it can be truly generalized, i.e., aiming to mimic different types of coordinates in different regions of a model domain(Bleck 2002; Burchard and Beckers 2004; Adcroft and Hallberg 2006; Song and Hou 2006). The hybrid models that have much in common with isopycnal models are POSEIDON (Schopf and Loughe 1995) and HYCOM (Bleck 2002). Other generalized vertical coordinate models include HYPOP (Dukowicz 2005) and GOLD (Adcroft et al. 2008; Hallberg and Adcroft 2009). The CHIME model (Megann et al. 2010) uses the hybrid-coordinate ocean model HYCOM, in which interior isopycnal layers transition to constant-depth levels in near-surface waters (Figure 2.18), should in principle combine the advantages of both model types without the weaknesses of either. The ocean interior is represented by layers of constant potential density, but light layers that would outcrop and disappear in a pure isopycnic model are reused as constant-depth near-surface coordinate levels with specified minimum thicknesses. It is therefore largely an isopycnic ocean model, which reduces the main deficiency of the latter, namely the loss of resolution in weakly stratified regions. However, the advantages offered by a hybrid vertical coordinate do not come without a price, and concerns associated with complexities introduced by variable-depth layer models arise. One of the main concerns is the potential in hybrid-coordinate models for excessive vertical diffusion caused by the dispersive character of vertical advection schemes. If left uncontrolled, this diffusion can exceed that found in z-coordinate models, as the interlayer mass exchange can be much larger than the vertical transport rate seen in fixed-grid models. Hybrid-coordinate models also have only approximate representation of the pressure gradient (Sun et al. 1999). However, due to the vast range of spatial scales that cannot explicitly be incorporated into global ocean models, it is unlikely that we will ever find a model satisfactory to all users. Models built around a hybrid vertical coordinate still provide flexibility not found in the classical z-level and isopycnic coordinate models, in suppressing certain types of truncation errors while resolving weakly stratified layers.

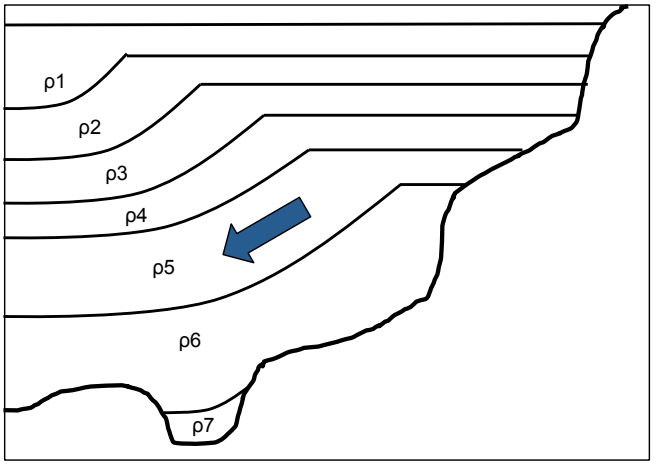

Figure 2.18: Schematic of hybrid vertical coordinate system.

In summary, the majority of climate models developed to date use a z-coordinate ocean

Table 2.2: Summary of main advantages and disadvantages of coordinate systems used in ocean models.

Vertical Coord.	**Main Advantages**	**Main Disadvantages**
z-coordinate (the model fields at each water column are defined at a set of constant depth, e.g. HadCM3)	(i) Good vertical resolution in the upper ocean (Sun and Bleck 2006); (ii) Upper ocean mixed layer well parametrized; (iii) Horizontal pressure gradient can be easily represented in an accurate manner; (iv) Equation of state for ocean water can be accurately represented in a straigthforward manner (McDougall et al. 2003).	(i) Too much diffusion as flow crosses coordinate surfaces (Sun and Bleck 2006); (ii) Excessive mixing at sill overflows which may have adverse consequence in long-term climate simulations (Sun and Bleck 2006); (iii) Excessive diapycnal mixing (Sun and Bleck 2006); (iv) Representation and parameterization of bottom boundary layer processes and flow are inaccurate; (v) Representation of tracer transport within the quasi-adiabatic interior is complicated.
ρ-coordinate (discretization of the vertical into potential density classes, e.g. MICOM)	(i) Better representations of near-adiabatic flows along sloping isopycnals; and (ii) Absence of spurious numerical mixing of dense waters at sill overflows (Roberts et al. 1996); (iii) Preservation of water properties over long time and length scales (Marsh et al. 1996); (iv) Tracer transports in the ocean interior are well represented (due to the natural ability to maintain water mass properties); (v) Bottom topography is represented in a piecewise linear fashion (avoiding need to distinguish bottom from side as done with z-coordinate models); (vi) Horizontal pressure gradient can be easily represented.	(i) Poor vertical resolution in weakly stratified regions (i.e. at high latitudes); (ii) Imprecise detrainment from the mixed layer; (iii) Representing the effects of a realistic (nonlinear) equation of state is complicated.
hybrid-coordinate (interior isopycnal layers transition to constant-depth levels in near-surface waters, e.g. HYCOM)	(i) Same as Isopycnic-coordinate model (MICOM) plus better resolution in weakly stratified regions (Bleck (2005)); (ii) Well controlled diffusion in ocean interior - T and S are preserved over long timescales (like MICOM); (iii) Good vertical resolution in upper ocean (better than MICOM); (iv) Reduction of numerically induced diapycnal fluxes (Bleck 2005); (v) Smooth lateral transition between deep-ocean and coastal-shelf domains (Bleck 2005); (vi) Simple modelling of abyssal dense overflow (Bleck 2005); (vii) Flexibility to accommodate massless layers on the sea floor (Bleck 2005).	(i) Excessive vertical diffusion (Bleck 2005); (ii) Approximate representation of pressure gradient (Sun et al. 1999); (iii) Need to cast transport equations in flux form and to use relatively complex lateral transport operators that maintain the physical integrity of mass field tracers when there are strong changes in layer thickness.

component which allows the ocean to have high resolution near the surface, but generally leads to excessive diapycnal mixing that may have adverse consequences in long-term climate simulations. Isopycnic models, which use potential density as their vertical coordinate, preserve the structure of water masses faithfully over long periods and distance but have poor vertical resolution in weakly stratified regions. Hybrid-coordinate models in which interior isopycnal layers transition to constant-depth levels in near-surface waters, should in principle combine the advantages of both model types without the weakness of either. Table 2.2 summarizes the main advantages and disadvantages of z-levels, isopycnic and hybrid coordinates.

2.1.4.2 Brief summary of systematic errors in HadCM3

HadCM3 is one of the models included in the climate change experiments described in the IPCC Third and Fourth Assessment Reports (IPCC 2001, 2007), and has been shown to have a remarkably stable climate when forced with preindustrial greenhouse gas concentrations. However, like most numerical models, HadCM3 has systematic errors which are not yet fully understood, and these may bias both the variability and predictability of the AMOC. As described by Gordon et al. (2000), the mean SST field in the model reproduces most of the characteristics of the observations in the World Ocean Atlas (Levitus et al. 1995) to within 1°C over much of the ocean. However, large discrepancies of over 3°C (and up to 6°C) occur in regions of large SST gradients, including the NAC region where the model is too cool. HadCM3 is also known to overestimate the land temperature variability (Collins et al. 2001). The mean SSS field is reproduced to within 1 psu in most regions (Pardaens et al. 2003). However, the model is too salty in the Gulf Stream region of the North Atlantic (∼2 psu), and too fresh in the Beaufort Gyre region of the Arctic Ocean (∼2 psu). In the upper ocean, the Labrador Sea and Arctic Ocean are relatively cool and fresh, while lower latitudes are warmer and saltier (Hawkins and Sutton 2007). Gamiz-Fortis and Sutton (2007) also showed that the temperature and salinity contrast between the Labrador Sea/Arctic Ocean and the North Atlantic is somewhat too large in HadCM3 (∼3 K, 1.5 psu) as compared to observations (∼0.5-1 K, 1.0 psu). Below the surface in the Atlantic, the model is generally too warm (∼2°C) and too salty (∼0.5 psu). Finally, HadCM3 simulates a NAO in Northern Hemisphere winter which has a spatial pattern consistent with the observations in the Atlantic region, but is too strongly teleconnected with the North Pacific (Collins et al. 2001).

We propose that the spurious numerical mixing that is commonplace in z-coordinate ocean models (Griffies et al. 2000) may artificially limit predictive skill in climate models that feature such an ocean component. Hybrid ocean models such as HYCOM (Bleck 2002) have the potential to overcome some of the weaknesses in conventional z-coordinate models. For example it is expected that the better preservation of interior

water masses in hybrid ocean models might have an influence on the decadal variability and predictability of climate models, since enhanced effective diapycnal diffusion typical of z-coordinate models will tend to erode interior gradients of temperature and salinity, including those corresponding to anomalies.

2.1.4.3 CHIME versus HadCM3

Megann et al. (2010) have shown the critical importance of changing just one component of the climate system, by comparing CHIME and HadCM3 control simulations. Their main findings are summarized here. They found that both models possess realistic and marked similarities in ocean heat transports and overturning circulation, with a maximum overturning in the North Atlantic of 18-20 Sv in both models and global northward heat transport consistent with observational estimates. They both have similar spatial distributions of wind stress and heat/freshwater fluxes, as well as warm sea surface biases at the eastern coasts (ascribed to errors in the cloud scheme of HadAM3). They also both show similar errors in the position of the Gulf Stream separation. However substantial differences between CHIME and HadCM3 are also evident. Although both models have large-scale surface temperature errors across most of the North Atlantic, the errors are warm in CHIME while they are cool in HadCM3. In addition, CHIME does not have the cold sea surface errors present in the North Pacific in HadCM3. However, it shows warm and salty errors in the North Atlantic, where HadCM3 has a smaller cold error associated with a southward deviation of the NAC and a fresh surface error over the whole North Atlantic. Moreover, both models show clear differences in separation position of the Kuroshio Current, which separates further south in HadCM3 and further north in CHIME than in observations. Both models also show similar differences in the position of the Gulf Stream separation, and the volume transport of the Gulf Stream at 65°W is smaller in CHIME (∼15 Sv) than in HadCM3 (∼23 Sv). Besides, some features of the climate system are more realistically represented in CHIME than in HadCM3. For instance, CHIME has significantly less mixing in the upper, intermediate and deep ocean than does HadCM3 resulting in the better representation and maintenance of key water masses. Namely, a better preservation of the signatures of AAIW and SAMW, more realistic structure of the southward-flowing NADW, a sharper and more realistic thermocline in the subtropical gyres, and reduced mixing of the dense overflow waters in the North Atlantic. These results were expected by the authors as the formulation of HYCOM is specifically designed to eliminate the spurious numerical diapycnal mixing present in z-coordinate models and therefore to better represent and preserve water properties over long time and length scales. Moreover, this more rigorously controlled diapycnal mixing is also apparent in other ocean features; whereas a global warming trend is evident in HadCM3 just below the surface to 800-1000 m depth, a similar warming trend in CHIME is more pronounced but shallower. However, CHIME also shows some

unrealistic patterns which are absent in HadCM3. For instance, the substantial warming and increasing salinity in the North Atlantic subpolar gyre in CHIME are clearly not realistic and not yet fully understood. In addition, CHIME has a less realistic gyre circulation in the North Atlantic than does HadCM3, which is quite surprising as it has been previously demonstrated that in ocean-only simulations the path of the NAC is more realistic in ocean-only isopycnic models forced by realistic surface fluxes than in comparable z-coordinate models (Roberts et al. 1996). Megann et al. (2010) attributed this unexpected result to the difference in wind stress between the two models in this region. Although the mixing in the Nordic Sea is realistic in HadCM3, the convection is too deep in CHIME (up to 4000 m) and extends not only across most of the Nordic Sea but through Fram Strait and as far as the Canadian Basin. This excessive mixing is consistent with the anomalously high surface salinity, and the resulting decrease in stratification, that develops in CHIME in the North Atlantic subtropical gyre and the Arctic.

Overall, while both HadCM3 and CHIME are considered "good" models from the point of view of their heat transports being within observational estimates, and possessing remarkably similar overturning circulations (despite their difference in temperature and salinity anomalies in the upper ocean in the North Atlantic), Megann et al. (2010) noted clear and marked differences between both climate models in their representation of the mean climate in control simulations which seem to be mainly caused by differences in interior mixing. The model differences associated with the more controlled diapycnal mixing in CHIME, are expected to be critical in long-timescale climate predictions, since the evolution of the ocean state is known to play a crucial role in climate dynamics of a decade and longer (Gordon et al. 2000). By reducing the extent of spurious mixing, CHIME may be characterized by possibly more realistic mechanisms and timescales of AMOC variability than those in HadCM3, and may have higher or at least substantially different predictive skills. CHIME thereby provides an invaluable check on the simulations made by e.g. Collins and Sinha (2003), Hawkins and Sutton (2007) from HadCM3, and therefore the robustness of its predictability skills on decadal timescales.

As already mentioned in *Sect. 1.5.2*, predictability experiments using CHIME could not be run until mid-2011. Predictability experiments with the well-established IPSL climate model have been carried out before then, which allowed us to develop an efficient experimental design prior to a similar such study with CHIME. The latest version of the IPSL model (IPSL-CM5A) and its various components are therefore now briefly presented.

2.2 The Institut Pierre Simon Laplace model (IPSL-CM5A)

The IPSL-CM5A model (Dufresne et al. 2012) has been recently developed at the Institut Pierre-Simon Laplace (IPSL) as part of the 5^{th} Phase of the Coupled Model Intercomparison Project (CMIP5). It is a full earth system model which, in addition to the physical atmosphere-land-ocean-sea ice model, also includes a representation of the carbon cycle, and stratospheric and tropospheric chemistry with aerosols. In the framework of this thesis, the low resolution version of the model is used (IPSL-CM5A-LR) to study the potential predictability of both the AMOC and North Atlantic Climate at decadal timescales. The model configuration is summarized below.

2.2.1 Brief model description

The model components are the atmospheric general circulation model LMDZ5A (Hourdin et al. 2012) associated with the ORCHIDEE land-surface model (Krinner et al. 2005) coupled with the ocean module NEMOv3.2 (Madec 2008), which includes the sea ice model LIM-2 (Fichefet and Maqueda 1997), and the oceanic bio-geochemistry model PISCES (Aumont and Bopp 2006). The coupling between oceanic and atmospheric models is achieved using OASIS3 (Valcke 2006). A general overview of these various components is now briefly given.

2.2.1.1 Atmospheric component: LMDZ5A

LMDZ5 is an atmospheric general circulation model developed at the Laboratoire de Météorologie Dynamique (Sadourny and Laval 1984). The dynamical part of the code is based on a finite-difference formulation of the primitive equations for the atmosphere. In the vertical, the model uses hybrid coordinates comprising 39 levels, with 15 levels above 20 km. It has a regular horizontal grid with 96 $\times$ 96 points corresponding to a resolution of 1.9° $\times$ 3.75°. In the LMDZ5A version (Hourdin et al. 2012), the physical parametrization is very close to that of the previous LMDZ4 version used for CMIP3 (Hourdin et al. 2006).

2.2.1.2 Land-surface component: ORCHIDEE

ORCHIDEE (ORganizing Carbon and Hydrology In Dynamic EcosystEms) simulates the energy and water cycles of soil and vegetation, the terrestrial carbon cycle, and the vegetation composition and distribution (Krinner et al. 2005). It is based on three different modules: (i) SECHIBA (Ducoudré et al. 1993; de Rosnay and Polcher 1998) which describes the exchanges of energy and water between the atmosphere and the biosphere, and the soil water budget, (ii) STOMATE (Saclay Toulouse Orsay Model

for the Analysis of Terrestrial Ecosytems, Krinner et al. 2005) which represents the phenology and carbon dynamics of the terrestrial biosphere, (iii) the global LPJ (Lund-Potsdam-Jena, Sitch et al. 2003) vegetation model that simulates vegetation dynamics.

2.2.1.3 Oceanic component: NEMOv3.2

NEMO (Nucleus for European Modelling of the Ocean) is a primitive equation model. The IPSL-CM5A model includes the NEMOv3.2 version, which uses a partial step formulation (Barnier et al. 2006) ensuring a better representation of bottom bathymetry and thus stream flow and friction at the ocean bottom than the previous IPSL-CM4 model. The configuration of the model is ORCA2 (Madec and Imbard 1996). In the horizontal direction, the model uses a curvilinear orthogonal grid: (i) south of 40°N, the grid is of isotropic Mercator type with a nominal resolution of 2°, (ii) a latitudinal grid refinement of 1/2° is used in the tropics, (iii) north of 40°N, the grid is non geographic and quasi-isotropic. The North Pole singularity is replaced by a line between points in Canada and Siberia. In the vertical direction, the model uses a full or partial step z-coordinate, or σ-coordinate, or a mixture of both. There are 31 vertical levels with the highest resolution for the upper 150 m. The distribution of variables is on a three-dimensional Arakawa C-type grid. Advection of temperature and salinity is done using a total variance dissipation scheme (Lévy et al. 2001; Cravatte et al. 2007). In the momentum equation, an energy and enstrophy conserving scheme is used (Arakawa and Lamb 1981; Le Sommer et al. 2009). The mixed layer dynamics are parameterized using the Turbulent Kinetic Energy (TKE) closure scheme of Blanke and Delecluse (1993) improved by Madec (2008). The horizontal eddy viscosity coefficient value is 4.10^4 m^2 s^{-1} and the lateral eddy diffusivity coefficient value is 10^3 m^2 s^{-1}.

2.2.1.4 Sea ice component: LIM-2

LIM-2 (Louvain-la-neuve sea Ice Model, version 2) is a two-level thermodynamic-dynamic sea ice model (Fichefet and Maqueda 1997, 1999). A three-layer model determines sensible heat storage and vertical heat conduction within snow and ice. The surface albedo is parameterized as a function of the surface temperature and the snow and ice thicknesses. For the momentum balance, sea ice is considered as a two-dimensional continuum in dynamical interaction with atmosphere and ocean. The sea ice and ocean models have the same horizontal grid.

2.2.1.5 Oceanic bio-geochemistry component: PISCES

PISCES (Pelagic Interaction Scheme for Carbon and Ecosystem Studies, Aumont and Bopp 2006) simulates the cycling of carbon, oxygen and of the major nutrients determining phytoplankton growth. The carbon chemistry of the model is based on the Ocean Carbon Model Intercomparison Project (OCMIP2) protocol (Najjar et al. 2007) and the parameterization proposed by Wanninkhof (1992) is used to compute air-sea exchange of CO_2 and O_2.

2.2.1.6 Atmosphere-Ocean-Sea ice component: OASIS

The Atmosphere-Ocean-Sea ice coupling in IPSL-CM5A-LR is very close, with some improvements, to the coupling used in IPSL-CM4 (presented in detail in Marti et al. 2010). The OASIS v3.0 coupler (Valcke 2006) is used to interpolate and exchange the variables and to synchronise the models.

2.2.2 Initial conditions and control run

The core of the predictability study with IPSL-CM5A is a 1000-year control integration. The initial state was taken at the end of a 400-year run in coupled mode, itself started after several hundreds of years of simulations of land and ocean carbon component separately to equilibrate the carbon pools (see Dufresne et al. 2012 for further details). The simulation uses constant pre-industrial boundary conditions of tropospheric greenhouse gases and aerosol concentrations, and constitutes the pre-industrial control simulation of the IPSL-CM5A-LR model used for the CMIP5 exercises. Figure 2.19 illustrates how well equilibrated the model is. There is almost no drift in surface temperature, surface salinity and heat budget, and no discernible difference between the flux at both the Top Of Atmoshere (TOA) and the surface. There is also no drift of the carbon flux over land and only a small one over the Ocean (see Dufresne et al. 2012 for further details).

2.2.3 How faithful is IPSL-CM5A-LR to the real climate system?

The global and North Atlantic climatology of IPSL-CM5A-LR have been described in several papers such as Dufresne et al. (2012), Hourdin et al. (2012), and Escudier et al. (2012). It has been shown that the 1000-year long simulation captures the main features of the observed climate, in spite of a few notable biases. Here is a summary of the main findings of the above-cited studies for the key oceanic and atmospheric fields, mainly in the Atlantic region (of interest here).

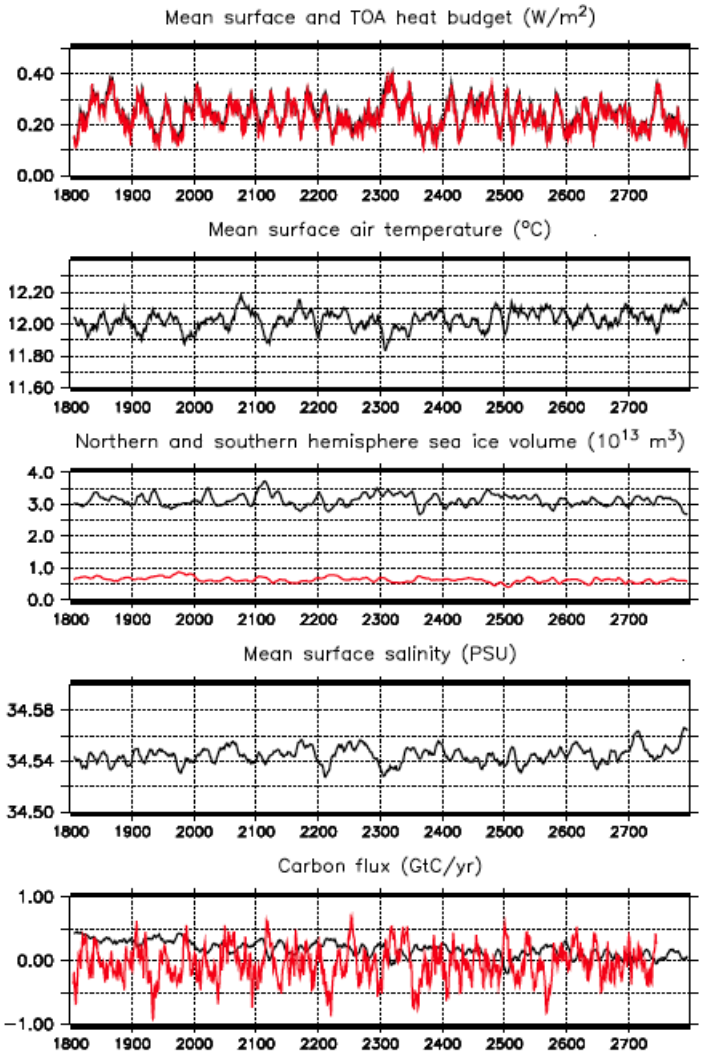

Figure 2.19: The time evolution of the global mean heat budget at surface and at the TOA (W m^{-2}), the global mean air surface temperature (°C), the sea-ice volume in the northern (black) and southern (red) hemisphere (10^3 m^3, the global mean surface salinity (psu), and carbon flux (GtC yr^{-1}) over ocean (black) and over land (red), for the 1000-year control integration of the IPSL-CM5A-LR model. (From Dufresne et al. 2012).

The Atlantic SST in IPSL-CM5A-LR captures the main features of the observed SST, but is clearly colder than observations over the whole North Atlantic (Figure 2.20, left-panel). Escudier et al. (2012) related the very large cold bias east of the Grand Banks to too weak and too zonal gradients in the vicinity of the Gulf Stream, partly due to a southward shift of the western boundary currents as in many other models (e.g. Danabasoglu 2008), and to the erroneous departure of the atmospheric jet stream from the coast and a poleward shift of the atmospheric jet (Guemas and Salas-Mélia 2011). Other biases include slightly too-cold SST in the tropics, and a strong cold bias in the Nordic Seas.

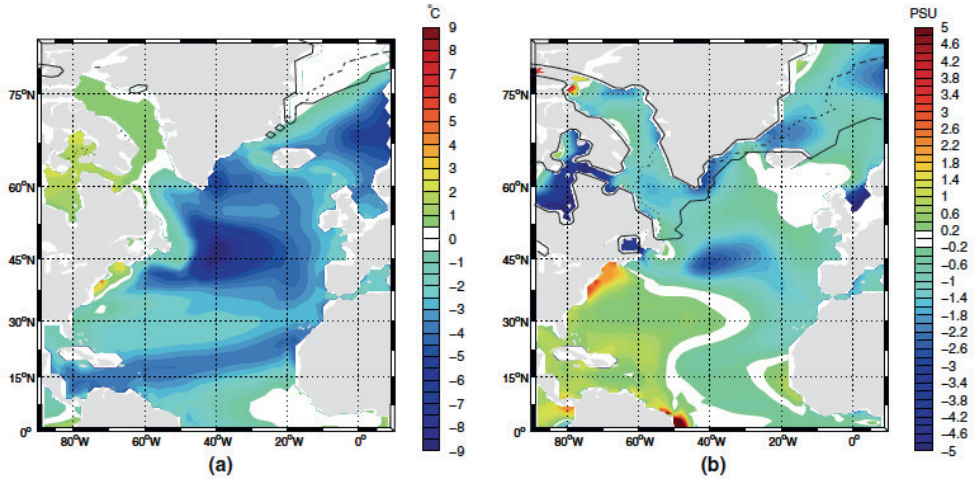

Figure 2.20: Bias of SST (left panel) and SSS (right-panel) in the Northern Atlantic averaged over the whole 1000 years of the IPSL-CM5A-LR model compared to observations. The mean of winter sea-cover in summer (left-panel) and winter (right-panel) is indicated as black continuous line for the model and dash-lined in observations. Observed SST are from Reynolds (1994), observed SSS are from Conkright et al. (2002) and observed sea-ice cover from Rayner et al. (2003). (From Escudier et al. 2012).

As shown by Escudier et al. (2012), the main features of the SSS fields are reproduced in IPSL-CM5-LR. Note, however, that the North Atlantic maxima are slightly shifted eastward as compared to the observations, and the subtropical maxima are slightly too strong (Figure 2.20, right-panel). A major fresh bias is also present in the northwestern Atlantic, probably due to an excess of freshwater forcing over the Labrador Sea as seen in the previous version of the model (Swingedouw et al. 2007). These fresher conditions, together with the cold bias identified earlier in the high-latitude North Atlantic, are associated with an overestimation of the winter sea-ice cover in the northern Atlantic and specifically in the Labrador and the Nordic Seas (Figure 2.20). This prevents a correct representation of deep convection in these areas, and could explain the lower range of its AMOC mean value (10.3 Sv, Escudier et al. 2012) compared to observational estimates (e.g. Ganachaud and Wunsch 2000; Cunningham et al. 2007).

In addition, the model has been shown to be globally too cold in term of SAT, with a pronounced bias in the mid-latitudes (Figure 2.21, Dufresne et al. 2012). These colder conditions clearly include most of the Atlantic region. Some warm biases are, nevertheless, worth pointing out over Siberia, Alaska and the Southern Ocean.

As with the previous version (IPSL-CM4), one important deficiency of IPSL-CM5A-LR is also the presence of a second zone of convergence south of the equator, both in the Pacific and Atlantic Oceans (Figure 2.22, Hourdin et al. 2012). Note that this double ITCZ is a classical bias of coupled models (see e.g. Dai 2006).

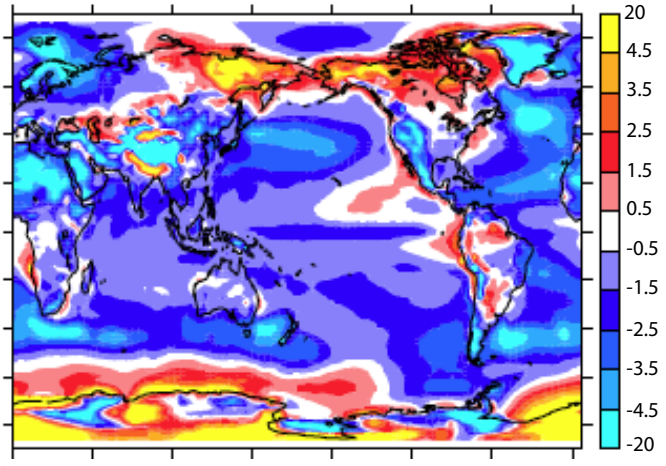

Figure 2.21: Bias in the climatology (period 1961-1990 in the IPSL-CM5A-LR model) of SAT compared to CRU estimate (Jones et al. 1999). (From Dufresne et al. 2012).

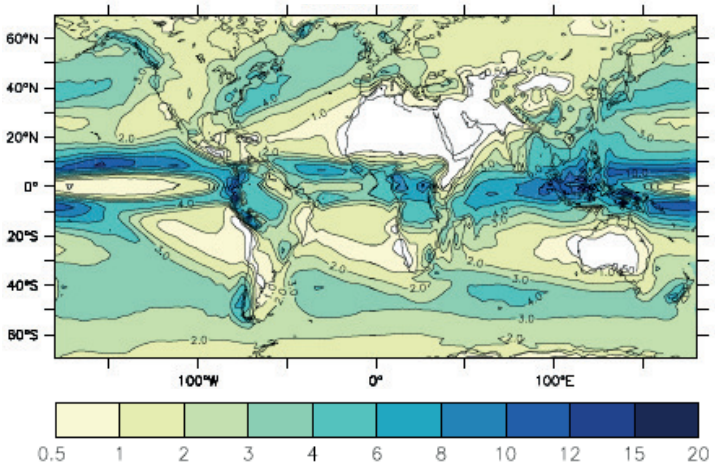

Figure 2.22: Annual mean rainfall (mm day^{-1}) in the prescribed SST simulation LMDZ5A-LR and in the "historical simulation" for the end of the 20th century with IPSL-CM5A-LR. (From Hourdin et al. 2012).

Despite its general cold bias and its too fresh northern Atlantic, the IPSL-CM5A-LR model has overall a realistic climate and can therefore be considered as a credible model for the study of climate predictability.

2.3 Summary of main characteristics of models used

Table 2.3 gives a summary of the main features of both models used in the framework of this thesis.

Table 2.3: Summary of main characteristics of both CHIME and ISPL-CM5A-LR models.

	CHIME	**IPSL-CM5A-LR**
Purpose in this thesis	Study of variability and predictability of AMOC and climate.	Study of predictability of AMOC and climate.
Reference	Megann et al. (2010)	Dufresne et al. (2012)
Atmosphere model	HadAM3 (Gordon et al. 2000)	LMDZ5A (Hourdin et al. 2012)
Ocean model	HYCOM v2.1.34 and v2.2.18 (*cD* and *E*3, respectively) (Bleck 2002)	NEMO v3.2 (Barnier et al. 2006)
Sea-ice model	From HadCM3 (Cattle and Crossley 1995)	LIM-2 (Fichefet and Maqueda 1997, 1999)
Land-surface component	MOSES (Cox et al. 1999)	ORCHIDEE (Krinner et al. 2005)
Atmosphere-ocean coupling	OASIS v2.4 and v3.0 (*cD* and *E*3, respectively) (Valcke et al. 2000; Valcke 2006)	OASIS v3.0 (Valcke 2006)
Oceanic biogeochemistry component	*none*	PISCES (Aumont and Bopp 2006)
Atmos. horizontal resolution	2.5° × 3.75°	1.9° × 3.75°
Ocean. horizontal resolution	Spherical bipolar grid (Sun and Bleck 2001): (i) 55°N-78°S = 1.25° × 1.25°, (ii) north of 55°N = bipolar grid.	ORCA2 grid (Madec and Imbard 1996): (i) south of 40°N = isotropic Mercator (resolution 2°), (ii) tropics = grid refinement of 1/2°, (iii) north of 40°N = non-geographic and quasi-isotropic grid.
Atmos. vertical coordinate	Hybrid (19 levels)	Hybrid (39 levels)
Ocean. vertical coordinate	Hybrid (25 levels)	z-coordinate or σ-coordinate or both (31 levels)
Mixing scheme	KPP (Large et al. 1994)	TKE (Blanke and Delecluse 1993)
Length of data analysed (years) in control run	*cD* (variability)=120; *E*3 (predictability) = 201	1000
Main biases in the Atlantic	(i) Substantial warming and increasing salinity in the North Atlantic subpolar gyre, (ii) Excessive mixing in the northern Atlantic high-latitudes.	(i) Significant cold and fresh biases in the northern Atlantic, (ii) Lack of deep convection in the Labrador and Nordic Seas.

Despite identified biases, both the CHIME and IPSL-CM5A models have overall a realistic climate and can therefore be considered as useful and credible tool for the study of climate variability and predictability. It is important to bear in mind that none of the existing models is able to accurately reproduce all aspects of past and current climate, and that no single model will ever be able to realistically reproduce climate as we experience it. By their very nature, models cannot capture all the factors involved in a natural system, and those that they do capture are often incompletely understood. This makes climate models impossible to truly verify or validate (Oreskes et al. 1994). Some may argue that long-term forecasts are useless because they cannot be properly evaluated and little can be learnt from a prediction without verification. Nevertheless, the models ability to reproduce many large-scale aspects of present-day climate, the fact that they are built on well-known physical processes (such as conservation of energy, mass and angular momentum), and the fact we can understand and interpret many of the results from known processes provide support for the models credibility, at least for large scales and certain variables. George Box is credited with the quote "All models are wrong, but some are useful" (Box 1979). Indeed, all climate models are known to be imperfect to some degree, but they can still help us to understand the things we observe or simulate and to test hypotheses. In the absence of better alternatives, it is likely to be better to use an "imperfect" model than, say, random guessing. Models represent the best tool we have available for explaining the current behaviour of our climate and predicting likely changes to the planet's future climate.

The next chapter will now discuss the different statistical tools and methods used here in both variability and predictability studies.

Chapter 3

Methodologies

This chapter gives a description of the methodologies used for studying the decadal variability and predictability of AMOC fluctuations and climate in the Atlantic sector. Data and statistical methods used for studying variability are first presented, prior to the methods and experimental design of the predictability experiments.

3.1 Climate variability study with CHIME: data and statistical methods

3.1.1 Data description

Monthly output data from *cD* are used. Analysed data comprise oceanic and atmospheric variables known to be directly or indirectly linked to climate variability. Ocean fields include salinity, temperature, surface potential density σ_2 with respect to the 2000 dbar surface (a measure of static stability), MLD, surface heat and freshwater fluxes. They also include the annual-mean meridional mass transport streamfunction of the Atlantic, and an AMOC index defined as its maximum at 30°N. Atmospheric fields comprise SAT, sea level pressure (SLP), and net precipitation. Note, that because of the spherical-tripolar grid used in the ocean component of CHIME, ocean fields have been re-gridded onto a regular 1.25°x1.25° grid north of 55°N.

We either use annual means, winter means (January-March) or September values for the different fields, and anomalies are calculated from the year 80-200 mean. Winter means are used to characterize activities in the high-latitude regions (as deep water is formed by convection in these regions mainly during the cold winter seasons) while September means rather characterize processes specific to the tropical regions (coincident with heaviest precipitation in the central Atlantic, at around the time of the northernmost position of the ITCZ). Note that the use of winter or September means does not give

qualitatively different results to the use of annual means but rather strengthens statistical robustness in some cases. When focusing on low-frequency variability, we apply 5-year or 10-year moving average filters to the data.

3.1.2 Statistical methods

In this study, the main statistical methods used include correlation, regression, spectral, composite, and Empirical Orthogonal Function (EOF) analyses. These methods are briefly described below.

Correlation coefficients

Correlation analysis gives a measure of the linear relationship between a set of variables. The Pearson's correlation coefficient, commonly simply referred to as the correlation coefficient, is a scaled version of the covariance (defined as the cross-product of the anomalies from the mean), where the covariance is divided by the standard deviation of the fields. The formula for the correlation of two n-length time series x and y is:

$$r = \frac{n\sum_{i=1}^{n} x_i y_i - (\sum_{i=1}^{n} x_i)(\sum_{i=1}^{n} y_i)}{\sqrt{[n\sum_{i=1}^{n} x_i^2 - (\sum_{i=1}^{n} x_i)^2][n\sum_{i=1}^{n} y_i^2 - (\sum_{i=1}^{n} y_i)^2]}} \tag{3.1}$$

The Least Squares Regression line

Simple regression analysis helps to determine the relationship between a dependent variable and an independent one. Most commonly, regression coefficients give the average value of the dependent variable when the independent variable is held fixed. Suppose that y is a dependent variable, and x is an independent variable, the equation of the least squares regression line of y on x is:

$$y = B_0 + B_1 x \tag{3.2}$$

where B_1 is the slope (also called the regression coefficient), and B_0 is the intercept:

$$B_1 = \frac{n\sum_{i=1}^{n} x_i y_i - (\sum_{i=1}^{n} x_i)(\sum_{i=1}^{n} y_i)}{n\sum_{i=1}^{n} x_i^2 - (\sum_{i=1}^{n} x_i)^2} \tag{3.3}$$

$$B_0 = \frac{\sum_{i=1}^{n} y_i - B_1(\sum_{i=1}^{n} x_i)}{n} \tag{3.4}$$

Power spectrum

The power spectra analysis uses, here, the Welch method of spectral estimation (Welch 1967) allowing us to measure the power of a signal at different frequencies. Note that no smoothing is applied to the data prior to the calculation of the spectrum. The Welch method is based on the concept of using periodigram spectrum estimates, which are the result of converting a signal from the time domain to the frequency domain. The power

of a red noise spectrum with the same $AR(1)$ coefficient fitted from the detrended given time series is also evaluated to test the statistical significance of its corresponding power spectrum.

Composite analysis

Composite analysis consists of averaging patterns with similar features (e.g. Figure 6 in Vellinga and Wu 2004), and can therefore help to better understand the possible influence of these particular features.

Empirical Orthogonal Function analysis

The method of EOF analysis (e.g. Von Storch and Zwiers 1999) is a decomposition of a data set in terms of orthogonal basis functions which are determined from the data. The basis functions are typically found by computing the eigenvectors of the covariance matrix of the data set. It is the same as performing a principal component analysis on the data, except that the EOF method finds both time series and spatial patterns. EOF analysis is therefore a useful way of determining the main modes of spatial and temporal patterns associated with the variability of a particular variable. When calculating EOFs, here, time series are normalized by the local variance and data are detrended.

Statistical significance

In this study, statistical significance of anomalies is tested using a z-test at the 90% confidence level. Significance of correlation and regressions coefficients is tested using Students t-test at either the 90% or 95% confidence level. Note that Quenouille (1952)'s method is used to account for the reduction of the effective numbers of degrees of freedom due to the autocorrelation in the datasets and the use of moving average. Degrees of freedom for moving averaged time series is determined as follows:

$$ne = \frac{n}{1 + 2\sum_{i=1}^{n-1} r_i r'_i} \tag{3.5}$$

where r_i and r'_i are autocorrelation of two time series with lag i years, and n is the number of data considered.

3.1.3 Domain of study

The domain of study for the present analysis is the Atlantic sector between 20°S-80°N and 90°W-30°E. We further consider regions where deep convection occurs in the model. The maximum MLD in March defines the deep convection sites as shown in Figure 3.1. Three deep convection sites are evident: (i) the GIN Seas, (ii) the Labrador Sea and (iii) a small region south of Iceland (extending down to about 57°N). Deep convection in the latter is significantly less than in the Labrador and GIN Seas. Furthermore, the Labrador and GIN Seas are both regions where MLD and AMOC fluctuations are most sensitively related (> 200 m Sv^{-1}). We therefore focus analysis on these two

main regions, for which the Labrador and GIN Seas domains have been respectively defined as 55°N-65°N/45°W-65°W and 65°N-80°N/15°W-15°E (see boxes, Figure 3.1). Corresponding convective indices have been calculated from the annual winter-mean MLD averaged over each domain.

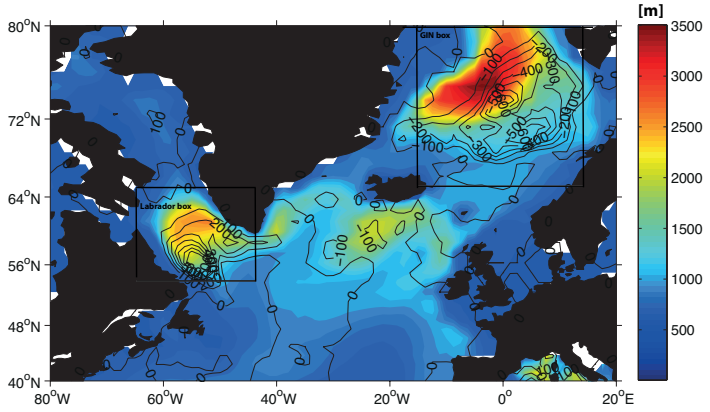

Figure 3.1: March MLD (m) averaged from year 80 to 200 (as colour-shaded) superimposed with its regression coefficients onto PC1 of the AMOC stream-function (m Sv^{-1}, shown as contours). The Labrador (GIN) Sea(s) box is defined as 55°N-65°N/45°W-65°W (65°N-80°N/15°W-15°E).

3.2 Climate predictability study with IPSL-CM5A-LR and CHIME: methods and experimental setup

3.2.1 Methods for measuring predictive skills

In the present study, two common methods are used to estimate potential predictability: (i) the diagnostic potential predictability (DPP) approach which only relies on a long control simulation, and (ii) the prognostic potential predictability (PPP) approach which requires re-running climate simulations with slightly perturbed initial conditions.

3.2.1.1 Diagnostic Potential Predictability (DPP) approach

The DPP approach uses the method of analysis of variance (Madden 1976; Rowell 1998) to examine the low-frequency variability (considered to be at least potentially predictable) of a given variable. As an estimate of DPP, we use the non-biased estimation of potential predictability variance fraction ($ppvf$) from Boer (2004) that attempts to separate the long-term variability from internal variability (considered as chaotic noise). The long-term variability that rises above this noise is deemed to arise from processes operating in the physical system that are assumed to be, at least potentially, predictable. The non-biased estimation of $ppvf$ (see Boer 2004 for further details) is defined as:

$$ppvf = \frac{\sigma_N^2 - \frac{1}{N}\sigma^2}{\sigma^2} \tag{3.6}$$

where σ_N^2 represents the variance of N-year means, and σ^2 represents the full variance of a given variable. The $ppvf$ varies between 0 and 1; a $ppvf$ close to 0 implies no long-term variability and thus no potential predictability. Conversely, $ppvf$ close to 1 implies large predictability. Statistical significance of $ppvf$ is judged using a F-test at the 90% or 95% confidence level. A threshold for "useful" potential predictability is however hard to define, as it is likely to be purpose and situation dependent.

Note that this approach is also of limited interest when applied to a single time series, that is when studying the temporal predictability of a given variable such as the AMOC index. In this study, we therefore restrict the use of this approach to the study of the spatio-temporal predictability of climate-related fields. Although the power of the DPP approach lies in the fact that it only relies on a long control simulation, it remains an easy and cheap statistical way to estimate the average predictive skill in a model, which differs from the prognostic approach described below.

3.2.1.2 Prognostic Potential Predictability (PPP) approach

In the PPP approach, the predictability is estimated prognostically by re-running a climate simulation (from the control integration) with slightly perturbed initial conditions supposed to represent atmospheric chaotic noise or uncertainty in the estimation of the climate state (e.g. Griffies and Bryan 1997a; Collins and Sinha 2003; Collins et al. 2006a; Msadek et al. 2010). This approach does not compare to observations directly, and only assesses the ability of the modeled climate to reproduce itself given a certain atmospheric noise. These experiments are thus often called "perfect ensemble" experiments. The PPP approach therefore represents an estimate of the upper limit of predictability based on having a perfect model and near perfect knowledge of the current state of the climate system (principally the state of the ocean). Although this situation is never likely to be achieved in practice, this approach is useful in identifying explicitly the climate predictability over a specific climate trajectory.

Practically, both the spread and the correlation of the members of each ensemble are useful and important tools to quantify the reproducibility and thus predictability of the simulated fields. In this study, we thus consider two deterministic measures (following the Assessment of Intraseasonal to Interannual Climate Prediction and Predictability report, National Research Council, NRC, 2010): the **Ensemble Spread (ES)** and **Ensemble Correlation (EC)**. Both these metrics have to be computed with respect to a target, a state that we wish to predict. At least two definitions of this target have been proposed in the literature: (i) the ensemble mean (e.g. as in Msadek et al. 2010, hereinafter M10) or (ii) each individual member successively (e.g. as in Collins and

Sinha 2003, hereinafter CS03). As illustrated below, ES computed with each definition only differs by a factor of proportionality. Both definitions are thus equivalent for this metric. In contrast, no such relationship of proportionality could be found for EC. Here, we will therefore consider these two definitions to evaluate possible differences in their respective scores of PPP. Both EC and ES metrics are now described considering the different definitions of target.

Ensemble Correlation (EC)

In the forecast framework, correlation addresses the question: "to what extent are the forecasts varying coherently with the observed variability?". In the M10 approach, predictability skill is evaluated by correlating each member of the ensemble to the ensemble mean whereas in the CS03 approach each member is correlated to each other. If M is the number of members, we therefore obtain M (resp. $M(M-1)/2$) individual correlations for M10 (resp. CS03). Independently of the approach used, the formula for the individual correlation of any pairs p is:

$$r_p = \frac{[T\sum_{t=1}^{t=T} A_t B_t] - [\sum_{t=1}^{t=T} A_t \sum_{t=1}^{t=T} B_t]}{\sqrt{[T\sum_{t=1}^{t=T} A_t^2 - (\sum_{t=1}^{t=T} A_t)^2] \times [T\sum_{t=1}^{t=T} B_t^2 - (\sum_{t=1}^{t=T} B_t)^2]}} \tag{3.7}$$

where T is the number of years over which we want the correlation for, and A and B are the time series (or members) forming the pair p. Once the individual correlations of all pairs have been calculated (M pairs for M10, $M(M-1)/2$ pairs for CS03), EC of the ensemble is computed as the mean of all individual correlations through a Fisher Transformation (Fisher 1921). The transformation is applied to each individual correlation r_p, and is defined by:

$$z_p = \frac{1}{2}\ln\left(\frac{1+r_p}{1-r_p}\right) = arctanh(r_p) \tag{3.8}$$

Then by calculating the mean z of all individual z_p, EC of a given ensemble is estimated by its inverse transformation:

$$EC = \frac{\exp(2z) - 1}{\exp(2z) + 1} \tag{3.9}$$

We will consider the two definitions of target (M10 and CS03) to evaluate possible differences in their respective score of predictive skills. Statistical significance of the resulting EC is judged using a one-tailed Students t-distribution test at the 90% confidence level with degrees of freedom corresponding to the average degrees of freedom of all individual correlations. The degrees of freedom of the latter takes into account the persistence in the two time series following Bretherton et al. (1999).

Ensemble Spread (ES)

ES or Root Mean Squared Error RMSE or again the Mean Squared Skill Score MSSS (as defined by the US CLIVAR working group on Decadal Predictability, http://clivar-dpwg.iri.columbia.edu) addresses the question: "how large are the typical errors in the forecast (among members) relative to those implied by baseline?". Consistently with EC, we consider the two definitions of the targets which arise from the literature: for a given lead-time LT, ES of an ensemble of individual members i is defined respectively as:

$$ES_{M10}(LT) = \sqrt{\frac{1}{M}\sum_{i=1}^{M}[X_i(LT) - \overline{X}(LT)]^2} \tag{3.10}$$

$$ES_{CS03}(LT) = \sqrt{\frac{2}{M(M-1)}\sum_{i=1}^{M}\sum_{j=i+1}^{M}[X_i(LT) - X_j(LT)]^2} \tag{3.11}$$

where we define: $\overline{X}(LT) = \frac{1}{M}\sum_{i=1}^{M} X_i(LT)$

We demonstrate below that there actually exists a relationship of proportionality between Equation 3.10 and Equation 3.11. Let consider the two following definitions of Mean Squared Error:

$$E_{M10} = \frac{1}{M}\sum_{i=1}^{M}(X_i - \overline{X})^2 \tag{3.12}$$

$$E_{CS03} = \frac{2}{M(M-1)}\sum_{i=1}^{M}\sum_{j=i+1}^{M}(X_i - X_j)^2 \tag{3.13}$$

By expanding $(X_i - \overline{X})^2$ in Equation 3.12 and after a few rearrangements we show that:

$$E_{M10} = \overline{X^2} - \overline{X}^2 \tag{3.14}$$

Then, if we introduce:

$$E = \frac{2}{M(M-1)}\sum_{i=1}^{M}\sum_{j=1}^{M}(X_i - X_j)^2 \tag{3.15}$$

We show by a recurrence reasoning that:

$$E = 2E_{CS03} \tag{3.16}$$

By expanding $(X_i - X_j)^2$ in Equation 3.15 and after a few rearrangements, we show that:

$$E = \frac{4}{M-1}(\overline{X^2} - \overline{X}^2) \tag{3.17}$$

By combining Equation 3.14, Equation 3.16 and Equation 3.17, we obtain the following relationship:

$$E_{CS03} = \frac{2M}{M-1} E_{M10} \tag{3.18}$$

Therefore,

$$ES_{CS03}(LT) = \sqrt{\frac{2M}{M-1}} ES_{M10}(LT) \tag{3.19}$$

And there exists a factor of proportionality $\sqrt{\frac{2M}{M-1}}$ between the ensemble spread of both CS03 and M10 definitions.

Generally, the trajectories of individual members diverge with time and thus ES increases with LT. When ES saturates at the control RMSE, we consider that there is no more potential predictability: the spread of the forecast is of similar magnitude as the natural spread of the modeled climate, and no predictability can be inferred. In CS03 (M10) the control RMSE is defined as $\sigma\sqrt{2}$ ($\sigma\sqrt{\frac{M-1}{M}}$), where σ is the standard deviation of the control integration. Statistical significance of ES as compared to the respective threshold (or control RMSE) is judged using a F-test at the 95% confidence level. The maximum LT at which a variable is said to be potentially predictable is the last significant LT before ES persistently exceeds the threshold.

As demonstrated above, ES computed with each definition (M10 and CS03) only differs by a factor of proportionality. Both definitions are thus equivalent for this metric. In contrast, no such relationship of proportionality could be found for EC. Here, we will therefore consider these two definitions of target to evaluate possible differences in their respective score of PPP.

Potential predictability criterion

With the objective of developing a common skill evaluation to enable us to compare decadal prediction systems across different modeling centers (Meehl et al. 2012), we propose here an approach of measuring predictive skills based on both ES and EC metrics. Indeed, note that EC alone does not indicate whether the forecast values are of the right magnitude (contrary to ES). In the same way, ES alone does not indicate the direction of the deviations (contrary to EC). We therefore explore the information given by both metrics, and consider that a variable is **potentially predictable** if it has a **(low) statistically significant ES** (below the saturation level defined as the control RMSE) **associated with a (high) statistically significant EC** (Figure 3.2, right panel). By combining these two metrics, we are in good agreement with Hawkins et al. (2011) who claim that prediction skills should be measured using more than one metric. However, it has to be kept in mind that, as will be illustrated later (in *chapters 5* and *6*), combining these two metrics might be too restrictive in some situations, and that information given by ES or EC alone should not be neglected.

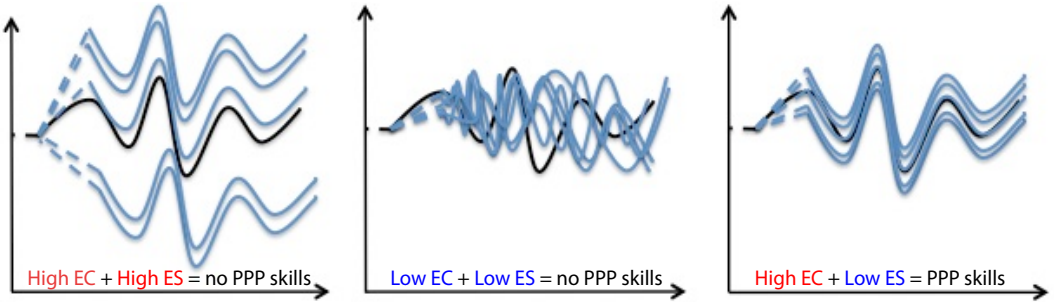

Figure 3.2: Schematic representation of two scenarios with no PPP skills (both left and middle panels) and one scenario with PPP skills (right panel) as defined here.

Note that deterministic measures of skills (such as $ppvf$, EC, ES) do not give information about the prediction probabilities; such information can complement the results already obtained from both the DPP and PPP approaches, and can be of particular importance for society-relevant variables such as surface temperature. This probabilistic information can be obtained through the calculation of the Probability Density Functions (PDFs) of a specific variable for each ensemble experiment.

Probability Density Functions

For a given variable x, the PDF fitted by a Gaussian distribution can be calculated by computing the mean μ and standard deviation σ of the M members of the ensemble experiment:

$$PDF(x) = \frac{1}{\sigma\sqrt{2\pi}} \exp \frac{-(x-\mu)^2}{\sigma} \tag{3.20}$$

Potential predictability may arise if the ensemble mean of the ensemble experiment is significantly shifted with respect to climatology resulting in biases in the probability of e.g. warmer temperatures. A variable x is therefore predictable if the forecast PDF distribution of x differs sufficiently from the climatological PDF distribution to influence relevant decision-makers (as illustrated in Figure 3.3).

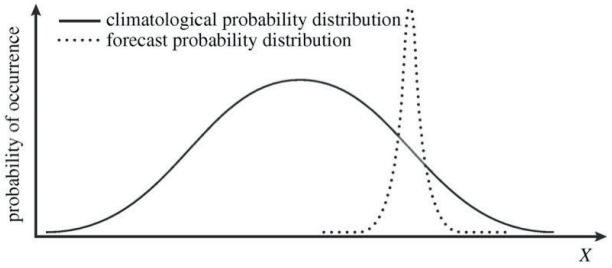

Figure 3.3: The solid line is a schematic illustration of the climatological probability of some climatic variable, such as decadal-mean surface temperature. The dashed line is a schematic illustration of a decadal forecast probability distribution showing clear predictability.

3.2.2 Model simulations with IPSL-CM5A-LR

3.2.2.1 Control integration for DPP

The DPP approach only relies on the IPSL-CM5A-LR control integration described earlier in *Sect. 2.2.2*. It is a 1000-year control simulation started from a suite of adjustment simulations lasting more than 1000 years. Using constant pre-industrial boundary conditions of tropospheric greenhouse gases and aerosol concentrations, this is the pre-industrial control simulation used for the CMIP5 exercises.

3.2.2.2 "Perfect ensemble" experiments for PPP

The core of the PPP approach is a series of 5 ensemble experiments using the same code as the control integration described above. Each ensemble starts from a different date of the control simulation and includes 10 members, started from slightly different initial conditions and integrated for 20 years. Initial conditions of the different members are obtained here by perturbing the SST from the control simulation with an anomaly chosen randomly for each grid point in the interval [-0.05°C, 0.05°C] with an equiprobable distribution for each value over this interval. This perturbation mimics a non-Gaussian white noise perturbation. No perturbation has been applied for the grid points under sea-ice cover. Figure 3.4 shows the five different starting dates of each ensemble experiment together with the time series of the AMOC index from years 1870 to 2200 in the control integration. One experiment starts from a year corresponding to relatively weak AMOC conditions (hereinafter W, year 1901), one from intermediate conditions (hereinafter I, year 2171), and one from strong conditions (hereinafter S, year 2071). We have also chosen to start some experiments respectively 5 and 15 years before the large AMOC maximum in 2071 to investigate how far ahead this extreme value can be captured (15P and 5P, starting dates 2056 and 2066, respectively). Note that other choices could have been made and because of the limited number of starting dates, this experimental set up was not designed to draw robust conclusions about a possible predictability-dependence on the AMOC initial state. It could nevertheless give useful indications about it.

3.2.3 Model simulations with CHIME

3.2.3.1 Control integration for DPP

The core of the DPP approach with CHIME is the 201-year control integration of *E3* (from year 105 to 305) as described earlier in *Sect. 2.1.2.2*. It has been run in fully coupled mode for 445 years from rest, using constant pre-industrial boundary conditions of tropospheric greenhouse gases and aerosol concentrations. There is evidence that this pre-industrial control simulation is not as reliable as *cD* (e.g. climate drift, missing

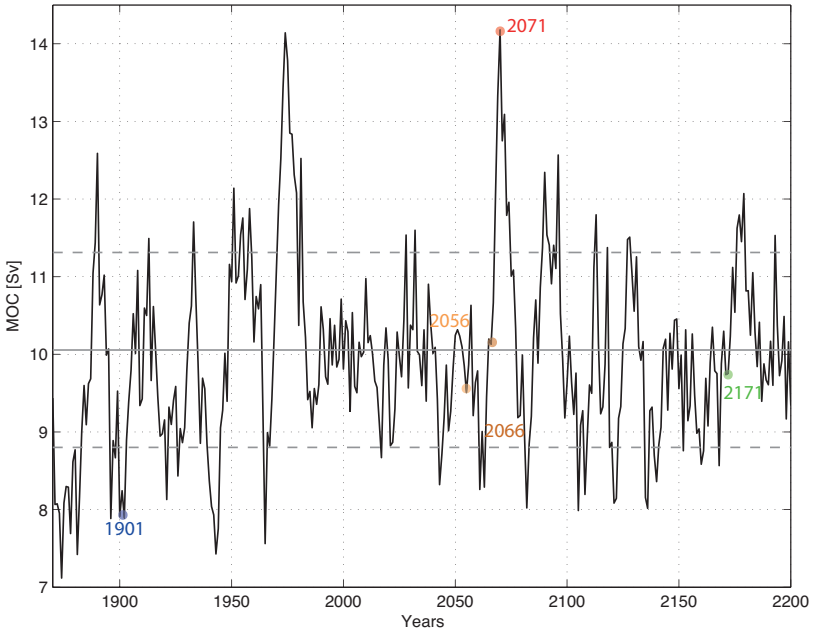

Figure 3.4: Time series of AMOC index in the IPSL control integration from year 1870 to 2200, with starting points of perfect ensemble experiments shown as coloured points. The 1000-year mean is shown as the horizontal line and the corresponding standard deviations are shown as the dashed lines.

data), and this has to be kept in mind through the rest of the study. Predictability experiments carried out with *E3* nevertheless give useful indication about the potential predictive skills of this new model. Results from these experiments could be used as benchmark for future experiments once a more reliable and longer control integration of CHIME (or similar model) will have been obtained.

3.2.3.2 "Perfect ensemble" experiments for PPP

The core of the PPP approach with CHIME is a series of 5 ensemble experiments run from the control integration *E3*. Each ensemble of 5 members was started from slightly different initial conditions and integrated for 20 years. To test the eventual sensitivity of predictive skills to the number of members considered, one of these experiments has been generated with 5 additional slightly different initial conditions, therefore accounting for 10 members in total (excluding the control integration). Because the new configuration of CHIME did not allow us to apply the same perturbation scheme than the one used in IPSL-CM5A, perturbations to the initial conditions in CHIME were obtained as follows: each of the ensembles were restarted from the same atmospheric state of the control integration, but the ocean of each one of the members was initialized from an ocean advanced by a day relative to the preceding member. Figure 3.5 shows the five different starting dates of each "perfect ensemble" experiment together with the time series of the AMOC index from year 105 to 305 in the control integration *E3*. To facilitate

the comparison of our results with those from IPSL-CM5A, we chose starting dates corresponding as close as possible to the AMOC initial states in the IPSL experiments. Therefore, one experiment starts from a year corresponding to strong AMOC conditions (hereafter S, year 260), two experiments start respectively 15 and 5 years before this strong event (hereafter 15P and 5P, year 245 and 255), and one experiment starts from intermediate conditions (hereafter I, year 105). Note that because of missing restart files, the experiment corresponding to relatively weak AMOC conditions (hereafter W) does not start from an extreme value (as in IPSL) but starts about 3 years prior it (year 280). We will still refer this experiment as starting from weak AMOC conditions. These experiments with CHIME could strengthen conclusions drawn from the IPSL-CM5A model about eventual predictability-dependency on the AMOC initial states.

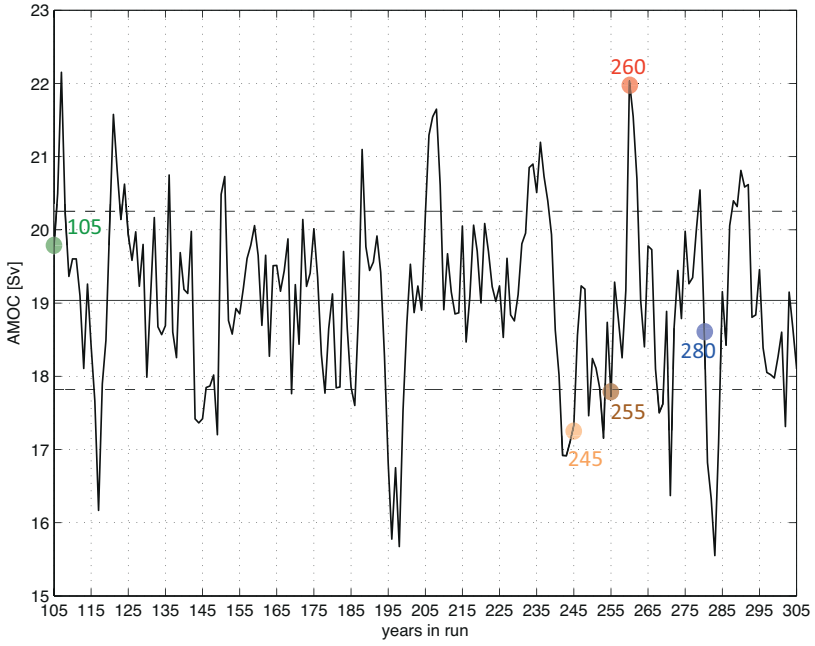

Figure 3.5: Time series of AMOC index in the CHIME control integration *E3* from year 105 to 305, with starting points of perfect ensemble experiments shown as coloured points. The 201-year mean is shown as the horizontal line and the corresponding standard deviations are shown as the dashed lines.

The next chapter will now address the first objective of this thesis by analyzing the natural decadal variability of the AMOC (and associated key variables) as seen in the CHIME model.

Chapter 4

Decadal-timescale changes of the AMOC and climate in CHIME

Results from this chapter have been accepted for publication in Climate Dynamics as: *Persechino A, Marsh R, Sinha B, Megann A, Blaker A, New A (2012) Decadal-timescale changes of the Atlantic meridional overturning circulation and climate in a coupled climate model with a hybrid-coordinate ocean component. Clim Dyn, 39(3):1021-1042.*

4.1 Aim of study

Mechanisms responsible for decadal variability of the AMOC are still under debate. Improving our understanding of such variability is prerequisite in the perspective of developing operational decadal predictions schemes. Focussing on the shorter decadal timescale (i.e. 15-30 years), this chapter therefore describes the natural variability of the AMOC and associated key variables as seen in CHIME, in order to better understand the key processes implicated in such variability. *Sect. 4.2* describes the structure and variability of the AMOC. Co-variability of ocean properties and surface climate are discussed in *Sect. 4.3*. Underlying physical mechanisms are considered in *Sect. 4.4*. A summary and discussion follow in *Sect. 4.5*, with concluding remarks in *Sect. 4.6*.

4.2 Internal AMOC variability in CHIME

4.2.1 Spin-up, trend and variability of the AMOC

The AMOC index time series is shown for the entire *cD* run in Figure 4.1a (black line). Despite the relatively short time series available, decadal-to-multidecadal timescale variability can still be easily distinguished from the spinup transient from year 80. The

amplitude of variability is about 2 Sv (ranging from 17.5 to 22 Sv). The average decadal mean (about 19.8±1.4 Sv) compares well with observational estimates (18±2-3 Sv) of Talley (2003), but is a little smaller than the mean of 22.8±1.6 Sv in the corresponding period of HadCM3 (Megann et al. 2010). The principal component associated with the main mode of variability of the AMOC streamfunction (PC1, further discussed in *Sect. 4.2.2*) is superimposed on the AMOC index (Figure 4.1a, grey line). The two time series are highly correlated, with correlation coefficient of 0.86 (Table 4.1). Although its corresponding power spectrum shows most energy (relative to a fitted first order autoregressive AR1 model, Chatfield 1975) at a period of about 30 years, this is well below the 80% confidence limit about the fitted red noise spectrum (Figure 4.1b). Although not significant, periods in the range 15-30 years almost reach this 80% confidence limit, so it appears that the PC1 of the AMOC in CHIME reveals an enhanced power compared to a fitted red noise spectrum for periods in this range.

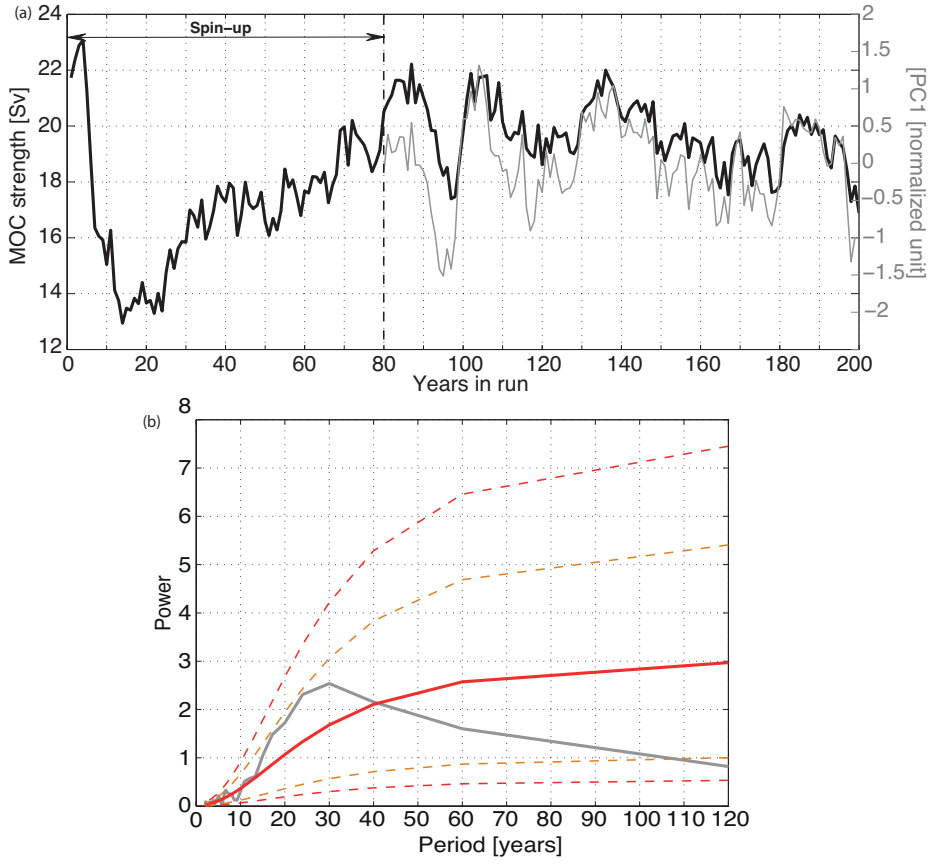

Figure 4.1: (a) Time series of the AMOC index from *cD* for the whole 200-year simulation (black line) superimposed with the PC1 time series of the AMOC streamfunction from year 80 (grey line), (b) Power Spectrum of the detrended PC1 (grey line) using the Welch method of spectra estimation. The smooth red solid line is the power of a red noise spectrum with the same AR(1) coefficient fitted from the detrended PC1 time series, and red (orange) dashed lines, which are the 95% (80%) confidence limits.

The mean AMOC streamfunction (Figure 4.2) has broadly similar features to the mean

Table 4.1: Maximum correlation coefficients between 10-year moving averages of the PC1 of AMOC and several different variables. Bold correlations are statistically significant at the 90% confidence limits.

Variable	**Max. Correlation Coefficient**	**Lag (years)**
AMOC index	**0.86**	Instantaneous
September northern tropical subtropical SST gradient	**0.79**	Near-instantaneous
Convective index (Labrador)	**0.90**	PC1 lags by ~ 2
Convective index (GIN)	**-0.70**	PC1 lags by ~ 1
Winter surface potential density (Labrador)	**0.86**	PC1 lags by ~ 2
Winter surface potential density (GIN)	**-0.83**	PC1 lags by ~ 1
Tropical Activity (TA)	**0.75**	PC1 lags by $\sim 8-9$

AMOC inferred from observations (Ganachaud and Wunsch 2000); the circulation associated with the NADW has a maximum transport of about 18 Sv at a depth of 800-1200 m occurring at about 30°N. NADW lies at a maximum depth of about 4000 m, which is considerably deeper than the observed depth at which NADW enters the DWBC (about 2000-2500 m, Reid 1989). This bias could be the result of either the weakened AABW cell found in CHIME (Megann et al. 2010) or an unrealistic degree of preservation of the density outflows from the Nordic Seas as a consequence of the isopycnic coordinate system (Roberts et al. 1996) that will result in a too-dense NADW cell. The 18 Sv of warm northward flow is found in the upper ocean (mainly in the Gulf Stream and NAC) with the strongest sinking occurring in a broad region between about 55°N and 65°N. There is also evidence for deep water formation in the Nordic Seas as far as 70°N. The inflow of AABW (the reverse cell below 4000 m) reaches barely 2 Sv; Megann et al. (2010) suggest that this is due to excessive wintertime ice cover in the Antarctic and hence insufficient heat loss to form realistic volumes of bottom water.

4.2.2 EOF analysis of AMOC variability

To analyze the spatial patterns associated with variability of the AMOC in CHIME, we have calculated EOFs (e.g. Von Storch and Zwiers 1999) based on 121 years of annual-mean AMOC streamfunction calculated from year 80 onwards (Figure 4.3). Prior to the calculations, time series are normalized by the variance, and detrended.

EOF1 explains 33.6% of the total variance (Figure 4.3a), and has a basin-wide structure similar to that of the streamfunction itself (Figure 4.2). It has a maximum value of

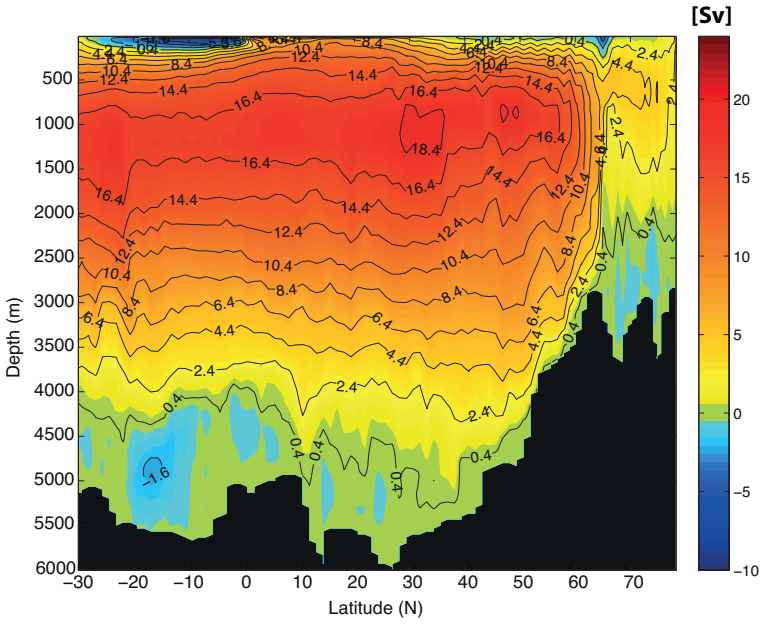

Figure 4.2: Annual mean streamfunction of zonally integrated volume transport (Sv) from 30°S to 80°N, averaged from years 80 to 200 in CHIME. Positive values mean clockwise circulation.

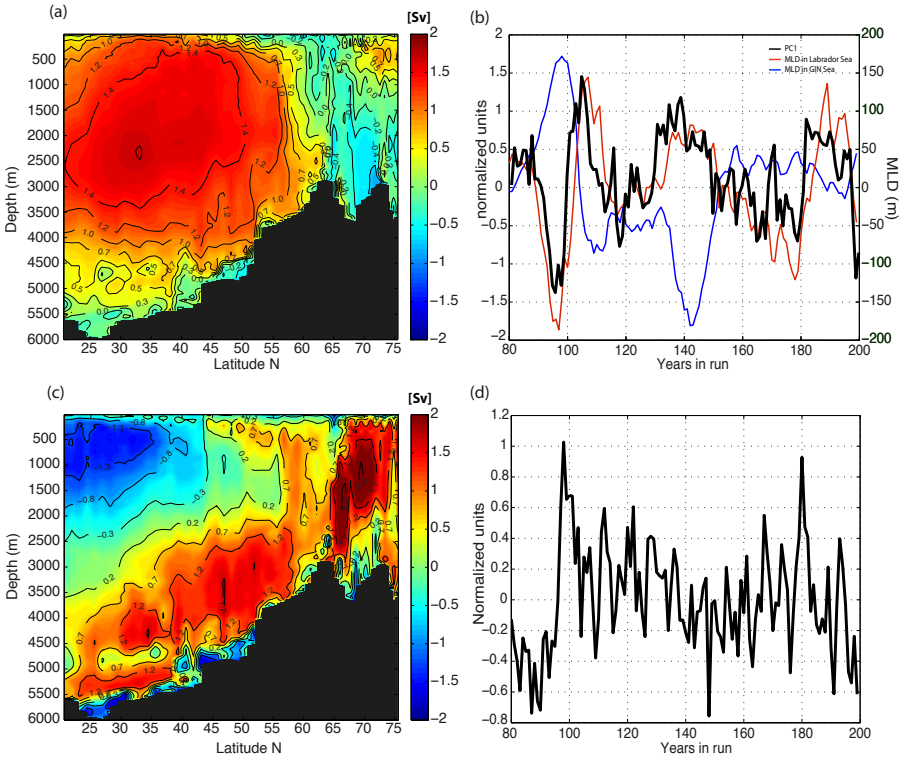

Figure 4.3: Detrended AMOC streamfunction (from year 80 to 200) in the North Atlantic (20°N to 75°N): (a) EOF1; (b) PC1 (black line) and 10-year moving average winter MLD in Labrabor Sea (red line) and GIN Seas (blue line); (c) EOF2 and (d) PC2.

about 1.6 Sv (for a fluctuation of one standard deviation of PC1) with the strongest sinking taking place primarily at about 55-60°N. As already mentioned in *Sect. 4.2.1*, PC1 (Figure 4.3b, black line) shows an enhanced power for periods in the range 15-30 years and is significantly correlated with the AMOC index; we shall therefore use PC1 of the AMOC as a reference time series in the following analyses. It would therefore seem that EOF1 thus describes AMOC changes associated with variability in the period range 15-30 years, most likely related to Labrador Sea Water (LSW) variability; the strongest sinking indeed occurs at about 55-60°N and PC1 shows a close link with convective activity (MLD) in the Labrador Sea (Figure 4.3b, red line). However, convective activity in the GIN Seas also seems to be closely linked to PC1 of the AMOC as seen by their apparent anti-phase relationship (Figure 4.3b, blue line). These close relationships between the AMOC and convective activities are further investigated in *Sect. 4.4*. It is clear, therefore, that EOF1, which shows the principal changes happening in the AMOC on decadal timescales, appears to capture not only the mechanism associated with LSW variability but also mechanisms associated with variability in the GIN Seas.
One further interesting feature of EOF1 is the anti-phase relationship between latitude ranges corresponding to the Labrador Sea and to the Nordic Seas (Figure 4.3a), which is confirmed by the clear anti-correlation between convective activities in these two regions (Figure 4.3b). In observational studies, convection in the Labrador Sea has indeed generally been found to vary out of phase with convection in the Greenland Sea (Dickson et al. 1996; Hurrell and Dickson 2004). However, this is not the case for all climate models, for example HadCM3 (e.g. Dong and Sutton 2005; Bingham et al. 2007) has generally weak convection in the Labrador Sea (possibly related to the substantial surface freshening that occurs in the subpolar gyre of that model). Mechanisms behind this anti-phase pattern in CHIME will be further investigated in *Sect. 4.4*.

EOF2, which accounts for about 12% of the total variance, shows a dipole pattern with mainly positive values from 40°N to 75°N below 2500 m, and negative values in the upper ocean south of 40°N (Figure 4.3c). The strongest variability in the sinking here takes place primarily at about 55-65°N and 65-70°N. The positive cell of EOF2 may arise through deeper sinking and return flow in the upper cell of the AMOC; this could be related to changes in surface winds and/or surface fluxes in the GIN Seas, leading to an increase in the density of the overflow waters. The strong amplitude of this second mode of AMOC variability close to the ocean bottom in the subpolar region and north of the sills suggests a role for both the denser LSW and Greenland Sea Water (GSW), and that these latter vary on interannual rather than decadal timescales (see Figure 4.3d). Indeed, the associated power spectrum (not shown) reveals an enhanced variability for statistically significant periods in the ranges 2-3 and 5-6 years at the 80% confidence limit. Although not significant, there is a peak at about 60 years suggesting also some multi-decadal variability; a longer simulation would, however, be needed to confirm this.

From this EOF analysis, we develop the following picture of the AMOC streamfunction

and its evolution in time: a primary mode of variability is associated with a decadal cycle related to convective activity in the Labrador and (inversely) the GIN Seas, while a secondary mode is rather associated with interannual variability of convective activity in these two regions. Note that, as shown by the standard deviation of the streamfunction in Figure 4.4, the strongest AMOC fluctuations occur within the NADW cell at the latitude range of the Labrador Sea (50-60°N) and to a lesser extent in the GIN Seas at about 70-75°N.

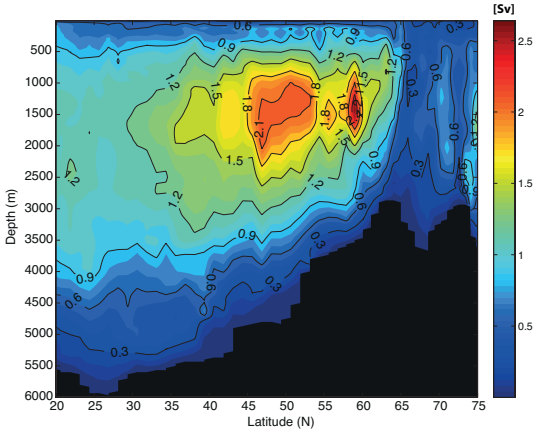

Figure 4.4: Standard deviation of the annual mean streamfunction (Sv) shown in Figure 4.2.

4.2.3 Evolution of the AMOC on a decadal timescale

To further examine the decadal variability of the AMOC, lead-lag regressions of the AMOC streamfunction on PC1 of the AMOC have been calculated and are shown in Figure 4.5. Because of the short control experiment length, most of the coefficients are not statistically significant (grey shading). Nevertheless, this figure still gives useful indications about the dynamical evolution of the decadal AMOC oscillation in CHIME. At lag -15 years, we found evidence for the NADW cell to be in its weak phase with an anti-clockwise anomalous circulation. Gradually, significant positive anomalies of meridional circulation develop in the tropics and extend northwards. At lag 0, the AMOC reaches a maximum with enhanced northward warm surface flow, stronger southward deep return flow, and enhanced downwelling at about 55-60°N. Thereafter, positive anomalies of meridional circulation gradually weaken and negative anomalies begin to appear in the tropics. Note that both EOF1 and EOF2 patterns of the AMOC are clearly identifiable here (e.g. at lag 0 and +6, respectively), underlining the contribution of these two modes to decadal variability of the AMOC. On a decadal timescale, streamfunction anomalies responsible for the reversal phase of the AMOC oscillation in CHIME seem to originate in low latitudes. The possibility that they may even originate in the South Atlantic through compensation in the flow of NADW across the Equator

(Schmitz and Richardson 1991) is not excluded. We note a link between the development of streamfunction anomalies in the low latitudes, and the associated northward transport of salinity anomalies (see *Sect. 4.4.3.1*).

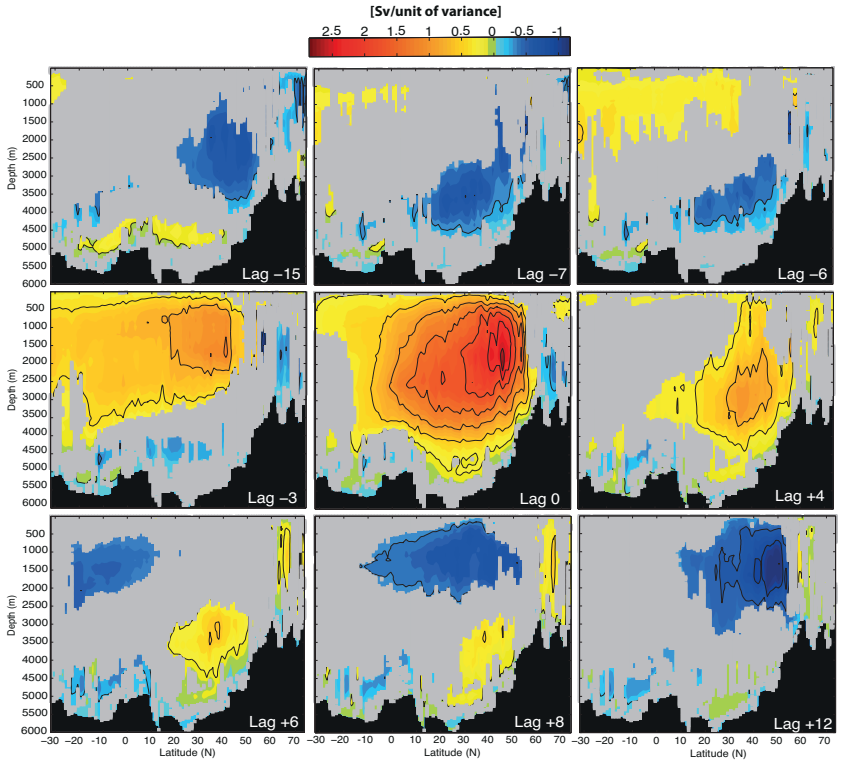

Figure 4.5: Lead-Lag regression coefficient maps of the AMOC streamfunction (Figure 4.2) at various lags to PC1 of the AMOC (Figure 4.3) (Sv unit of variance^{-1}). The grey shading indicates 90% confidence level for zero correlation.

4.3 Associated signals and impacts

The associated signals and impacts of AMOC variability in CHIME are considered in the ocean and the atmosphere respectively.

4.3.1 Ocean

A composite of winter SST anomaly patterns (relative to the year 80-200 winter mean) induced by AMOC fluctuations was obtained by averaging anomalies over years when the AMOC is strongest (i.e. when exceeding the AMOC standard deviation, Figure 4.6). Significance of anomalies at each grid point was assessed by testing the null hypothesis that they were taken from a distribution that has the same mean as all the years (using a z-test at the 90% confidence level). When the AMOC is in its strong state, most of the upper ocean, from the subtropics to the mid-latitudes (mainly over the Gulf Stream

path) and the Nordic Seas becomes warmer, whereas the northern tropics becomes significantly cooler. This cooling could be explained by the stronger heat transport associated with stronger AMOC conditions that takes away heat from the low latitudes towards the higher latitudes but also by associated changes in atmospheric forcing such as the NAO. The role of the atmosphere in this cooling is supported by the fact that the SST pattern has similarities with the structure of observed SST correlated with the NAO (e.g. Visbeck et al. 2001), and that at about 300-800 m depth this temperature pattern looks significantly different from the surface pattern (Figure 4.7). In CHIME, a northern tropical-subtropical SST dipole is identified, in contrast to HadCM3 where the SST dipole is cross-equatorial (Vellinga and Wu 2004). The difference in the dipoles probably results from differences in the SST patterns between the two models as identified by Megann et al. (2010). A strong AMOC state in CHIME will therefore tend to warm the subtropics to the mid-latitudes and the Nordic Seas, and to cool the northern tropical SST, causing a northern tropical-subtropical SST gradient (a link strengthened by the strong and significant near-instantaneous correlation found between this gradient and the PC1 of AMOC, Table 4.1).

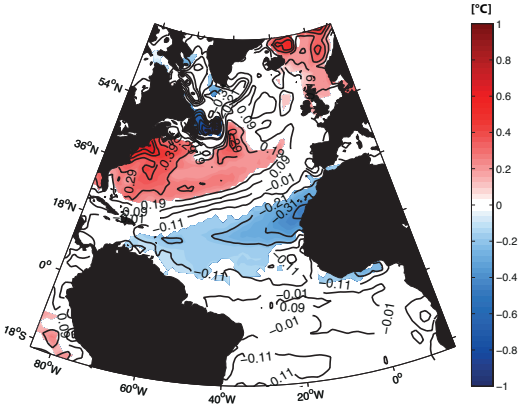

Figure 4.6: Composite of winter anomaly patterns of SST induced by AMOC fluctuations, obtained by averaging anomalies over years when the AMOC (defined as the PC1 of the MOC) is strongest. Colours indicate where the null hypothesis of equal means is rejected at the 10% level.

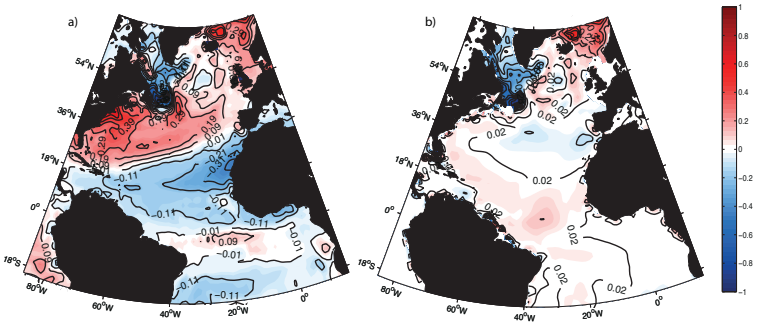

Figure 4.7: Same as Figure 4.6 for (a) SST and (b) sea temperature at 300-800 m depth (layer 13) with no statistical significance test applied.

The leading mode of multi-decadal SST variability in the North Atlantic is known as the Atlantic Multi-decadal Oscillation or AMO (e.g. Kerr 2000), for which an index is traditionally defined as the basin-averaged (90°W-30°E, 0-70°N) SST anomaly (e.g Knight et al. 2005), although the definition of AMO index might alternatively be defined in terms of the timescale of variability (Frankcombe et al. 2010). While the North Atlantic SST anomaly pattern in Figure 4.6 is characterized as a sub-basin scale tropical-subtropical SST dipole, positive anomalies are predominant and the strongest in the Northern Hemisphere, suggesting an AMO-type response as seen in the observations (e.g. Sutton and Hodson 2005). This pattern is also somewhat reminiscent of SST anomaly patterns identified in previous studies as characteristic of multi-decadal variability on 20-30 year timescales (e.g. Figure 8 in Frankcombe et al. 2010). Figure 4.8a shows the AMO index (traditionally defined), after linear detrending (green line), alongside our index for the leading (decadal) mode of AMOC variability (blue line). On inspection, SST variability appears to lag AMOC variability. This is confirmed by lagged cross-correlations between the two time series, shown in Figure 4.8b. The strongest and statistically most significant correlation is obtained when a 10-year moving average is applied to both time series; a maximum correlation of about 0.64 is for the PC1 of the AMOC leading the AMO by about 4 years (Figure 4.8b, dashed line).

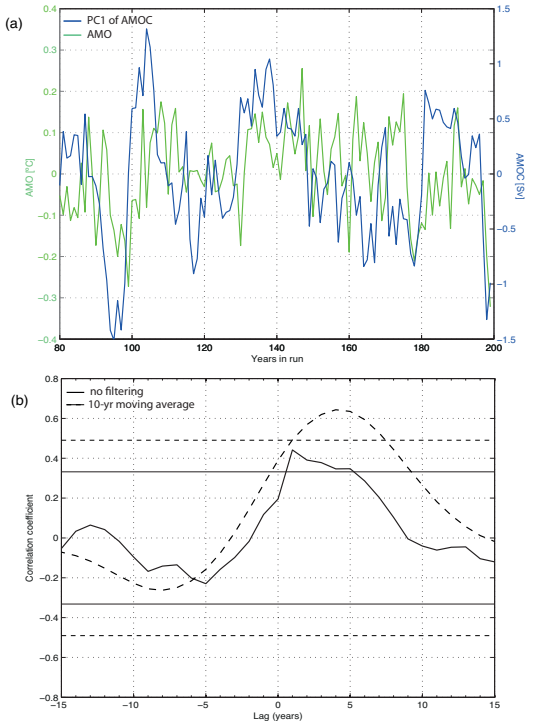

Figure 4.8: Measures and relationships between AMO and AMOC indices: (a) time series of the area-averaged (90°W-30°E, 0-70°N) annual SST anomaly after linear detrending (green line), shown alongside the PC1 of AMOC (blue line); (b) lagged cross-correlations plot between the two time series (solid line) and their 10-year moving averaged time series (dashed line); horizontal lines correspond to their corresponding 95% confidence limit for zero correlation. Positive lags are for PC1 leading the AMO.

We further investigate the extent to which decadal variability in CHIME is associated with sub-surface thermal anomalies, as recently linked to observed multi-decadal variability (Frankcombe et al. 2008, 2010). Figure 4.9 shows sub-surface temperature anomalies (colour-shaded) as a function of longitude and time, averaged over CHIME layers 10-12 (spanning an approximate depth range 150-400 m in the subtropics) and the latitude range 10-30°N (best representative of westward propagation by layer anomalies). The time series at each longitude is detrended and smoothed with a 5-year moving average. There is an overall impression of westward translation of sub-surface anomalies on a timescale of 7-10 years, similar in magnitude (±0.4°C) to observations (Frankcombe et al. 2008).

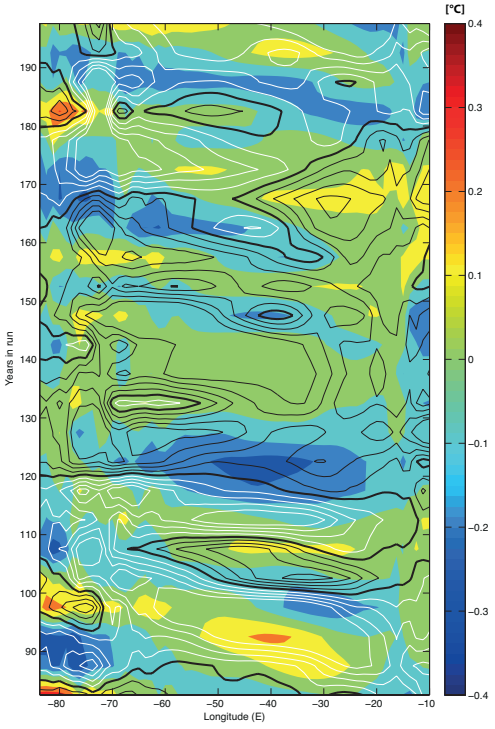

Figure 4.9: Sub-surface anomalies as a function of longitude and time, averaged over CHIME layers 10-12 and the latitude range 10-30°N, detrended and smoothed with a 5-year moving average. Temperature anomalies are colour-coded. Thickness anomalies are contoured, with a contour interval of 2.5 m (the zero contour is bold; positive anomalies are indicated by thin black contours; negative anomalies are indicated by thin white contours).

In CHIME, layer temperature anomalies are accompanied by salinity anomalies (not shown) that have the opposite effect on density, as layer densities below the mixed layer are prescribed. As a consequence, there is no associated density perturbation and these temperature and salinity anomalies are advected as passive tracers of water mass variability. A degree of westward propagation (in temperature and salinity) is associated with perturbations in layer thickness, although this is only clear over years 80-120. Anomalies in cumulative thickness of layers 10-12 (corresponding to the depth

range of about 150-400 m), in the range ±10 m, are indicated in Figure 4.9 by the over-plotted contours. These thickness anomalies are indicative of density anomalies, and are likely implicated in AMOC variability.

When and where layer interfaces are displaced anomalously upwards or downwards, the associated temperature and salinity anomalies may be substantial (reaching ±2.0°C and ±0.5 psu), but inspecting animations of temperature and salinity anomalies at selected latitudes, these anomalies do not clearly propagate westwards for much of the period (consistent with the layer thickness anomalies in Figure 4.9). In conclusion, the majority of sub-surface temperature variability seen to translate westwards does not cause AMOC variability but passively advects with the evolving velocity field. Averaged over the subtropics, temperature anomalies also spread downwards from a surface origin, on decadal timescales, accompanied by salinity anomalies that ensure constant layer density (not shown).

Previous studies have established that multi-decadal (20-30 year) variability may be understood as the thermal wind response to a surface thermal anomaly in the north-central part of the Atlantic basin, inducing westward Rossby wave propagation across the basin on near-decadal timescales (Colin de Verdière and Huck 1999), and subsequent adjustment of meridional temperature (hence density) gradients that lead to a dynamical response of the AMOC (te Raa and Dijkstra 2002). While westward translation of sub-surface temperature anomalies in the subtropics of CHIME appear on first inspection to be consistent with this mechanism, the accompanying salinity anomalies (in isopycnal layers) preclude any density perturbation. In contrast, thickness anomalies of ±10 m are a signature of interior density anomalies, but the associated temperature and salinity anomalies do not clearly propagate. We proceed in later sections to attribute the source of AMOC variability in CHIME to the advection of mixed layer salinity anomalies from low to sub-polar latitudes, while mixed layer temperature anomalies are strongly and quickly damped through surface heat fluxes. Regarding the latter process, there is however evidence for local correlation of anomalies in SST and surface heat flux associated with the NAO, as outlined in *Sect. 4.4.3.2*.

4.3.2 Atmosphere

Figure 4.10 shows composite atmospheric anomaly patterns when the AMOC is strongest, for winter anomalies of SAT, SLP, and September anomalies of net precipitation. Only significant values (at the 90% level) are coloured. When the AMOC is strongest, SAT along the western coast of North America (i.e. over the Gulf stream path) and in the Nordic Seas becomes significantly warmer in contrast to both the northern tropics and the Labrador Sea areas where it becomes significantly cooler (Figure 4.10a). This is consistent with the anti-phase relationship previously identified between the Labrador and GIN Seas (see *Sect. 4.2.2*). This SAT pattern somewhat resembles that of the SST

in Figure 4.6, and the anomalies vary from about 0.1°C in the tropics and subtropics, to over 1°C in the Nordic Seas. Over land, the strongest AMOC conditions are associated with a significant warming of northern Europe (in good agreement with e.g. Pohlmann et al. 2006) and the central eastern seaboard of North America.

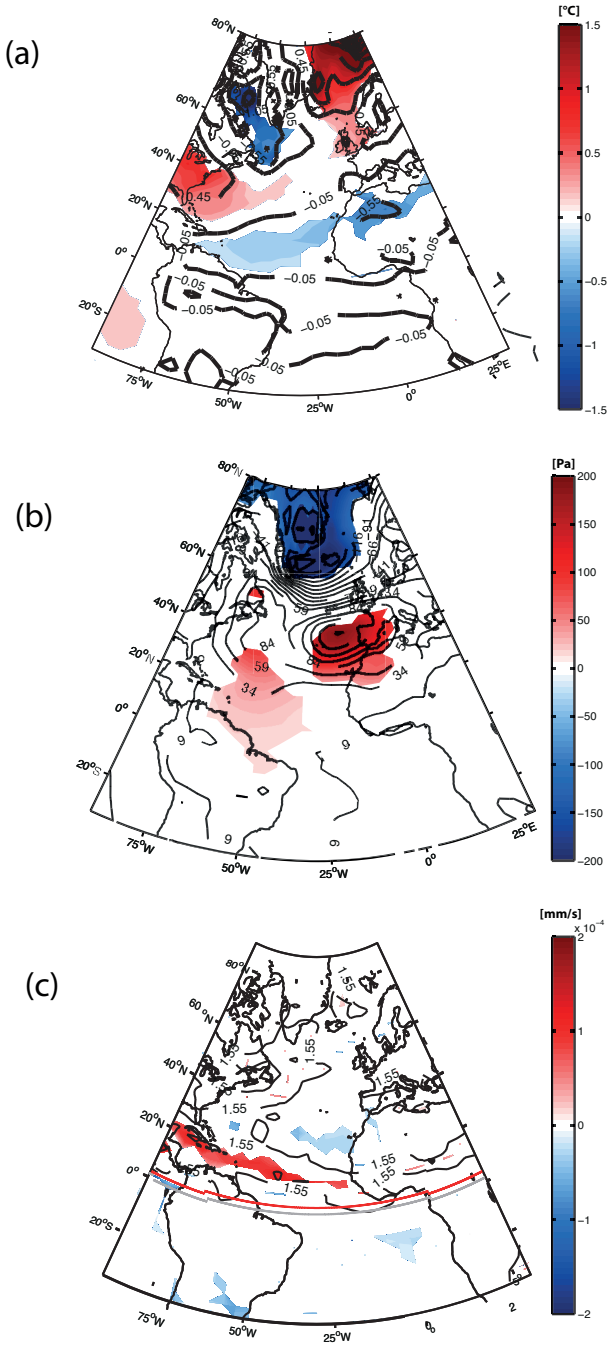

Figure 4.10: Same as Figure 4.6 but for (a) winter SAT (°C), (b) winter SLP (Pa) and (c) September net precipitation (mm s^{-1}) also indicating ITCZ position averaged over all years (grey line) and over years corresponding to strong AMOC conditions (red line). Colours indicate where the null hypothesis of equal means is rejected at the 10% level.

Under the same strong AMOC conditions, lower SLP appears near the Icelandic Low, while higher SLP appears over the Azores (Figure 4.10b). This pattern resembles the NAO in a positive phase, possibly reflecting some oceanic influence on this leading atmospheric mode. In CHIME, strong AMOC conditions therefore seem to be associated with a positive phase of the NAO. This NAO-like pattern is consistent with the NAO-like response to the AMOC intensification identified by Mignot and Frankignoul (2010) in the IPSL-CM4 model, although the sensitivity of SLP to changes in the AMOC in CHIME is about three times higher.

While few significant precipitation anomalies appear under strong AMOC conditions, some notable changes develop over the western tropics of the North Atlantic, with positive anomalies of up to 20 cm yr^{-1}, suggesting a northward shift of the ITCZ (Figure 4.10c), probably as a consequence of the tropical-subtropical SST gradient that accompanies strong AMOC conditions (Figure 4.6). For a given year, the ITCZ position has been defined as the latitudinal position at which September precipitation reaches its maximum in the central Atlantic (i.e. at about 30°W, similar to Biasutti et al. 2006). We can see that the ITCZ position is indeed about 2.2° further north (red line) than the average position (grey line), which corresponds to a northward shift of about 230 km. With stronger precipitation expected north of the Equator, freshwater anomalies are expected to develop locally. A similar relationship between displacement of the ITCZ and lower frequency (centennial) variability of the AMOC has also been identified in HadCM3 by Vellinga and Wu (2004); however, in that study the northward shift of the ITCZ is caused by a cross-equatorial SST gradient, whereas in our case it seems to be associated with a northern tropical-subtropical SST gradient (see Figure 4.6).

4.4 Physical mechanisms

4.4.1 Relation of AMOC to convective activity and density anomalies

If we examine how convective indices (as defined in *Sect. 3.1.3*) evolve over time in both the Labrador and GIN Seas (Figure 4.3b, red and blue lines, respectively), an anti-phase relationship is clear, as already mentioned in *Sect. 4.2.2*. The maximum correlation coefficient of -0.7 is obtained for a slight lead, by 1 year, of convection in the Labrador Sea over that in the GIN Seas (Figure 4.11). Correlation of these two convective indices with the PC1 of AMOC shows strong statistically significant relationships (Table 4.1); the Labrador (GIN) Sea(s) has a maximum (minimum) correlation coefficient of about 0.9 (-0.7) with the AMOC, when the latter lags by about 2 years (1 year). Note that the correlation is negative in the GIN Seas where it is positive in the Labrador Sea; an increase in MLD in the Labrador (GIN) Sea(s) is therefore associated with an increase (decrease) of the AMOC, 2 years (1 year) later.

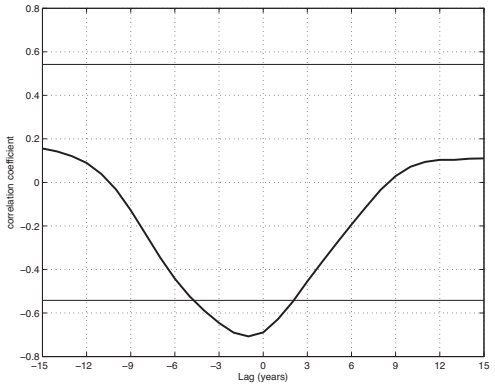

Figure 4.11: Lagged cross-correlations between the 10-year moving average winter MLD in the Labrador and GIN Seas (positive lags for the GIN Seas leading the Labrador Sea); horizontal black lines correspond to the 95% confidence limit for zero correlation.

In addition, if we examine how winter surface potential density (hence static stability) is spatially correlated (instantaneously) to AMOC fluctuations, the strongest correlations occur in both the Labrador and GIN Seas (Figure 4.12). Correlations between winter surface density averaged over these two regions and AMOC fluctuations are very similar to those with the convective indices; surface density in the Labrador (GIN) Sea(s) is indeed strongly correlated (anti-correlated) with the AMOC intensity, with an average correlation coefficient of 0.86 (-0.83) (Table 4.1). There is therefore evidence that in CHIME, AMOC fluctuations are principally related to surface density in the Labrador Sea, reinforcing the suggestion that the first mode of AMOC variability (EOF1) is directly influenced by the convective activity in the Labrador Sea. Note that the significant correlations with the northern tropics (although weakest than in the high-latitudes) suggest that this region also plays an important role in controlling AMOC fluctuations (as confirmed later).

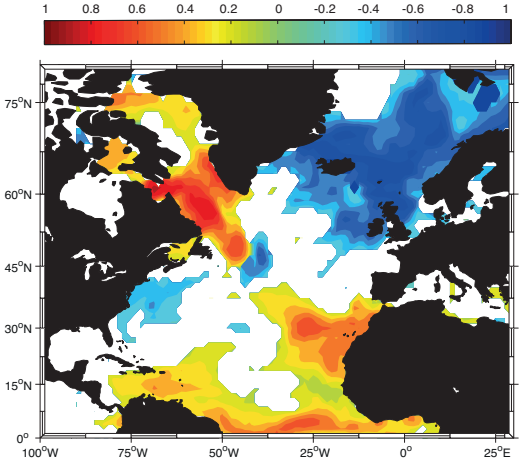

Figure 4.12: Instantaneous correlation map of 10-year moving average of winter surface density and PC1 of AMOC. Blank areas are not statistically significant at the 95% confidence level.

In summary, we have shown that surface density in the Labrador (GIN) Sea(s) is strongly correlated (anti-correlated) with AMOC fluctuations and explains about 64% of the AMOC variance. Convective activity in the Labrador and GIN Seas in CHIME therefore varies in anti-phase; an increase in surface density in the Labrador (GIN) Sea(s) is associated with an increase (decrease) in the AMOC strength. This result is consistent with the opposite signs of EOF1 of the AMOC streamfunction, at the latitudes of Labrador and GIN Seas, seen in Figure 4.3a. In the following section, we therefore investigate factors influencing surface density in the two convective regions.

4.4.2 Relative roles of temperature and salinity variability in driving density fluctuation

Figure 4.13 shows the influence of winter SSS and SST on winter surface density fluctuations in both convective regions. In the GIN Seas, surface density is strongly anti-correlated with SST with a maximum instantaneous correlation of -0.93 (grey dashed line). A decrease in SST in the GIN Seas will therefore increase surface density in this region, while the role of SSS is negligible (grey solid line). In the Labrador Sea, by contrast, surface density is significantly correlated with SSS, with a maximum correlation of 0.8 when this latter leads by 3 years (black solid line). A decrease in SSS in the Labrador Sea will therefore most effectively decrease surface density in this region 3 years later, while in the meantime the role of SST is largely negligible (dashed black line).

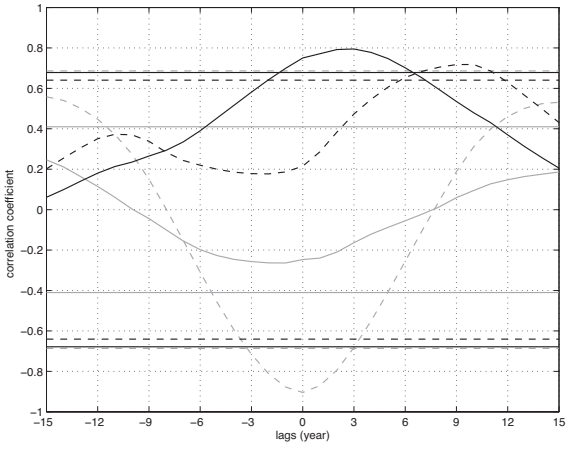

Figure 4.13: Lagged cross-correlations of 10-year moving average between winter SSS (solid lines) / SST (dashed lines) and winter surface density in the Labrador Sea (black lines) / GIN Seas (grey lines). Horizontal lines correspond to their respective 95% confidence limit for zero correlation.

Figure 4.14 shows the extent to which properties in these two convective regions are connected. Although both SST and SSS do not seem to be individually connected (see both dashed and solid grey lines), densities are significantly anti-correlated with a

maximum coefficient of about -0.70 (black solid line) at no lag. This anti-correlation is again consistent with results from *Sect. 4.4.1.* This significant relationship between densities in these two convective regions exists despite the different mechanisms that seem to control them. Therefore we can expect that the process that controls the SSS in the Labrador Sea is anti-correlated to what causes changes in the SST in GIN Seas.

In summary, surface density changes in the Labrador Sea are salinity-dominated, while they are temperature-dominated in the GIN Seas. Different mechanisms are therefore likely to control surface density variability (with implications for the AMOC) in the two convective regions, although those mechanisms appear to be anti-correlated.

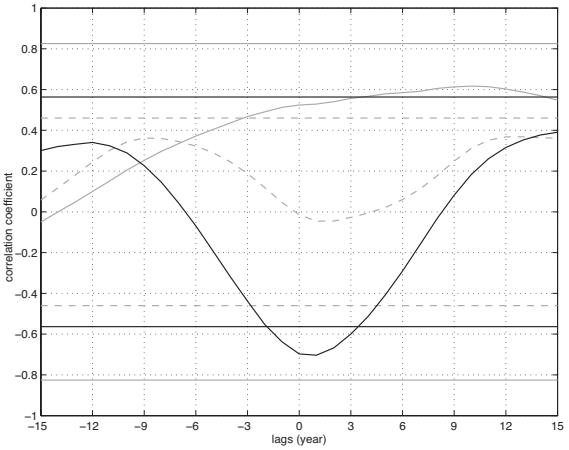

Figure 4.14: Lagged cross-correlations of 10-year moving average between winter SSS (grey solid line), winter SST (grey dashed line), and winter surface density (black solid line) between the two convection regions (i.e. both the Labrador and GIN Seas). Horizontal lines correspond to their respective 95% confidence limit for zero correlation.

4.4.3 Origins of anomalies in convective regions

In this section, we investigate the origins of SST and SSS anomalies in both the convective regions and the underlying oceanic and atmospheric processes.

4.4.3.1 Long-range preservation of salinity anomalies

Figure 4.15 shows maps of pentadal salinity anomalies from years 170 to 189 on three model layers in the upper branch of the AMOC, representative of the surface, and depth ranges around 90-150 m and 200-650 m. These maps reveal how a positive salinity anomaly present in the tropics during the pentad 170-174 develops on a 15-year timescale. At the surface, the anomaly spreads northward along the Guyana Current and through the Caribbean, into the western subtropical gyre, and eventually into the interior of the subpolar gyre (Figure 4.15a). This spreading is also evident at depth, where

the anomaly reaches the deep convection regions after about 15 years (Figure 4.15b,c). This is evidence for long-range preservation of salinity anomalies, en route from the tropics to the high latitudes, on a timescale of about 15 years.

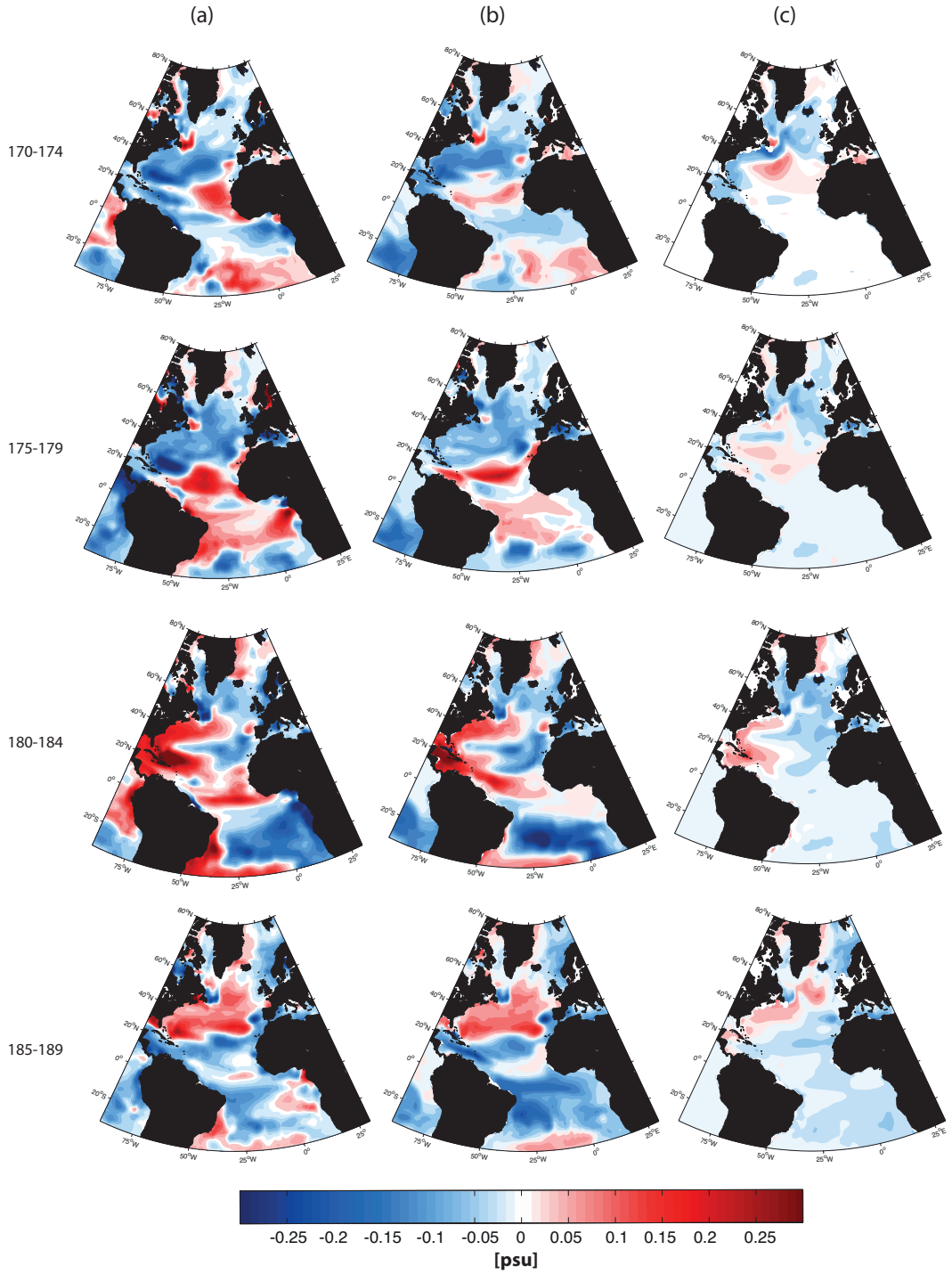

Figure 4.15: Pentadal anomalous salinity maps from year 170 to 189 on three model layers: (a) layer 1 (surface, constant-depth layer everywhere), (b) layer 9 (σ_2=34.10 kg m^{-3}, varying between about 90-150 m depth, non-isopycnic beyond 25°N), and (c) layer 14 (σ_2=36.05 kg m^{-3}, varying between about 200-650 m depth, non-isopycnic beyond 50°N).

The mechanism linking tropical and convective regions likely plays a role in the reversal phase of the AMOC oscillation. It is noteworthy that the AMOC appears to strengthen from low latitudes (see Figure 4.5), suggesting an element of feedback as the salinity anomalies are also more rapidly advected northwards in the strengthening phase. As the AMOC dynamically evolves, transports start declining to the south, reducing the import of high salinity waters. Note that, this finding contrasts with several studies using the HadCM3 model where the reversal of the oscillation on multi-decadal timescales has been mainly attributed to anomalies originating from the high latitudes (e.g. Dong and Sutton 2005; Hawkins and Sutton 2007). Our finding is, however, consistent to some extent with Vellinga and Wu (2004), who showed that in HadCM3 the reversal oscillation is caused by anomalous advection of salinity anomalies from the tropics. But in their study, this happens on a centennial timescale rather than on a decadal timescale as identified in CHIME.

As previously shown in *Sect. 4.4.2*, salinity will predominantly affect surface density (with implications for the AMOC) in the Labrador Sea, while it does not directly affect density in the GIN Seas. Therefore, to obtain a better idea of how surface density in the Labrador Sea is correlated to salinity in the North Atlantic, linear lagged-correlation maps between salinity contributions to winter surface density in the Labrador Sea are analyzed (Figure 4.16). The earliest correlations with SSS anomalies appear in the tropical western Atlantic (originating either from there or from the South Atlantic) about 15 years before a positive density anomaly in the Labrador Sea. With an AMOC cycle in the period range of 15-30 years (*Sect. 4.2.1*), this 15-year lead time corresponds to half of the maximum identified period of the longer decadal mode. At this stage, most of the northern North Atlantic is fresher than normal, consistent with the AMOC being in a weak phase. These fresh conditions gradually diminish and give way to more saline conditions over subsequent years, and the implication is that it takes about 15 years for the tropical positive anomalies to advect to the subpolar sinking region. These maps clearly reinforce the notion of northward transport of salinity anomalies, as previously shown.

In summary, SSS in the high-latitude regions seems to be strongly correlated to tropical SSS anomalies about 15 years earlier. These tropical anomalies will therefore also affect surface density in the Labrador Sea 15 years later while it will not be the case in the GIN Seas, where surface density is SST-dominated. There is therefore evidence for a 30-year cycle related to convective activity in the Labrador Sea in the primary mode of AMOC variability (EOF1) to be associated with the northward transport of northern tropical SSS anomalies.

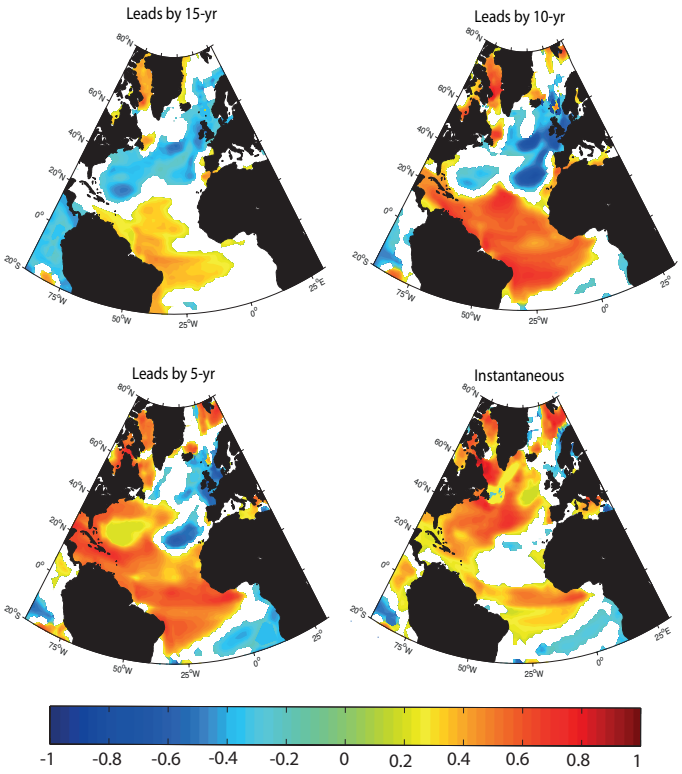

Figure 4.16: Cross-correlations maps between annual SSS contributions and winter surface density in the Labrador Sea when SSS leads. Blank areas are not statistically significant at the 95% confidence level.

4.4.3.2 Relative role of the NAO

As seen in Figure 4.10b, strong AMOC conditions in CHIME are associated with a positive NAO-like pattern. In both the Labrador and GIN Seas, winter surface density has a statistically significant relationship with the NAO index (as defined in *Chapter 2*), with a maximum positive correlation of 0.74 and negative correlation of -0.70, respectively, when the NAO leads by about 1-2 years (Table 4.2). The anti-phase behavior between the two convective regions in the model is once again underlined by these correlations of opposite sign. This result is consistent with observational studies, as convection in the Labrador Sea generally varies in phase with the NAO-index, while in the GIN Seas it varies out of phase (e.g. Hurrell and Dickson 2004). The above results therefore suggest that surface density in both the Labrador and GIN Seas is influenced by NAO fluctuations. This influence on AMOC variability has been extensively investigated. The balance of evidence from previous modelling (e.g. Delworth and Greatbatch 2000; Eden and Willebrand 2001; Bentsen et al. 2004; Guemas and Salas-Mélia 2008) and observational studies (e.g. Dickson et al. 1996; Curry et al. 1998) suggests that both heat flux changes and wind-stress variations are important means by which the NAO influences the AMOC, across a wide range of frequencies.

In CHIME, the influence of the NAO on surface density in both convective regions seems to act through different processes. Indeed, although the NAO fluctuation explains about 50% of SST variability in the GIN Seas (r $\approx$ 0.70), no significant relationship with SST has been found in the Labrador Sea (Table 4.2). There is also no significant correlation between the NAO and SSS in the latter region, although SSS has been found to be the dominant factor influencing surface potential density there (see *Sect. 4.4.2*). Although we found evidence for the NAO to influence surface density through its impact on local SST in the GIN Seas, other processes seem to be involved in the Labrador Sea. Below, we consider regional NAO influences in more detail.

Table 4.2: Maximum correlation coefficients between 10-year moving averages of the NAO index and several different variables. Bold correlations are statistically significant at the 90% confidence limits.

Variable	**Max. Correlation Coefficient**	**Lag (years)**
Winter surface potential density (Labrador)	**0.74**	NAO leads by $\sim 1-2$
Winter surface potential density (GIN)	**-0.70**	NAO leads by $\sim 1-2$
Winter SST (GIN)	**0.70**	NAO leads by ~ 2
Winter SST (Labrador)	0.46	NAO lags by ~ 10
Winter SSS (Labrador)	0.46	NAO leads by ~ 4
Winter heat fluxes (GIN)	-0.15	NAO leads by ~ 5
Winter heat fluxes (Labrador)	**-0.60**	Instantaneous
Winter freshwater fluxes (GIN)	-0.45	NAO lags by ~ 7
Winter freshwater fluxes (Labrador)	**-0.65**	NAO leads by $\sim 4-5$
PC1 of AMOC	**0.82**	NAO leads by ~ 1
PC2 of AMOC	**-0.60**	Instantaneous
Tropical Activity (TA)	**0.56**	NAO lags by $\sim 8-9$

First let us consider the influence of the NAO on surface density in the Labrador Sea. We have shown the NAO to have statistically significant relationships with buoyancy fluxes in the Labrador Sea; an increase in the NAO index leads to a decrease in local surface heat fluxes (stronger ocean cooling) near-instantaneously (r $\approx$ -0.60, Table 4.2) and to a decrease in freshwater fluxes (ocean freshwater loss) about 4-5 years later (r $\approx$ -0.65, Table 4.2). Because the NAO affects surface density earlier (after $\sim$1-2 years) than freshwater fluxes (after $\sim$ 4-5 years), the NAO-induced freshwater flux anomalies cannot be regarded as directly influencing SSS (and therefore surface density) to an important extent in the Labrador Sea. However, with its near-instantaneous correlation with heat fluxes, the possibility of the NAO to influence local SSS through ocean mixing processes

is not ruled out. In this scenario, the convective mixing associated with stronger surface heat loss will more extensively mix fresh surface waters with saline deep waters. In addition, the strong and significant anti-correlation found between SSS and heat fluxes in the Labrador Sea (r ≈ -0.72 when heat fluxes lead by ∼ 1 year, not shown) supports this mechanism.

In contrast to the case of the Labrador Sea, the NAO index does not correlate with surface heat and freshwater fluxes in the GIN Seas (Table 4.2). Therefore, the way by which the NAO affects local SST does not seem to be through its local impact on simultaneous heat fluxes. This can be further investigated by examining the covariance between anomalous SST and anomalous net surface heat flux ($\overline{T'Q'}$, noting that Q includes both radiative and turbulent heat fluxes) as shown in Figure 4.17. If covariances are examined for the winter season of all years of the analysis period, significant values are observed in four main regions of the North Atlantic. Negative values occur over the Labrador Sea/western subpolar gyre and over the Greenland Sea, whilst positive values occur over the Florida Current/Gulf Stream region and over the upwelling region off West Africa. This implies that, over the oceanic deep convection regions, surface heat flux tends to damp SST variability (reducing temperature variance: in other words, positive SST anomalies result in increased oceanic heat loss). Further south, at the eastern and western boundaries of the subtropical gyre, the opposite is true and heat fluxes tend to amplify SST variability.

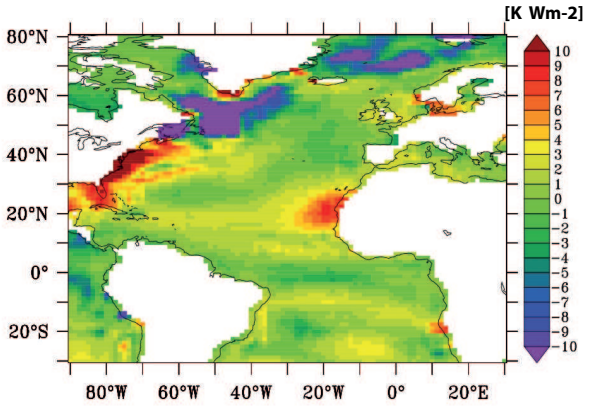

Figure 4.17: SST-Heat Flux covariance ($\overline{T'Q'}$) in K Wm^{-2} calculated for winter mean anomalies over years 81-192 of the model experiment.

However, the simultaneous correlation contains contributions both from the atmospheric response to the SST (i.e. damping in this case) and also from the SST response to the atmosphere (Schneider and Fan 2007). We have calculated lag correlations between winter SST and heat flux during the previous summer (Figure 4.18). There are positive values over the Greenland Sea, so we speculate that this may be a partial mechanism for the correlation between the NAO and SST in the GIN Seas, although other processes such as advection and mixing may also be involved. Such a link between the NAO and SST may be more fully explored using a method such as the Interactive Ensemble

Coupled Global Climate Model (Fan and Schneider 2012), but this lies beyond the scope of the present study.

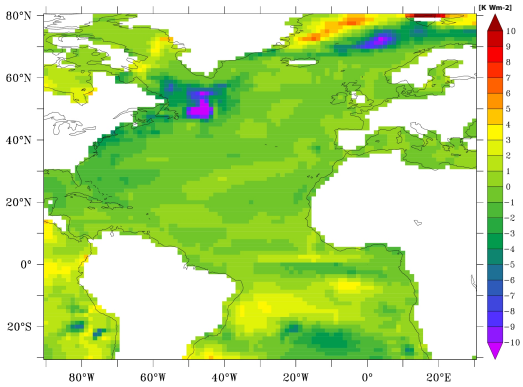

Figure 4.18: SST-Heat Flux covariance ($\overline{T'Q'}$) in K Wm^{-2} calculated for winter mean SST anomalies and heat flux anomalies during the previous summer.

In CHIME, we therefore find evidence that the NAO strongly influences surface density in both the Labrador and GIN Seas (with implications for the AMOC) on interannual timescale but through different mechanisms. In summary, an increasing NAO index will lead to an increase in surface density in the Labrador Sea about 1-2 years later through a local (indirect) influence on SSS. By driving anomalous heat fluxes, the NAO forces variation of Labrador SSS through ocean mixing processes, and subsequently variations of the AMOC (as SSS is the dominant factor controlling surface density in this region). Meanwhile, an increasing NAO index will lead to a decrease in surface density in the GIN Seas about 1-2 years later through a local influence on SST. Processes other than the direct impact of the NAO on heat fluxes, seem to control these local SST anomalies; the lagged response of surface heat fluxes (as discussed earlier) or the mechanical action of the NAO-induced wind (e.g. Pickart et al. 2003; Mignot and Frankignoul 2010) are regarded as plausible candidates. Note that a majority of previous modelling studies (e.g. Delworth and Greatbatch 2000; Bentsen et al. 2004) showed that the link between the NAO and AMOC is via the restricted area of the Labrador Sea. This differs from our study, where a link between the atmosphere and the AMOC includes a statistically-significant relationship between the NAO index and surface density in the GIN Seas. This result however supports the finding of some observational studies, such as Dickson et al. (1996), Belkin et al. (1998), and Alekseev et al. (2001), that emphasize the importance of the GIN Seas in explaining the influence of the NAO on AMOC fluctuations.

The second mode of AMOC variability in CHIME, that we attribute to the interannual anti-phase variability related to convective activity in the Labrador Sea and the GIN Seas (see *Sect. 4.2.2*), thus seems to be associated with a local influence of the NAO on surface density in these two regions. The statistically significant correlation of -0.60 found between the NAO index and PC2 of the AMOC supports the above statement (Table 4.2). The implication is that a large part of the variability of the AMOC, being

driven by the NAO, is a passive response to intrinsic internal atmospheric variability, rather than being part of a coupled ocean-atmosphere mode, and that this passive response to the atmosphere is associated mainly with the Labrador Sea. This is consistent with similarity of the AMOC PC1 power spectrum to that of red noise. However there is enhanced power in 15-30 year periods and we argue that this is due to advection of salinity anomalies from the tropics (earlier *Sect. 4.4.3.1*) and links between the position of the ITCZ and the NAO (next *Sect. 4.4.3.3*).

4.4.3.3 A link between tropical activity and NAO

In addition to the NAO-related mechanism affecting surface density in the GIN Seas, the close link between the convective activity in this latter region and the PC1 of the AMOC (see *Sect. 4.2.2*) also suggests the existence of a decadal-timescale mechanism affecting GSW variability. With evidence from previous studies that the North Atlantic climate variability is affected by tropical Atlantic ocean-atmosphere interaction (e.g. Rajagopalan et al. 1998; Okumura et al. 2001; Terray and Cassou 2002), we propose that the NAO and tropical activity are connected on a decadal timescale in our model.

We characterize the tropical activity (TA) in the Atlantic as the averaged September SSS over the northern tropical Atlantic (reflecting the northward shift of the ITCZ under strong AMOC conditions, leading to the development of freshwater anomalies in the northern tropics). In support of the above hypothesis (for an existing link between the tropics and the high latitudes in the model), TA is indeed statistically correlated with NAO variability with a maximum correlation coefficient of about 0.56 when TA leads by 8-9 years (Table 4.2). Although the mechanisms behind such a link still require clarification, this significant relationship suggests that the anomalous shift of the ITCZ affects the high latitude atmosphere (more specifically the NAO) about 8-9 years later, coincident with a decrease in surface density in the Labrador Sea and a decrease in SST (and hence increase in surface density) in the GIN Seas. This teleconnection between TA and NAO is consistent with previous studies (cited earlier).

In addition to the long-range preservation of SSS anomalies originating from the tropics and affecting LSW variability, the decadal cycle related to both LSW and GSW variability identified in the primary mode of AMOC variability (EOF1) therefore seems to be associated with mechanisms, still not clearly identified, that connect tropical activity to the NAO. The strong significant correlations found between the PC1 of the AMOC and both TA (r=0.75, Table 4.1) and the NAO (r=0.82, Table 4.2) support the above statement. With a lead-time of about 8-9 years, we note that this connection between the tropics and the high latitudes corresponds to just over half of the identified minimum period of the primary decadal mode of the AMOC (in the range 15-30 years).

4.5 Summary and discussion

This first study of natural variability in CHIME follows an initial study of the spinup and the equilibrium state in comparison with HadCM3 (Megann et al. 2010). The following summary and discussion covers two aspects of the study: (i) the characteristics of a strong AMOC state (prerequisite for understanding mechanisms behind decadal AMOC fluctuations); (ii) the processes and lead/lag timescales implicated in the decadal variability of the AMOC.

4.5.1 Fingerprints of a strong AMOC state

Strong AMOC conditions are associated with warmer SST over most of the North Atlantic from the subtropics to the high-latitudes, and cooler SST over the northern tropics. Despite being further north than other studies, this SST pattern (i.e. a northern tropical-subtropical gradient) reflects an AMO-type response in good agreement with previous studies (e.g. Sutton and Hodson 2005; Frankcombe et al. 2010). In sub-surface layers, temperature anomalies translate westwards and downwards in the subtropics, on decadal timescales. While this behaviour is also characteristic of the AMO (Frankcombe et al. 2008, 2010), we find that our index of mode-1 AMOC variability leads the AMO index by 2-3 years, suggesting that, in CHIME at least, sub-surface temperature variability is a response to AMOC variability rather than a cause. Accompanying sub-surface salinity anomalies exactly compensate for the temperature anomalies in isopycnic layers, and the small perturbations in horizontal density gradients (in the subtropics) that are associated with layer thickness anomalies do not appear to lead AMOC anomalies.

Strong AMOC conditions tend to coincide with warm SAT from the subtropics to the high latitudes, except in the Labrador Sea where SAT becomes cooler. Over land, parts of northern Europe and central North America also become warmer. Coincident with the strong AMOC are also a positive-state NAO and maximum northward shift of the ITCZ. Associated with the positive NAO are positive surface heat flux anomalies (reduced ocean heat loss) which reinforce higher SST in the GIN Seas, helping to suppress convection (see *Sect. 4.5.2*). With northward displacement of the ITCZ and associated net surface freshwater influx (P-E $>$ 0), a negative anomaly develops in surface salinity across the tropics.

4.5.2 Key processes implicated in decadal AMOC fluctuations

Power spectral analysis reveals an enhanced power at a decadal timescale in CHIME, for periods in the range 15-30 years. Overall, the main modes of variability are described by changes associated with primarily a decadal cycle and secondarily an interannual

cycle related to convective activity in the Labrador and (inversely) the GIN Seas. Accompanying decadal AMOC variability are anomalies in basin-scale hydrography and air-sea heat fluxes at key locations. Associated variability in the atmosphere includes the NAO (varying in phase with the AMOC) and the ITCZ (migrating north/south with a strengthening/weakening AMOC).

An out-of-phase relationship in MLD between sinking regions indicates that strong sinking in the Labrador Sea is coincident with weak sinking in the GIN Seas, associated with positive and negative surface density anomalies respectively. Positive density anomalies in the Labrador Sea are associated with anomalously high surface salinity, while negative density anomalies in the GIN Seas are associated with anomalous surface warmth. Therefore, SSS (SST) anomalies in the GIN (Labrador) Seas are negligible compared to SST (SSS) in affecting surface density, and hence AMOC fluctuations. The linkage of the Labrador Sea and the GIN Seas with the AMOC differ substantially between models, but is in good agreement with Medhaug et al. (2011) using the isopycnic-ocean Bergen Climate Model.

Surface salinity in the Labrador Sea (and hence surface density) appears to be associated with the northward spreading of anomalies originating from the tropical Atlantic around 15 years earlier. Tropical SSS anomalies may have formed locally through air-sea interaction as a consequence of the ITCZ shift, leading to anomalous surface freshwater gain in the northern tropical Atlantic under strong AMOC conditions. Although a significant shift of the ITCZ has been identified in the model, other processes responsible for the development of SSS anomalies are not to be excluded such as changes in the Amazon River outflow, or inter-basin exchange (Biastoch et al. 2008, 2009). In addition, there is evidence for the anomalous shift of the ITCZ affecting the high-latitude atmosphere, more specifically the NAO about 8-9 years later. Such a decadal teleconnection between the tropical Atlantic and the NAO has already been identified in the observations. A strong tropical-extratropical link was indeed suggested by Rajagopalan et al. (1998) who emphasizes a strong broadband coherence in the 8- to 20-year period between the NAO and the tropical Atlantic cross-ITCZ SST difference. Although mechanisms behind such a link remain largely unclear, Tourre et al. (1999) emphasizes a timescale defined by the ability of upper ocean anomalies to persist, even after the atmospheric anomalies decay, and during which ocean-atmophere interaction is maintained on the Atlantic basin-scale. The 8-9 year timescale found in CHIME suggests a preference for a teleconnection via the ocean rather than the atmosphere, but a mixture of both oceanic and atmospheric teleconnections cannot be ruled out. Indeed both teleconnections have already been identified in modulating, for example, the tropical Pacific decadal variability (Liu et al. 2002). The decadal teleconnection between the tropical Atlantic and the NAO identified in CHIME needs to be clarified by further studies. As a consequence of this teleconnection, changes in NAO forcing will first near-instantaneously affect heat fluxes in the

Labrador Sea, which in turn will affect (increase) local SSS (and hence surface density) through ocean mixing processes. In the meantime, NAO will near-instantaneously impact SST in the GIN Seas, although the precise mechanism for this is still unclear. Air-sea fluxes, related to opposite phases of the NAO, are therefore contributing to the convection in the Labrador Sea and in the GIN Seas, in good agreement with Medhaug et al. (2011). To summarise, in a positive (negative) NAO state, coincident with strong (weak) AMOC conditions, orientation of the Atlantic storm track will favour warmer (colder) conditions in the GIN Sea and saltier (fresher) conditions in the Labrador Sea.

In CHIME, we therefore find evidence for surface density in both the Labrador Sea and the GIN Seas to be influenced by the tropical activity about a decade earlier but through different mechanisms. The fact that one unit change of surface density in the GIN Seas has stronger impact on AMOC fluctuations than one unit change in the Labrador Sea (about 14 Sv kg^{-1} m^3 and 7 Sv kg^{-1} m^3, respectively) and that the Labrador Sea has in contrast a dominant influence on AMOC strength (as shown by their positive correlations) suggests that variability in the latter region is higher than in the GIN Seas. To summarize, a teleconnection (still to be clarified) may link ITCZ changes to the NAO, affecting the surface density in the GIN Seas, while both tropical-extratropical teleconnection (hence the NAO) and slower ocean advection (of tropical SSS anomalies) affect surface density in the Labrador Sea. Which of these processes is more important in controlling decadal AMOC variability? Our results show that the first principal component of the AMOC has a slightly stronger correlation with the NAO index (r=0.82, Table 4.2) than the northern tropical-subtropical SST gradient (resulting in a shift of the ITCZ) (r=0.79, Table 4.1), suggesting that the NAO-related mechanism is slightly dominant and that the latter leads the AMOC by about 1 year. We also emphasize that, although the processes described above contribute to AMOC variability on decadal timescales, a large part of the variability of the AMOC is therefore likely to be a passive response to intrinsic internal atmospheric variability (in common with most climate models, e.g. Delworth et al. 1993; Dong and Sutton 2005), rather than being part of a coupled ocean-atmosphere mode (e.g. Timmerman et al. 1998). We argue that the enhanced power in 15-30 year periods is due to advection of salinity anomalies from the tropics and links between the tropical Atlantic and the high-latitude atmosphere.

4.6 Conclusions

The sequence of events based on the range of statistical evidence presented in previous sections allows us to schematically summarize the main processes implied in about one half of a decadal-timescale AMOC primarily driven by the Labrador Sea cycle in CHIME, as shown in Figure 4.19. Strong AMOC conditions are accompanied by the development of freshwater anomalies in the northern tropics (as a consequence of the northward shift of the ITCZ). Accompanying this variation of tropical SSS, concurrent changes

in the tropical atmosphere lead to a decrease in the NAO about 8-9 years later, via a teleconnection that still needs to be clarified. This weaker NAO decreases surface density (and hence SSS) in the Labrador Sea, through reduction in surface heat loss and the convective mixing of fresh surface and saline deep waters. Simultaneously, surface density will increase in the GIN Seas, due to decreased SST, possibly through the mechanical action of the NAO-induced wind (Pickart et al. 2003; Mignot and Frankignoul 2010) or a lagged response to increases in surface heat loss. Meanwhile, northward transport of freshwater anomalies from the tropics to the high-latitudes, via the Gulf Stream, further decreases SSS in the Labrador Sea and hence surface density in this region. Associated with increased (decreased) surface density in the GIN (Labrador) Seas, the AMOC is now in a weak state.

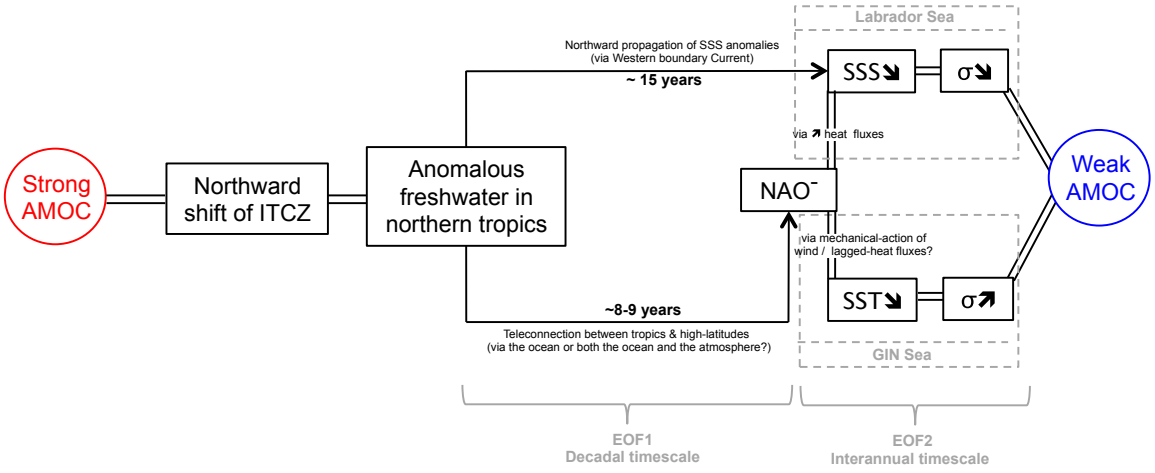

Figure 4.19: Simplified schematic of mechanism responsible for one half of the decadal AMOC cycle primarily driven by the Labrador Sea variability in CHIME. Double lines are used when the timescale of the interaction is near-instantaneous (< 3 years).

The long-range links between the tropical Atlantic activity and subsequent convective activity in both the Labrador and GIN Seas regions in CHIME suggest that European climate is potentially predictable on substantially longer timescales than the 5-10 years typically asserted from experiments with climate models that feature an orthodox z-level coordinate ocean component (e.g. Latif et al. 2006). The evaluation of the predictive skills of this hybrid-coordinate ocean component model will therefore be the subject of *Chapter 6*. As already mentioned in the previous chapters, predictability experiments with the well-established IPSL climate model have been carried out prior to similar such study with CHIME. The results of these experiments are the subject of the next chapter.

Chapter 5

Decadal predictability of the AMOC and climate in IPSL-CM5A-LR

Results from this chapter have been accepted for publication in Climate Dynamics (SI: IPSL & CNRM climate models for CMIP5) as: *Persechino A, Mignot J, Swingedouw D, Labetoulle S, Guilyardi E (2012) Decadal Predictability of the Atlantic Meridional Overturning Circulation and Climate in the IPSL-CM5A-LR model. Clim Dyn, doi: 10.1007/s00382-012-1466-1.*

5.1 Aim of study

Although a considerable number of studies have addressed decadal predictability of the climate system in the last few years due to the impetus of the "near-term" CMIP5 protocol (Taylor et al. 2009), the assessment of decadal climate predictability remains unclear as the level of predictability differs from one study to another (e.g. Meehl et al. 2009). This may be subject to model differences and uncertainties, as well as differences in the experimental protocol and metrics used. It is therefore important to carefully define predictability and to use several metrics to better understand the limit and extent of predictable fields.

In this chapter, we explore the decadal predictability of the AMOC and associated oceanic and atmospheric fields as they are represented in the IPSL-CM5A-LR model (Dufresne et al. 2012) under pre-industrial control conditions, using both diagnostic potential predictability (DPP) and prognostic potential predictability (PPP) approaches. In the DPP approach, the predictability is analysed by decomposing the variance of a climate variable into a long timescale component considered as potentially predictable, and

an unpredictable noise component (see *Sect. 3.2.1.1*). The core of this approach relies on the 1000-year-long control integration of the IPSL-CM5A-LR model (see *Sect. 2.2.2*). In the PPP approach, the predictability is estimated prognostically, by re-running a climate simulation with slightly perturbed initial conditions (see *Sect. 3.2.1.2*). The core of this approach is a series of five "perfect ensemble" experiments using the same code as the IPSL-CM5A-LR control integration used in the DPP approach; each ensemble includes 10 members, started from slightly different initial conditions and integrated for 20 years (see *Sect. 3.2.2.2*). The spread and the correlation of the members of each ensemble are then evaluated to quantify the reproducibility and thus predictability of the simulated fields. We thus consider two deterministic measures: the Ensemble Spread (ES) and Ensemble Correlation (EC), previously described in *Chapter 3*. We explore the information given by both metrics, and consider that a variable is potentially predictable if it has a (low) statistically significant ES associated with a (high) statistically significant EC. As illustrated below, combining these two metrics might be too restrictive in some situations, and information given by ES or EC alone should not be neglected.

The aim of this study is to address the following questions: (i) Where do climate-related fields exhibit the strongest sensitivity to decadal AMOC fluctuations in the model? (ii) Are specific changes in the AMOC potentially predictable and which observations of the ocean state are likely to be of greatest value to constrain predictions? (iii) What is the predictability of the Atlantic climate and how is it related to low-frequency AMOC variability?

The control integration is analysed in *Sect. 5.2* to investigate the impact of decadal AMOC fluctuations on the Atlantic climate. In *Sect. 5.3*, the potential predictability of the AMOC is investigated using "perfect ensemble" experiments. *Sect. 5.4* addresses the potential predictability of climate and its link with decadal AMOC variability. A summary and discussion follow in *Sect. 5.5*, with concluding remarks in *Sect. 5.6*.

5.2 Fingerprints of AMOC variability

In the IPSL-CM5A-LR model, AMOC variability has been associated with a 20-year cycle described as an ocean-atmosphere coupled mode driven by the subpolar region, and involving deep convection in the Nordic Seas, at the southern tip of Greenland, and south of Iceland (Escudier et al. 2012). Prior to the study of potential predictability in the AMOC, the regional impacts of AMOC variability are investigated in the control integration. To do so, we use regressions of 5-year moving averaged surface temperature and precipitation onto the 5-year moving averaged AMOC index when this latter leads by 10 years (lags at which regression coefficients are the strongest, Figure 5.1). Despite some significant signals in the tropical Pacific, the main significant impacts are restricted

to the North Atlantic surrounding regions. We therefore concentrate on this basin in the following.

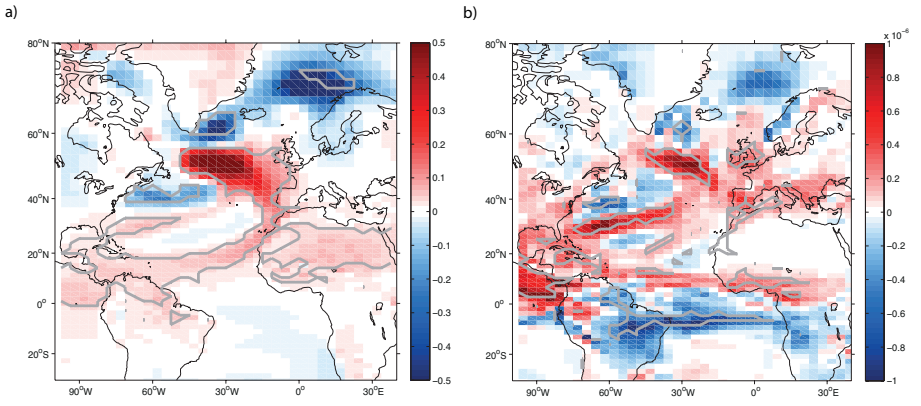

Figure 5.1: Lagged regression of the 5-year moving average (a) surface air (sea) temperature at ground (sea) level (°C Sv^{-1}), and (b) precipitation (mm day^{-1} Sv^{-1}) onto the 5-year moving average AMOC index at the lag where regression coefficients are the strongest (i.e. when the AMOC leads by 10 years). Statistical significance of regression values has been tested using Students *t*-test, and Quenouille (1952)'s method was used to calculate the effective degrees of freedom. The grey contour indicates 90% confidence level for zero correlation.

5.2.1 Impacts on surface temperature

Figure 5.1a shows that the AMOC impact on temperature at the decadal timescale is dominant over the ocean, and in particular north of the NAC. Anomalously strong AMOC conditions are associated with significantly warm SST anomalies in the subpolar gyre, in both the eastern and southern branch of the subtropical gyre, and cold SST anomalies along the eastern coast of Greenland, south of the Denmark Strait and in the Norwegian Sea, with a typical amplitude of about 0.5°C Sv^{-1}. SST anomalies from the tropics to the subpolar regions in the Northern Hemisphere remain predominantly positive in contrast to the Southern Hemisphere where there are some hints of negative anomalies. Consistent with this result, Figure 5.2 that shows the time series of surface temperature averaged over the mid- to subpolar Atlantic sector, also shows clear evidence for extreme warm temperatures over this region about 6 years after the extreme AMOC event of 2071 (identified in Figure 3.4). Under anomalously strong AMOC conditions, an inter-hemispheric SST dipole pattern (although weak) therefore seems to emerge, as also identified in HadCM3 (Vellinga and Wu 2004). This pattern is also consistent with the AMO pattern in IPSL-CM5A-LR (Gastineau et al. 2012) as well as in an earlier version of the IPSL model (IPSL-CM4, Msadek and Frankignoul 2009). This suggests that as in other models (Kushnir 1994; Kerr 2000; Delworth and Mann 2000) an AMO-type response is associated with decadal AMOC fluctuations in IPSL-CM5A-LR. The SST pattern, identified in the latter, also resembles the observed AMO (e.g. Sutton

and Hodson 2005), except for the localised significant negative anomalies in the high-latitudes of the North Atlantic. This result is consistent with previous modelling studies that found decadal AMOC fluctuations to be associated with an SST pattern resembling the observed AMO (Kushnir 1994; Kerr 2000; Delworth and Mann 2000).

As indicated above, decadal AMOC fluctuations have a much weaker impact over land. Anomalously strong AMOC conditions tend to be followed by significantly warmer conditions in Central America, subtropical Africa, and a few marine-influenced regions of Western Europe (with amplitude of anomalies up to $+0.1°C\ Sv^{-1}$). Such links over land are consistent with previous studies (e.g. Pohlmann et al. 2004).

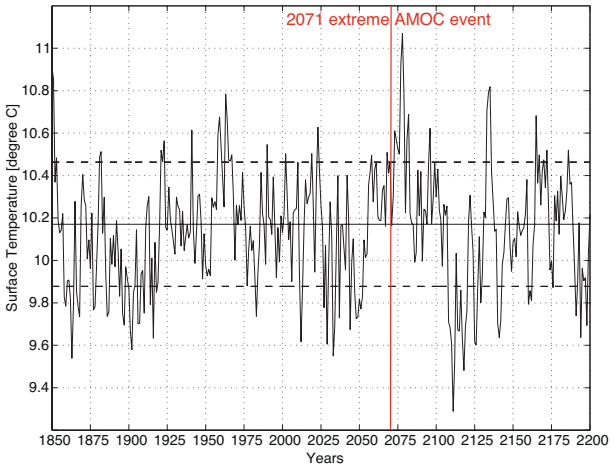

Figure 5.2: Time series of surface temperature averaged over the mid- to sub-polar Atlantic sector (30°N-60°N/70°W-0°) from 1850 to 2200. The 1000-year mean is shown as the horizontal line and the corresponding standard deviations are shown as the dashed lines

5.2.2 Impacts on precipitation

In terms of precipitation, the tropical Atlantic Ocean clearly shows strong sensitivity to decadal AMOC fluctuations (Figure 5.1b): stronger AMOC conditions are associated with significantly drier (wetter) southern (northern) tropics. This suggests a northward shift of the ITCZ over the tropical Atlantic, as also identified in other climate models (e.g. Vellinga and Wu 2004; Swingedouw et al. 2009; Persechino et al. 2012a). The ITCZ shift is also seen to extend to the Pacific Ocean, consistent with Xie et al. (2008) and Swingedouw et al. (2009). The strong sensitivity of tropical precipitation to AMOC fluctuations probably happens through the influence of SST anomalies identified earlier (Figure 5.1a), consistent with the well-established strong coupling between the ocean and the atmosphere in this region (e.g. Chiang et al. 2008 and references therein). Significant precipitation anomalies are also found from the subtropics to the high-latitudes, largely resembling the corresponding SST anomalies.

The oceanic precipitation signal is again seen to leak over the adjacent continental areas, as for temperature. At mid-latitudes, strong AMOC conditions are in particular associated with significantly wetter conditions over the British Isles (Figure 5.1b). The signal identified over the tropical Atlantic also extends over the adjacent continents with significantly drier (wetter) conditions in the southern (northern) tropical regions of both America and Africa when the AMOC is increasing. This is consistent with several studies that already investigated the link between decadal modulation of Sahelian rainfall, ITCZ shift and the AMO (Folland et al. 1986; Rowell et al. 1995; Zhang and Delworth 2006; Knight et al. 2006; Ting et al. 2009).

In view of these major climatic impacts of the AMOC, an important question remains whether AMOC fluctuations are potentially predictable. The ability to predict such fluctuations is now investigated using the PPP approach as described in *Sect. 3.2.1.2*.

5.3 Potential predictability of AMOC fluctuations

Figure 5.3 shows the AMOC trajectories of each individual member, for each start date, together with the ensemble mean. At first sight, all ensemble means follow the initial control run relatively well, although with less variability due to the averaging effect. In particular, the extreme AMOC event at year 2071 is relatively well-captured (although underestimated in terms of amplitude) by both experiments starting 15 and 5 years before this peak.

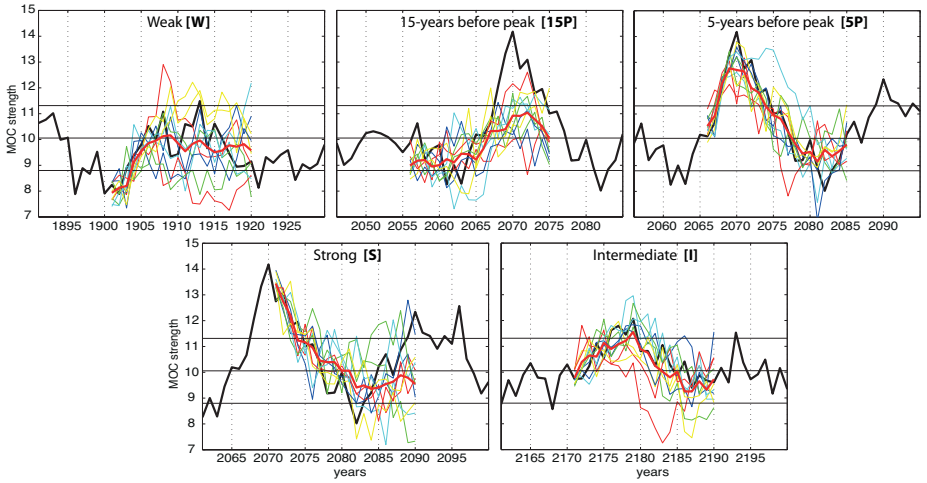

Figure 5.3: "Plumes" of maximum-annual mean AMOC between 20°N and 50°N from ensembles of the IPSL-CM5A-LR in which the initial conditions have been perturbed. Five ensembles are shown starting from different dates in the control simulation. The individual ensemble members are shown as coloured lines, the ensemble mean as the red thick line, and the control run as the thick black line. The middle horizontal black line is the mean AMOC, and both upper and lower horizontal black lines show standard deviations highlighting the range of variability of the MOC.

5.3.1 Are changes in the AMOC potentially predictable?

5.3.1.1 Comparing the level of predictive skills to different definitions of metrics

Figure 5.4 shows ES of the AMOC index as a function of lead-time up to 2 decades for each experiment and both M10 (in grey) and CS03 (in black) definitions (further details in *Sect. 3.2.1.2*). This figure confirms the relation of proportionality derived earlier between both definitions, with a factor of $\sqrt{\frac{2M}{M-1}}$ (M being the number of members). The last statistically significant lead-time before ES persistently exceeds the threshold is independent of the definition used, and represents the maximum lead-time of predictability as inferred from ES alone. Figure 5.5 shows EC computed between lead-time 1 year and varying lead-times, ranging 5 to 20 years (5 years corresponding to the minimum lead-time of predictability found from ES, Figure 5.4). EC has generally higher scores for M10 than for CS03. Indeed, the ensemble mean (used in M10) is smoother and holds some information from each member, allowing higher correlations than one to one correlations among members (as used in CS03). However, in most cases, when EC is statistically significant (or not), it is generally also the case for the other definition. Note two exceptions (experiments W and I). However, from a predictability point of view, the statistical significance of EC at the lead-time at which ES saturates (information given in Figure 5.4) is the same whichever the definition used. The main disadvantage of using EC_{CS03} is that too much weight could be given to an individual member that heavily diverges from the others, while EC_{M10} tends to average out extremes by the use of the ensemble mean. On the other hand, the latter can be seen as too lax as it involves a smoother baseline.

We showed that, overall, both definitions of EC and ES deliver similar messages, although EC_{CS03} seems to be slightly more severe than EC_{M10}. We therefore prefer to opt for the most cautious/severe definition, and will use the CS03 definition hereafter.

5.3.1.2 How far ahead is the AMOC potentially predictable?

Figure 5.6 shows a summary of results combining both ES_{CS03} (Figure 5.4, black line) and EC_{CS03} (Figure 5.5, black line) for the AMOC index. The predictive skill of each experiment is determined by the maximum lead-time at which ES saturates and its corresponding EC. Experiment S shows overall the highest PPP skill as its ES saturates at the longest lead-time and is associated with a high statistically significant EC (lower-right plot, Figure 5.6); this experiment suggests a limit of predictive skill for the AMOC index of about 13 years. This result is consistent with a simple stochastic assumption for example (e.g. Frankignoul and Hasselmann 1977; Frankignoul 1985), which would predict that when starting from an extreme AMOC value, we expect most

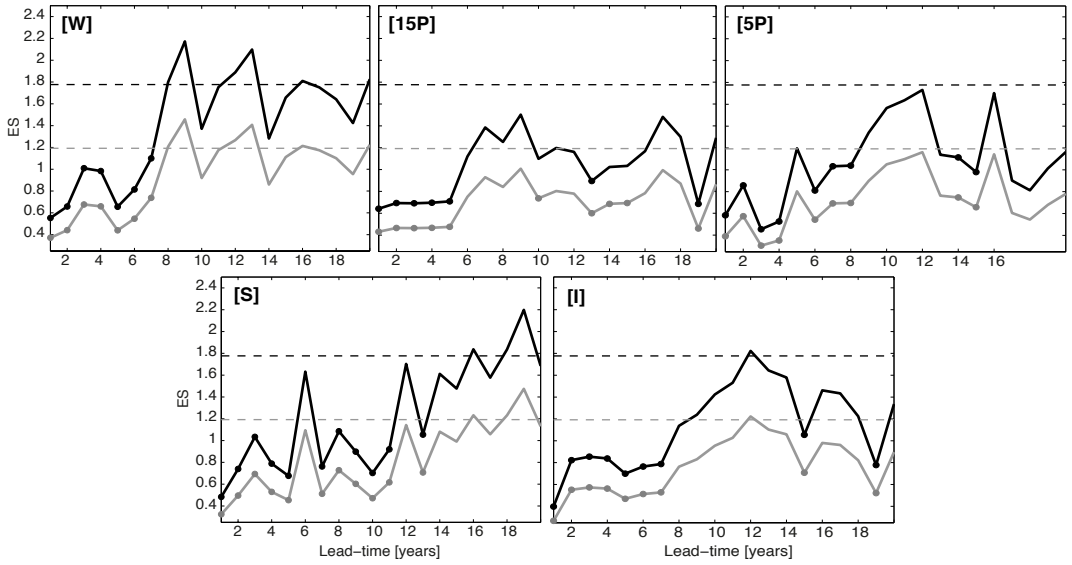

Figure 5.4: ES of AMOC index for each of the five ensemble experiments for M10 (grey line) and CS03 (black line) definitions for lead-time up to 20 years. The threshold at which ES saturates (implying no potential predictability) is shown as the black (grey) horizontal dashed line for CS03 (M10). Dots indicate that ES is statistically smaller than the corresponding threshold at the 95% level based on a F-test.

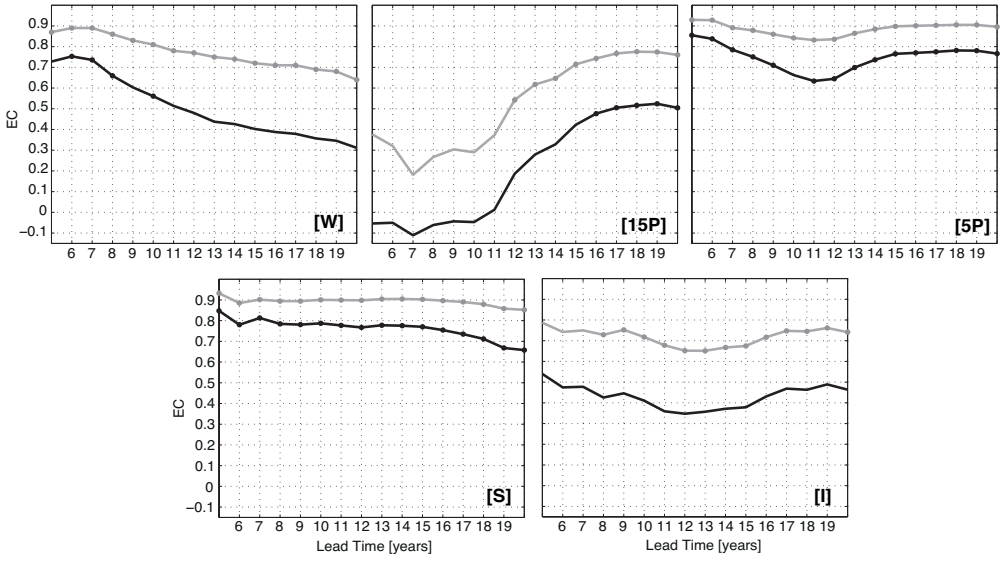

Figure 5.5: EC of AMOC index (as calculated by the Fisher transformation) for each of the five ensemble experiments for M10 (grey line) and CS03 (black line) definitions for lead-time from 5 to 20 years. Dots indicate that EC is statistically significant at the 90% confidence level using a one-tailed t-test.

of the members to take the same direction towards a neutral state, thereby yielding high predictability. Nevertheless, the predictability timescale found here is longer than the persistence time estimated from the AMOC index autocorrelation function in a red noise framework (e.g. Frankignoul et al. 2002) which amounts to 4-5 years (not shown).

This indicates that a simple autoregressive model provides low predictability for AMOC index behavior. Once back towards neutral (close to the mean) conditions (after about 13 years), experiments S indeed loses its predictive skills with a continually growing (decreasing) ES (EC) with lead-time. Similarly to S, experiment W is expected to have a similar predictive skill since it starts from an extreme state (more than one standard deviation σ away from the mean, Figure 5.3). Although the EC associated with the maximum lead-time is statistically significant and high (0.74), ES however saturates twice as rapidly as in experiment S (at about 7 years, Figure 5.6). This lower PPP skill could be explained by its starting date not being in such an extreme state as S; indeed, the starting value is superior (inferior) to 2σ in S (W). Alternatively, it might come from the dynamics itself, suggesting that the AMOC has more PPP skills when it starts from an anomalously strong overturning than from a weak one or a value close to its mean. The fact that the initial state corresponding to an anomalously strong AMOC is more predictable than those corresponding to a weak AMOC is in good agreement with several previous studies (e.g. Collins and Sinha 2003; Collins et al. 2006a). Consistent with the idea that extreme states are associated with better predictive skills, both experiments I and 15P that start from neutral mean states have no predictive skills (as defined in *Sect. 3.2.1.2*); indeed EC is not significant for lead-times of 5 to about 15 years (Figure 5.6). However, ES saturates after 5 and 7 years respectively. Based on ES only, this could still indicate a weak predictability. The above results suggest that predictability depends on the AMOC initial state, although the limited number of experiments limits the robustness of this claim.

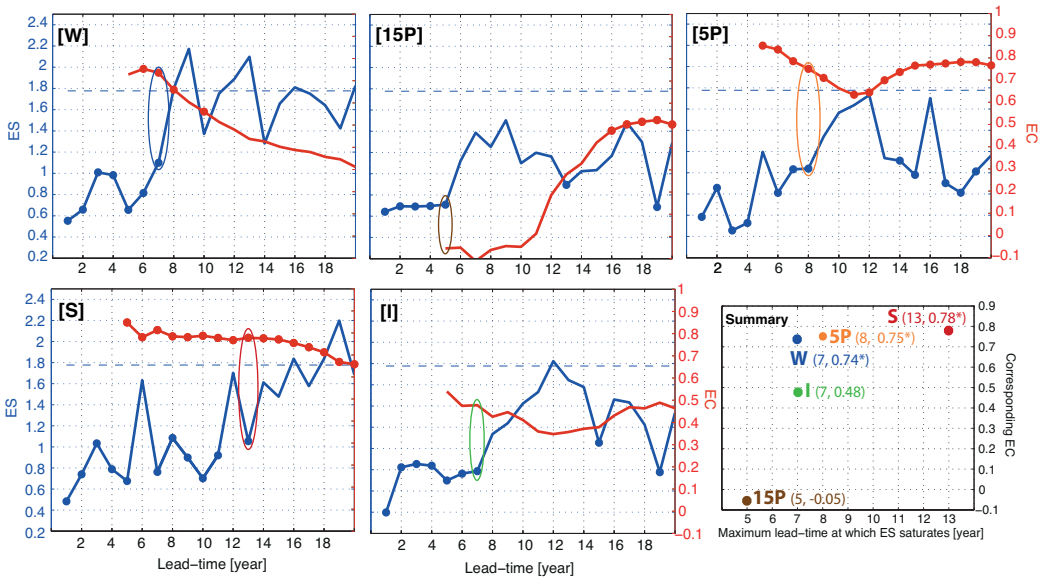

Figure 5.6: Plots of results from CS03 definition showing ES (blue line) and EC (red line) against lead-times for each of the five ensemble experiments. Dots indicate statistical significance at the 95% (90%) confidence level for ES (EC). The summary plot shows the maximum lead-time at which ES saturates with its corresponding EC (as indicated by the oval circles) for each experiment (statistically significant ECs at the 90% are marked with an asterisk).

Given the AMOC impact on climate (Figure 5.1), the ability of the model to predict an extremum such as the one of the year 2071 (Figure 5.3) could be of great interest. Such an ability is identified in experiment 5P, which shows the second highest predictive skills (after S) with a limit of predictive skill of about 8 years (that is after the peak has been captured, Figure 5.6). In contrast, strictly speaking, experiment 15P has no predictive skills (as defined in *Sect. 3.2.1.2*). Nevertheless, this experiment still succeeds in capturing the peak of the year 2071 as seen in the plumes in Figure 5.3, where most of the members exhibit a positive AMOC anomaly at 15 years lead-time. This feature is somewhat reflected in the statistically significant EC calculated for a lead-time longer than 15 years (i.e. when the peak is included). Although Figure 5.3 shows that the amplitude of the peak is not well reproduced, there is some evidence for the ability of the model to capture an extreme AMOC event up to 15 years in advance. Note here that, despite the fact that ES saturates very rapidly and is not associated with a significant EC, EC alone still gives useful information about this ability to capture a peak. This underlines the importance of considering each metric (ES and EC) separately in addition to their combined information, in order to identify interesting features such as extreme events.

By averaging the maximum lead-time at which ES saturates for the five ensemble experiments, we found an average saturation level reached after 8 years. Note, however, that at this lead-time, the average EC amounts to 0.51 which is not significant at the 90% level when considering the average number of degrees of freedom over each starting date. Indeed, Figure 5.5 and Figure 5.6 show that EC strongly depends on the starting date. For such a limited number of starting dates, it is thus of limited use for an estimation of the average predictive skill. It seems therefore reasonable to claim that, based on ES alone, the average predictive skills of the AMOC is of about 8 years in the IPSL-CM5A-LR model. Again, this lead-time is more than the persistence time of the AMOC index, confirming an important role of oceanic dynamics on the predictability of the AMOC.

Figure 5.6 also brings out some other interesting features worth pointing out. There is some evidence for both ES and EC not to be independent metrics; a decreasing (increasing) ES is generally associated with increasing (decreasing) EC. This claim is further supported in *Appendix A*. There is also some apparent return of predictive skills for both experiments 15P and 5P. There is, indeed, some evidence for ES returning below the saturation level and recovering statistical significant a few years after saturation, with corresponding EC which also recovers significance. Note that this increasing of EC is relatively small in 5P (<0.1), compared to 15P (>0.5); the reason for the significant increase in this latter is certainly due to its ability to capture the extreme AMOC event present in the second decade (at least in terms of its presence and its sign). Although this apparent "return" of skill has already been pointed out by several studies, its origin still remains unclear. For example, Newman et al. (2003) suggest that this reflects

variations of the actual noise rather than a true skill, while Hermanson and Sutton (2009) rather suggest that this might be a consequence of the use of a simple univariate measure to quantify predictability. Here, it is not to be excluded that this "return" of skill in the second decade could be related to the peak of energy at 20 years (as found in the control simulation, Escudier et al. 2012), which might increase correlation and then predictability for larger timescale. The origin of this phenomenon definitely merits further attention and should be the main focus of further studies.

5.3.2 An early warning system to predict extreme AMOC events?

Even though such events are rare and may be viewed as "surprises", providing an early warning system is extremely desirable considering their possible major climatic impacts. Results above showed clear evidence for the ability of the model to capture extreme AMOC events. More specifically experiment 15P gives hope for predicting such events earlier than the 8-year average predictive skills identified by the PPP approach. Given the lack of AMOC observations, we investigate here whether there exist monitorable precursors to such extreme events and whether they are themselves predictable. Note that these are likely to be strongly model-dependent.

As briefly mentioned in *Sect. 5.2*, Escudier et al. (2012) identified a 20-year cycle associated with the AMOC variability in the IPSL-CM5A-LR control integration. Figure 5.7 shows a simplified schematic of the mechanism responsible for one half of this cycle. They have shown that, for example, a deceleration of the East Greenland Current (EGC) brings less cold and fresh water into the Labrador Sea giving rise to positive temperature and salinity anomalies in the upper 200 m around 3 years after the deceleration. These anomalies then propagate along the subpolar gyre and reach the Nordic Seas in about 7 years. As they pass over the convection sites, the salinity anomalies favour deep convection, thereby inducing an AMOC intensification after 9 years. In the Nordic Seas, the positive temperature anomalies also induce an anomalous decrease of sea-ice cover which in turn triggers a positive anomalous atmospheric temperature. The direct atmospheric response to this temperature anomaly is a local below-normal SLP anomaly and a localised cyclonic atmospheric circulation, associated to anomalous southward wind stress along the eastern coast of Greenland. This leads to an intensification of the EGC which turn creates negative temperature and salinity anomalies in the Labrador Sea. This process lasts 10 years, and the second phase of the cycle begins. A more detailed mechanism of the cycle can be found in Escudier et al. (2012). Even though the AMOC is not taking an active part in this variability mechanism, it is still influenced by the cycle through deep convection anomalies. Escudier et al. (2012) found therefore evidence for the EGC intensity and water properties in the Labrador Sea to be precursors of changes in the model's AMOC, with a lead-time of about 14 years for the EGC and 11 years for the Labrador Sea salinity.

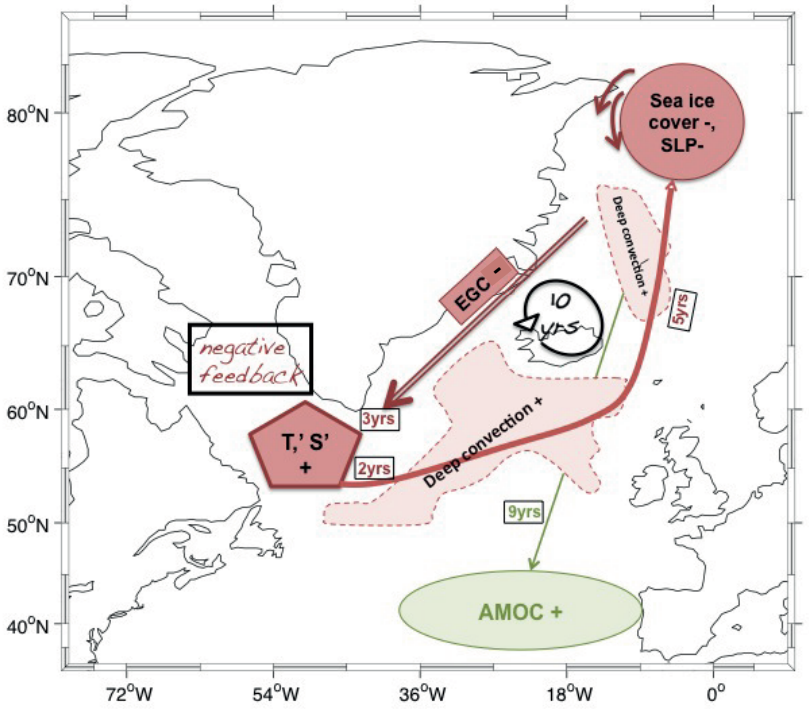

Figure 5.7: Schematic view of mechanisms responsible for one half of the decadal AMOC cycle in IPSL-CM5A-LR. Items in red are actively involved in the 20-year cycle. T' stands for upper ocean temperature anomaly, S' for upper ocean salinity anomaly. EGC is the East Greenland Current and SLP the sea level pressure. Starting from a positive temperature and salinity anomaly, the signs in the red boxes indicate the sign of the correlation among items, and the number in the square black boxes the time lag in years. Items in green are periodically perturbed by the 10-year cycle but not actively taking part in its generation. The signs and the number of years denote correlation and time lags as above. (Adapted from Escudier et al. 2012).

Using this apparent predictability in a practical way requires that a large change in the main identified precursors always lead to a corresponding change in the AMOC index. Figure 5.8 shows time series of the AMOC index, SSS in the Labrador Sea and the EGC index (defined as the southward meridional transport across the Denmark Strait of waters with a salinity lower than 34 psu) in the control integration for each ensemble with the corresponding plumes superimposed. It is found that of the 6 identified "events" (represented as letters in Figure 5.8), for which within 5 years at least one of the precursors changes by more than 2σ and the other one by at least 1.5σ, 5 are followed by an AMOC change of the correct predicted sign, of which 4 show a change larger than 1.5σ. This large change in AMOC occurs about 15 (13) years after a large change in EGC (SSS in the Labrador Sea). This result is consistent with the lead-times summarized in Figure 5.7, and therefore illustrates the potential predictive role of these two variables. Large magnitude of change in precursors (around 0.9-1.2 Sv and 0.5-0.7 psu) therefore suggests the potential predictability of extreme AMOC events through observations of properties in the Labrador Sea and Denmark Strait. This also suggests that in the case

of extreme AMOC events, there is the possibility for longer lead-time of predictability (13 or 15 years, depending on the predictor) than the average 8 years found above (see *Sect. 5.3.1*). Note that this longer lead-time has previously been discussed for the experiment 15P alone. Its ability to capture the peak 15 years later is indeed linked to the state of its EGC precursor, which is extreme at the beginning of the experiment (point C, Figure 5.8).

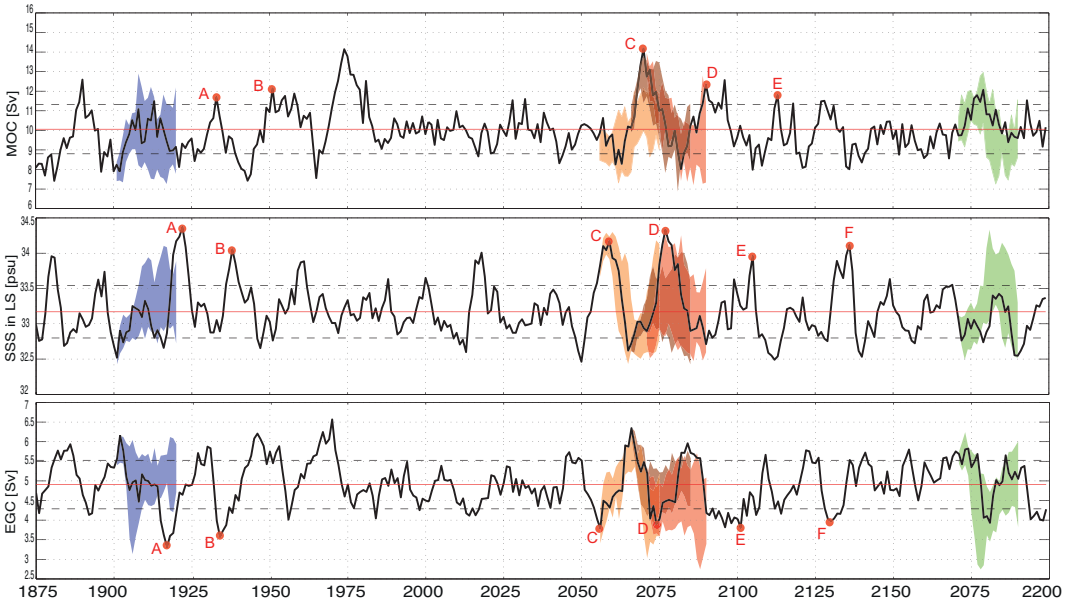

Figure 5.8: Time series of AMOC index (top panel), SSS in Labrador Sea (middle panel), and EGC index (bottom panel). Thick black line is the control integration, dashed lines are the standard deviation, red line is the mean, and envelope of each experiment is shown as coloured shading. Letters (A-B-C-D-E-F) correspond to identified "events" (see text for further details).

Finally, hope for predictability of an extreme AMOC to go even beyond this suggested decadal lead-time could arise if these two precursors exhibit in turn some potential predictability skills. Indeed, both the EGC and SSS in the Labrador Sea have been found to have some robust predictability for lead-times up to 9 and 7 years, respectively (not shown). The possibility of predicting an extreme EGC event at least 9 years in advance gives hope for the predictability of an extreme AMOC event beyond 2 decades ahead, although this has not been tested prognostically.

We therefore found convincing evidence that extreme changes in the AMOC as seen in the IPSL-CM5A-LR model might be potentially predictable up to 2 decades ahead from the monitoring of its high-latitude Atlantic precursors. Hawkins and Sutton (2008) already found such a relationship with the HadCM3 model. If a comparable mechanism to the one identified in the IPSL-CM5A-LR model (Escudier et al. 2012) occurs in the real ocean, which remains to be demonstrated (encouraging elements can be found in Swingedouw et al. 2012), then the ability to predict AMOC fluctuations is promising for potential predictability of climate at multi-decadal timescales.

5.4 Spatio-temporal predictability of Atlantic climate

Potential predictability of both surface temperature and precipitation is now evaluated using and comparing both the DPP and PPP approaches. As mentioned in *Sect. 3.2.1.1*, a threshold for "useful" potential predictability is often hard to define in the DPP approach, as it only relies on a long control integration. On the other hand, it remains a cheap (in terms of computation time) and easy way to evaluate average predictive skills from long time series. This differs from the PPP approach which is much more expensive, but better evaluates the growth of perturbations in initial conditions and therefore the effective predictability within models. Given a choice of starting dates, this approach can also illuminate the link between temperature and precipitation predictability and the AMOC.

5.4.1 Potential predictability of surface temperature

Figure 5.9 shows predictability maps of Atlantic surface temperature up to 1 and 2 decades as identified by both the DPP and PPP approaches in the IPSL-CM5A-LR model. For the former approach, the maps show the $ppvf$ for 10 and 20-year means and are shown in Figure 5.9a. For the PPP approach, regions combining surface temperature with both statistically significant EC and ES statistically smaller than the saturation level at the considered lead-time (i.e. regions potentially predictable as defined in *Sect. 3.2.1.2*) are shown in Figure 5.9b as a function of the number of experiments for which these conditions are met.

Over the ocean, the regions of highest (more than half of the experiments) predictive skills at both 1 and 2 decades identified by the PPP approach coincide to some extent with those of highest $ppvf$ scores (for which 10 to 40% of the variance is in the considered decadal band, Figure 5.9a). These regions mainly include the convection sites (as identified by Escudier et al. 2012) together with the NAC path, and are in good agreement with results from the diagnostic multi-model predictability studies of Boer (2004) and Boer and Lambert (2008). The PPP approach also brought some hints of potential predictability (less than half of the experiments) for the two timescales in regions including the southeastern branch of the subtropical gyre and the tropics (more specifically the western deep tropics up to 1 decade extending to the northern western tropics up to 2 decades). These two regions are also identified by the DPP approach, although some discrepancies are present in the tropics; up to 2 decades, strongest signals are identified in the southern tropics rather than in the northern tropics. Interestingly, these regions of weak signals (i.e. the southeastern branch of the subtropical gyre and the tropics) are each identified in experiments including the extreme AMOC event of 2071, namely in experiment 15P and S mainly over 2 decades (see *Appendix B*, Figure B.1). Although it remains difficult to draw robust conclusions from the limited number of experiments,

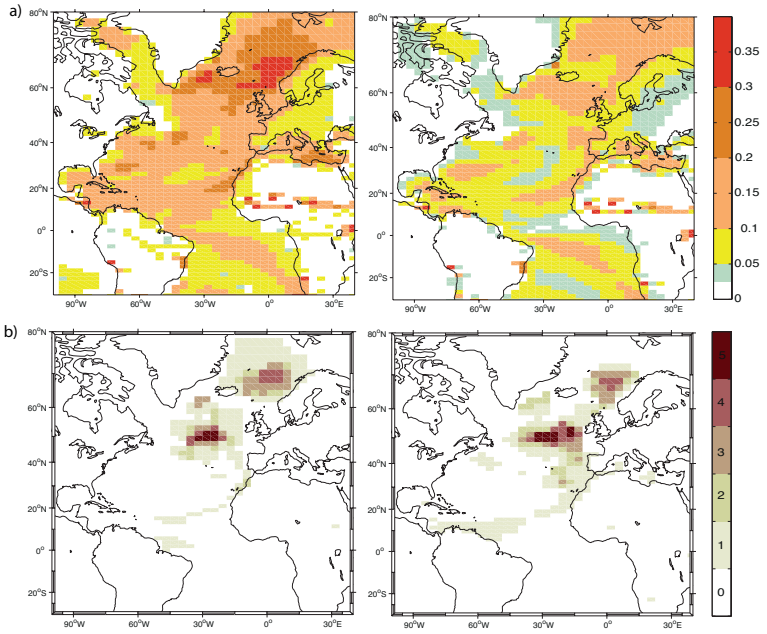

Figure 5.9: Potential predictability of surface temperature in the Atlantic sector identified by: (a) the DPP approach showing maps of the internally generated decadal *ppvf* for 10-year (left panel) and 20-year (right panel) means in the unforced control climate of IPSL-CM5A-LR (the colored areas are significant at the 95% level according to a F-test); (b) the PPP approach showing maps of the number of starting dates (out of 5) where grid points are potentially predictable (i.e. where it combines both statistically significant EC at the 90% confidence level according to a Student's t-test and normalized ES smaller than saturation level at the 95% level according to a F-test) up to one (left panel) and two (right panel) decades.

this suggests that an extreme AMOC event might favour the potential predictability of these regions. However, the reason for the weak scores in these regions in the 5P experiment remains to be clarified.

In general, in both approaches, potential predictability over land is less significant than over the ocean. It is found over the coastal areas bordering some of the potentially predictable oceanic regions (that mainly include the maritime-influenced regions of western Africa, the western coast of the Iberian peninsula, and the northern coasts of the British Isles and South America), and it seems to be favored by extreme AMOC events (see *Appendix B*, Figure B.1). The DPP approach identifies additional land areas located further away from the coast (i.e. in Europe, in both the African and South American continents). Note, however, that these additional land areas are regions of low *ppvf* values (<0.1, Figure 5.9a).

Finally, the evidence of a relationship between the potential predictability of surface temperature and the AMOC is due to the fact that the major regions identified as potentially predictable by both approaches, are also remarkably similar to the regions significantly sensitive to decadal AMOC fluctuations (as shown in Figure 5.1a).

5.4.2 Potential predictability of precipitation

Potential predictability of precipitation (Figure 5.10) is considerably smaller than for surface temperature, in good agreement with the multi-model approach of Boer and Lambert (2008). Similar to the latter study, the Nordic Seas are the most prominent regions where precipitation seems to be predictable at both timescales. There are also some patches of predictability over the subpolar gyre in both approaches. Note that the DPP approach identifies additional regions (both oceanic and continental) mainly over the tropics (Figure 5.10a). As for surface temperature, these additional regions have low $ppvf$ values. Furthermore, as for regions of weak signals for surface temperature, regions identified by both approaches appear in experiments including the extreme AMOC state of the year 2071 (experiments 15P and S, see *Appendix B*, Figure B.2).

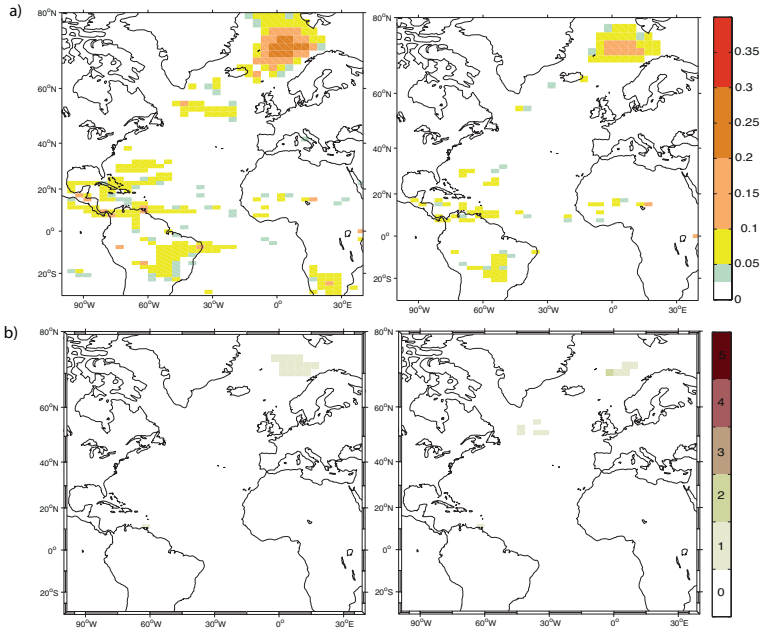

Figure 5.10: Potential predictability of precipitation in the Atlantic sector as defined in Figure 5.9.

As with surface temperature, the evidence for a link between an extreme AMOC event and predictability of precipitation in the above identified regions is due to the fact that they are also regions sensitive to decadal AMOC fluctuations (as shown in Figure 5.1b). The possibility for a link between precipitation at high latitude and the AMOC would not be surprising since by controlling a significant part of freshwater fluxes there, precipitation control the AMOC precursors identified in the model. These results suggest the mechanisms responsible for climate predictability to be strongly linked to the mechanisms behind decadal AMOC variability. Note, nevertheless, that this link between regions potentially predictable and those sensitive to decadal AMOC fluctuations is less clear for precipitation than for temperature, and this could also explain the weaker PPP skills in precipitation in the tropical and subtropical regions, given our experimental set-up for the prognostic approach largely focused on specific AMOC events.

5.5 Summary and discussion

5.5.1 Potential predictability of the AMOC

The predictive skills of the AMOC index have been quantified by the prognostic (PPP) approach for five experiments starting from different AMOC initial states, using both the ensemble spread (ES) and the ensemble correlation (EC). In most cases, ES (EC) increases (decreases) with lead-time, and hence predictability is lost after a certain lead-time. In some cases, an apparent "return" of skill is detected a few years after saturation. This has to be interpreted carefully as it could simply reflect noise rather than predictability (e.g. Newman et al. 2003). Our experiments showed that it could nevertheless also be related to the large variability of the AMOC at the 20-year timescale found in the control simulation (Escudier et al. 2012). EC was found particularly useful to detect such features in the simulations.

It is difficult to determine average predictability skills in the "perfect model" experiments as it implies averaging skills over several starting dates which themselves have very different predictability skills. Nevertheless, it seems reasonable to claim that the modeled AMOC has an average predictive skill of 8 years in the IPSL-CM5A-LR model, when considering the average lead-time at which ES saturates. The corresponding EC averaged over all starting dates is not significant. Note that the AMOC index has also been found to have a persistence time (estimated from the AMOC index autocorrelation function in a red noise framework) of about 4-5 years, which is less than the average predictive skills found here. This suggests a role of the oceanic dynamics in this predictability. The average lead-time of predictability of the AMOC index found in the IPSL-CM5A-LR model is somewhat shorter than those identified in most similar published studies, for which the predictability lead-time could reach 2 decades ahead (e.g. Collins and Sinha 2003; Msadek et al. 2010; Pohlmann et al. 2004; Collins et al. 2006a). It is, however, somewhat in agreement with Teng et al. (2011) who found the AMOC to be predictable for only one decade in the CCSM3 model. Hermanson and Sutton (2009) identified a shorter lead-time in the HadCM3 model, with an average predictive skill of about 5 years. The IPSL-CM5A-LR model belongs to the middle-range of timescale of AMOC predictive skills identified so far in the literature. Such a comparison with existing studies should, however, be considered carefully because of the many differences in the experimental protocol used among predictability studies.

When considering the predictive skills of each ensemble experiment separately, there is evidence for predictive skills to depend on the AMOC initial state. Indeed, the highest skills have been found (in descending order) in the experiments starting (i) from a strong AMOC initial state (up to 13 years), (ii) 5 years before a maximum peak (up to 8 years) and (iii) from a weak AMOC initial state (up to 7 years). In contrast, no predictive skills (as defined in *Sect. 3.2.1.2*) have been found for experiments starting

from an intermediate AMOC initial state and 15 years before a maximum peak. This is essentially because the ensemble correlation rapidly becomes insignificant. Based on ES alone, these starting dates could be considered as being predictable 7 and 5 years ahead respectively. Nevertheless, generally, predictive skills have therefore been identified for experiments starting or nearly-starting from an extreme AMOC state. The above results also suggest better predictive skills for an initial state corresponding to an anomalously strong AMOC than those corresponding to a weak AMOC, in good agreement with the perfect model studies of Collins and Sinha (2003) and Collins et al. (2006a). However, the number of members (10) for each experiment is somewhat low to fully assess the robustness of such an impact of the AMOC initial state on its predictability. Note furthermore that, although no predictive skills (as defined from both EC and ES) have been identified in the experiment starting 15 years before a peak, this specific experiment still showed the ability of the model to capture relatively well an extreme AMOC event on a longer lead-time than the average one identified by the PPP approach.

In view of the major climatic impact induced by such extreme events, the development of an early warming system would be of great value. The present study shows that this is made possible through the monitoring of the high-latitude precursors of the AMOC in this model (which are the EGC and the upper-ocean properties in the Labrador Sea), which leads to an increase in predictive skills of extreme AMOC events up to 2 decades ahead. The perspective of an early warning system of such events thus motivates the monitoring of the EGC strength and water properties in the Labrador Sea. In this perspective, observation programs across e.g. the WOCE-AR7/A1 section for the Labrador Sea (http://cchdo.ucsd.edu/atlantic.html) and the East Greenland shelf and slope of south of Denmark Strait (Brearley et al. 2012), as well as the maintenance of mooring arrays in these areas, are likely to be of greatest added value to constrain prediction of the AMOC. Similar observational targets have also been pointed out by Hawkins and Sutton (2008) using the HadCM3 model.

5.5.2 Potential predictability of the North Atlantic climate

Changes in the AMOC have been found to have significant and widespread climate impacts. The prospect for predictability of decadal AMOC fluctuations is therefore promising for potential predictability of climate. This latter has been investigated using both diagnostic (DPP) and PPP approaches. They give overall very similar results, and strongly agree on the regions that exhibit the highest predictive skills. Some discrepancies, nevertheless, arise for regions where only some hints of predictability have been identified. Indeed, these regions are often larger in the DPP approach than in the PPP approach. In other words, the DPP estimation seems less discriminate. To strengthen the robustness of our results, note that the regions claimed to have some hints of predictability below are regions identified by both the DPP and PPP approaches.

The far North Atlantic (that includes the convection sites of the model and the NAC path) has been identified as the region exhibiting the highest predictive skills. Surface temperature is potentially predictable up to 2 decades in advance there, in good agreement with previous studies (e.g. Collins 2002; Boer 2004; Pohlmann et al. 2004; Hawkins et al. 2011; Branstator et al. 2012). Note that this ability to predict the North Atlantic subpolar gyre also gives hope for potential multi-year forecasts of tropical storm and hurricane frequency (Smith et al. 2010). Some hints of potential predictability are also identified at this timescale in the subtropics (mainly over the southern part of the eastern branch of the subtropical gyre) and the tropics (mainly over the north western tropics). The predictability found in the latter region is clearly different from results of Pohlmann et al. (2004) in the ECHAM5-MPI/OM climate model, and also contrasts with Collins (2002), who found signals only up to the interannual timescales in the tropics in HadCM3. To some extent our result, however, agrees with Hawkins et al. (2011) who also found decadal predictability in the tropics in the HadCM3 model, but only up to 1 decade ahead and restricted to the southern tropics. Land areas display little potential predictability compared to oceans. Potential predictability at decadal timescales is generally restricted to the coastal areas bordering some of the oceanic regions identified above; they mainly include the coast of western Africa, the western coast of the Iberian Peninsula, both the northern coast of the British Isles and South America. Signals over maritime Europe as identified by Boer and Lambert (2008) and Pohlmann et al. (2004) are not brought out as clearly in our study. Although potential predictability is largely absent for precipitation (as noted by Pohlmann et al. 2004; Boer and Lambert 2008; Boer 2011 in particular), there are some hints of potential predictability up to 2 decades over the convection sites of the Nordic Seas and the subpolar gyre.

Similarly to the AMOC, regions with weak but significant predictability (i.e the tropics and subtropics for temperature, the Nordic Seas and subpolar gyre for precipitation) seem to depend at least partly on the AMOC state. Results suggests that extreme AMOC events might favour the potential predictability of regions of weak signals, as the latter are in most cases identified when the predicted time-period includes such events. Although the origin of a possible link between climate predictability and extreme AMOC still needs to be clarified, the likelihood for such a link is strengthened by the fact that regions identified as potentially predictable (for both surface temperature and precipitation) are also all strongly influenced by decadal AMOC fluctuations. This suggests that the mechanisms responsible for climate predictability are to some extent linked to the decadal AMOC variability. More research to understand the specific mechanisms that lead to predictability is, however, still needed. The present study nevertheless underlines that the potential predictability of the AMOC could therefore lead to significant decadal predictability of climate (where the AMOC has a sufficiently strong impact), and may therefore be of economic and societal importance (e.g. Meehl et al. 2009).

5.5.3 Evaluation of different methods for quantifying predictive skills

Different definitions of predictability, different experimental protocols and metrics have often been used among the previous studies to evaluate predictive skills. It therefore remains difficult to estimate the weight of the metrics on the level of predictability found here in the IPSL-CM5A-LR model by comparing this level to those found in previous studies. Nevertheless, from a methodological point of view, our study still puts forward some interesting results regarding the evaluation of predictive skills.

Regarding the PPP approach, we showed that combining ES and EC should be preferred in principle but it is sometimes difficult to apply in practice. For the evaluation of average predictive skills, EC was found insignificant. In the case of 15P, it reduced the quantification of predictability skill for weak lead-times but greatly helped to highlight the ability of the model to capture the late peak. We thus still claim that both metrics should be considered in parallel. Our results also suggest that considering either the ensemble mean of an experiment or each individual member as a baseline in the calculation of both metrics does not affect the overall results.

As already mentioned, both DPP and PPP approaches generally brought out the same main features concerning both temperature and precipitation predictability. Marginal discrepancies concerned the regions of weak signals. Because of the difficulty to define a "useful" threshold of potential predictability in the DPP approach, the PPP approach allows more detailed analysis. It however relies on the subjective choice of starting dates, number of members and experiments.

Despite the limited number of experiments starting with similar AMOC states, another aspect brought out by the PPP approach is that both the AMOC and some regions might have higher predictive skills under specific initial states, often when the predicted time period includes an extreme AMOC. This result needs to be confirmed by further work. Although reliable estimates of skill conditional on specific initial states are difficult to determine (due to the small sample for verification), more systematic experiments starting with similar initial states (i.e. weak, intermediate, strong, just before a peak) should therefore be undertaken. It could even be extended to further scenarios such as starting just after a peak. Note that, this dependence on initial states already exists with seasonal-to-interannual climate forecasts dependent on the phase of El-Niño Southern Oscillation (e.g. Chen et al. 2004), and it is expected to be the case with decadal predictions (Griffies and Bryan 1997a). The present study suggests that forecasts starting from an extreme phase of natural internal variability can be more skillful than those starting from average conditions. In that sense, studying skill from case studies may prove more useful to understand predictability mechanisms than computing average skill from numerous start dates as done in most previous studies.

5.6 Conclusions

In conclusion, the decadal predictability of the AMOC and associated oceanic/atmospheric variables in IPSL-CM5A-LR can be summarized in the following key points:

• The AMOC has an average prognostic predictability of about 8 years.

• In about 80% of the cases, an extreme AMOC event can be predicted up to 2 decades in advance from the monitoring of its high-latitude precursors (which are the East Greenland Current and water properties in the Labrador Sea).

• The far North Atlantic (that includes the convection sites, the NAC path, and the subpolar gyre region) exhibits the highest predictive skills for surface temperature up to 2 decades in advance. Some hints of predictability are also identified up to 2 decades in the subtropics (over the southern part of the eastern branch of the subtropical gyre) and the tropics (over the northern western tropics).

• There is little potential predictability for surface temperature over land, which is restricted to the coastal areas bordering some of the predictable oceanic regions.

• Potential predictability is largely absent for precipitation, despite some hints of predictability up to 2 decades in the Nordic Seas.

• Predictive skills of AMOC, surface temperature and precipitation seem to be favoured by extreme AMOC events in maximum states.

• All regions identified as potentially predictable are strongly influenced by decadal AMOC fluctuations, suggesting that the mechanisms responsible for climate predictability are to some extent linked to the decadal AMOC variability.

It is also important to bear in mind that here we have assessed the upper limit of both the AMOC and climate predictability as both perfect model and near perfect knowledge of the current state of the climate system are assumed. Indeed, climate models still have significant biases compared to observations, and their possible impacts on the level of predictability skill of a model cannot be ignored. As an illustration, Branstator et al. (2012) found that, using six state-of-the-art AOGCMs, the average lead-time of predictability for subsurface temperature (especially in the North Atlantic) varied considerably between the models highlighting how poorly the North Atlantic predictability must be represented in some, or perhaps all, of the six models. Therefore, bearing in mind the possible impact of the limitations of the IPSL-CM5A-LR model, its lack of deep convection in the Labrador Sea (Swingedouw et al. 2007) might well affect the effective level of predictability skill. This problem should be addressed in future work. The 20-year variability cycle in the subpolar North Atlantic in the model also greatly influences the present results and its occurrence in the real world further needs to be assessed. The possibility that lower predictability limits would arise in a

real predictive system with this model cannot be ruled out (see Swingedouw et al. 2012). However, to the extent that both diagnostic and prognostic approaches are appropriate measures of skill, the present results give some indications as to where and to what extent skillful decadal forecasts might be possible.

Results from *Chapter 4* suggested that hybrid-coordinate ocean component model such as CHIME might have better predictive skills than climate models that feature an orthodox z-coordinate level coordinate ocean component such as IPSL-CM5A-LR. To strengthen or weaken this claim (as well as the robustness of the results found here), similar analyses have therefore been repeated with the CHIME model by following an experimental design as similar as possible to the one used here with the IPSL-CM5A-LR model. This is the subject of the next chapter.

Chapter 6

Decadal predictability of the AMOC and climate in CHIME

6.1 Aim of study

In this chapter, we explore the decadal predictability of the AMOC and associated oceanic and atmospheric fields as they are represented in the CHIME model (Megann et al. 2010) under control conditions, using both the diagnostic (DPP) and prognostic (PPP) approaches. Results from this study will complement those from IPSL-CM5A-LR (*Chapter 5*) by strengthening or questioning some of the claims previously drawn.

In the DPP approach, we analyze the 201-year-long control integration $E3$ of CHIME (see *Sect. 2.1.2.2*), and use the non-biased estimation of $ppvf$ (from Boer 2004) as an estimate of predictive skills. In the PPP approach, five "perfect ensemble" experiments are performed from the same control integration. Each experiment consists of five ensemble members (excluding the control run) starting from slightly different initial conditions and integrated for 20 years. As with IPSL-CM5A-LR (*Chapter 5*) and following the CS03 definition of target, both Ensemble Spread (ES) and Ensemble Correlation (EC) are evaluated in CHIME to quantify the reproducibility and thus predictability of the simulated fields, and we consider that a variable is potentially predictable if it has a (low) statistically significant ES associated with a (high) statistically significant EC.

Note that because different control integrations are used in the variability and predictability study with CHIME (cD and $E3$, respectively), we have to be aware of the eventual differences in their AMOC characteristics (both spatially and temporally). Indeed, all these discrepancies have to be kept in mind as analogies are drawn between the mechanisms of AMOC variability and predictability.

First, both spatial and temporal variability associated with the AMOC are therefore compared in both cD and $E3$ in *Sect. 6.2*. The control integration $E3$ is then analyzed

in *Sect. 6.3* to investigate the impact of strong AMOC fluctuations on both oceanic and atmospheric fields in the Atlantic sector. In *Sect. 6.4*, the potential predictability of the AMOC, as identified by the PPP approach, is investigated using "perfect ensemble" experiments. Using both DPP and PPP approaches, *Sect. 6.5* addresses the potential predictability of both associated oceanic and atmospheric fields as well as its link with decadal AMOC variability. A summary and discussion follow in *Sect. 6.6*, with concluding remarks in *Sect. 6.7*.

6.2 Internal AMOC variability: discrepancies between *E3* and *cD*

6.2.1 Spin-up, trend and variability of AMOC

The AMOC index time series are shown for both control integrations in Figure 6.1. As already mentioned in *Sect. 2.1.2.2*, the AMOC index in $E3$ has the most stabilized state between year 105 and 305. During this period it has an oscillation amplitude of about 3 Sv (ranging from 16 to 22 Sv) against an amplitude of about 2 Sv (ranging from 17.5 to 22 Sv) in cD during its corresponding near-stabilized period (from year 80 to 200). The average decadal mean is slightly weaker by about 1 Sv in $E3$ (18.7 $\pm$ 1.9 Sv against 19.8 $\pm$ 1.4 Sv in cD), which is still well within the observational estimates (18 $\pm$ 2-3 Sv) of Talley (2003).

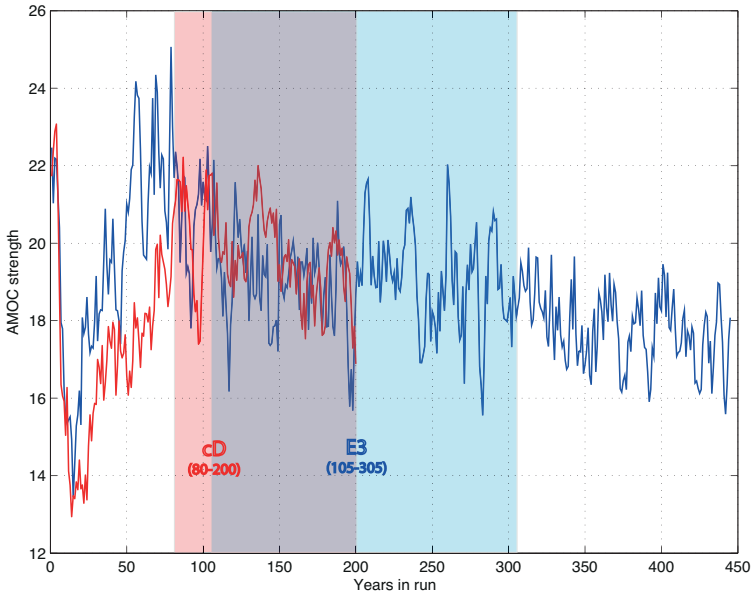

Figure 6.1: Time series of AMOC index of cD (in red) and $E3$ (in blue). Red (blue) shading corresponds to the time period analyzed in cD ($E3$) and the grey shading corresponds to their common time period.

Figure 6.2 shows the mean AMOC streamfunction for both runs averaged over their corresponding periods of analysis, along with their spatial differences. At first sight, they both have a similar spatial structure. There are however some differences worth pointing out. In both runs, the circulation associated with the NADW is maximum at a depth of about 800-1200 m, spreading from 30°N to 60°N. The maximum transport is, however, slightly stronger in $E3$ ($\sim$ 20 Sv, Figure 6.2a, right panel) than in cD ($\sim$ 18 Sv, Figure 6.2a, left panel). The NADW cell also lies at a slightly shallower depth in $E3$ (extending to $\sim$ 3500 m against 4000 m in cD) resulting in a weaker transport (up to 4 Sv) between about 1500 m and 4000 m depth (Figure 6.2b). This shallower NADW cell in $E3$ may be a consequence of its stronger AABW cell (about - 4 Sv against - 2 Sv in cD). The deep sinking regions seem similar in both runs, although in the Labrador Sea, the sinking is slightly stronger in $E3$ (Figure 6.2b) consistent with the higher maximum transport of the NADW cell in the latter. Despite these few discrepancies, it seems reasonable to claim that the structure of the AMOC streamfunction in both runs is similar.

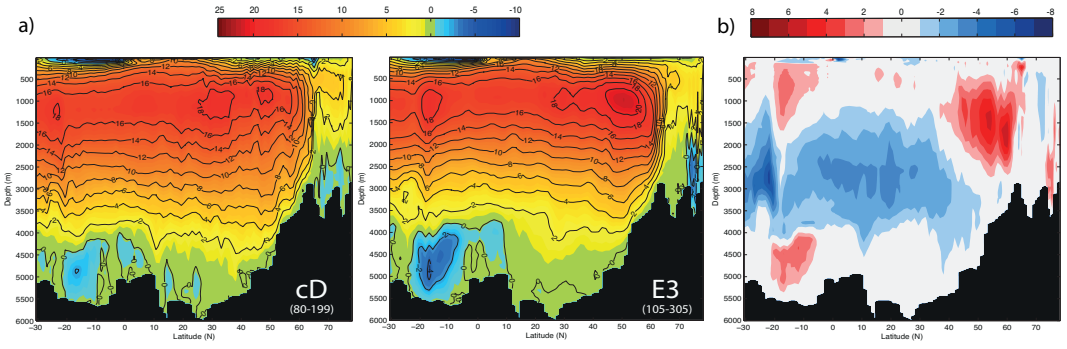

Figure 6.2: (a) Annual mean streamfunction of zonally integrated volume transport (Sv) from 30°S to 80°N, averaged from years 80-199 (105-305) for cD ($E3$). (b) Differences in annual mean streamfunction (Sv) between $E3$ and cD; positive (negative) values correspond to stronger (weaker) transport in $E3$.

6.2.2 EOF analysis of AMOC variability

The first two EOFs of the AMOC streamfunction in $E3$ (based on 201 years of annual-mean calculated from year 105 to 305) are shown in Figure 6.3. Prior to the calculations, time series are normalized by the variance, and detrended. If we compare the spatial structures of these two EOFs with those of cD (see Figure 4.3), they look to some extent similar at first sight.

The first EOF mode (EOF1) in both $E3$ and cD explains a similar amount of variance (32% and 33%, respectively). In *Sect. 4.2.2*, the primary mode of AMOC variability in cD has been associated with a decadal cycle (ranging from a 15-30 years period) related to convective activity in the Labrador and (inversely) the GIN Seas. With a similar spatial structure to cD, EOF1 in $E3$ suggests that its main mode of variability might

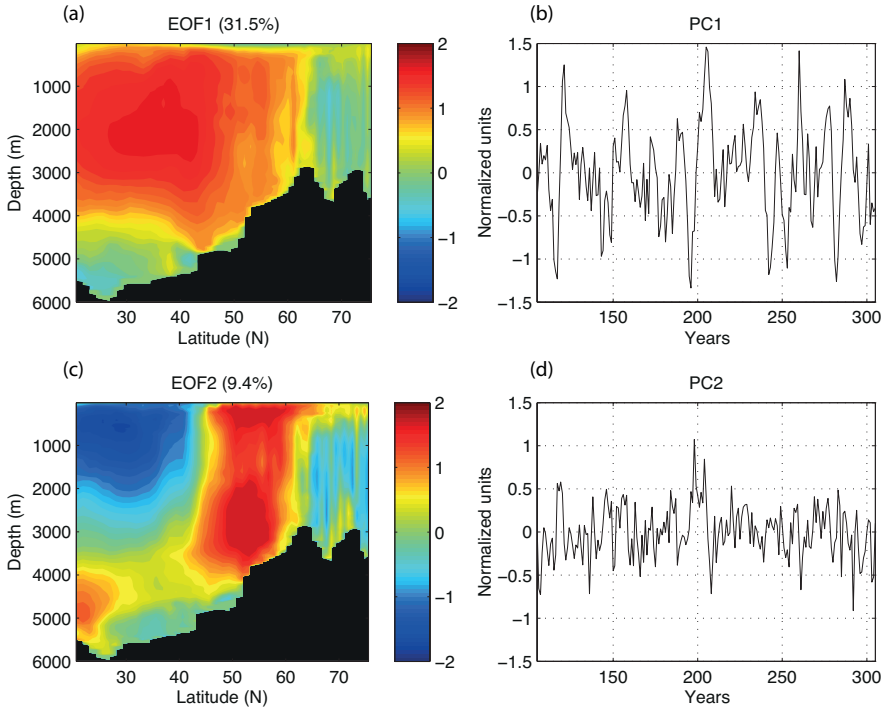

Figure 6.3: Detrended AMOC streamfunction (from year 105 to 305) in the North Atlantic(20°N to 75°N): (a)EOF1; (b)PC1; (c) EOF2 and (d) PC2.

also be related to the same convective activity. The statistically significant correlation between the 10-year moving average of PC1 and the detrended convective index in the Labrador Sea (defined as the averaged March MLD in the region 55°N-65°N/45°W-65°W, Figure 6.4, red line) supports the link between EOF1 and LSW variability. They are correlated at the 95% confidence level with a coefficient of 0.42 (not shown), when PC1 leads by about 3 years (similar lag found in *cD*, see Table 4.1). However, in contrast to *cD*, no such correlation has been found with the convective index in the GIN Seas (defined as the averaged March MLD in the region 65°N-80°N/15°W-15°E, Figure 6.4, blue line). Nevertheless, convective activity in both the Labrador and GIN Seas seems to have an anti-phase relationship as supported by their statistical significant correlation of about -0.30 when the Labrador Sea leads by 1 year (not shown), consistent with *cD* (see Figure 4.11). Although the correlation coefficient is weaker in *E*3, this result suggests that a link between these two convective regions exists, and that despite no evidence for a statistical relationship between PC1 and convective index in the GIN Seas, EOF1 in *E*3 might still be associated with this latter region through its link with the Labrador Sea. The main mode of variability in *E*3 also seems to be associated with a decadal cycle. Indeed, the power spectrum of PC1 shows the strongest energy (relative to a fitted first order autoregressive AR1 model, Chatfield 1975) at a statistical significant peak (at the 95% confidence limit) of about 15 years (Figure 6.5). Although well below the 80% confidence limit, there is also a second large peak at about 25-30 years period above the fitted red noise spectrum. These two peaks are well within the 15-30 years range period found in *cD* see Figure 4.1b). Note also the strong instantaneous correlation

coefficient of about 0.82 between PC1 of the AMOC streamfunction and the AMOC index (Figure 6.6), as for cD (see Table 4.1).

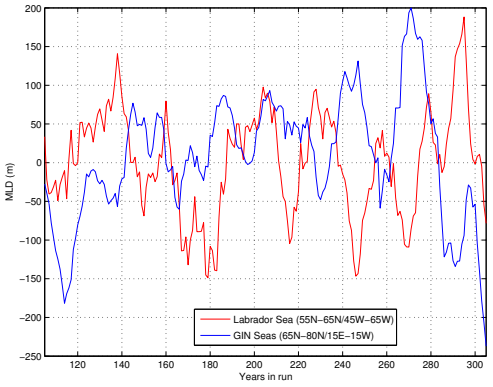

Figure 6.4: Time series of detrended 10-year moving average March MLD in the Labrador (in red) and GIN (in blue) Seas in $E3$.

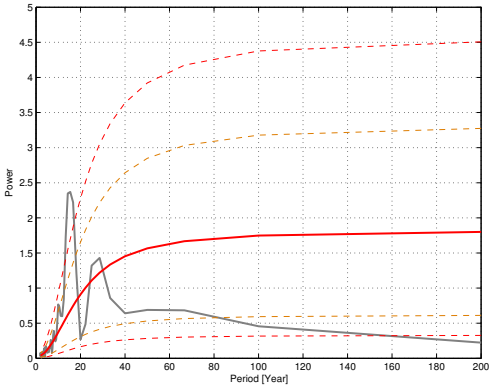

Figure 6.5: Power Spectrum of the detrended PC1 time series of the AMOC streamfunction (grey line) in $E3$ using the Welch method of spectra estimation. The smooth red solid line is the power of a red noise spectrum with the same AR(1) coefficients fitted from the detrended PC1 time series, and red (orange) dashed lines, which are the 95% (80%) confidence limits.

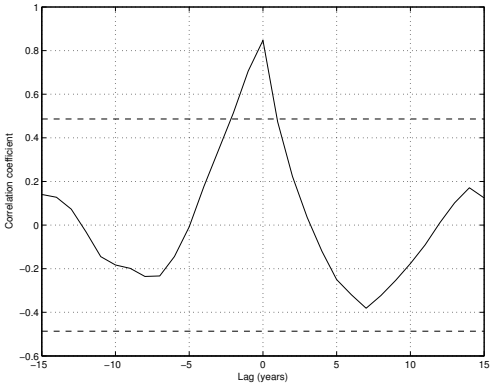

Figure 6.6: Lagged cross-correlations plot between PC1 of the AMOC streamfunction and the AMOC index in $E3$; horizontal dashed lines correspond to the 95% confidence limit for zero correlation.

The second EOF mode (EOF2) in both $E3$ (Figure 6.3c) and cD (see Figure 4.3c) explains a similar amount of variance (about 9% and 12%, respectively). The secondary mode of AMOC variability in cD has been associated with interannual variability related convective activity in both the Labrador and GIN Seas (see *Sect. 4.2.2*). Although EOF2 has overall a similar spatial structure in both runs, there are significant differences in the high latitude regions. Indeed, in contrast to cD, the strongest variability in $E3$ occurs in the Labrador Sea and is less in the GIN Seas. However, in both cases, PC2 seem to vary on interannual rather than decadal timescales.

In comparison with cD, the two first modes of AMOC variability in $E3$ seem to mainly be related to convective activity in the Labrador Sea with a lesser role for the GIN Seas. The reduced variability in this latter (compared to cD) may be partly caused by the closure of the Bering Strait in $E3$ therefore affecting the highest latitude regions that include the GIN Seas. Nevertheless, these two runs agree in that the leading mode of AMOC variability is driven by convective activity in the Labrador Sea. It therefore seems reasonable to assume that the mechanisms controlling the decadal AMOC fluctuations are similar in both runs, keeping in mind that further analyses would be necessary to confirm this.

6.3 Fingerprints of AMOC variability

Prior to the study of the AMOC potential predictability skills in CHIME, the regional impacts of the AMOC are investigated in $E3$. To do so, we carried out composite analyses of several oceanic/atmospheric variables thought to be sensitive to decadal AMOC fluctuations. Note that winter or September means were used when the statistical significance of results was more robust than with the use of annual mean; this however does not give qualitatively different results.

6.3.1 Impacts on sea surface temperature

A composite of annual SST anomaly pattern (relative to the 105-305 annual mean) induced by AMOC fluctuations was obtained by averaging anomalies over years when the AMOC is strongest (i.e. when exceeding one standard deviation, Figure 6.7). Although the relatively short control integration length limits the statistical significance of the results, the SST pattern looks somewhat similar to that identified in cD (see Figure 4.7a). When the AMOC is in its strong state, most of the upper ocean, from the subtropics to the mid-latitudes (mainly over both the Gulf Stream and NAC paths) and the Nordic Seas becomes warmer, whereas SST south of about 25°N tends to become cooler. This pattern somewhat reflects an AMO-type response in good agreement with previous studies (e.g. Sutton and Hodson 2005; Frankcombe et al. 2010); this AMOC-AMO connection in CHIME has been discussed in detail in *Sect. 4.3.1*.

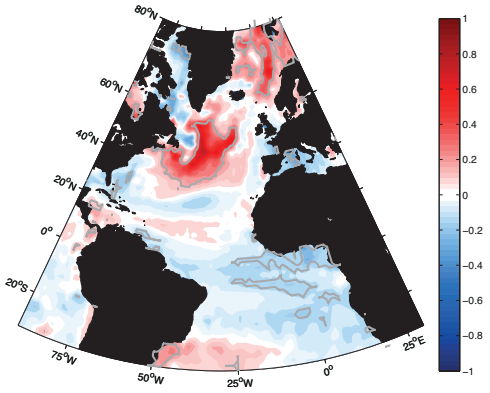

Figure 6.7: Composite of annual anomaly patterns of SST (°C) induced by AMOC fluctuations, obtained by averaging anomalies over years when PC1 of the AMOC streamfunction is strongest. Grey contours indicate where the null hypothesis of equal means is rejected at the 10% level.

6.3.2 Impacts on surface air temperature

A composite of winter SAT anomaly pattern (relative to the 105-305 winter mean) induced by strong AMOC conditions is shown in Figure 6.8. Note that, as in the case of SST, the relatively short control experiment length limits the statistical significance of the results. Nonetheless, it seems reasonable to claim that stronger AMOC conditions mainly affect SAT in the North Atlantic region from the subtropics to the high latitude, and that pattern somewhat resembles that of the SST described earlier. When the AMOC is strongest, SAT in the Nordic Seas, the eastern branch of the subtropical gyre and along the NAC path tends to become warmer in contrast to both the Labrador Sea and to a lesser extent the tropical Atlantic where it tends to become cooler. As found in *cD*, this pattern is consistent with the anti-phase relationship previously identified between the Labrador and GIN Seas (see *Sect. 6.2.2*). Strong AMOC conditions also have impacts over land. Strongest conditions are mainly associated with a warming of both Europe and North America, which is consistent with similar previous studies (e.g. Pohlmann et al. 2004). In contrast, most of Greenland and land in the Southern Hemisphere tend to cool. This SAT pattern does agree in many ways with the one identified in *cD* (see Figure 4.10a), mainly in terms of warming of the Nordic Seas, North America and Europe, and cooling of the Labrador Sea. Although cooler conditions are identified in both runs in the tropics, those identified in the northern tropics in *cD* are not as clearly identified in *E*3. To summarise, this composite analysis reveals that most of the Northern (Southern) Hemisphere Atlantic sector tends to become warmer (cooler) under strong AMOC conditions.

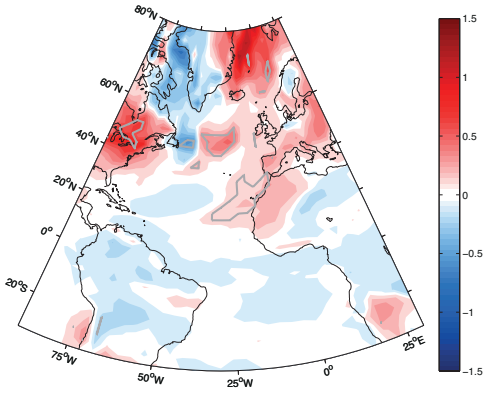

Figure 6.8: Composite of winter anomaly patterns of SAT (°C) induced by AMOC fluctuations, obtained by averaging anomalies over years when PC1 of the AMOC streamfunction is strongest. Grey contours indicate where the null hypothesis of equal means is rejected at the 10% level.

6.3.3 Impacts on precipitation

Figure 6.9 shows a composite of September precipitation anomaly pattern induced by strong AMOC conditions. Similarly to *cD* (see Figure 4.10c), few significant anomalies appear. There are still some notable changes over the western tropics of the North Atlantic with positive anomalies up to 20 cm yr^{-1}, suggesting a northward shift of the ITCZ. Although the tropical-subtropical SST gradient is less pronounced in *E*3 than in *cD* (*Sect. 6.3.1*), it seems reasonable to assume that the northward shift of the ITCZ is probably a consequence of this SST gradient. Under strong AMOC conditions, the Northwestern tropical Atlantic is expected to become wetter, and freshwater anomalies are therefore expected to develop locally as already mentioned for *cD*. The strong oceanic precipitation signal in this region also seems to leak over the adjacent continental areas.

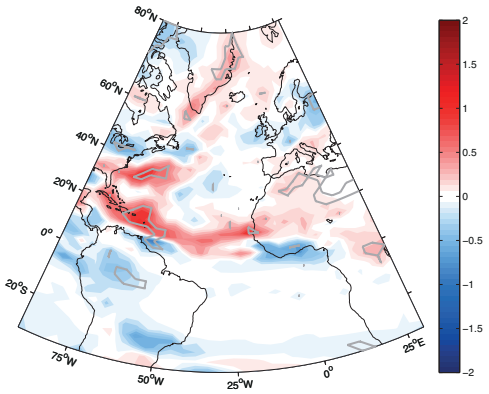

Figure 6.9: Composite of September anomaly patterns of precipitation (mm day^{-1}) induced by AMOC fluctuations, obtained by averaging anomalies over years when PC1 of the AMOC streamfunction is strongest. Grey contours indicate where the null hypothesis of equal means is rejected at the 10% level.

6.3.4 Impacts on sea level pressure

Figure 6.10 shows a composite of winter SLP anomaly pattern induced by strong AMOC conditions. Lower SLP tends to appear in most of the Northern Hemisphere except for the Labrador Sea and Greenland where SLP becomes higher. This pattern looks significantly different from the one identified in *cD* (see Figure 4.10b), where strong AMOC conditions were associated with a positive NAO-like pattern, this latter having been found to play a predominant role in explaining decadal AMOC fluctuations. Although the SLP pattern identified here could put into question the role of the NAO in explaining such fluctuations in *E*3, the missing January data for atmospheric fields in *E*3 (see *Sect. 2.1.2.2*) could well be the reason of the absence of the NAO-like pattern.

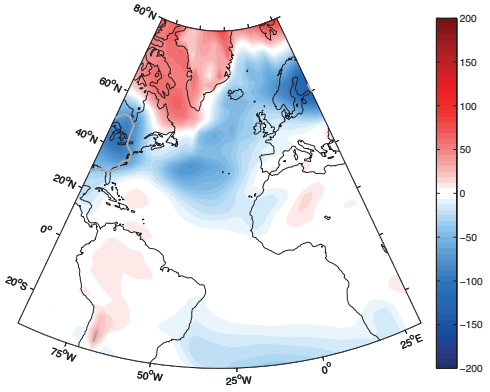

Figure 6.10: Composite of winter anomaly patterns of sea level pressure (Pa) induced by AMOC fluctuations, obtained by averaging anomalies over years when PC1 of the AMOC streamfunction is strongest. Grey contours indicate where the null hypothesis of equal means is rejected at the 10% level.

As in the case of *cD*, a clear link between AMOC strength and both surface temperature and precipitation has been identified in *E*3 (mainly over oceanic regions), reinforcing the existence of such a link in CHIME. In view of these major climatic impacts, the important question remains of whether AMOC fluctuations are potentially predictable in this model.

6.4 Potential Predictability of AMOC fluctuations

6.4.1 How far ahead is the AMOC potentially predictable?

The potential predictability of the AMOC is investigated using the PPP approach, for which five "perfect ensemble" experiments are performed starting from different AMOC initial states (strong, intermediate, weak, 5 and 15 years before a peak). Each experiment consists of six members (including the control integration) for 20-year long simulation.

Figure 6.11 shows the trajectories of each individual member, for each start date, together with the ensemble mean. At first sight and without taking into account the lowest variability due to the averaging effect, few ensemble means appear to closely follow the control run. Note that the extreme AMOC event at year 260 is relatively well captured when starting 5 years prior this peak (experiment 5P) while this is not really the case when starting 15 years before (experiment 15P).

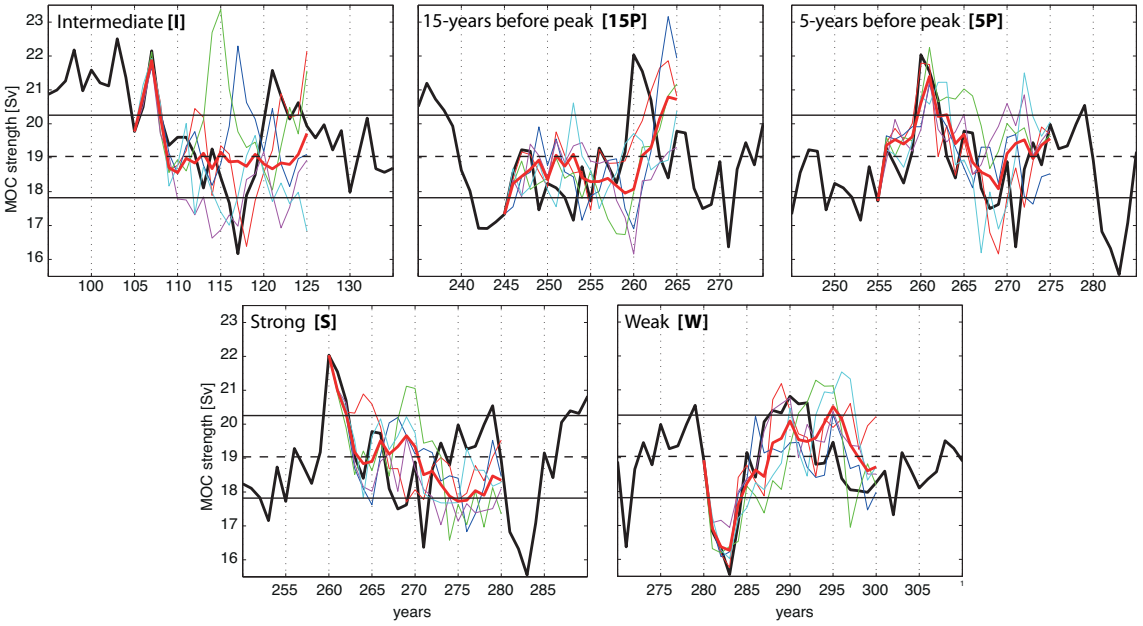

Figure 6.11: "Plumes" of maximum-annual mean AMOC at 30°N from ensembles of the CHIME model in which the initial conditions have been perturbed. Five ensembles are shown starting from different dates in the control integration *E*3. The individual ensemble members are shown as coloured lines, the ensemble mean as the red thick line, and the control run as the black thick line. The black horizontal dashed line is the mean AMOC, and both upper and lower horizontal solid lines show standard deviations highlighting the range of variability of the AMOC.

Figure 6.12 shows ES as a function of lead-time up to 2 decades for each experiment. The last statistically significant lead-time before ES persistently exceeds the threshold represents the maximum lead-time of predictability as inferred from ES alone. The longest lead-time of predictability is obtained for experiment 15P with a saturation level reached after about 10 years. In contrast, experiment S saturates the most quickly, after only 2 years. This latter result is quite surprising in view of previous similar studies (e.g. Collins et al. 2006a; Collins and Sinha 2003) and our experiments with IPSL (see *Sect. 5.3.1*) for which experiments starting from strong initial AMOC states are usually associated with an ES saturating at the longest lead-time. As for experiments 5P, W, and I, they all have an ES saturating after about 5-6 years. Figure 6.13 shows EC computed between lead-time 1 year and varying lead-times, ranging 5 to 20 years. Experiment W shows the highest scores with statistically significant EC superior to 0.7 for all lead-times from 5 to 20 years. Such EC (although slightly weaker) are found

for experiment I, but only up to 11 years. Experiment 5P shows weakest scores with statistically significant EC between about 6-9 years and 12-16 years. As for experiments S and 15P, no statistically significant ECs have been found.

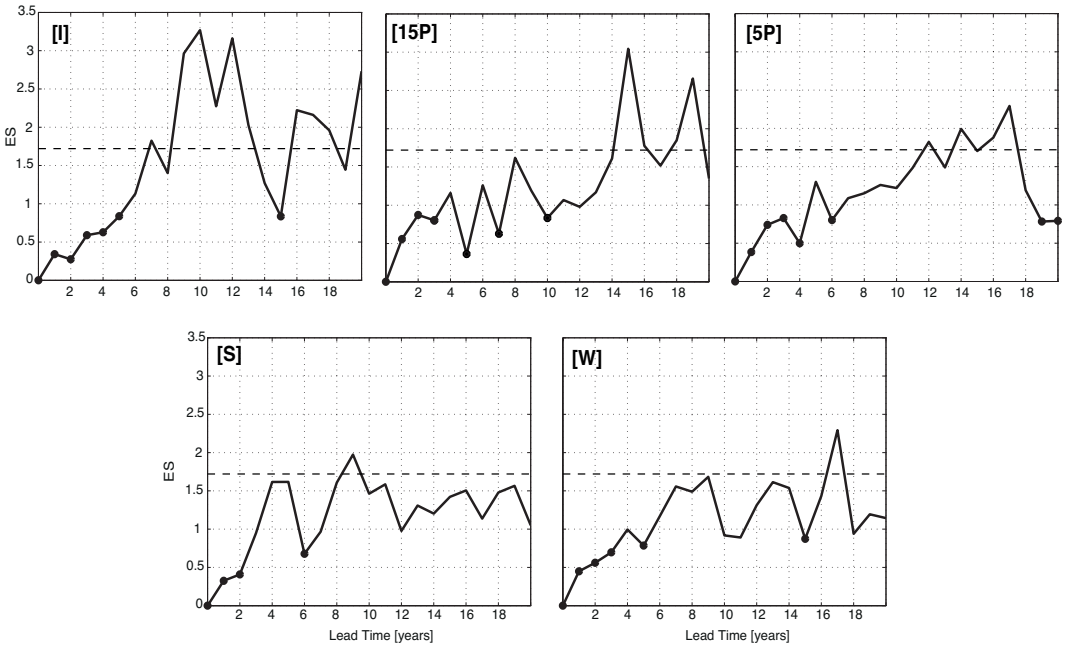

Figure 6.12: ES of AMOC index for each of the five experiments for lead-time up to 20 years. The threshold at which ES saturates (implying no potential predictability) is shown as the black horizontal dashed line. Dots indicate that ES is statistically smaller than the threshold at the 95% level based on a F-test.

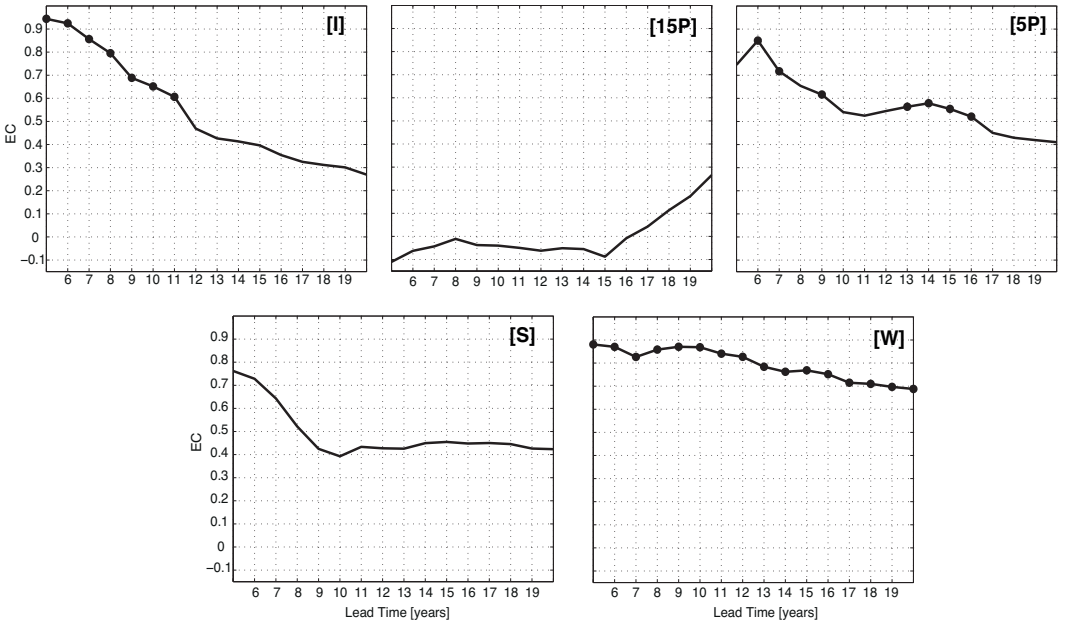

Figure 6.13: EC of AMOC index (as calculated by the Fisher transformation) for each of the five ensemble experiments for lead-time from 5 to 20 years. Dots indicate that EC is statistically significant at the 90% confidence level using a one-tailed Student t-test.

To have a better idea of the predictive skill of each experiment, information given by both ES and EC are summarized in Figure 6.14. As with the IPSL predictability study, the predictive skill of each experiment is determined by the maximum lead-time at which ES saturates and its corresponding EC.

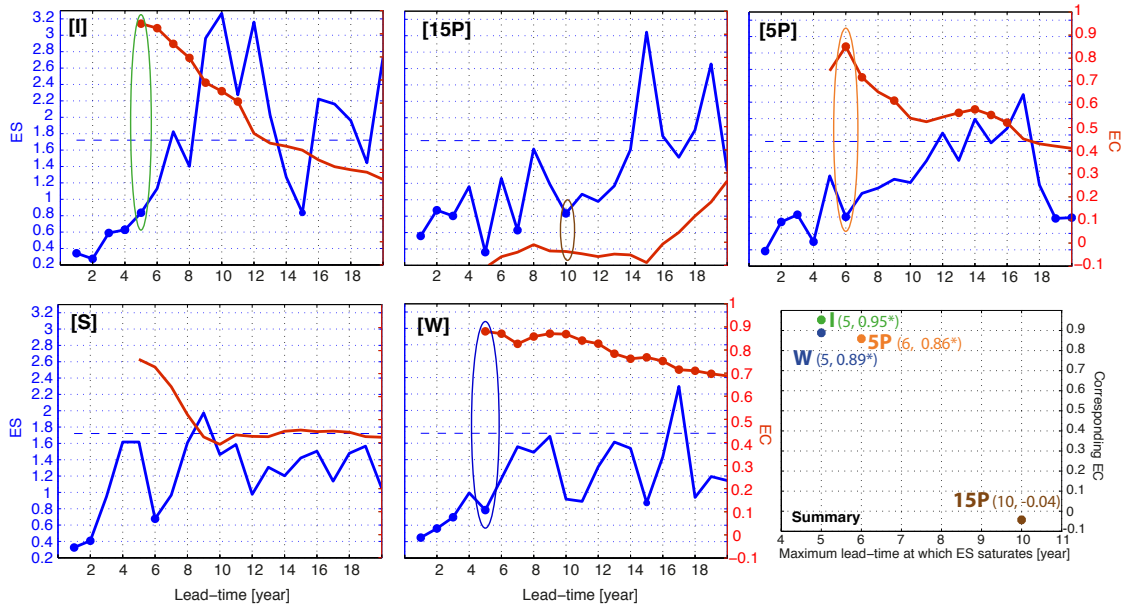

Figure 6.14: Plots showing ES (blue line) and EC (red line) against lead-times for each of the five ensemble experiments. Dots indicate statistical significance at the 95% (90%) confidence level for ES (EC). The summary plot shows the maximum lead-time at which ES saturates with its corresponding EC (as indicated by the oval circles) for each experiment (statistically significant ECs at the 90% are marked with an asterisk).

Experiment 5P shows overall the highest PPP skills as it corresponds to the experiment with the longest saturation lead-time (obtained from ES) and a corresponding EC statistically significant and superior to 0.8 (lower-right plot, Figure 6.14); this experiment therefore suggests a limit of predictive skills of the AMOC index of about 6 years. Experiment 5P is closely followed by experiments I and W, which both have high statistically significant EC but ES that saturates slightly more quickly (after about 5 years).

In contrast, strictly speaking, both experiments 15P and S have no predictive skills (as previously defined in *Sect. 3.2.1.2*). Indeed, while ES of experiment 15P saturates at the longest lead-time (10 years), its corresponding EC is remarkably low (-0.04). As illustrated earlier in the IPSL predictability study, information given by ES or EC alone should not be neglected as they can still give useful information about for specific feature such as the ability to capture an extreme event. So based on ES of experiment 15P only, this could still indicate a strong predictability (up to 10 years), but it is nevertheless not strong enough to predict the peak of year 260. In addition, the fact that the longest lead-time at which ES saturates is obtained for the experiment showing the lowest EC somewhat contrasts with results obtained with the IPSL-CM5A model. Indeed in the

latter, it seems that the more the lead-time (at which ES saturates) increases, the more EC increases (see lower-right plot, Figure 5.5). This is clearly not the case with CHIME (lower-right plot, Figure 6.14). To some extent, experiment 15P weakens the claim drawn from the IPSL predictability study that ES and EC are dependent metrics (see *Sect. 5.3.1*). Surprisingly, there is also no predictive skill (as defined in *Sect. 3.2.1.2*) for the experiment starting from strong initial AMOC state (i.e. experiment S). Based on ES only, this could still indicate very weak predictability only up to 2 years. This result clearly contrasts with those from the IPSL predictability study (see *Sect. 5.3.1*) and previous similar studies (e.g. Collins and Sinha 2003; Collins et al. 2006a) that showed that experiments starting from anomalously strong AMOC are usually associated with the best predictive skills. Because, here, the experiments have fewer members than these previous studies, we question whether this influence the PPP skills and whether this could be the reason of the lowest skills of experiments S in CHIME. We therefore test the eventual sensitivity of PPP skills to the number of members by generating five additional members for experiments S. Figure 6.15 shows the plumes, ES and EC of the AMOC index when considering these additional members (now accounting for 11 members in total). Results show that the lead-time at which ES saturates still remains the shortest of the five ensemble experiments (from 2 years with 6 members to 3 years with 11 members) and that no statistically significant EC is obtained for any lead-times. One of the plausible explanations for this surprising short predictability lead-time is that strong AMOC conditions might be associated with an excessive convective mixing in CHIME that reduces its predictive skills. This result also suggests that increasing the number of members does not significantly affect the PPP skills of the AMOC, and strengthens the robustness of results found for experiment S in CHIME.

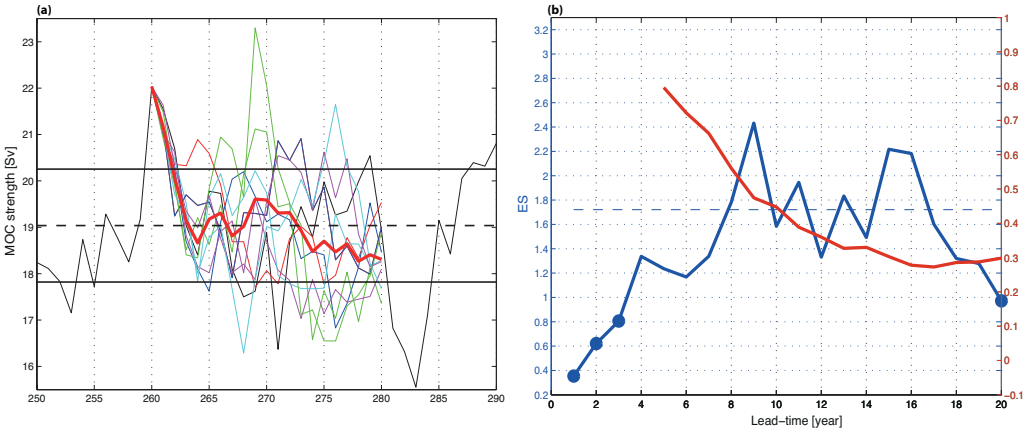

Figure 6.15: (a) "Plumes" of maximum-annual mean AMOC at 30°N, and (b) plot of ES (blue line) and EC (red line) against lead-times (dots indicate statistical significance at the 95% confidence level), for experiment S when considering 11 members.

Although the highest predictive skill in CHIME has not been found when starting from a maximum AMOC extreme state as with IPSL (see *Chapter 5*) or HadCM3 (e.g. Collins

and Sinha 2003), there is nevertheless some evidence in CHIME for the AMOC predictive skills to be favoured by its extreme states. Indeed the highest potential predictability has been found for experiment 5P that is only 5 years prior a maximum extremum, and closely followed by experiment W that starts from a minimum AMOC extreme state. The latter result somewhat contrasts with previous studies which generally found that experiments starting from a minimum AMOC extreme have significantly lower predictive skills than experiments starting from a maximum AMOC extreme. The results obtained with CHIME therefore question the stronger influence of a maximum AMOC extreme on predictive skills.

By averaging the maximum lead-time at which ES saturates for the five ensemble experiments, we found an average saturation level reached after about 6 years. However, at this lead-time, the average EC amounts to 0.66 which is not statistically significant at the 90% level when considering the average number of degrees of freedom over each starting date. As already pointed out in the IPSL predictability study, EC (which can strongly depends on the starting dates) is of limited use for an estimation of the average predictive skill. It seems therefore reasonable to claim that, based on ES alone, the average predictive skills of the AMOC is of about 6 years in the CHIME model. Note that this lead-time is somewhat shorter than the one found in the previous chapter with the IPSL-CM5A model (8 years, see *Sect. 5.3.1*). However, this result is in good agreement with Hermanson and Sutton (2009) who found an average predictive skill of the AMOC of about 5 years with the HadCM3 model.

6.4.2 Probability Density Functions of AMOC

Although deterministic measures of predictive skills (such as EC, ES) are a good way of evaluating the effective predictability within models, such metrics do not give information about the prediction probabilities. As stated in *Sect. 3.2.1.2*, a shift in the mean of the ensemble can be complementary and useful for prediction. For each experiment, we therefore examine the Probability Density Functions (PDFs) of the AMOC index (Figure 6.16), fitted by assuming a Gaussian distribution (to be consistent with the central limit theorem for a process arising from numerous independent disturbances, Wunsch and Heimbach 2012) and computing the mean and standard deviation of the 6 members (including the control integration). If the ensemble mean of the ensemble experiment is significantly shifted with respect to climatology, it will result in biases in the probability of e.g. stronger AMOC conditions; information of considerable interest in view of its possible climatic impacts.

At first sight, shifts with respect to climatology are most significant when calculating over the first decade (Figure 6.16a) than over the two decades (Figure 6.16b), consistent with a decrease in predictive skills beyond one decade for the AMOC index in CHIME (as identified earlier). For the first decade, all experiments (including those with no

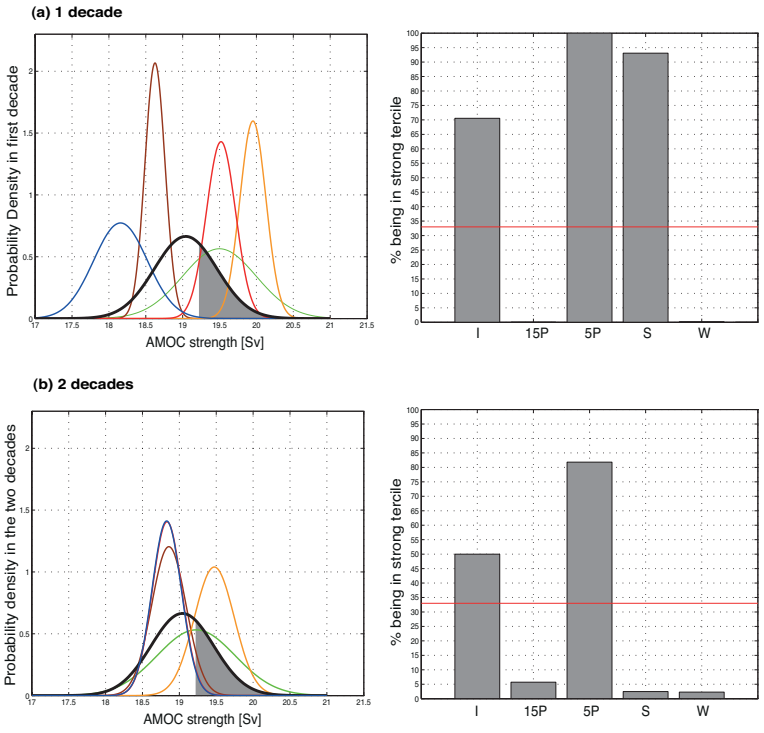

Figure 6.16: Left panels - Fitted PDFs of decadal mean of the AMOC index in the (a) first and (b) two decade(s). Black solid line represents the climatological PDF computed from the 201-year control integration $E3$ with the stronger tercile shown as grey shading; Colored lines represent the PDF of each experiment S (red), W (blue), I (green), 15P (brown), 5P (orange). Right panels - Probability of decadal-mean AMOC being in the strong tercile (the upper third of the climatological PDF) for each experiment; the climatological probability of this event is 33% (shown as the horizontal red line).

PPP skills as defined here, see previous section) have significant shifts with respect to climatology, and are therefore useful in that sense. Experiments 5P, I, and S (15P and W) show a significant increase in the probability of stronger (weaker) conditions over the first decade. For example, the probability of decadal-mean AMOC strength being in the strong tercile (the upper third of the climatological PDF) for experiment 5P (W) is more than 99% (less than 1%), that is higher (lower) than the 33% expected from chance. A reliable forecast that says that "the decadal-mean of AMOC strength has more than 99% (or less than 1%) chance of being significantly stronger than normal in the coming decade" could be of considerable value. The above results show evidence for useful prediction probability skills in regard to the AMOC index of CHIME.

6.4.3 An early warning system to predict extreme AMOC events?

Results from *Sect. 6.4.1* also showed the ability of the model to capture a maximum extreme AMOC (e.g. year 260) about 5 years in advance (experiment 5P, Figure 6.11), similarly to the IPSL-CM5A model. However it does not seem to be able to capture such

a peak 15 years in advance (experiment 15P, Figure 6.11), in contrast to IPSL. From experiment W, we can also see the ability of the model to capture well the minimum extreme AMOC of year 283 about 3 years in advance. However, in contrast to 5P, experiment W starts when the AMOC is already in its decreasing trend; it is therefore difficult to draw robust conclusions about the ability of the model to capture such a minimum peak only based on this experiment. There is nevertheless some evidence for the ability of the CHIME model to capture extremum states. Similarly to the IPSL model, we can investigate whether some of the AMOC precursors can increase the predictive average lead-time found with the PPP approach (i.e. the 6-year lead-time). According to the mechanisms identified in *Chapter 4*, northern tropical Atlantic SSS can be considered as a precursor of AMOC changes in CHIME, with a lead-time of about 15 years (see Figure 4.19). As already mentioned in *Chapter 5*, for this apparent predictability to be useful requires that a large change in the main identified precursor always leads to a corresponding change in the AMOC index. It is important to bear in mind that these mechanisms and the location of the precursor site are model-dependent.

Figure 6.17 shows time series of the AMOC index (upper panel) and the northern tropical Atlantic SSS averaged from 0-15°N (lower panel) in the control integration $E3$. It is found that of the 11 identified "events", for which the precursor changes by more than 1.5σ, 6 are followed by an AMOC change of the correct predicted sign around 15 years later, of which 5 show a change larger than 1.5σ. In CHIME, there is therefore evidence for large changes in the precursor to lead to large changes in the AMOC (after $\sim$ 15 years) in about 50% of the cases.

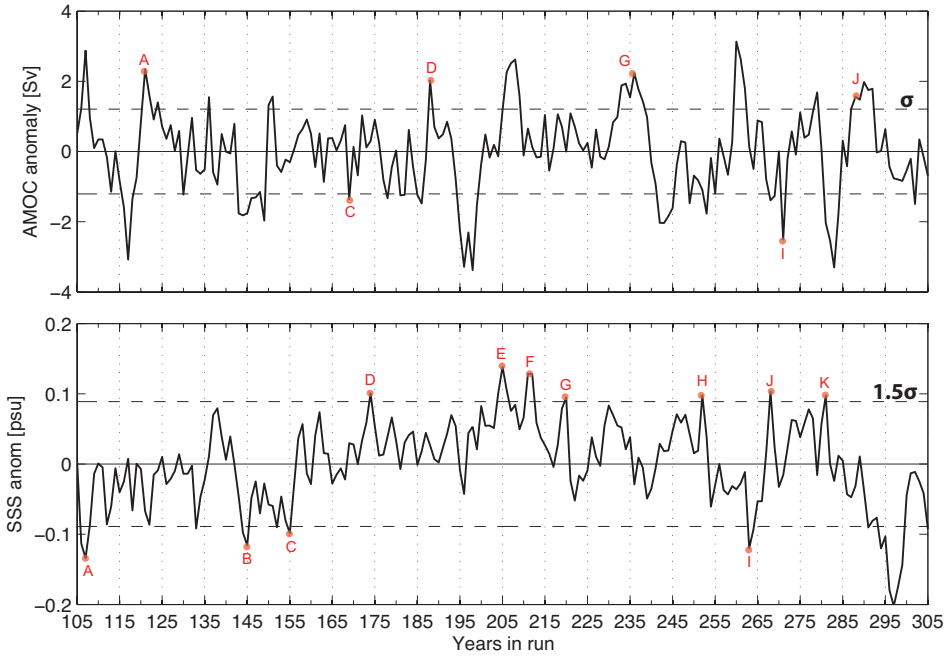

Figure 6.17: Time series of detrended AMOC index and northern tropical Atlantic SSS (averaged from 0-15°N/0-80°W). Alphabetical letters correspond to identified events (see text for further details).

Note that in the IPSL-CM5A model, large changes in the AMOC precursors (located in the northern North Atlantic) lead to large changes in the models AMOC in about 80% of the cases (see *Sect. 5.3.2*). It is, however, important to note that this apparent difference in the ability to predict extreme AMOC events might not be significant since fewer initial events (for which the precursors are in an extreme state) have been identified in IPSL-CM5A than in CHIME (6 "events" against 11, respectively). Nevertheless, several factors could still explain the plausible difference in the ability of these two models to predict extreme AMOC events from their corresponding precursors. For example, this could be due to the difference in the localization of their AMOC precursors; while the one in CHIME is situated in the tropics, both precursors in IPSL-CM5A are in the high latitude regions (Escudier et al. 2012) that are closer to the deep convection sites. In CHIME, the precursor may be relatively too remote, and might therefore lose its predictive skill over longer distances, compared to IPSL-CM5A. Large changes in the IPSL-CM5A precursors might therefore lead to more systematic large changes in the AMOC. We also have to keep in mind that the AMOC precursor considered here for $E3$ with CHIME has been identified from a different CHIME control integration (cD, see *Chapter 4*). Although there is some evidence that both $E3$ and cD have similar mechanisms controlling the decadal AMOC fluctuations (see *Sect. 6.2*), the northern tropical Atlantic SSS anomalies might not be the most appropriate precursor in $E3$.

Despite all these above qualifications, it seems reasonable to say that an early warning system of extreme AMOC events can still be possible with CHIME (while less reliable than with IPSL-CM5A). In about 50% of the cases, the monitoring of large changes in the northern tropical SSS could lead to the prediction of an extreme AMOC event about 15 years later, therefore increasing the average lead-time of predictability found from the PPP approach when directly applied to the AMOC index (6 years, see *Sect. 6.4.1*). Note that, as already mentioned in the IPSL predictability study, hope for the predictability of an extreme AMOC event to go even beyond this suggested decadal lead-time of predictability could arise if its precursor itself is predictable. However, in contrast to the AMOC precursors in IPSL-CM5A, the PPP approach reveals no potential predictability of the AMOC precursor in CHIME. Indeed, the northern tropical Atlantic SSS has been found to have an average predictive skill that saturates after only 2 years associated with a very low and non-significant EC (<0.15, not shown).

In summary, we found convincing evidence that extreme changes in the AMOC as seen in the CHIME model might be potentially predictable up to 15 years ahead from the monitoring of tropical precursors. If a comparable mechanism to the one identified in the CHIME model (*Chapter 4*) occurs in the real ocean (which remains to be demonstrated), then the ability to predict decadal AMOC fluctuations is promising for potential predictability of climate at multi-decadal timescales.

6.5 Spatio-temporal predictability of Atlantic climate

Potential predictability of climate-related fields such as SST, SAT and precipitation is now evaluated in CHIME using and comparing both the DPP and PPP approaches.

6.5.1 Potential predictability of sea surface temperature

Figure 6.18 shows predictability maps of Atlantic SST up to 1 and 2 decades as identified by both the DPP and PPP approaches in the CHIME model. For the former approach, the maps show the *ppvf* for 10 and 20-years means and are shown in Figure 6.18a. For the PPP approach, regions combining SST with both ES statistically smaller than the saturation level at the considered lead-time and statistically significant EC (i.e. regions potentially predictable as defined in *Sect. 3.2.1.2*) are shown in Figure 6.18b as a function of the number of experiments for which these conditions are met.

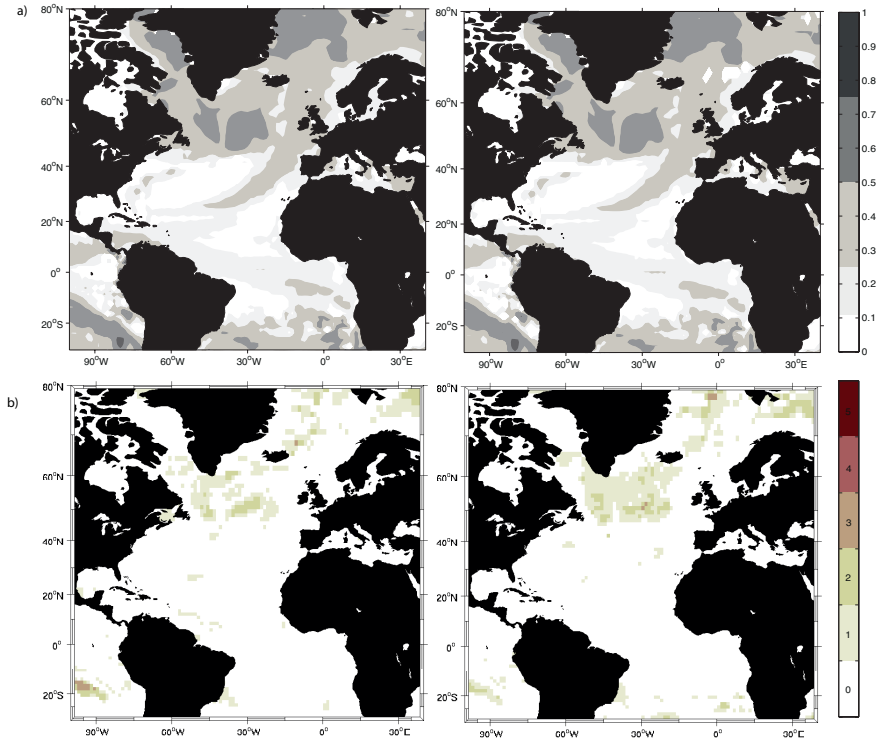

Figure 6.18: Potential predictability of SST in the Atlantic sector identified by: (a) the DPP approach showing maps of the internally generated decadal *ppvf* for 10-year (left panel) and 20-year (right panel) means in the unforced control climate of CHIME (the colored areas are significant at the 95% level according to a F-test); (b) the PPP approach showing maps of the number of starting date (out of 5) where grid points are potentially predictable (i.e. where it combined both statistically significant EC at the 90% confidence level according to a Student t-test and normalized ES smaller than saturation level at the 95% level according to a F-test) up to one (left panel) and two (right panel) decades.

Note that there are less marked differences between the two timescales in CHIME than in IPSL-CM5A (see Figure 5.8), mainly for the DPP approach. *ppvf* values are largely statistically significant over the Atlantic Ocean (Figure 6.18a). We recognize the "reverse C shape" pattern in CHIME for mid-latitude SST as already identified in IPSL-CM5A (see Figure 5.9). This particular pattern has also been identified by Delworth et al. (2007) in the EOF analysis of observed annual mean SST data for the period 1870-2005 (Figure 6.19), suggesting that predictability might be associated with variance. The highest scores are mainly found in the northern North Atlantic, specifically in Baffin Bay, the subpolar gyre region and the Greenland Sea, where 50 to 75% of the variance exists in the decadal bands (Figure 6.18a). These two latter regions are the only ones identified as potentially predictable by the PPP approach. Note that their signals are however weak as these regions are identified in a maximum of only 2 ensemble experiments (i.e. for less than 50% of the experiments). The PPP approach does not seem to identify regions with less than 50% of variance in the decadal bands, as it does not even identify the eastern branch of the subtropical gyre and the southern tropics that still have significant fractions of variance ($0.25 < ppvf < 0.50$, Figure 6.18a). As already mentioned in the IPSL predictability study (see *Chapter 5*), this discrepancy between the two approaches might arise both from the difficulty of the DPP approach to define a threshold for "useful" potential predictability and from the limited number of starting dates in the PPP approach. Nevertheless, the latter approach still clearly brings out most of the regions exhibiting the highest fraction of variance in the decadal band as identified by the DPP approach, strengthening the likelihood of these regions to be potentially predictable. As mentioned earlier, they include the subpolar gyre region and the Greenland Sea.

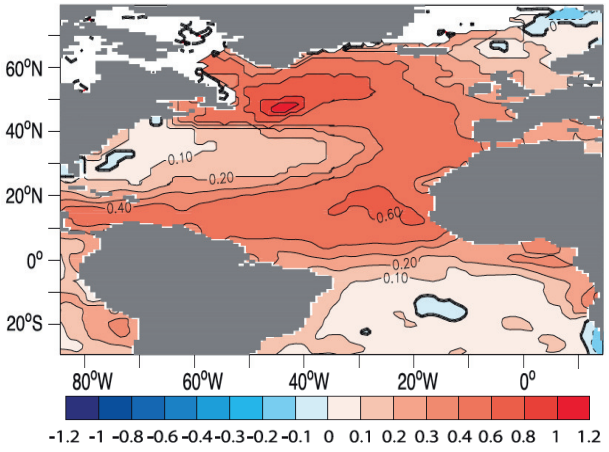

Figure 6.19: Output from and EOF analysis of observed annual mean SST over the period 1870-2005 obtained from the HADISST data set, Rayner et al. (2003). The values plotted are the linear regression of the original SST time series on the standard deviation of the PC1 time series, and then multiplied by 2 (yielding a map corresponding to SST anomalies associated with a two standard deviation fluctuation of this EOF). Units are K. Contour intervals are 0.1 between -0.4 and 0.4, and 0.2 otherwise. (From Delworth et al. 2007).

The influence of strong AMOC states alone on the predictive skills of regions of weak predictability signals claimed in the IPSL predictability study (see *Sect. 5.4*) does not really apply to the CHIME experiments. Although the predictability of SST in the subpolar gyre region and the Greenland Sea seems to indeed arise from experiments including or starting from a strong AMOC state (i.e. experiments 15P and S, especially up to 2 decades), most of the SST predictability in CHIME comes from experiment W, that is when starting from a weak AMOC state (see *Appendix C*, Figure C.1). Although the experimental set up was not designed to draw robust conclusions about a possible predictability-dependence on the AMOC initial states, there is still some evidence in CHIME that SST predictability is favoured by extreme AMOC events in a maximum state (like in IPSL-CM5A) but also in a minimum state.

6.5.2 Potential predictability of surface air temperature

Figure 6.20 shows predictability maps of Atlantic SAT up to 1 and 2 decades as identified by both the DPP and PPP approaches. As in the case of SST, the SAT pattern is barely modified between the two timescales considered here (especially for the DPP approach), in contrast to results found with IPSL-CM5A (see Figure 5.8). The only noticeable exception is for the Nordic Seas in the DPP approach (Figure 6.20a) where the predictive skills slightly extend to the surrounding areas when the timescale is decreasing.

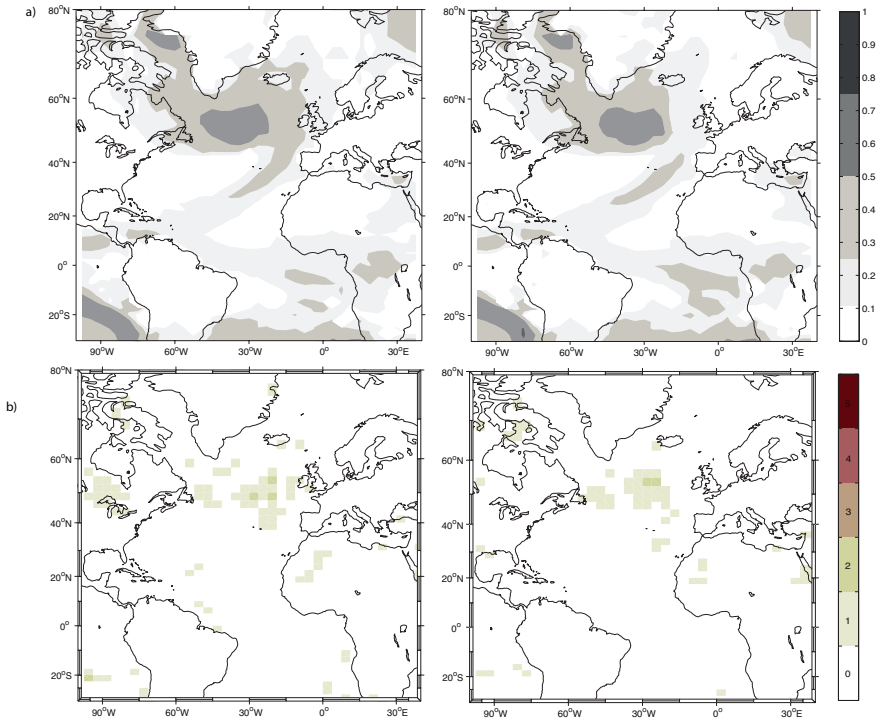

Figure 6.20: Potential predictability of SAT in the Atlantic sector as defined in Figure 6.18.

As expected, the *ppvf* pattern of SAT over the ocean somewhat resembles that of the SST (Figure 6.18). Note, however, the exception of the Greenland Sea where SST is identified as potentially predictable but not SAT. The reason for this discrepancy between the two variables remains unclear. Statistically significant DPP skills for which more than 25% of the variance is in the decadal bands mainly include most of the northern North Atlantic (Figure 6.20a), in good agreement with the diagnostic multi-model approach of Boer (2004) and Boer and Lambert (2008). Some hints of predictability are also visible in the eastern branch of the subtropical gyre and the tropics up to 2 decades ahead, where 10 to 25% of the variance exists in the decadal band (Figure 6.20a). Overall, the highest scores over the ocean are found, as with SST, in Baffin Bay and the subpolar gyre region for which 50% to 75% of the variance exists in the decadal bands. The latter region is the only one identified as potentially predictable by the PPP approach. Note that, as with SST, regions identified as predictable by the PPP approach are characterized by a high fraction of SAT variance in the decadal bands (above 25%).

Over land, potential predictability is generally less than over the ocean. There are however some areas for which 10 to 50% of the variance exists in the two decadal bands (Figure 6.20a). These regions include Central America, Northeast and Tropical Africa, Iceland, Eastern Canada and the Western part of the British Isles. The PPP approach only identified the latter region and Central Canada (rather than Eastern) as potentially predictable up to 1 decade ahead. As with the ocean, predictability over land is identified in less than 50% of all the ensemble experiments in the PPP approach. In contrast to the western part of the British Isles, there is no evidence for Central Canada to be potentially predictable in the DPP approach (with less than 10% of the variance in the decadal band). This discrepancy may arise from the January missing months in the control integration $E3$, on which the DPP approach relies.

Despite some discrepancies between the two approaches, we can be strongly confident in the robustness of our results concerning the potential predictability of SAT over the ocean in the subpolar gyre region, and over land in the western part of the British Isles, as these regions are identified by both approaches.

As with SST, the regions of weak signals identified by the PPP approach here in CHIME (i.e. the subpolar gyre region, Canada and the western part of the British Isles) seem to be favoured when the predicted time period includes or starts from a maximum AMOC extreme state; they are indeed identified for experiments 15P and S only (see *Appendix C*, Figure C.1). "Plumes" of SAT averaged over both the North Atlantic subpolar region and the Western UK confirm this finding (Figure 6.21). These plumes, indeed, show clear evidence for the subpolar gyre region (Western UK) to have better predictive skills for experiment 15P (S); this is the experiment in which most of the members seems to follow each other the most closely, and in which the spread of the prediction plume seems to be the smallest, mainly over the first decade. Note that averaging SAT over a quite large region might hide predictive skills of some local areas which

could be of primary importance to decision makers in sectors such as, e.g. agriculture, fisheries. When studying predictability of climate-related fields, it therefore seems more judicious to examine maps of predictive skills rather than "plumes" averaged over a specific region. As in IPSL-CM5A, predictive skills are not identified in experiment 5P although it includes the extreme AMOC peak of year 260. The reason for the weak scores in these regions in 5P also remains to be clarified. Note that, in contrast to SST, the predictive skills of SAT are low for experiment W.

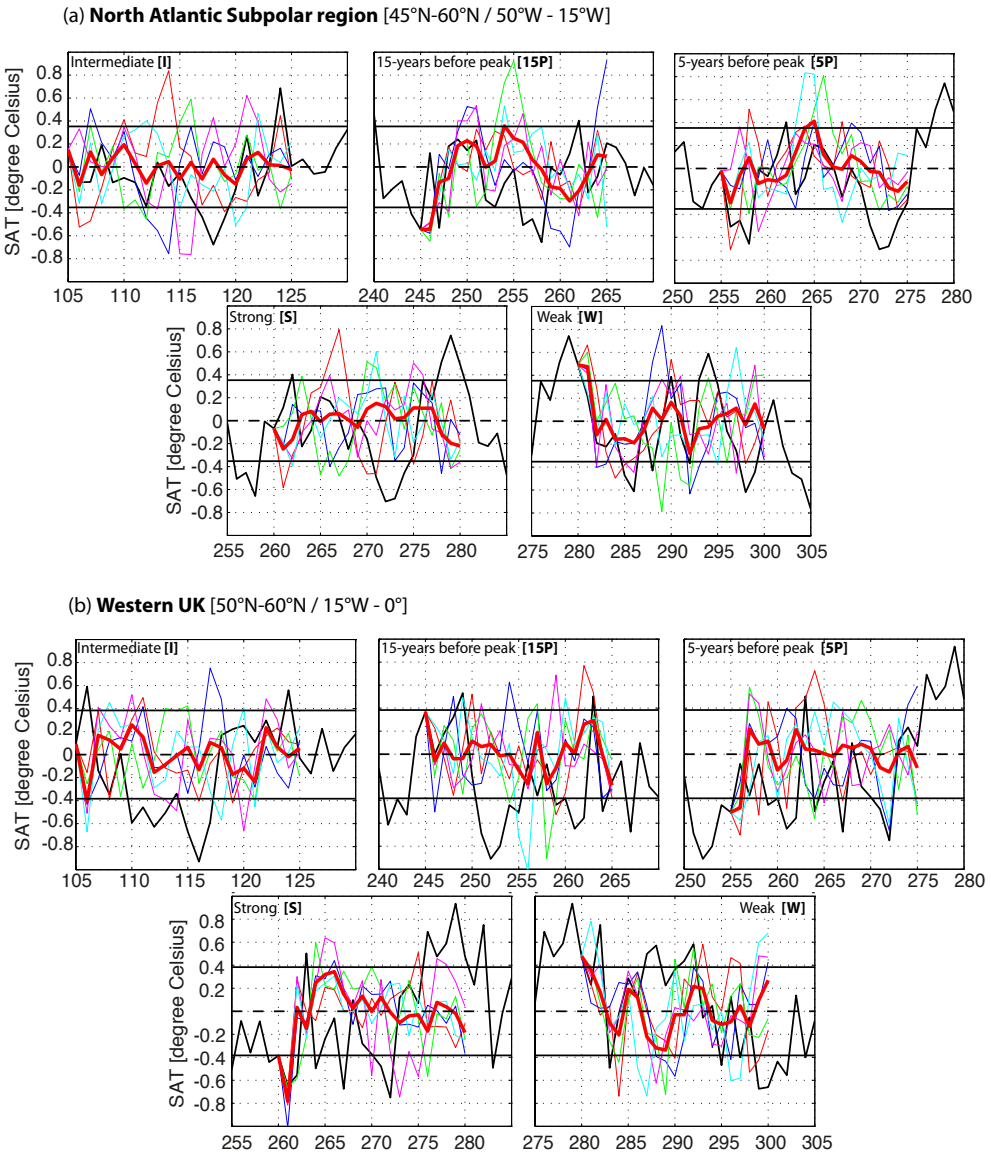

Figure 6.21: "Plumes" of detrended SAT averaged over (a) the North Atlantic Subpolar region [45°N-60°N/50°W-15°W] and (b) the Western UK, from ensembles of the CHIME model in which the initial conditions have been perturbed. The individual ensemble members are shown as coloured lines, the ensemble mean as the red thick line, and the control run as the black thick line. Both upper and lower horizontal black lines show standard deviations highlighting the range of variability of the SAT.

6.5.3 Potential predictability of precipitation

The potential predictability of precipitation (Figure 6.22) is considerably smaller than for SST and SAT, in good agreement with the multi-model approach of Boer and Lambert (2008). As with surface temperature, the *ppvf* pattern for precipitation does not significantly differ between the 10-year and the 20-year timescales. Although weak, a few patches of predictability (for which 10 to 50% of the variance exist at the two decadal bands) are found in the subpolar gyre region, the southern tropical Atlantic and over Central America (Figure 6.22a). Although these two latter regions are not identified in Boer and Lambert (2008), the subpolar gyre region is identified with a significant fraction of variability (comprised between 5% and 30%) up to 2 decades ahead. However, none of the above regions have been identified by the PPP approach in CHIME (Figure 6.22b). As already mentioned earlier, the discrepancy between these two approaches might come from the difficulty in defining a "useful" threshold of predictability in the DPP approach. It seems therefore cautious to claim that predictability of precipitation is absent in CHIME.

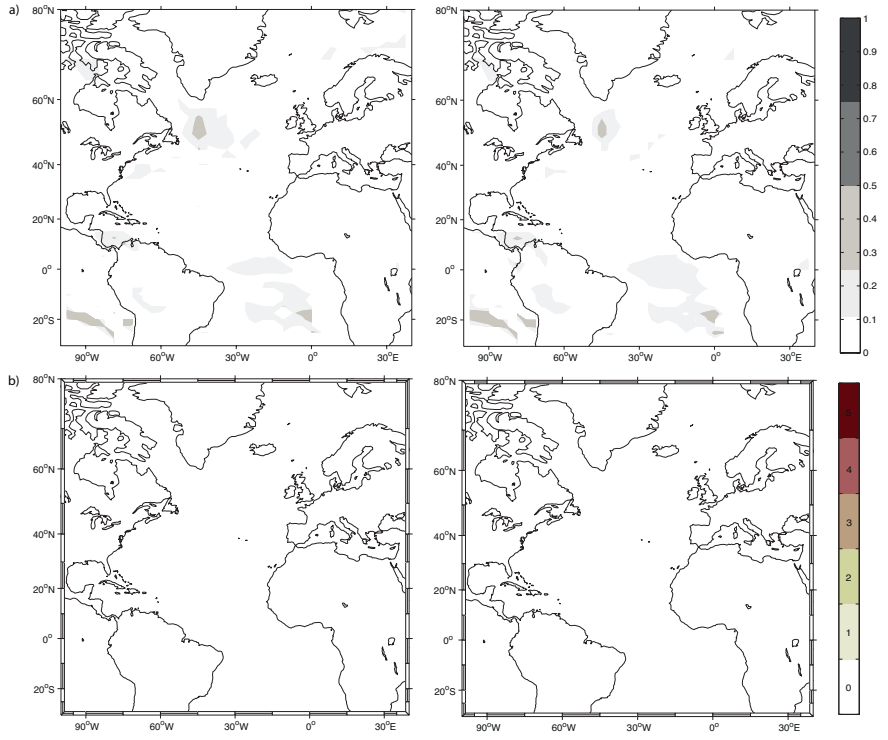

Figure 6.22: Potential predictability of precipitation in the Atlantic sector as defined in Figure 6.18.

Although not as obvious as in the IPSL-CM5A model, the above results suggest some dependence of predictability skills on the AMOC initial state, at least for SST and SAT, in CHIME. Indeed, they seem to be favoured by extreme AMOC states although the role of minimum versus maximum extreme states still needs to be clarified. The likelihood for a link between extreme AMOC events and predictability of temperature

is strengthened by the fact that regions identified as potentially predictable by both approaches here are also the regions most sensitive to strong AMOC conditions (as seen in Figure 6.7, Figure 6.8). In contrast to IPSL-CM5A, this link has however not been found for precipitation in CHIME. Nevertheless these above results still suggest that, in CHIME, the mechanism responsible for temperature predictability could be linked to the one behind decadal AMOC variability as found in IPSL-CM5A.

6.6 Summary and discussion

In this study, we have focused on the prognostic predictability of the AMOC as represented in the CHIME model, along with the diagnostic (DPP) and prognostic (PPP) predictability of associated oceanic and atmospheric fields. In the DPP approach, we analyzed the 201 years of the control integration $E3$, while "perfect ensemble" experiments using the same control integration are performed in the PPP approach.

6.6.1 Potential predictability of the AMOC

The predictive skills of the AMOC index have been quantified by the PPP approach for five experiments starting from different AMOC initial states, using both the ensemble spread (ES) and the ensemble correlation (EC). As for the IPSL predictability study, ES (EC) generally increases (decreases) with lead-time, and hence predictability is lost after a certain lead-time. Note, however that, this relationship between ES and EC does not clearly exist for experiment 15P, therefore weakening the claim drawn in *Chapter 5* that ES and EC are dependent metrics.

Although it remains difficult to determine an average predictability skill in the "perfect ensemble" experiments (as it implies averaging skills over several starting dates which themselves have very different predictability skills), it seems reasonable to claim that the modeled AMOC has an average predictive skill of about 6 years in the CHIME model (when considering the average lead-time at which ES saturates). This average lead-time of predictability is somewhat shorter than the one found with the IPSL-CM5A-LR model (8 years, see *Chapter 5*). This is, however, in good agreement with Hermanson and Sutton (2009) who found an average predictive skill of the AMOC of about 5 years with the HadCM3 model. Given the more coherent internal structure of the anomalies in CHIME compared to non-isopycnic coordinate ocean component models (such as HadCM3 and IPSL), CHIME would be expected to have significantly better predictive skills than non-isopycnic models. This does not actually seem to be the case here.

When considering the predictive skills of each ensemble experiment separately, there is evidence for predictive skills to depend on the AMOC initial state. Although the highest predictive skill in CHIME has not been found when starting from a maximum AMOC

extreme state as was the case with IPSL-CM5A (see *Chapter 5*) or HadCM3 (e.g. Collins and Sinha 2003), there is nevertheless some evidence in CHIME for the AMOC predictive skills to be favoured by its extreme states. Indeed the highest potential predictability has been found for the experiment starting 5 years prior to maximum extrema (experiment 5P), and closely followed by the experiment starting from a minimum AMOC extreme state (experiment W). Reliable probability forecasts have also been found for these two experiments; experiment 5P (W) suggests that the decadal-mean AMOC strength has more than 99% (less than 1%) chance of being significantly stronger than normal in the next decade. As briefly mentioned above, these results with CHIME somewhat differ from those with IPSL-CM5A (see *Chapter 5*) and HadCM3 (e.g. Collins and Sinha 2003) as the highest predictive skill has not been found when starting from a maximum AMOC peak (i.e. for experiment S). Even after having added additional members to experiment S (in order to test the robustness of its result), the AMOC predictive skills have been found to be one of the lowest in CHIME. In contrast to this latter finding, the predictive skills associated with experiments starting from a minimum AMOC extreme in both IPSL-CM5A and HadCM3 were significantly lower than when starting from a maximum AMOC. The results obtained with CHIME therefore question the stronger influence of a maximum AMOC extreme on its predictive skills.

Although they occur rarely, the ability to predict extreme events is of considerable value in view of its major climatic impacts. The model has shown its ability to capture relatively well the timing of an extreme AMOC event about 5 years in advance (experiment 5P). It has also been shown that by monitoring its precursor, the AMOC predictive skills of such events can go beyond this 5 years lead-time and beyond the average lead-time of predictability (of about 6 years). Indeed, an extreme AMOC event can be predicted up to 15 years in advance from the monitoring of its tropical precursor in 50% of the cases, which is the northern tropical Atlantic SSS in CHIME. Note that despite some evidence that the mechanism controlling decadal AMOC fluctuations in cD is very similar to the one in $E3$, it has to be kept in mind that this tropical precursor might not be the most appropriate one in $E3$. Nevertheless, our finding tends to suggest the need for intense observation in the tropical Atlantic Ocean to constrain prediction of the AMOC. In such perspective, the maintenance of, e.g. mooring arrays in this area, is likely to be of greatest value provided the real world has a similar mechanism of variability.

6.6.2 Potential predictability of the North Atlantic climate

Changes in the AMOC have also been found to have significant and widespread climate impacts; the potential predictability of these climate impacts have been evaluated here using both DPP and PPP approaches. First, note that independently of the approach used, there is not much difference in the spatial distribution of their potentially predictable regions between the 10-year and 20-year timescales. As was the case with

IPSL-CM5A, the DPP estimation seems less discriminant and regions found to be potentially predictable by the PPP approach correspond to the regions showing the highest fraction of variance in the decadal band in the DPP approach. However, in contrast to IPSL-CM5A, these regions identified by the PPP approach only reveal some hints of predictability (i.e. they are identified in less than 50% of the "perfect ensemble" experiments). But the fact that they are also identified in the DPP approach strengthens our confidence in the predictability skills of these regions. To therefore strengthen the robustness of our results, note that the regions claimed to have some hints of predictability below are regions identified by both approaches.

The North Atlantic subpolar gyre has been identified as a region where SST and SAT are potentially predictable up to 2 decades ahead, in good agreement with the IPSL predictability study (see *Chapter 5*) and previous similar studies (e.g., Collins 2002; Boer 2004; Pohlmann et al. 2004; Hawkins et al. 2011; Branstator et al. 2012). As previously mentioned in *Chapter 5*, the ability to predict this region is promising for the potential multi-year forecast of tropical storm and hurricane frequency (Smith et al. 2010). There are also some hints of SST predictability in the Nordic Seas (and more specifically in the Greenland Sea), which are clearly absent for SAT. This region has also been identified in most of the above-cited studies, for which the predictability of SAT over the ocean is generally similar to that of SST (e.g. Pohlmann et al. 2004). While this discrepancy between SST and SAT in the Nordic Seas in CHIME could be a consequence of the January missing months in the atmospheric data of $E3$, the fact that this discrepancy is also evident from the PPP approach refutes this hypothesis. Because of the strong link between sea ice and SAT in these high-latitude regions (e.g. Bengtsson et al. 2004; Wu et al. 2004) we can speculate that sea-ice affects predictive skills and therefore plays an important role. This difference between the predictability of SST and SAT in the Nordic Seas therefore requires further investigation. Land areas display little potential predictability compared to oceans. We can, however, be confident about the potential predictability of SAT over the British Isles (mainly the western part) up to at least 1 decade. Nonetheless signals over maritime Europe as identified by Boer and Lambert (2008) and Pohlmann et al. (2004) are not brought out as clearly in our study with CHIME. Potential predictability is absent for precipitation in CHIME. This result contrasts with those from the IPSL predictability study (see *Chapter 5*) and e.g. Hawkins et al. (2011) study (with the HadCM3 and HadGEM1 models), for which precipitation in some part of the tropics has been identified as potentially predictable. The lack of signal in the tropics in CHIME might be a consequence of the absence of an ENSO cycle in the control integration $E3$. The latter is indeed thought to affect the tropical Atlantic activity (e.g. Saravanan and Chang 2000), and might therefore affect some of the AMOC precursors as identified in CHIME. The absence of ENSO might bias the lead-time of AMOC predictability found in CHIME.

Although, the experimental set up was not designed to draw robust conclusions about

any predictability-dependence on the AMOC initial states, this study nevertheless gave some useful indications about it. The weak signals of SST predictability identified by the PPP approach (in the subpolar gyre region and Nordic Seas) seem to be favoured by extreme AMOC events, both in maximum and minimum states. This trend towards better predictive skills when the AMOC is at near extremum has already been brought out for the predictability of the AMOC index in IPSL-CM5A. Although SAT also shows some dependence on extreme AMOC events, it differs from SST and AMOC index insofar as there is no evidence for its predictive skills to be favoured by a minimum AMOC state (in good agreement with results from the IPSL predictability study, see *Chapter 5*). Finally, the likelihood for a link between SST and SAT predictability and the AMOC is strengthened by the fact that regions where both SST and SAT have been found to be potentially predictable are also regions strongly sensitive to strong AMOC conditions. This suggests that the mechanisms responsible for climate predictability are to some extent linked to the mechanisms responsible for decadal AMOC variability. As previously underlined in *Chapter 5*, more research to understand the specific mechanisms that lead to predictability is, however, still needed.

6.6.3 Evaluation of different methods for quantifying predictive skills

From a methodological point of view, this study also put forward some interesting results regarding the experimental protocol of predictability study and the evaluation of predictive skills.

Overall, the DPP approach identifies more widespread predictable areas than the PPP approach does. Although only marginal discrepancies have been identified between the DPP and PPP approaches in the IPSL-CM5A model, these discrepancies are more marked in CHIME. Indeed, in the latter model, it seems that the PPP approach is only able to identify regions with a fraction of variance in the decadal band superior to 50%. Note, however, that regions with such fraction of variance are not necessarily identified in the PPP approach. Nevertheless, as with IPSL-CM5A, both approaches agree in CHIME insofar as regions identified by the PPP approach correspond to the regions exhibiting the highest fraction of variance in the DPP approach. Discrepancies between the two approaches usually concern the regions of weak predictability signals, which have low fractions of variance in DPP and are not identified in PPP. The most striking example is for precipitation, for which some regions with (weak) significant fraction of variance at the decadal timescale have been identified by the DPP approach (e.g. in the subpolar gyre region, the southern tropics), and none of them have been identified by the PPP approach. As with IPSL-CM5A, these discrepancies could arise, for example, from the difficulty to define a "useful" threshold of potential predictability in the DPP approach, or from the subjective choice of starting dates, number of members and experiments in the PPP approach. Note that, in contrast to IPSL-CM5A, there is one exception in

CHIME for which some predictability signals (although weak) are identified in the PPP approach and not in the DPP approach (concerning e.g., SAT in central Canada). Here, we rather attribute this discrepancy to the January missing months in the atmospheric data of $E3$, probably affecting results from the DPP approach.

Regarding the PPP approach, we showed that combining ES and EC should be preferred in principle but it is sometimes difficult to apply in practice such in the case of evaluating average predictive skills. Both metrics should therefore be considered in parallel. Results from this study also suggest that the predictability of AMOC, SST, and SAT might be favoured by extreme AMOC events; however, the role of minimum versus maximum extreme states still needs to be clarified. More systematic experiments starting with similar initial states should therefore be encouraged. If the role of weak states is confirmed in CHIME, this finding will contrast with those found in the IPSL predictability study (see *Chapter 5*) and previous similar studies (e.g. Collins and Sinha 2003; Collins et al. 2006a) for which weak states are generally associated with lower predictive skills than strong states. The present study with CHIME therefore suggests that a forecast starting from an extreme phase of natural internal variability can be more skillful than one starting from average conditions. As already mentioned in *Chapter 5*, in that sense, studying skill from case studies may prove more useful to understand predictability mechanisms than computing average skills from numerous start dates, as done in most previous studies. This study also pointed out that increasing the number of members from 6 to 11 in experiment S did not affect its predictive skills. Although only based on one ensemble experiment, this study suggests that experimental protocol for predictability studies should privilege the number of ensemble experiments over the number of ensemble members, in good agreement with Meehl et al. (2012).

6.7 Conclusions

In conclusion, the decadal predictability of the AMOC and associated oceanic/atmospheric variables in CHIME can be summarized in the following key points:

• The AMOC has an average prognostic predictability of about 6 years.

• In about 50% of the cases, an extreme AMOC event can be predicted up to 15 years in advance from the monitoring of the northern tropical Atlantic SSS.

• Over the ocean, the North Atlantic subpolar gyre region (Nordic Seas) is potentially predictable for both SST and SAT (SST only) on decadal timescales.

• Over land, there is little evidence of decadal predictability of SAT except for the limited area of the western part of the British Isles.

• Decadal predictability is absent for precipitation.

• Predictive skills of AMOC, SST and SAT seem to be favoured by extreme AMOC events; however, the role of minimum versus maximum extreme states still needs to be clarified.

• All regions identified as potentially predictable are strongly influenced by decadal AMOC fluctuations, suggesting that the mechanisms responsible for climate predictability are to some extent linked to the mechanisms responsible for decadal AMOC variability.

As with the IPSL predictability study, it is important to bear in mind that here we have assessed the upper limit of both the AMOC and climate predictability as both a perfect model and near perfect knowledge of the current state of the climate are assumed. For example, the substantial warming and increasing salinity in the North Atlantic subpolar gyre and the excessive mixing in the Northern high-latitudes in CHIME (Megann et al. 2010) might well affect its effective level of predictability skill. In addition, the limitations of this study with CHIME include the absence of the ENSO cycle in the control integration, as well as the problems linked to the January missing months for the atmospheric data. Nevertheless, we still believe that the result of this study give some indications as to where and to what extent skillful decadal forecasts might be possible. They also complement results from the IPSL predictability study (in *Chapter 5*) by strengthening or questioning some of the claims drawn in that study. To some extent, the effect of the vertical representation of the ocean component on the predictability skills of the model can also be addressed. These above aspects will be briefly discussed in the following and final chapter of this thesis.

Chapter 7

Discussion and Conclusions

This thesis has addressed the decadal variability and predictability of the AMOC and associated key variables in two different climate models. We first analyzed the decadal variability of the AMOC in the new coupled climate model CHIME (Megann et al. 2010), and then explored the AMOC's potential predictability on decadal time scales using both the IPSL-CM5A (Dufresne et al. 2012) and CHIME models.

The fact that CHIME shares its atmosphere and ice components with the widely used IPCC-class model HadCM3 (Gordon et al. 2000) means that comparison between the two models makes possible an assessment of the extent to which the structural biases inherent in the vertical representation of the ocean affect the decadal variability and predictability of the AMOC. Comparing our results from the variability study carried out with CHIME here with those obtained from existing similar studies with HadCM3 (e.g. Vellinga and Wu 2004; Dong and Sutton 2005) should give us a reasonable idea of the influence of the ocean component on the decadal variability associated with the AMOC. However, to evaluate the impact of the vertical representation of the ocean on predictive skills, such comparisons with existing studies is more difficult, first, because of the limited number of studies with HadCM3, and second because of the many differences in the experimental protocols for predictability studies. Since a near-identical experimental protocol has been used for CHIME and IPSL-CM5A, a comparison of the results between these two models here can still be useful considering that this latter model belongs to the new generation of z-coordinate models (and can therefore be seen as a more up to date z-coordinate model than HadCM3). However, it has to be kept in mind that these two models differ in more than just the representation of the ocean vertical coordinates, so the comparison between these two models has to be carefully interpreted. It is also important to remind that conclusions based on CHIME are only preliminary since, in the framework of this study, the model was only in its early stage of development. Some issues were not completely resolved at the time of simulations, and their impacts on our present results are difficult to assess.

In this concluding chapter, a comparison of results regarding the decadal variability (predictability) of the AMOC and key variables in CHIME and HadCM3 (IPSL-CM5A) is made. The outcomes and limitations of this study are then discussed and also placed into a "bigger-picture" context. Suggestions for future work are also discussed.

7.1 Comparing climate models with different vertical representation of the ocean

7.1.1 Decadal variability: CHIME versus HadCM3

Note that in CHIME, run $E3$ used for predictability study exhibits similar AMOC characteristics as run cD, as shown in Figure 7.1. Run cD of CHIME is used below for comparisons with HadCM3.

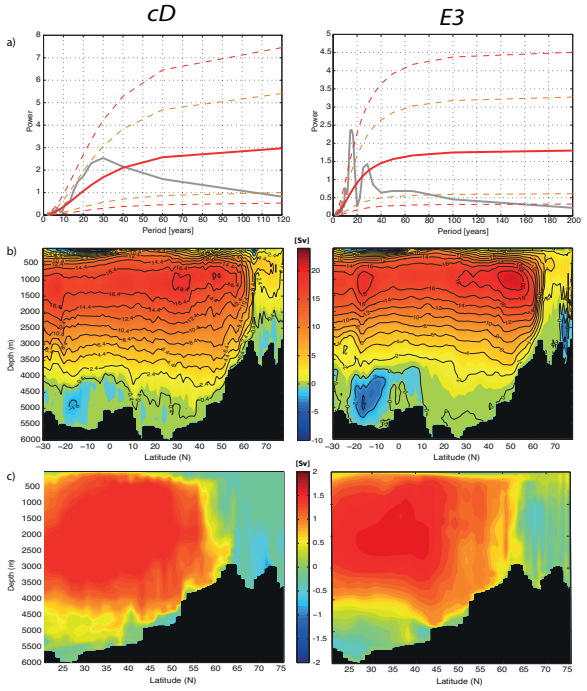

Figure 7.1: Main AMOC characteristics in CHIME (cD - left panels; $E3$ - right panels): (a) Power Spectrum of the detrended PC1 of AMOC - the smooth red solid line is the power of a red noise spectrum with the same AR(1) coefficient fitted from the detrended PC1 time series, and red (orange) dashed lines, which are the 95% (80%) confidence limits; (b) Annual mean streamfunction of zonally integrated volume transport - positive values mean clockwise circulation; (c) EOF1 of AMOC streamfunction.

It has generally been shown that AMOC oscillations are mostly irregular and their periods change considerably among models; while ECHAM5/Max Planck Institute Ocean Model (MPI-OM, Jungclaus et al. 2005) has one of the longest periods with 70-80 years, HadCM3 (Dong and Sutton 2005, Figure 7.2a) and Parallel Climate Model (PCM, Dai

et al. 2005) show the shortest periods with about 25 years. While it has been difficult to estimate the period of AMOC variability in CHIME due to limited integration length, its power spectra nevertheless revealed an enhanced power for periods in the range 15-30 years (Figure 7.1a). CHIME therefore shows a low-range period of AMOC variability that includes the 25-year period found in HadCM3. Although longer CHIME integrations are needed to better establish this range of periodicity, our evidence suggests that CHIME and HadCM3 share similar decadal timescale AMOC oscillations.

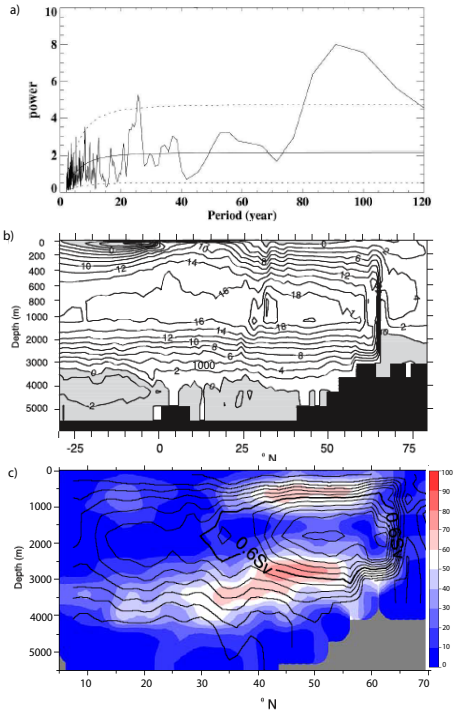

Figure 7.2: Main AMOC characteristics in HadCM3: (a) Power Spectrum of the detrended AMOC index - the smooth solid line is the power of a red noise spectrum with the same AR(1) coefficient as the data and dashed lines, which are 90% confidence limits (from Dong and Sutton 2005); (b) Annual mean streamfunction of the zonally integrated volume transport (from Megann et al. 2010); (c) Streamfunction of EOF1 contoured (interval 0.2 Sv) and colours representing the percentage of the total low frequency period accounted for by the mode - solid (dashed) lines indicate positive (negative) values (from Bingham et al. 2007).

In both CHIME and HadCM3, the circulation associated with the NADW has a maximum transport of about 18 Sv (Figure 7.1b - left panel, and Figure 7.2b, respectively), well within the CMIP3 range (10 to 30 Sv, Gregory et al. 2005). There are, however, some structural differences in the respective meridional overturning streamfunctions. In CHIME, for example, the strongest sinking occurs in a broader region (between about 55-65°N) than in HadCM3 (primarily occurring at 65°N). Megann et al. (2010) explained that this difference could be partly due to the deeper mixing in the subpolar gyre in CHIME and to the reduced mixing in the Labrador Sea in HadCM3. Note, however, that compared to observations, CHIME overestimates winter mixed layer depth in the

Labrador Sea while HadCM3 underestimates it. The AMOC also comprises NADW outflow of about 16 Sv at the Equator in CHIME against 14 Sv in HadCM3 (Dong and Sutton 2005), and the outflow extends deeper in CHIME (to about 4000 m, against 3600 m in HadCM3, Megann et al. 2010). The dominant mode of AMOC variability (EOF1) in CHIME (Figure 7.1c - left panel) has a spatial structure very similar to that in HadCM3 (Figure 7.2c), and the amount of total variance explained is similar in both models (about 34%). There are nevertheless significant differences; for example, the maximum value for a fluctuation of one standard deviation of PC1 is more than double in CHIME (about 1.6 Sv) compared to HadCM3 (about 0.7 Sv). Another significant difference is that the phases of EOF1 in the Labrador Sea and Nordic Seas are of opposite sign in CHIME while they remain similar in HadCM3, with the caveat that Labrador Sea convection is much weaker in HadCM3 than in CHIME. In that sense, CHIME seems more realistic; in observational studies, it has been established that convection in the Labrador Sea is generally out of phase with convection in the Greenland Sea (e.g. Hurrell and Dickson 2004). Therefore, different mechanisms appear to control AMOC variability on decadal timescales in CHIME and HadCM3.

Regarding these mechanisms, it has been shown that phase reversal of the AMOC oscillation in CHIME seems linked to the northward shift of the ITCZ, and hence to the development of salinity anomalies in the tropics. This finding contrasts with several studies using HadCM3 where the reversal phase of the oscillation has been mainly attributed to anomalies originating from high latitudes (Hawkins and Sutton 2007) but is to some extent in agreement with Vellinga and Wu (2004) who attributed this reversal oscillation to advection of salinity anomalies from the tropics. However, this advection happens on a centennial timescale rather than on the decadal timescale identified in CHIME. A plausible explanation of the faster advection of anomalies in CHIME could come from the better preservation of water masses, compared to HadCM3 (as discussed by Megann et al. 2012); so an anomalous water mass maintains its structure better in CHIME, and can be more effectively advected "intact" to high latitudes. Note, however, that centennial mechanisms (as identified by Vellinga and Wu 2004) may also be active in CHIME but these cannot be investigated using the short integration available to us. The cause of the northward shift of the ITCZ in CHIME also differs from HadCM3 in the sense that this shift is associated with a northern tropical-subtropical SST gradient and not a cross-equatorial gradient as identified in HadCM3 (Vellinga and Wu 2004) and observations (e.g. Chiang et al. 2002). This more northward SST gradient in CHIME may be a consequence of the strong warm surface bias in the North Atlantic (Megann et al. 2010). Despite these differences, CHIME is similar to HadCM3 in that a significant part of the AMOC variability is likely to be a passive response to the internally generated atmospheric variability linked to NAO (e.g. Dong and Sutton 2005), rather than being part of a coupled ocean-atmosphere mode (e.g. Vellinga and Wu 2004). The main characteristics of decadal AMOC fluctuations in CHIME and HadCM3 are summarized in Table 7.1.

Table 7.1: Summary of main characteristics of decadal AMOC fluctuations in CHIME (run *cD*) and HadCM3 (from previous existing studies).

	CHIME	**HadCM3**
AMOC cycle	15-30 years	25 years (Dong and Sutton 2005)
Main NADW characteristics	Max. transport = 18 Sv; Outflow at equator = 16 Sv; Max. outflow depth = 4000 m	Max transport = 18 Sv; NADW outflow at equator = 14 Sv; Max. outflow depth = 3600 m (Dong and Sutton 2005)
Region of strongest sinking	55-65°N	65°N (Dong and Sutton 2005)
Winter MLD	Overestimated compared to observations	Underestimated compared to observations (Dong and Sutton 2005)
Relationship between convection in Labrador and Nordic Seas	Out-of-phase relationship as in observations (Hurrell and Dickson 2004)	In-phase relationship (Dong and Sutton 2005; Bingham et al. 2007)
Trigger of reversal phase of AMOC oscillation	Development of salinity anomalies in the tropics (caused by northward shift of ITCZ), then propagating northward on decadal timescale	(i) Development of salinity anomalies in the high latitudes caused by transport variation of freshwater and sea-ice from the Arctic (Hawkins and Sutton 2007); (ii) Development of salinity anomalies in the tropics (caused by northward shift of ITCZ), then propagating northward on centennial timescale (Vellinga and Wu 2004)
Causes of ITZC shift	Northern tropical-subtropical SST gradient	Cross-equatorial SST gradient (Vellinga and Wu 2004)
Mechanisms	Internal ocean-only mode excited by atmosphere noise (NAO) for a significant part of AMOC variability	(i) Internal ocean-only mode excited by atmosphere noise (NAO) (Dong and Sutton 2005); (ii) Coupled ocean-atmosphere mode (Vellinga and Wu 2004)

7.1.2 Decadal predictability: CHIME versus IPSL-CM5A

By comparing results from predictability studies that use experimental protocols as similar as possible, the comparison of both the CHIME and IPSL results contributes to the coordinated effort of determining a common skill evaluation framework to evaluate decadal predictions. Indeed, as pointed out by Meehl et al. (2012), this is highly desirable to allow a comparison of decadal prediction systems across different modeling centres. In addition, with some evidence for better preservation of water masses and for a more coherent internal structure to the anomalies than in non-isopycnic coordinate ocean component models (such as HadCM3 and IPSL-CM5A), CHIME might be expected to have significantly better predictive skills than non-isopycnic models. With no clear indications of such better predictive skills in the present study, this expectation is not borne out here, as summarized below.

Decadal predictability of the AMOC

First, the 6-year average lead-time of predictability found in CHIME is slightly shorter than the one found with the IPSL-CM5A model (8 years, Table 7.2). Note that CHIME also has a similar average predictability to the one found in HadCM3 for the AMOC index with a lead-time of about 5 years (Hermanson and Sutton 2009). It seems therefore reasonable to claim that the AMOC index in CHIME has an average lead-time of predictability similar to those of the two non-isopycnic models, IPSL-CM5A and HadCM3. When considering the predictive skills of each ensemble separately, the longest lead-time at which ES saturates is about 10 years in CHIME (Table 7.2, experiment 15P), against 13 years in IPSL-CM5A (Table 7.2, experiment S), and 20 years in HadCM3 (Collins and Sinha 2003). The above results are somewhat surprising since, for the reasons mentioned earlier, CHIME is expected to have, overall, significantly better predictive skills than non-isopycnic models. We can question whether the shorter predictability timescale in CHIME compared to IPSL-CM5A is a consequence of: (i) excessive convective mixing that takes place in the northern latitude regions in CHIME (Megann et al. 2010), hence reducing its predictive skills; (ii) faster-growing modes in CHIME (although the more controlled diapycnal mixing in isopycnic models is expected to have slower growing modes than non-isopycnic models); (iii) the absence of ENSO cycle that could bias the lead-time for predictability in CHIME given the influence of this cycle on the tropical Atlantic region (Saravanan and Chang 2000) which is key in driving decadal AMOC fluctuations in the model; (iv) the different perturbation scheme used to generate the ensemble members in both models (predictability experiments perturbing only the upper ocean state - like in IPSL-CM5A - may overestimate the predictability time, Zanna et al. 2012).

Experiments starting from weak AMOC state (W), and starting 15 and 5 years before a maximum AMOC extreme (15P and 5P, respectively), have similar predictive skills in both CHIME and IPSL-CM5A (Figure 7.3, Table 7.2). On the other hand, both models

Table 7.2: Summary of predictive skills in CHIME and IPSL-CM5A showing the maximum lead-time at which ES saturates with its corresponding EC. (*) are significant EC at the 90% level.

	CHIME: Max. ES	**CHIME: Corresponding EC**	**IPSL-CM5A: Max. ES**	**IPSL-CM5A: Corresponding EC**
I	5	0.95*	7	0.48
15P	10	-0.04	5	-0.05
5P	6	0.86*	8	0.75*
S	2	*none*	13	0.78*
W	5	0.89*	7	0.74*
Average	**6**	**0.66**	**8**	**0.74**

differ in their predictive skills for experiments starting from strong (S) and intermediate (I) AMOC initial states (Figure 7.3, Table 7.2). Indeed, although some skills have been identified for S (I) in IPSL-CM5A (CHIME), they have not been identified in CHIME (IPSL-CM5A). The fact that predictive skills have identified for experiment I in CHIME and not IPSL-CM5A, might be explained by the fact that the starting date in CHIME is not in such an intermediate state as in IPSL-CM5A but rather closer to a strong state (Figure 7.3). The most striking difference between the two models concerns experiment S. Although the highest predictive skills have been found for this experiment in IPSL-CM5A, this is actually the experiment in which the predictive skills are the weakest in CHIME. The fact that skills are higher for W than S in CHIME is quite unexpected, considering that the contrary has generally been found in most previous studies (e.g. Collins and Sinha 2003). One of the plausible explanations is that strong AMOC conditions might be associated with an excessive convective mixing in CHIME that reduces its predictive skill. The better predictive skill of W over S in CHIME, therefore questions the well-established better skill of experiments starting from strong AMOC conditions over those starting from weak AMOC conditions. Another intriguing result is that experiments 15P in both CHIME and IPSL-CM5A have remarkably low ensemble correlation compared to the other experiments (Figure 7.3, Table 7.2).

It has also been shown that by monitoring the AMOC precursors, the ability to predict extreme AMOC events, in both CHIME and IPSL-CM5A, can go beyond the average lead-time of predictability (up to about 2 decades). However, large changes in the AMOC precursors lead to large changes in the model's AMOC in about 80% of the cases in IPSL-CM5A, against only 50% in CHIME. It is, however, important to note that this apparent difference in the ability to predict extreme AMOC events might not be significant since fewer initial "events" (for which the precursors are in an extreme state) have been identified in IPSL-CM5A than in CHIME (6 "events" against 11, respectively). Nevertheless, several factors could still explain the plausible difference in the ability of

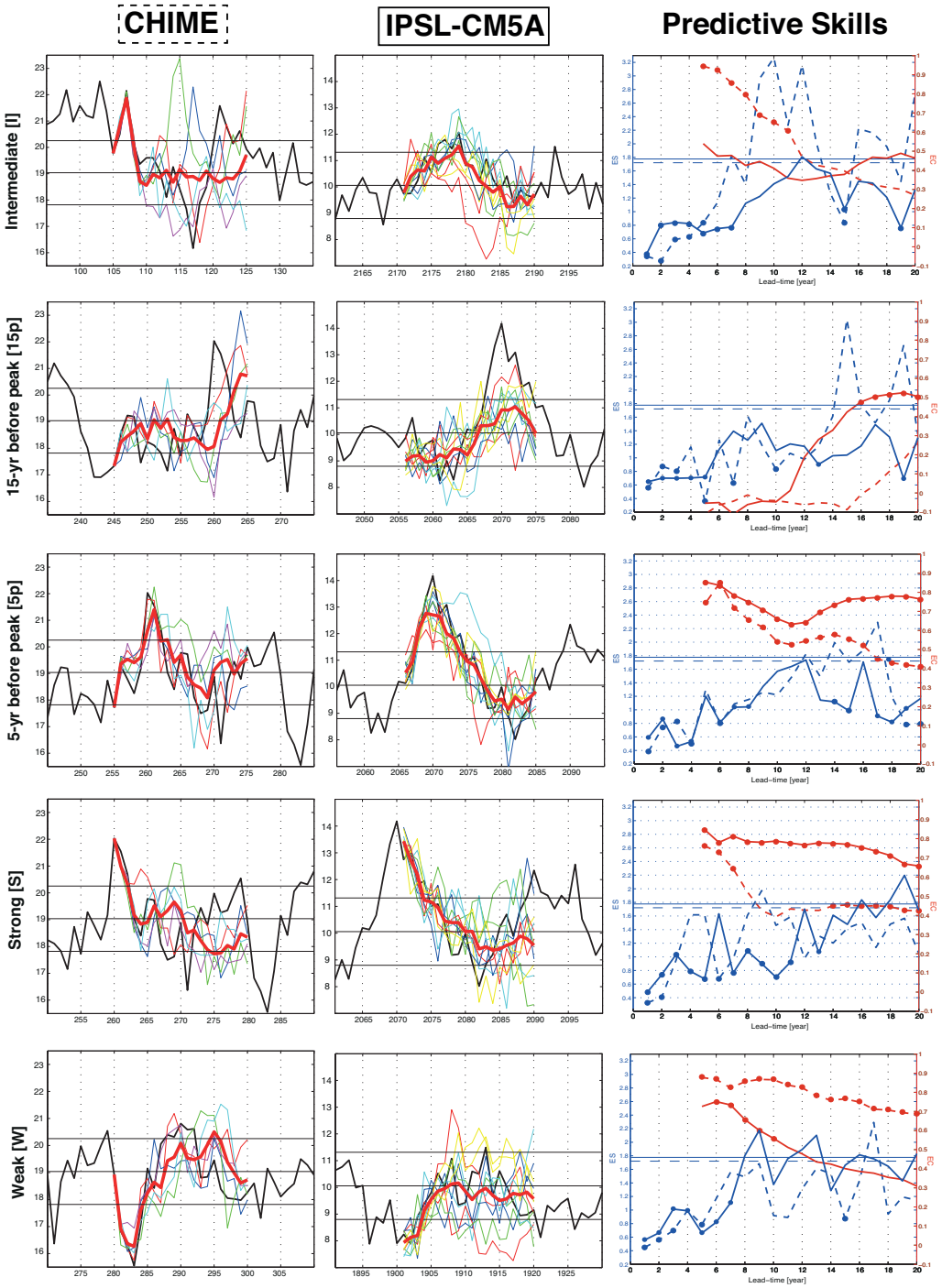

Figure 7.3: "Plumes" of AMOC index in CHIME (left-column) and IPSL-CM5A (middle-column) for each experiment. The members are shown as coloured lines, the ensemble mean (control run) as the red (black) thick lines. The middle horizontal black line is the mean AMOC, and both upper and lower horizontal black lines show standard deviation. Summary of predictive skills (right-column) in CHIME (dashed lines) and IPSL-CM5A (solid lines) showing ES (in blue) and EC (in red) against lead-times. Dots indicate statistical significance at the 95% (90%) confidence level for ES (EC).

these two models to predict extreme AMOC events from their corresponding precursors. It is important to bear in mind that the AMOC precursor considered here with CHIME has been identified from a different control integration, and might therefore not be the most appropriate one (hence explaining its weaker ability in predicting extreme events). On the other hand, if the same precursor does really apply, then the difference in the ability to predict extreme AMOC events in the two models might be explained by the difference in the localization of their precursors; while the one in CHIME is situated in the tropics, both precursors in IPSL-CM5A are in the high latitude regions (Escudier et al. 2012). In CHIME, the precursor may be relatively remote from the deep convection sites compared to IPSL-CM5A precursors, and CHIME might therefore lose predictive skill correspondingly.

Decadal predictability of the North Atlantic climate

In terms of decadal predictability, an interesting feature worth pointing out concerns the differences between CHIME and IPSL in the DPP approach: indeed, CHIME has generally higher $ppvf$ values than IPSL-CM5A (reaching up to 0.75 and 0.40, respectively, Figure 7.4 and Figure 7.5). Strictly speaking, these higher values in CHIME mean that its low-frequency variability is more easily distinguishable from the internal variability than in IPSL-CM5A, hence suggesting the potentially better predictive skills of climate in CHIME. In contrast, the comparisons of the evaluation skills by the PPP approach suggest better predictive skills in IPSL-CM5A than in CHIME. Indeed, predictability signals in CHIME are rarely identified in more than 50% of the experiments, while in IPSL-CM5A some signals can be identified in all experiments (Figure 7.4 and Figure 7.5). The evidence for slightly weaker predictive skills of the AMOC index in CHIME compared to IPSL-CM5A suggests that the DPP approach might actually overestimate the predictive skills of climate in CHIME. We speculate whether that is due to the significantly shorter control integration length used in CHIME (201-year) than in IPSL-CM5A (1000-year). This shorter control integration length might also explain why the spatial distribution of the $ppvf$ values in CHIME barely differs between the 10-year and 20-year timescales, in contrast to IPSL-CM5A.

Over the ocean, both models exhibit the highest predictive skills for surface temperature in the far North Atlantic (roughly in the subpolar gyre region and the Nordic Seas) out to about 2 decades (Figure 7.4). They, however, differ in the sense that the IPSL-CM5A model also identifies some hints of decadal predictability in both the subtropics and the tropics, which are clearly absent in CHIME. This absence of signals might be a consequence of the absence of an ENSO cycle in run $E3$ of CHIME; indeed, ENSO is known to affect the tropical Atlantic activity (e.g. Saravanan and Chang 2000), and therefore the predictability in this region. Over land, both models agree on the significantly smaller predictability of surface temperature compared to the ocean. However there are more hints of predictability signals in IPSL-CM5A (which are restricted to the coastal areas bordering some of the oceanic predictable regions) than in CHIME (which

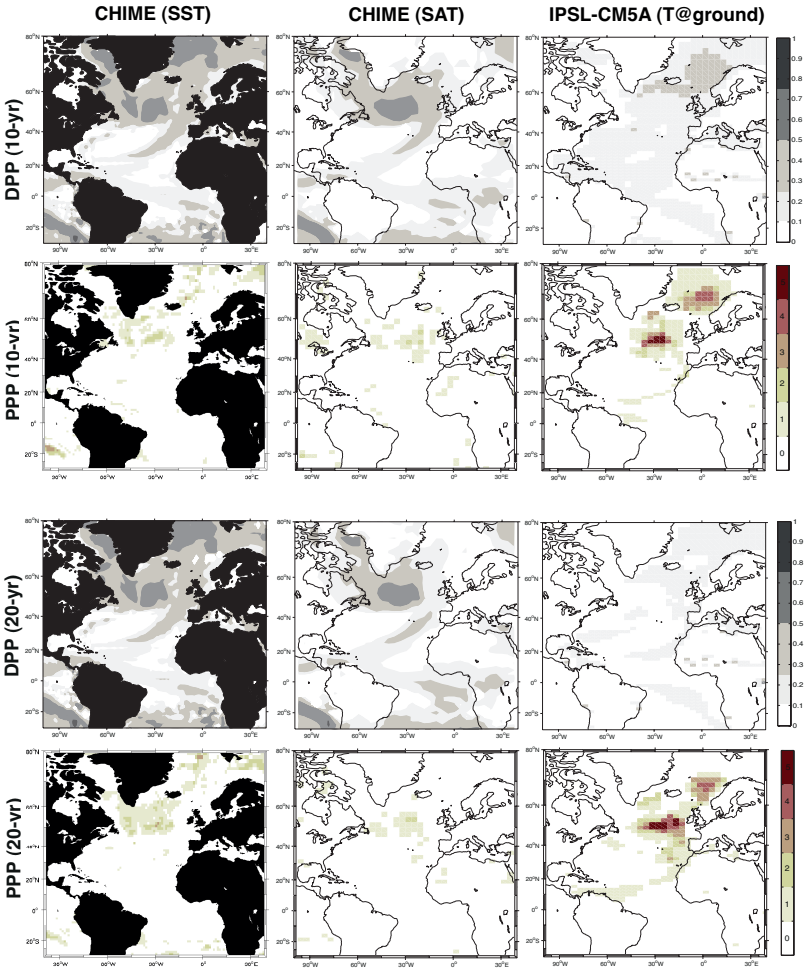

Figure 7.4: Potential predictability of SST (left-column) and SAT (middle-column) in CHIME, and surface temperature (at ground level) in IPSL-CM5A (right-column). The DPP maps show $ppvf$ for 10-year and 20-year means (the colored areas are significant at the 95% level according to a F-test); The PPP maps show the number of starting dates (out of 5) where grid points are potentially predictable (i.e. where it combines a normalized ES smaller than saturation level at the 95% level according to a F-test, and a statistically significant EC at the 90% confidence level according to a Students t-test) up to 10 and 20 years.

are only found over the western part of the British Isles). Predictability of precipitation on decadal timescales is largely absent in both models (Figure 7.5). The weaker predictability of precipitation compared to temperature is in agreement with Boer and Lambert (2008) and Goddard et al. (2012); in general, precipitation is a more localized variable in both space and time, and thus subject to larger noise-like variability that is not predictable. Although weak, there are still a few signals in ISPL-CM5A (some patches over the Nordic Seas and the subpolar gyre region) whereas no signals have been identified in CHIME.

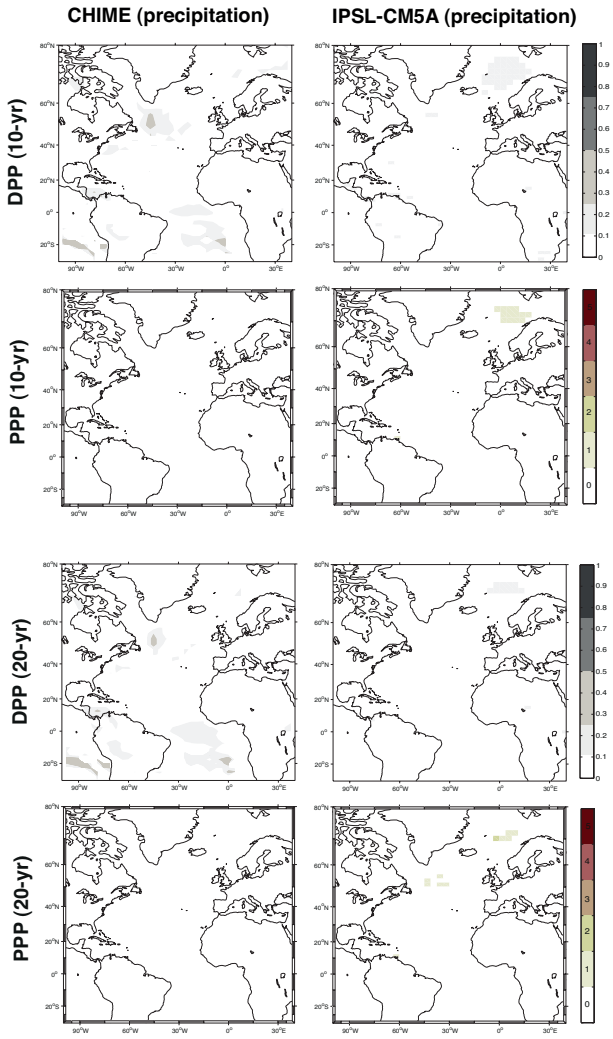

Figure 7.5: Same as Figure 7.4 but for precipitation.

In addition, climate predictability seems to have some dependence on the AMOC initial state in both models. Indeed, there is some evidence for better predictive skills of surface temperature (at ground level) in IPSL-CM5A and SAT in CHIME, when the AMOC is near extremum in a maximum state. However, predictability of SST in CHIME differs compared to IPSL insofar as predictive skills seem to also be favoured when the AMOC is near extremum in a minimum state. A plausible explanation of this difference between the two models could be the use of SST data in CHIME instead of surface temperature at ground level as in IPSL-CM5A (although both SST and surface temperature at ground level patterns in IPSL-CM5A have been found to be similar). Nevertheless, the fact that predictability of the AMOC itself shows better predictive skills when starting from a minimum AMOC state than a strong state, suggests that the minimum state has a significant influence in CHIME. Results with CHIME therefore challenge the better predictive skills of strong AMOC initial states over the weak states, found in other models.

Finally, the fact that, for both models, regions identified as potentially predictable are also strongly sensitive to decadal AMOC fluctuations strengthens the likelihood for a link between climate predictability and the AMOC. This suggests that the mechanisms behind climate predictability are to a large extent linked to the ones responsible for decadal AMOC variability.

Evaluation of different methods for quantifying predictive skills

In both models, the DPP approach identifies more widespread predictable regions than the PPP approach (Figure 7.4 and Figure 7.5). As already mentioned in *Chapters 5* and *6*, these discrepancies might arise, first, from the difficulty to define a "useful" threshold of potential predictability in the DPP approach, and second, from the subjective choice of starting dates, number of members and experiments in the PPP approach. However it seems reasonable to conclude that, both approaches agree insofar as, in both models, regions identified as potentially predictable by the PPP approach correspond to those with the highest decadal fractions of variance in the DPP approach. The two approaches are complementary, thus strengthening the robustness of the results.

In addition, in the PPP approach, there is evidence supported by both models that the two metrics used here to evaluate predictive skills (EC and ES) are not independent. Indeed, a decreasing (increasing) ES has been generally associated with increasing (decreasing) EC (Figure 7.3, right-column). Besides, this hypothesis has been supported analytically for centred and normalized data (see *Appendix A*). However, there is one exception in CHIME that weakens the robustness of this claim, with an increasing ES associated with an increasing EC over time (Figure 7.3, experiment 15P, dashed-lines). This draws into question the robustness of such a simple relationship in the real world.

Although the experimental set up was not designed to draw robust conclusions about any predictability-dependence on the AMOC initial states, both CHIME and IPSL-CM5A have still given some useful indications. In both models, predictability of both the AMOC and climate seems to be sensitive to the initial AMOC conditions with transitions around extreme states appearing as the most predictable events (in good agreement with e.g. Griffies and Bryan 1997b; Collins and Sinha 2003; Collins et al. 2006a). However, the role of minimum versus maximum extreme states still needs to be clarified. This result nevertheless suggests that skill from case studies may prove more useful for understanding predictability mechanisms than computing average skills from numerous start dates, as in most previous studies.

The main results of the decadal predictability studies carried out with CHIME and IPSL-CM5A are summarized in Table 7.3.

Table 7.3: Summary of main findings about decadal predictability in CHIME and IPSL-CM5A.

	CHIME	**IPSL-CM5A**
Average predictive skills of AMOC	6 years	8 years
Experiments for which AMOC is predictable	5P > W = I	S > 5P > W
% of cases where extreme AMOC event predictable from its precursor(s)	50%	80%
DPP scores	Up to 0.75	Up to 0.40
PPP scores	Predictability signals in up to 40% of experiments	Predictability signals in up to 100% of experiments
Surface temperature predictability over the ocean	Up to 2 decades in far North Atlantic	Up to 2 decades: (i) far North Atlantic (highest skills), (ii) Subtropics (hints), (iii) Tropics (hints)
Surface temperature predictability over land	Up to 1 decade in Western part of British Isles (hints)	Up to 2 decades in coastal areas bordering oceanic predictable regions (hints)
Precipitation predictability	Absent	Up to 2 decades: (i) Nordic Seas (hints), (ii) North Atlantic subpolar gyre (hints)
Climate predictability mechanisms	Evidence for links with mechanisms responsible for decadal AMOC fluctuations	Evidence for links with mechanisms responsible for decadal AMOC fluctuations
DPP versus PPP	Regions identified in PPP corresponds to regions with the highest decadal fraction of variance	Regions identified in PPP corresponds to regions with the highest decadal fraction of variance
EC and ES relationship	Dependent metrics, except for experiment 15P	Dependent metrics
Predictability-dependence on AMOC initial states	(i) AMOC and SST: favoured by extreme states (maximum and minimum), (ii) SAT: favoured by extreme states (maximum)	(i) AMOC: favoured by extreme states (maximum and minimum), (ii) SAT, SST and precipitation: favoured by extreme states (maximum)

7.2 Decadal variability of AMOC and climate in CHIME

7.2.1 Limitations and future work

Outcomes rarely come without limitations. Here are some issues from this study on decadal variability with CHIME and some suggestions for future work.

The first limitation of our study arises from the short control integration length available (120 years). A longer integration ($\sim$ 1000 years) would be needed to clarify the periodicity of decadal AMOC fluctuations in CHIME, and to check whether or not it is significantly different from a simple red noise model. All the analyses should be repeated with this longer run to validate the findings of this study.

If the mechanism of decadal AMOC fluctuations is confirmed, then further investigation might be needed to better understand the processes behind some (tele)connections. For example, the way in which the NAO affects SST in the GIN Seas still remains unclear since processes other than the direct impact on heat fluxes seems to control these local SST anomalies. As already mentioned in *Chapter 4*, such a link could be more fully explored using a method such as the Interactive Ensemble Coupled Global Climate Model (Fan and Schneider 2012). Further analysis focused on the mechanical action of the wind on local SST could also be useful. Another example is the decadal teleconnection between the tropical Atlantic ocean-atmosphere and the high latitude stormtrack (i.e. the NAO); although such a teleconnection has already been identified in the observations (Rajagopalan et al. 1998), the processes behind it still remain unclear and therefore need to be carefully considered.

In addition, to further establish the extent to which the salinity preservation and the speed of the northward advection are particular to CHIME, it would be necessary to undertake a more in-depth intercomparison with a climate model typical of the majority that feature a more orthodox z-coordinate ocean component. In comparison with HadCM3, the early evidence is that CHIME does indeed better preserve the properties of intermediate waters such as AAIW, over long distances (Megann et al. 2010). However, HadCM3 may not be the most appropriate model for such comparison, due to the limited role that Labrador Sea convection plays in driving AMOC variability in this model. It also has to be kept in mind that any model inter-comparison has to take into account a possible dependency of each model on a considerable number of model choices (e.g. topography, boundary conditions, mixing parameterizations) that can have significant impact on the behavior of the basin-scale circulation.

Last but not least, it remains to be demonstrated that the mechanism of decadal AMOC fluctuation identified in CHIME (namely the development and poleward advection of tropical salinity anomalies) occurs in the real world. Undertaking comparison with multi-decadal observations would therefore be necessary. However, such observations are

at present inadequate for this purpose, due to under-sampling of much of the Atlantic sector prior to the Argo era. This study therefore underlines the necessity of a sustained observation network particularly in the tropical Atlantic. The continuity of observational programs such as the Tropical Atlantic Climate Experiment (TACE, Schott et al. 2004), and observational networks such as the Pilot Research Moored Array in the Tropical Atlantic (PIRATA, Servain et al. 1998) are thus of primary importance to obtain decade-long timeseries of observations. Then, if a comparable mechanism to the one identified in the CHIME model occurs in the real world, the long-range links between the tropical Atlantic activity and subsequent convective activity in both the Labrador and GIN Seas promise potential predictability of the AMOC and climate.

7.2.2 What have we learnt?

The key messages from the present study are summarised below, and placed into a "bigger-picture" context. First, in common with most previous modelling studies, a large part of the variability of the AMOC on decadal timescales is likely to be a passive response to intrinsic internal atmospheric variability (e.g. Jungclaus et al. 2005; Danabasoglu 2008; Delworth and Greatbatch 2000), rather than being part of a coupled ocean-atmosphere mode (e.g. Timmerman et al. 1998). Second, our study underlines the key role that the tropical Atlantic region is playing in controlling decadal AMOC fluctuations. Although this finding is supported by some studies (e.g. Vellinga and Wu 2004; Mignot and Frankignoul 2005), most of them support the dominant role of high-latitude processes (e.g. Delworth et al. 1997; Jungclaus et al. 2005; Hawkins and Sutton 2007; Escudier et al. 2012). These discrepancies amongst the different existing climate models underline the current poor understanding of the mechanisms controlling the variability of the AMOC on decadal timescales. As underlined by Liu (2012), it is generally difficult in a climate model to clarify the role of ocean-atmosphere feedback and to distinguish a coupled mode from a damped oceanic mode unambiguously, based on the diagnosis of a control simulation alone. Indeed, model complexity limits the extent to which model processes, interactions and uncertainties can be understood and evaluated. te Raa et al. (2004) noted that, although quantitative aspects of the variability like period and spatial pattern are changing, the physical mechanisms of decadal variability in the more complex simulations can be attributed to the same processes as in the simplest model configuration. This suggests that simple (or idealized) models might actually be more appropriate to identify the nature of decadal variability. The use of complex climate models is, nevertheless, essential to explore the role of non-linear dynamics in generating this variability.

The present study also underlines, that although quantitative aspects of the variability like periods and spatial pattern can be somewhat similar, different vertical coordinate

choice of the ocean component significantly affects the processes behind decadal variability. It is quite worrying to see how the choice of vertical coordinate alone gives rise to such discrepancies. With some evidence for better preservation of water masses and a more coherent internal structure to the anomalies than non-isopycnic coordinate ocean component models (Megann et al. 2010), isopycnic models are expected to be more realistic. However, better observations, in particular long-term records of observed changes, are essential to support (or not) this assumption, and hence to help to understand processes critical to improving model performance. Recently, Johns et al. (2011) supported the idea that monitoring the AMOC is of primary importance since they found observational evidence for the direct influence of the AMOC on the climate system. Significant resources have been and are continuing to be devoted to field programs intended to provide direct measures of AMOC strength (e.g. Send et al. 2011; Rayner et al. 2011). However, variations in the AMOC are not easily interpreted as diagnostic of the ocean circulation or its climate impacts, and to progress we need to pick apart the different components of the flows and come to understand how and why they vary (Wunsch and Heimbach 2012). The requirements on future observational systems are far greater that what is now available.

7.3 Decadal predictability of AMOC and climate in CHIME

7.3.1 Limitations and future work

Although "perfect ensemble" experiments show considerable promise for predicting internal variability, particularly in the North Atlantic (e.g. Collins et al. 2006a; Hurrell et al. 2009), there are critical obstacles that must be overcome if such potential predictability is to be achieved in reality. For example, there are limitations linked to the restricted number of experiments that can be run. This limitation has to be kept in mind here, especially when drawing conclusions about any possible predictability-dependence on the AMOC initial states. Although the present study permitted some useful indications about this, more systematic experiments starting with similar initial states should be undertaken to confirm the results of this study. This should also help to clarify the role of minimum versus maximum AMOC extreme states on predictive skills, and other interesting features such as the remarkably low ensemble correlation of experiments 15P (compared to the other experiments) found in both CHIME and IPSL-CM5A. The problem of model error is also a technical obstacle that needs to be overcome in the idealized model experiment framework. It has, indeed, to be kept in mind that here we have assessed the upper limit of predictability as both perfect model and near perfect knowledge of the current state of the climate system are assumed. However, climate models still have significant biases compared to observation, and their possible impacts on the level of predictability skill of a model cannot be ignored. For example, as

already mentioned in *Chapter 6*, the substantial warming and increasing salinity in the North Atlantic subpolar gyre and the excessive mixing in the northern high-latitudes in CHIME (Megann et al. 2010) might well affect the effective level of predictability skill. An essential component of evaluating decadal prediction will therefore be to determine the effect of model systematic errors on the predictions, both in the simulation of mean climate and coupled processes that contribute to decadal time scale variability; this is an important aspect of the research activities involved with decadal prediction in CMIP5 (Taylor et al. 2009). In addition, different definitions of predictability, different experimental protocols and different metrics are often used in idealized model experiments to evaluate predictive skills, making the comparisons among existing studies difficult. The development of a common skill evaluation framework to evaluate decadal predictions should therefore be encouraged to allow a comparison of decadal prediction systems across different modeling centres (Meehl et al. 2012). For example, the impact of different perturbation schemes (used to generate the ensembles) on the level of predictive skills should be seriously considered in forthcoming studies; there is indeed some recent evidence for predictability experiments in which only the atmospheric state is perturbed (equivalent to perturb the upper ocean only), that may strongly overestimate the ocean predictability time (Zanna et al. 2012). Whether SST alone is sufficient to constrain the AMOC is indeed unclear (Dunstone and Smith 2010).

In addition, one important limitation of our predictability study with CHIME is its relatively short control integration length (compared to IPSL-CM5A), therefore affecting the statistical significance of the results. These results also rely on a control integration for which the reliability is questionable, notably because of the absence of the ENSO cycle known to significantly influence the tropical Atlantic Ocean (e.g. Saravanan and Chang 2000; Giannini et al. 2001; Huang et al. 2002); a key region in the processes driving decadal AMOC fluctuations in CHIME. To validate the CHIME predictability results, this study should be repeated using a longer and more reliable control integration. Confidence in decadal forecasts also requires an understanding of the physical mechanisms giving rise to any predicted changes in climate. The next step would therefore be to undertake a more in-depth investigation of the specific mechanisms that lead to predictability, consisting of further study of e.g. links between water properties and pressure gradient, the large scale mixing of anomalous properties.

Furthermore, the fact that CHIME has similar (or even shorter) level of predictive skills than do non-isopycnic models (such as IPSL-CM5A, HadCM3) is surprising given that isopycnic models are expected to have better predictive skills because of their supposed better preservation of water masses and more coherent internal structure of the anomalies. The origin of this unexpected result merits further attention and investigation. In addition, experiments starting from strong AMOC states have often been associated with the better predictive skills, as found in most previous studies (e.g. Collins and

Sinha 2003; Collins et al. 2006a) and in our IPSL study. Yet, in CHIME this experiment is actually associated with the lowest skills. The possibility that strong AMOC conditions in CHIME might be associated with an excessive convective mixing (reducing its predictive skill) is not excluded. This surprising result therefore needs further clarification.

Finally, which of the two models shows the most "realistic" predictive skills of decadal AMOC fluctuations remains difficult to say since sufficiently long observational time series are at present unavailable. However, the current RAPID-WATCH program (Cunningham 2008), which aims at delivering a decade long (2004-2014) time series of observations of the AMOC is of considerable value in such perspective. With some evidence that extreme AMOC events can be predictable beyond a decade, the continuity of such observational programs should be encouraged. Obtaining decade-long time series of observations is of primary importance for verification purposes, but also for accurate initialization of the ocean state in coupled climate models. Indeed, initializing models with the observed state of the climate is thought to improve decadal forecast skills (e.g. Keenlyside et al. 2008; Smith et al. 2010) and is at the heart of the decadal predictability problem (e.g. Meehl et al. 2012; Hurrell et al. 2012). Because of the under-sampling of much of the Atlantic sector prior to the Argo era, a comprehensive global climate observing system, with a particular emphasis on the ocean (e.g. Trenberth 2008) should be maintained. Sustained observation should particularly be encouraged in the tropical Atlantic (e.g. TACE, Schott et al. 2004) since our findings suggest the need for intense observation in this key region to constrain prediction of the AMOC.

7.3.2 What have we learnt?

Contrary to expectations, the choice of vertical coordinate of the ocean component does not significantly affect the level of predictive skills of a model. The present study shows evidence for the strength of the AMOC to have an average predictive skill of about 7 years, and that, on decadal timescales, surface temperature has the highest predictive skills in the high latitude regions and potential predictability for precipitation is largely absent. Because the level of predictability differs from one study to another and that different experimental protocol are used among the existing predictability studies, it remains difficult to evaluate the realism of decadal predictability. A common skill evaluation framework should therefore be encouraged. The decadal prediction evaluation framework described in the present study should be taken as a methodological set-up, since we do not claim it is mature enough to propose any reliable prediction to be used for societal application. For example, uncertainties in the forecast is something to absolutely consider for a prediction system to be reliable, and these are not taken into consideration in the prediction evaluation framework described here. But our approach

still gives some indications as to where and to what extent skillful decadal forecasts might be possible.

In addition, the assumptions, conditions, uncertainties and underlying framework of models would ideally need to be communicated to the decision-makers, for them to be able to evaluate the relevance of the information provided by the models, and to make informed decisions. This turns out to be too complex and time consuming, so it is the scientist's duty to provide guidance on the interpretations of the model results. The question of whether we should believe anything that our models predict about future climate is related to how well we can quantify the uncertainty in model projections. Stainforth et al. (2007) showed that it is not clear that weighted combinations of results from today's complex climate models based on their ability to reproduce a set of observations can provide decision-relevant probabilities. As long as all of our current models are far from being empirically adequate, they consider this to be futile as all models have effectively zero weight relative to the real world. Stainforth et al. (2007) have thus described several methods for presenting the results of large ensembles without assuming realism for any individual model in order to increase our ability to communicate the appropriate degree of confidence in said results. They suggested, for example, that confidence may come from physical understanding of processes involved or from the failure to simulate the variables of interest under present-day climate.

The present study also shows evidence that decadal predictability of the AMOC and associated impacts on climate may be sensitive to the initial oceanic conditions with transitions around extreme states appearing as the most predictable events, in good agreement with several existing studies (e.g. Collins and Sinha 2003; Collins et al. 2006a). This suggests the need for accurate knowledge of the current state of the ocean. As already mentioned earlier, significant resources are being devoted to provide direct measure of AMOC strength, but variations in the latter are not easily interpreted as diagnostic of the ocean circulation or its climate impacts (Wunsch and Heimbach 2012). The global three-dimensional ocean circulation should therefore be described with all of its space and time structure. For instance, Zanna et al. (2012) pointed out the strong sensitivity of the AMOC to deep perturbation in the high latitude regions and that errors there could limit the predictability of the AMOC. These requirements on observational system are far greater than what is available at present.

7.4 Concluding remarks

This project provides a contribution to better understanding of the mechanisms driving decadal AMOC fluctuations while underlining the complexity of such mechanisms and the major disagreements amongst the existing modeling studies. Although additional efforts are still needed to bridge some of the gaps linked to the mechanisms of decadal

variability, this project also contributes to better understanding of the predictability limits for decadal AMOC variations and associated key variables, by giving some indications as to where and to what extent skillful decadal forecasts might be possible. This project also contributes to the development of a common skill evaluation framework to evaluate decadal predictions, which is highly desirable to allow a comparison of decadal systems across different modeling centres. The decadal prediction system described here should, however, be taken as a methodological set-up, since we do not claim it is mature enough to propose any reliable prediction to be used for societal application.

It is worth noting that at present, only a handful of people think about how to make the best use of the huge amounts of data generated by climate models, how to synthesize data for the non-expert, how to effectively communicate the results and how to characterize uncertainty. The realistic communication of scientific uncertainty and the relevance of today's "best available information" may prove critical for maintaining credibility in the future as model-based information improves.

It is also important to bear in mind that none of the existing models is able to accurately reproduce all aspects of past and current climate, and that no single model will ever be able to realistically reproduce climate as we experience it. By their very nature, models cannot capture all the factors involved in a natural system, and those that they do capture are often incompletely understood. Nevertheless, the models ability to reproduce many large-scale aspects of present-day climate, the fact that they are built on well-known physical processes (such as conservation of energy, mass and angular momentum), and the fact we can understand and interpret many of the results from known processes provide support for the models credibility, at least for large scales and certain variables. In the absence of better alternatives, it is likely to be better to use an "imperfect" model than, say, random guessing. They are the best tool we have available for explaining the current behaviour of our climate and predicting likely changes to the planet's future climate.

Ultimately, not just the quality but also the value of decadal forecasts should be quantified in terms of the societal or economic value of the predicted information to climate-related decisions or impacts studies. As the science of decadal prediction is developed, the skill of such predictions in relation to their usefulness and application must also be evaluated.

Appendix A

Relationship between ES and EC

We consider here centred and normalized (by the standard deviation) data in time t. We consider the CS03 definition of ES and EC:

$$ES^2 = \frac{2}{M(M-1)} \sum_{i=1}^{M} \sum_{j=i+1}^{M} (X_i(t) - X_j(t))^2 \tag{A.1}$$

$$EC = \frac{2}{M(M-1)} \sum_{i=1}^{M} (\sum_{j=i+1}^{M} corr(X_i(t), X_j(t))) \tag{A.2}$$

where the discrete time correlation using centred and normalized data is:
$corr(X_i(t), X_j(t)) = \frac{1}{T} \sum_{t=1}^{T} X_i(t) X_j(t)$

We consider the average of ES over the period of time T: $< ES^2 >_T = \frac{1}{T} \sum_{t=1}^{T} ES^2(t)$

By expanding $(X_i(t) - X_j(t))^2$ in Equation A.1 and after a few rearrangements, we can show that:

$$< ES^2 >_T = \frac{1}{T} \sum_{t=1}^{T} \frac{2}{M(M-1)} \sum_{i=1}^{M} \sum_{j=i+1}^{M} (X_i^2(t) + X_j^2(t) - 2X_i(t)X_j(t)) \tag{A.3}$$

$$< ES^2 >_T = \frac{2}{M(M-1)} \sum_{i=1}^{M} \sum_{j=i+1}^{M} \frac{1}{T} \sum_{t=1}^{T} (X_i^2(t) + X_j^2(t)) - \frac{4}{M(M-1)} \sum_{i=1}^{M} \sum_{j=i+1}^{M} \frac{1}{T} \sum_{t=1}^{T} X_i(t) X_j(t) \tag{A.4}$$

Since the variables are centred and normalized: $\frac{1}{T} \sum_{t=1}^{T} X_i^2(t) + X_j^2(t) = 2$

Hence, we obtain the following result: $\boldsymbol{< ES^2 >_T = 2(1 - EC)}$

For the real case, where the data are not normalized and centred, which is more appropriate for ES estimation, no such simple relationship can be found analytically, but we hypothesize that ES and EC remain related. A few illustrations of such link are evidenced in *Sect. 5.3.1.2* and provide support in favour of this hypothesis.

Appendix B

Predictability maps of climate in IPSL-CM5A-LR

We present the individual predictability maps for temperature and precipitation for each starting date in the PPP protocol. These individual results are aggregated in Figure 5.8b and Figure 5.9b.

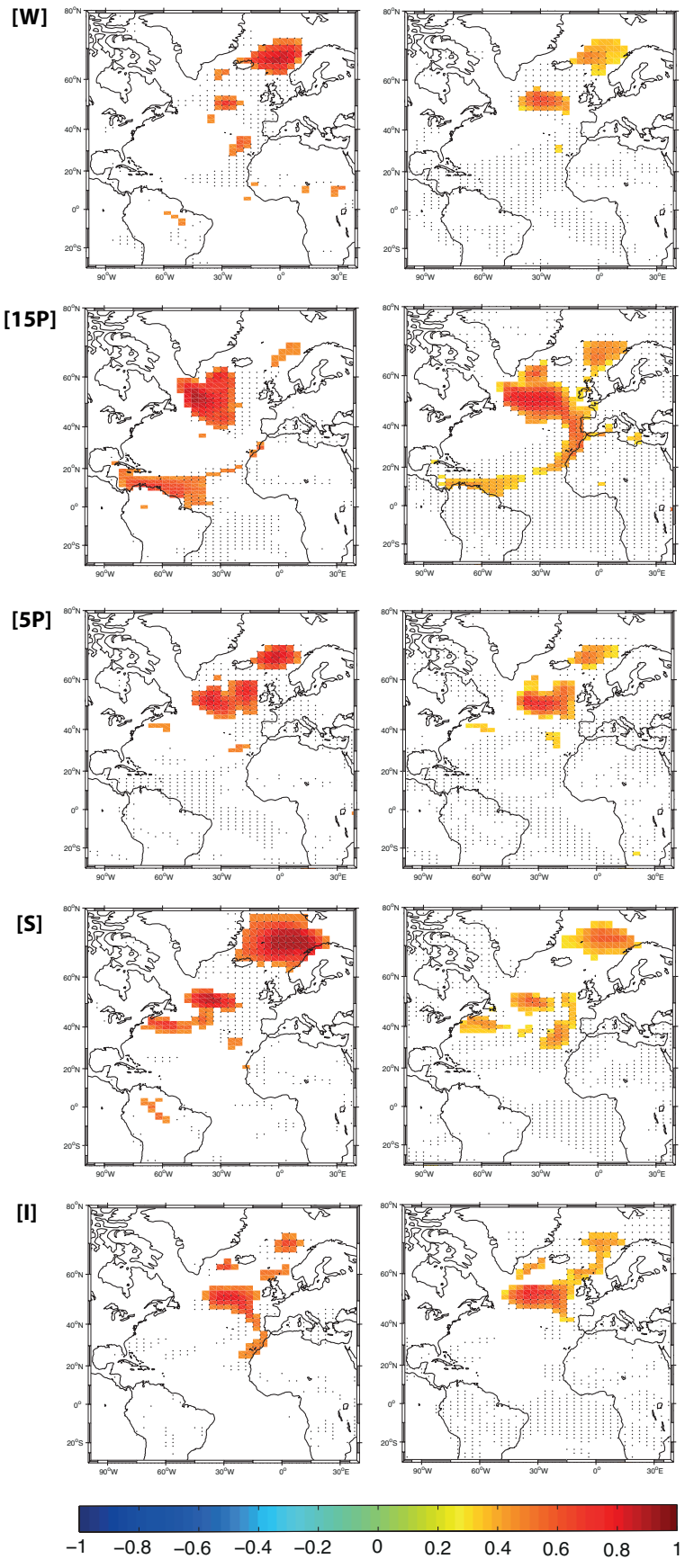

Figure B.1: **Surface Temperature** - Colours represent EC computed as in CS03 for each starting date and years 1-10 (left panels), 1-20 (right panels) of each ensemble experiment. Areas where the correlation is not statistically significant at the 90% level are shown in white. Dots represent grid point where the ES is statistically significantly smaller than the control RMSE at the 95% level.

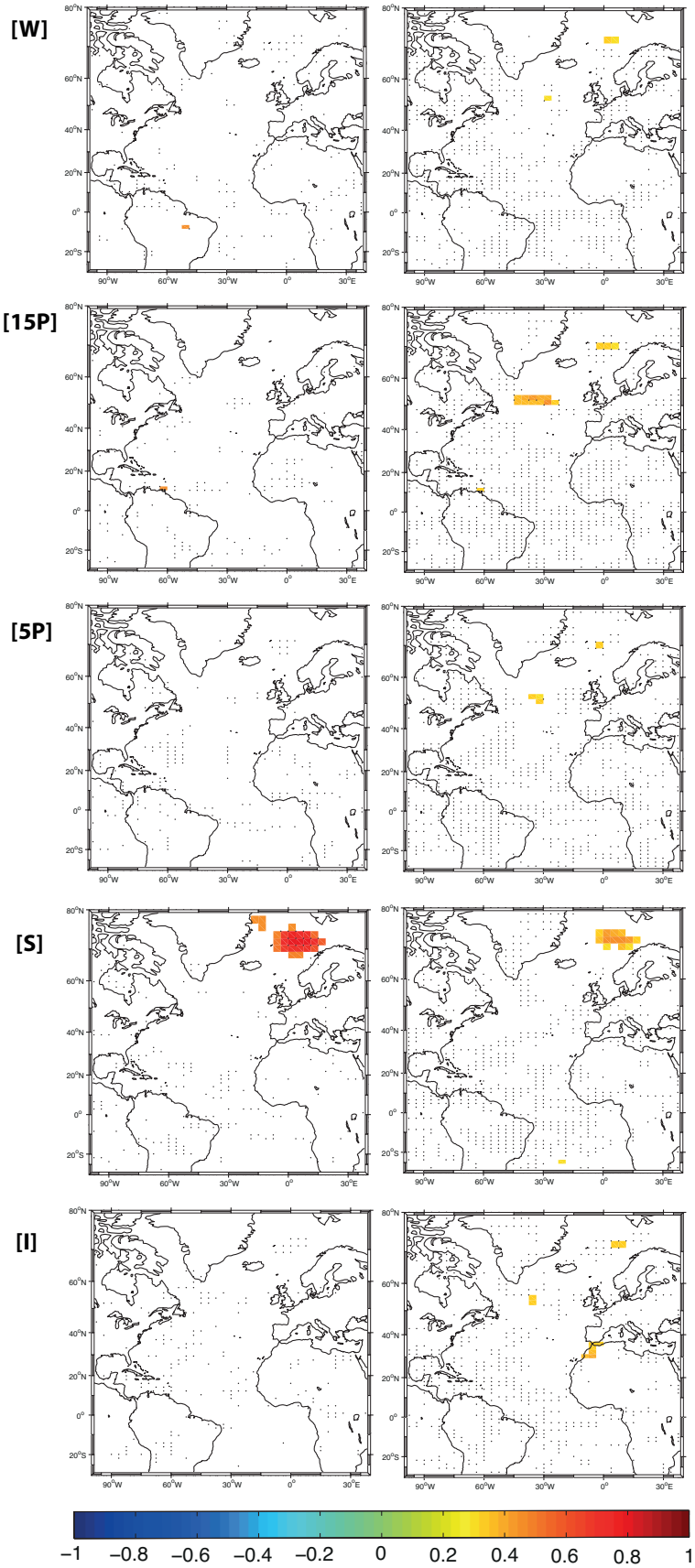

Figure B.2: **Precipitation** - Colours represent EC computed as in CS03 for each starting date and years 1-10 (left panels), 1-20 (right panels) of each ensemble experiment. Areas where the correlation is not statistically significant at the 90% level are shown in white. Dots represent grid point where the ES is statistically significantly smaller than the control RMSE at the 95% level.

Appendix C

Predictability maps of climate in CHIME

We present the individual correlation maps for SST and SAT for each starting date in the PPP protocol. These individual results are aggregated in Figure 6.18b and Figure 6.19b.

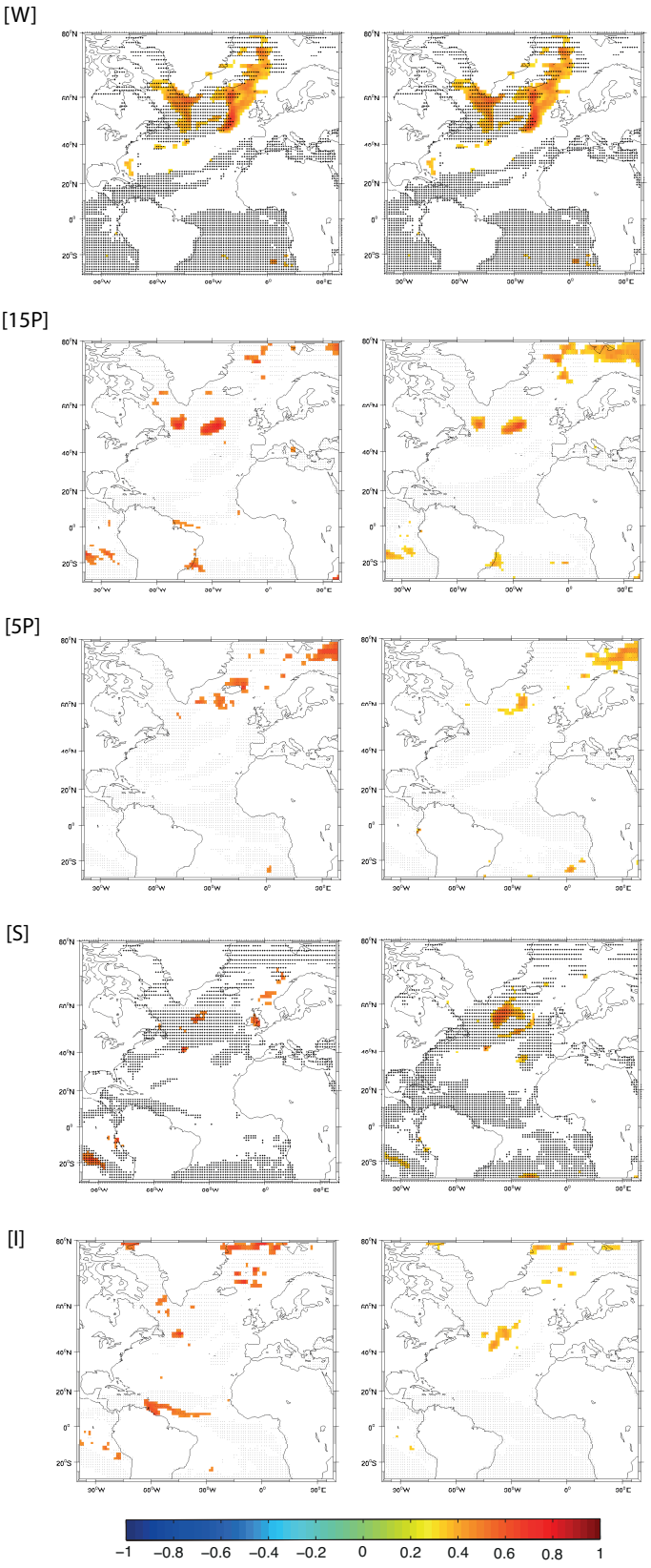

Figure C.1: **Sea Surface Temperature** - Colours represent EC computed as in CS03 for each starting date and years 1-10 (left panels), 1-20 (right panels) of each ensemble experiment. Areas where the correlation is not statistically significant at the 90% level are shown in white. Dots represent grid point where the ES is statistically significantly smaller than the control RMSE at the 95% level.

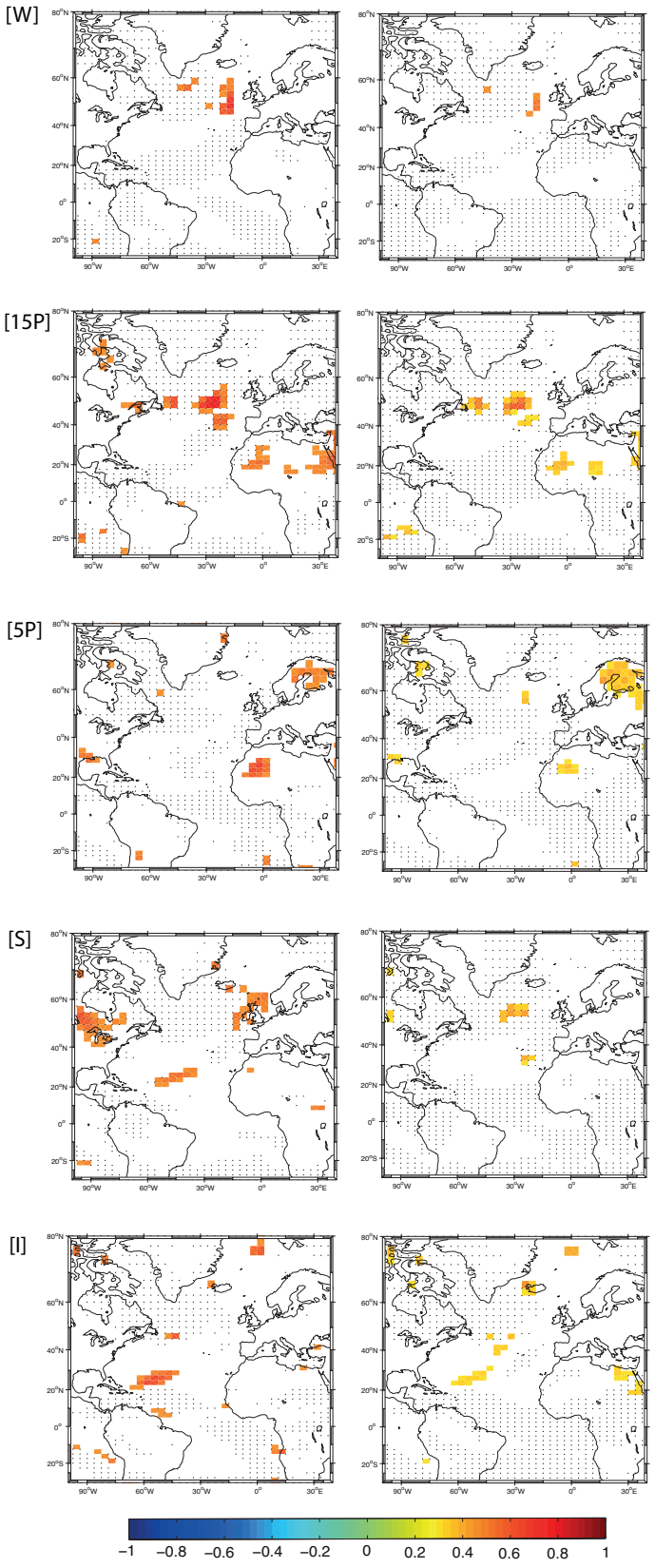

Figure C.2: **Surface Air Temperature** - Colours represent EC computed as in CS03 for each starting date and years 1-10 (left panels), 1-20 (right panels) of each ensemble experiment. Areas where the correlation is not statistically significant at the 90% level are shown in white. Dots represent grid point where the ES is statistically significantly smaller than the control RMSE at the 95% level.

References

A. Adcroft and R. Hallberg. On methods for solving the oceanic equations of motion in generalized vertical coordinates. *Ocean Model.*, 11:224–233, 2006.

A. Adcroft, R. Hallberg, and M. Harrison. A finite volume discretization of the pressure gradient force using analytic integration. *Ocean Model.*, 22:106–113, 2008.

G.V. Alekseev, O.M. Johannessen, A.A. Korablev, V.V. Ivanov, and D.V. Kovalesky. Interannual variability of water mass in the Greenland Sea and the adjacent areas. *Polar Res.*, 20:207–210, 2001.

R.B. Alley and P.U. Clark. The deglaciation of the Northern Hemisphere: A global perspective, in mechanisms of global climate change at millennial timescales. *Geophys. Monogr. Ser.*, 112:142–182, 1999.

A. Arakawa and V.R. Lamb. A potential enstrophy and energy conserving scheme for the shallow water equations. *Mon. Wea. Rev.*, 109(1):18–36, 1981.

O. Aumont and L. Bopp. Globalizing results from ocean in situ iron fertilization studies. *Global Biogeochem. Cycles*, 20(GB2017), 2006. doi: 10.1029/2005GB002591.

J. Bader and M. Latif. The impact of decadal-scale Indian Ocean sea surface temperature anomalies on Sahelian rainfall and the North Atlantic Oscillation. *Geophys. Res. Lett.*, 30(2169), 2003. doi: 10.1029/2003GL018426.

M.A. Balmaseda, M.K. Davey, and D.L.T Anderson. Seasonal dependence of ENSO prediction skill. *J. Climate*, 8:2705–2715, 1995.

B. Barnier, G. Madec, T. Penduff, J.-M. Molines, A.-M. Treguier, Julien Le Sommer, A. Beckmann, A. Biastoch, C. Bning, J. Dengg, C. Derval, E. Durand, S. Gulev, E. Remy, C. Talandier, S. Theetten, M. Maltrud, J. McClean, and B. De Cuevas. Impact of partial steps and momentum advection schemes in a global ocean circulation model at eddy-permitting resolution. *Ocean Dyn.*, 56:543–567, 2006. doi: 10.1007/s10236-006-0082-1.

C.N. Barron, P.J Martin, A.B. Kara, R.C. Rhodes, and L.F. Smedstad. Formulation, implementation and examination of vertical coordinate choices in the Global Navy Coastal Ocean Model (NCOM). *Ocean Model.*, 11:347–375, 2006.

I.M. Belkin, S. Levitus, J.I. Antonov, and S.A. Malmberg. "Great Salinity Anomalies" in the North Atlantic. *Prog. Oceanogr.*, 41:1–68, 1998.

L. Bengtsson, V.A. Semenov, and O.A. Johanessen. The early twentieth-century warming in the Arctic. A possible mechanism. *J. Climate*, 17:4045–4057, 2004.

M. Bentsen, H. Drange, T. Furevik, and T. Zhou. Simulated variability of the Atlantic meridional overturning circulation. *Clim. Dyn.*, 22, 2004. doi: 10.1007/s00382-004-0397-x.

A. Biastoch, C.W Boning, J. Getzlaf, J.M. Molines, and G. Madec. Causes of interannual-decadal variability in the meridional overturning circulation of the mid-latitude North Atlantic Ocean. *J. Climate*, 21:6599–6615, 2008. doi: 10.1175/2008/jCLI2404.1.

A. Biastoch, C.W Boning, F.U. Schwarzkopf, and J.R.E. Lutjeharms. Increase in Agulhas leakage due to poleward shift in the Southern Hemisphere westerlies. *Nature*, 462:495–498, 2009. doi: 10.1038/nature08519.

M. Biasutti, A.H. Sobel, and Y. Kushnir. GCM precipitation biases in the Tropical Atlantic. *J. Climate*, 19:935–958, 2006.

R.J. Bingham, C.W. Hughes, V. Roussenov, and R.G. Williams. Meridional coherence of the North Atlantic meridional overturning circulation. *Geophys. Res. Lett.*, 34 (L23606), 2007. doi: 10.1029/2007GL031731.

A.T. Blaker, B. Sinha, V.O. Ivchenko, N.C. Wells, and V.B. Zalesny. Identifying the roles of the ocean and atmosphere in creating a rapid equatorial response to a Southern Ocean anomaly. *Geophys. Res. Lett.*, 33(6), 2006. doi: 10.1029/2005GL025474.

B. Blanke and P. Delecluse. Variability of the Tropical Atlantic Ocean simulated by a general circulation model with two different mixed-layer physics. *J. Phys. Oceanogr.*, 23(7):1363–1388, 1993.

R. Bleck. An oceanic general circulation model framed in hybrid isopycnic-cartesian coordinates. *Ocean Mod.*, 4:55–88, 2002.

R. Bleck. Hybrid coordinate ocean model (HYCOM) user's manual: details of the numerical code. 2005. Available from http://hycom.rsmas.miami.edu.

R. Bleck and S.G. Benjamin. Regional weather prediction with a model combining terrain-following and isentropic coordinates. Part 1: Model description. *Mon. Weather Rev.*, 121:1770–1785, 1993.

R. Bleck and D.B. Boudra. Initial testing of a numerical ocean circulation model using a hybrid (quasi-isopycnic) vertical coordinate. *J. Phys. Oceanogr.*, 11:755–770, 1981.

R. Bleck, Jr. G.R. Halliwell, A.J. Wallcraft, S. Carroll, K. Kelly, and K. Rushing. Hybrid coordinate ocean model (HYCOM) user's manual: details of the numerical code. 2002. Available from http://hycom.rsmas.miami.edu.

R. Bleck, C. Rooth, D. Hu, and L.T. Smith. Ventilation patterns and mode water formation in a wind- and thermodynamically driven isopycnic coordinate model of the North Atlantic. *J. Phys. Oceanogr.*, 22:1486–1505, 1992.

R. Bleck and L.T. Smith. A wind-driven isopycnic coordinate model of the North and Equatorial Atlantic Ocean. 1: Model development and supporting experiments. *J. Geophys. Res.*, 95:3273–3285, 1990.

G.J. Boer. A study of atmosphere-ocean predictability on long time scales. *Clim. Dyn.*, 16:469–472, 2000.

G.J. Boer. Decadal potential predictability in coupled models. *CLIVAR Exchanges*, 129 (3), 2001. International CLIVAR Project Office.

G.J. Boer. Long-timescale potential predictability in an ensemble of coupled climate models. *Clim. Dyn.*, 23:29–44, 2004.

G.J. Boer. Decadal potential predictability of twenry-first century climate. *Clim. Dyn.*, 36:1119–1133, 2011. doi: 10.1007/s00382-010-0747-9.

G.J. Boer and S.J. Lambert. Multi-model decadal potential predictability of precipitations and temperature. *Geophys. Res. Lett.*, 35(L05706), 2008. doi: 10.1029/2008GL033234.

A. Born and J. Mignot. Dynamics of decadal variability in the Atlantic subpolar gyre: a stochastically forced oscillator. *Clim. Dyn.*, 2011. doi: 10.1007/s00382-011-1180-4.

G.E.P. Box. *Robustness in statistics*. Robustness in the strategy of scientific model building. New York, NY: Academic Press, 1979.

G. Branstator, H. Teng, G. Meehl, M. Kimoto, J. Knight, M. Latif M, and A. Rosati. Systematic estimates of initial value decadal predictability for six AOGCMs. *J. Climate*, 25:1827–1846, 2012.

J.A. Brearley, R.S. Pickart, H. Valdimarsson, S. Jonsson, R.W. Schmitt, and T.W.N. Haine. The East Greenland boundary current system south of Denmark Strait. *Deep Sea Res. Part I*, 63:1–19, 2012. doi: 10.1016/j.dsr.2012.01.001.

C.S Bretherton, M. Widmann, V.P. Dymnikov, J.M. Wallace, and I. Bladé. The effective number of spatial degrees of freedom of a time-varying field. *J. Climate*, 12:1990–2009, 1999.

W.S. Broecker. Thermohaline circulation, the achilles heel of our climate system: Will man-made co_2 upset the current balance. *Science*, 278(5343):1582–1588, 1997.

K. Bryan, S. Manabe, and R.C. Pacanowski. A global ocean-atmosphere climate model II. The oceanic circulation. *J. Phys. Oceanogr.*, 5:30–46, 1975.

H.L Bryden, H.R. Longworth, and S.A. Cunningham. Slowing of the Atlantic meridional overturning circulation at 25°N. *Nature*, 438:655–657, 2005.

H. Burchard and J.M. Beckers. Non-uniform adaptive vertical grids in one-dimensional numerical ocean models. *Ocean Model.*, 6:51–81, 2004.

H. Cattle and J. Crossley. Modelling Arctic climate change. *Philos. Trans. Roy. Soc. London*, 352A:201–213, 1995.

E.P. Chassignet, H. Arango, D. Dietrich, T. Ezer, M. Ghil, D.B. Haidvogel, C.-C. Ma, A. Mehra, A.M. Paiva, and Z. Sirkes. DAMEE-NAB: the base experiments. *Dyn. Atmos. Oceans*, 32:155–184, 2000.

E.P. Chassignet, H.E. Hurlburt, O.M. Smedstad, G.R. Halliwell, P.J. Hogan, A.J. Wallcraft, and R. Bleck. *Ocean weather forecasting: an integrated view of oceanography.* Ocean prediction with the HYbrid Coordinate Ocean Model (HYCOM). pages 413–426. Springer, Berlin, 2006.

E.P. Chassignet, H.E. Hurlburt, O.M. Smedstad, G.R. Halliwell, P.J. Hogan, A.J. Wallcraft, and R. Bleck. Ocean prediction with the HYbrid Coordinate Ocean Model (HYCOM). *J. Mar. Syst.*, 65:60–83, 2007.

E.P. Chassignet, L.T. Smith, R. Bleck, and F.O. Bryan. A model comparison: Numerical simulations of the North and Equatorial Atlantic oceanic circulation in depth and isopycnic coordinates. *J. Phys. Oceanogr.*, 26:1849–1867, 1996.

E.P. Chassignet, L.T. Smith, G.R. Halliwell, and R. Bleck. North Atlantic simulation with the HYbrid Coordinate Ocean Model (HYCOM): Impact of the vertical coordinate choice, reference density and thermobaricity. *J. Phys. Oceanogr.*, 33:2504–2526, 2003.

C. Chatfield. *The analysis of timeseries: theory and practice.* Chapman and Hall, London, 1975.

D. Chen, M.A. Cane, A. Kaplan, S.E. Zebiak, and D. Huang. Predictability of El-Niño over the past 148 years. *Nature*, 428:733–736, 2004.

J.C.H. Chiang, W. Cheng, and C.M. Bitz. Fast teleconnections to the Tropical Atlantic sector from the Atlantic thermohaline adjustment. *Geophys. Res. Lett.*, 35(L07704), 2008. doi: 10.1029/ 2008GL033292.

J.C.H. Chiang, Y. Kushnir, and A. Giannini. Deconstructing Atlantic intertropical convergence zone variability: influence of the local cross-equatorial sea surface temperature gradient and remote forcing from the Eastern Equatorial Pacific. *Geophys. Res. Lett.*, 107(4004), 2002. doi: 10.1029/2000JD000307.

P.U. Clark, N.G. Pisias, T.F Stocker, and A.J. Weaver. The role of the thermohaline circulation in abrupt climate change. *Nature*, 415:863–869, 2002.

A. Colin de Verdière and T. Huck. Baroclinic instability : An oceanic wavemaker for interdecadal variability. *J. Phys. Oceanogr.*, 29:893–910, 1999.

M. Collins. Climate predictability on interannual to decadal timescales: The initial value problem. *Clim. Dyn.*, 19:671–692, 2002.

M. Collins, M. Botzet, A.F. Carril, H. Drange, A. Jouzeau, M. Latif, S. Masina, O.H. Otteraa, H. Pohlmann, A. Sorteberg, R. Sutton, and L. Terray. Interannual to decadal climate predictability in the North Atlantic: A multimodel-ensemble study. *J. Climate*, 19:1195–1203, 2006a.

M. Collins and B. Sinha. Predictable decadal variations in the thermohaline circulation and climate. *Geophys. Res. Lett.*, 30(6), 2003. doi: 10.1029/2002GLO16504.

M. Collins, S. Tett, and C. Cooper. The internal climate variability of HadCM3, a version of the Hadley Centre coupled model without flux adjustments. *Clim. Dyn.*, 17:61–81, 2001.

W.D. Collins, C.M. Bitz, M.L. Blackmon, G.B. Bonan, C.S. Bretherton, J.A. Carton, P. Chang, S.C. Doney, J.J. Hack, T.B. Henderson, J.T. Kiehl, W.G. Large, D.S. Mckenna, B.D. Santer, and R.D. Smith. The Community Climate System Model version 3 (CCSM3). *J. Climate*, 19:2122–2143, 2006b.

M.E. Conkright, R.A. Locarnini, H.E. Garcia, T.D. Obrien, T.P. Boyer, C. Stephens, and J.I. Antonov. *World Ocean Atlas 2001: Objective Analyses, Data Statistics, and Figures, CD-ROM Documentation*, volume 17. NOAA Silver Spring, 2002.

D. Conway, A. Persechino, S. Ardoin-Bardin, H. Hamandawana, C. Dieulin, and G. Mahe. Rainfall and water resources variability in Sub-Saharan Africa during the 20^{th} century. *J. Hydrometeor.*, 10(1):41–59, 2009. doi: 10.1175/2008JHM1004.1.

R. Courant, K. Friedrich, and H. Lewy. On the partial difference equations of mathematical physics. *IBM J. Res. Dev.*, 11(2):215–234, 1967.

P.M. Cox, R.A. Betts, C.B. Bunton, R.L.H. Essery, P.R. Rowntree, and J.Smith. The impact of new land surface physics on the GCM simulation of climate and climate sensitivity. *Clim. Dyn.*, 15:183–203, 1999.

S. Cravatte, G. Madec, T. Izumo, C Menkes, and A. Bozec. Progress in the 3-D circulation of the Eastern Equatorial Pacific in a climate ocean model. *Ocean Model.*, 17 (1):28–48, 2007. doi: 10.1016/j.ocemod.2006.11.003.

S.A. Cunningham. Monitoring the Atlantic Meridional Overturning Circulation at 26.5°N: RAPID-WATCH. Research and Consultancy Report 59, Nation Oceanoprahy Centre, Southampton, 2008.

S.A. Cunningham, S.G. Alderson, B.A. King, and M. A. Brandon. Transport and variability of the Antarctic Circumpolar Current in Drake Passage. *J. Geophys. Res.*, 108, 2003. doi:10.1029/2001JC001147.

S.A. Cunningham, T. Kanzow, D. Rayner, M.O. Baringer, W.E Johns, J. Marotzke, H.R. Longworth, E.M. Grant, JJ-M. Hirschi, L.M. Beal, C.S. Meinen, and H.L. Bryden. Temporal variability of the Atlantic meridional overturning circulation at 26.5°N. *Science*, 317(5840):935–938, 2007. doi: 10.1126/science.1141304.

S.A. Cunningham and R. Marsh. Observing and modeling changes in the Atlantic MOC. *Wiley Interdiscip. Rev. Clim. Change*, 1:180–191, 2010. doi: 10.1002/wcc.22.

J. Cuny, P.B. Rhines, and R. Kwok. Davis Strait volume, freshwater and heat uxes. *Deep-Sea Res.*, 52:519–542, 2005.

R.G. Curry, R. Dickson, and I. Yashayaev. A change in the freshwater balance of the Atlantic Ocean over the past four decades. *Nature*, 426, 2003. doi: 10.1038/nature02206.

R.G. Curry, M.S. McCartney, and T.M. Joyce. Oceanic transport of subpolar climate signals to mid-depth subtropical waters. *Nature*, 391:575–577, 1998.

S. Cusack, J.M. Edward, and J.M. Crowther. Investigating k-distribution methods for parametrizing gaseous absorption in the Hadley Centre climate model. *J. Geophys. Res.*, 104:2051–2057, 1999.

S. Cusack, A. Slingo, J.M. Edwards, and M. Wild. The radiative impact of a simple aerosol climatology on the Hadley Centre climate model. *Q. J. R. Meteorol. Soc.*, 124: 2517–2526, 1998.

A. Czaja and J. Marshall. Observations of atmosphere-ocean coupling in the North Atlantic. *Q. J. R. Meteorol. Soc.*, 127:1893–1916, 2001.

A. Dai. Precipitation characteristics in eighteen coupled climate models. *J. Climate*, 19 (18):4605–4630, 2006.

A. Dai, A. Hu, G.A. Meehl, W.M. Washington, and W.G. Strand. Atlantic thermohaline circulation in a coupled model: Unforced variations versus forced changes. *J. Climate*, 18:3270–3293, 2005.

G. Danabasoglu. On multidecadal variability of the Atlantic meridional overturning circulation in the community climate system model version 3. *J. Climate*, 21:5524–5544, 2008. doi: 10.1175/2008JCLI2019.1.

P. de Rosnay and J. Polcher. Modelling root water uptake in a complex land surface scheme coupled to a GCM. *Hydrol. Earth Syst. Sci.*, 2(2-3):239–255, 1998. doi: 10.1175/2008JCLI2019.1.

T. Delworth and K.W. Dixon. Implications of the recent trend in the Arctic/North Atlantic Oscillation for the North Atlantic thermohaline circulation. *J. Climate*, 13: 3721–3727, 2000.

T. Delworth and R.J. Greatbatch. Multidecadal thermohaline circulation variability driven by atmospheric surface flux forcing. *J. Climate*, 13:1481–1495, 2000.

T. Delworth, S. Manabe, and R.J. Stouffer. Interdecadal variations of the thermohaline circulation in a coupled ocean-atmosphere model. *J. Climate*, 6:1993–2011, 1993.

T. Delworth, S. Manabe, and R.J. Stouffer. Multidecadal climate variability in the Greenland Sea and surrounding regions: A coupled model situation. *Geophys. Res. Lett.*, 24:257–260, 1997.

T. Delworth and M.E Mann. Observed and simulated multi-decadal variability in the Northern Hemisphere. *Clim. Dyn.*, 16:661–676, 2000.

T. Delworth, R. Zhang, and M. Mann. Decadal to centennial variability of the Atlantic from observations and models. *Geophys. Monogr.*, 173:131–148, 2007.

M. Deque, C. Dreveton, A. Braun, and D. Cariolle. The ARPEGE-IFS atmosphere model: a contribution to the French community climate modelling. *Clim. Dyn.*, 10: 249–266, 1994.

C. Deser and M.L. Blackmon. Surface climate variations over the North Atlantic Ocean during winter: 1900-1989. *J. Climate*, 23:333–351, 2010.

C. Deser, R. Tomas, M. Alexander, and D. Lawrence. The seasonal atmospheric response to projected Arctic sea ice loss in the late twenty-first century. *J. Climate*, 6:1743–1753, 1993.

R.R. Dickson, J. Lazier, J. Meincke, P. Rhines, and J. Swift. Long-term coordinated changes in the convective activity of the North Atlantic. *Prog. Oceanogr.*, 38:241–295, 1996.

H.A. Dijkstra, L.A. Te Raa, M. Schmeits, and J. Gerrits. On the physics of the Atlantic Multidecadal Oscillation. *Ocean Dyn.*, 56:36–50, 2006.

B. Dong and R. Sutton. Adjustment of the coupled ocean-atmosphere system to a sudden change in the thermohaline circulation. *Geophys. Res. Lett.*, 29(1728), 2002. doi: 10.1029/ 2002GL015229.

B. Dong and R. Sutton. Mechanism of interdecadal thermohaline circulation variability in a coupled ocean-atmosphere GCM. *J. Climate*, 18:1117–1135, 2005.

H. Drange and R. Bleck. Multidimensional forward-in-time upstream-in-space-based differencing for fluids. *Mon. Weather Rev.*, 125:616–630, 1997.

N. Ducoudré, K. Laval, and A. Perrier. SECHIBA, a new set of parameterizations of the hydrologic exchanges at the land-atmosphere interface within the LMD atmospheric general circulation model. *Clim. Dyn.*, 6:248–273, 1993.

J.-L. Dufresne, M.A. Foujols, S. Denvil, A. Caubel, O. Marti, O. Aumont, Y. Balkanski, S. Bekki, H. Bellenger, R. Benshila, S. Bony, L. Bopp, P. Braconnot, P. Brockmann, P. Cadule, F. Cheruy, F. Codron, A. Cozic, D. Cugnet, N. deNoblet, J.-P. Duvel, C. Ethé, L. Fairhead, T. Fichefet, S. Flavoni, P. Friedlingstein, J.-Y. Grandpeix, L. Guez, E. Guilyardi, D. Hauglustaine, F. Hourdin, A. Idelkadi, J. Ghattas, S. Joussaume, M. Kageyama, G. Krinner, S. Labetoulle, A. Lahellec, M.-P. Lefebvre, F. Lefevre, C. Levy, Z.X. Li, J. Lloyd, F. Lott, G. Madec, M. Mancip, M. Marchand, S. Masson, Y. Meurdesoif, J. Mignot, I. Musat, S. Parouty, J. Polcher, C. Rio, M. Schulz, D. Swingedouw, S. Szopa, C. Talandier, P. Terray, and N. Viovy. Climate change projections using the IPSL-CM5 earth system model: from CMIP3 to CMIP5. *Clim. Dyn.*, 2012. In revision.

J.K. Dukowicz. HYPOP: A new type of Hybrid Eularian-Lagragian Ocean Model. 2005. Los Alamos Report LA-UR-05-9487.

N.J. Dunstone and D.M. Smith. Impact of atmosphere and sub-surface ocean data on decadal climate prediction. *Geophys. Res. Lett.*, 37(L02709), 2010. doi:10.1029/2009GL041609.

N.J. Dunstone, D.M. Smith, and R. Eade. Multi-year predictability of the Tropical Atlantic atmosphere driven by the high latitude North Atlantic Ocean. *Geophys. Res. Lett.*, 38(L14701), 2011. doi: 10.1029/2011GL047949.

C. Eden and J. Willebrand. Mechanism of interannual to decadal variability of the North Atlantic circulation. *J. Climate*, 14:2266–2280, 2001.

J.M. Edwards and A. Slingo. Studies with a flexible new radiation code. I: Choosing a configuration for a large-scale model. *Q. J. R. Meteorol. Soc.*, 122(531):689–719, 1996.

R. Escudier, J. Mignot, and D. Swingedouw. A coupled ocean-sea ice-atmosphere decadal variability mode in the North Atlantic in an AOGCM. *Clim. Dyn.*, 2012. doi: 10.1007/s00382-012-1402-4.

T. Ezer and G. Mellor. A generalized coordinate ocean model and a comparison of the bottom boundary layer dynamics in terrain following and z-level grids. *Ocean Model.*, 6:379–403, 2004.

M. Fan and E.K. Schneider. Observed decadal North Atlantic tripole SST variability. Part I: weather noise forcing and coupled response. *J. Atmos. Sci.*, 69:35–50, 2012.

T. Fichefet and M.A.M. Maqueda. Sensitivity of a global sea ice model to the treatment of ice thermodynamics and dynamics. *J. Geophys. Res.*, 102:2609–2612, 1997.

T. Fichefet and M.A.M. Maqueda. Modelling the influence of snow accumulation and snow-ice formation on the seasonal cycle of the Antarctic sea-ice cover. *Clim. Dyn.*, 15(4):251–268, 1999. doi: 10.1007/s003820050280.

R.A. Fisher. On the "probable error" of a coefficient of correlation deduced from a small sample. *Metron.*, 1(4):3–32, 1921.

C.K. Folland, D.E. Parker, and T.N. Palmer. Sahel rainfall and worldwide sea temperatures, 1901-85. *Nature*, 320:602–607, 1986.

K. Fraedrich and K. Müller. Climate anomalies in Europe associated with ENSO extremes. *J. Climatol.*, 12:25–31, 1992.

L.H. Frankcombe, H.A. Dijkstra, and A. von der Heydt. Sub-surface signatures of the Atlantic Multidecadal Oscillation. *Geophys. Res. Lett.*, 35(L19602), 2008. doi: 10.1029/2008GL034989.

L.H. Frankcombe, A. von der Heydt, and H.A. Dijkstra. North Atlantic multidecadal climate variability: An investigation of dominant time scales and processes. *J. Climate*, 23:3626–3638, 2010.

C. Frankignoul. Sea surface temperature anomalies, planetary waves, and air-sea feedback in the middle latitudes. *Rev. Geo. phys.*, 23:357–390, 1985.

C. Frankignoul and K. Hasselmann. Stochastic climate models. Part II: Application to sea-surface temperature variability and thermocline variability. *Tellus*, 29:284–305, 1977.

C. Frankignoul, E. Kestenare, and J. Mignot. The surface heat flux feedback. Part II: direct and indirect estimates in the ECHAM4/OPA8 coupled GCM. *Clim. Dyn.*, 19: 649–655, 2002.

S.R. Gamiz-Fortis and R.T. Sutton. Quasi-periodic fluctuations in the Greenland-Iceland-Norwegian Seas region in a coupled climate model. *Ocean Dyn.*, 57:541–557, 2007. doi: 10.1007/s10236-007-0116-3.

A. Ganachaud and C. Wunsch. Improved estimates of global ocean circulation, heat transport and mixing from hydrographic data. *Nature*, 408:453–457, 2000.

G. Gastineau, F. D'Andrea, and C. Frankignoul. Atmospheric response to the North Atlantic ocean variability on seasonal to decadal timescales in IPSL-CM5. *Clim. Dyn.*, 2012. doi: 10.1007/s00382-012-1333-0.

A. Giannini, J.C.H. Chiang, M.A. Cane, Y. Kushnir, and R. Seager. The ENSO teleconnection to the Tropical Atlantic Ocean: contributions of the remote and local SSTs to rainfall variability in the Tropical Americas. *J. Climate*, 14:4530–4544, 2001.

P. Gloersen, W.J. Campbell, D.J. Cavalieri, J.C. Comiso, C.L. Parkinson, and H.J. Zwally. Satellite passive microwave observations and analysis of Arctic and Antarctic sea ice, 1978-1987. *Annals of Glaciology*, 17:149–154, 1993.

L. Goddard, P. Gonzalez, S. Mason, A. Greene, and the US CLIVAR Working Group on Decadal Predictability. A verification framework for interannual-to-decadal prediction experiments. *Clim. Dyn.*, 2012. Submitted.

P.J. Goodman. Thermohaline adjustment and advection in an AOGCM. *J. Phys. Oceanogr.*, 31:1477–1497, 2001.

H. Goose, J.M. Campin, T. Fichefet, and E. Deleersnijder. Sensitivity of a global ice-ocean model to the Bering Strait throughflow. *Clim. Dyn.*, 13:349–358, 1997.

A.L. Gordon. Interocean Exchange of Thermocline Water. *J. Geophys. Res.*, 91(C4): 5037–5046, 1986.

A.L. Gordon, S.E. Zebiak, and K. Bryan. Climate variability and the Atlantic Ocean. *Eos Trans.*, AGU 73:161–165, 1992.

C. Gordon, C. Cooper, C. Senior, H. Banks, J. Gregory, T. Johns, J. Mitchell, and R. Wood. The simulation of SST, sea ice extents and ocean heat transports in a coupled model without flux adjustments. *Clim. Dyn.*, 16:147–168, 2000.

D. Gregory and S. Allen. The effect of convective scale down-drafts upon NWP and climate simulations. pages 122–123. Ninth conf. numerical weather prediction, Denver, Colorado, American Meteorological Society, 1991.

D. Gregory, R. Kershaw, and P.M. Inness. Parametrization of momentum transport by convection. II: tests in single-column and general circulation models. *Q. J. R. Meteorol. Soc.*, 123:1153–1183, 1997.

D. Gregory and D. Morris. The sensitivity of climate simulations to the specification of mixed phase clouds. *Clim. Dyn.*, 12:641–651, 1996.

D. Gregory and P.R. Rowntree. A mass flux convection scheme with representation of cloud ensemble characteristics and stability dependent closure. *Mon. Weather Rev.*, 118:1483–1506, 1990.

D. Gregory, G.J. Shutts, and J.R. Mitchell. A new gravity-wave-drag scheme incorporating anisotropic orography and low-level wave breaking: impact upon the climate of the UK Meteorological Office United Model. *Q. J. R. Meteorol. Soc.*, 124:463–494, 1998.

J.M. Gregory, K.W. Dixon, R.J. Stouffer, A.J. Weaver, E. Driesschaert, M. Eby, T. Fichefet, H. Hasumi, A. Hu, J.H. Jungclaus, I.V. Kamenkovich, A. Levermann, M. Montoya, S. Murakami, S. Nawrath, A. Oka, A.P. Sokolov, and R.B. Thorpe. A

model intercomparison of changes in the Atlantic thermohaline circulation in response to increasing atmospheric co_2 concentration. *Geophys. Res. Lett.*, 32(L12703), 2005. doi: 10.1029/2005GL023209.

S.M. Griffies, C. Böning, F.O. Bryan, E.P. Chassignet, R. Gerdes, H. Hasumi, A. Hirst, A.M. Treguier, and D. Webb. Developments in ocean climate modelling. *Ocean Mod.*, 2:123–192, 2000.

S.M. Griffies and K. Bryan. Predictability of North Atlantic multidecadal climate variability. *Science*, 275:181–184, 1997a.

S.M. Griffies and K. Bryan. A predictability study of simulated North Atlantic multidecadal variability. *Clim. Dyn.*, 8:459–488, 1997b.

A.M. Grötzner, M. Latif, A. Timmermann, and R. Voss. Interannual to decadal predictability in a coupled ocean-atmosphere general circulation model. *J. Climate*, 12: 2607–2624, 1999.

V. Guemas and D. Salas-Mélia. Simulation of the Atlantic meridional overturning circulation in an atmosphere-ocean global coupled model. Part I: a mechanism governing the variability of ocean convection in a preindustrial experiment. *Clim. Dyn.*, 31: 29–48, 2008.

V. Guemas and D. Salas-Mélia. Differing impacts of resolution changes in latitude and longitude on the mid-latitudes in the LMDZ GCM. *J. Climate*, 24(22):5831–5849, 2011. doi: 10.1175/2011JCLI4093.1.

M.M. Hall and H.L. Bryden. Direct estimates and mechanisms of ocean heat transport. *Deep Sea Res.*, 29:339–359, 1982.

R. Hallberg and A. Adcroft. Reconciling estimates of the free surface height in Lagrangian vertical coordinate ocean models with mode-split time stepping. *Ocean Model.*, 29:15–26, 2009.

R. Hallberg and A. Gnanadesikan. The role of eddies in determining the structure and response of the wind-driven southern hemisphere overturning: Results from the Modeling Eddies in the Southern Ocean (MESO) project. *J. Phys. Oceanogr.*, 36: 2232–2252, 2006.

R.W. Hallberg. Some aspects of the circulation in ocean basins with isopycnals intersecting the sloping boundaries. 1995. Ph.D. thesis, University of Washington, Seattle, 244 pp.

R.W. Hallberg. Stable split time stepping schemes for large-scale ocean modelling. *J. Comput. Phys.*, 135:54–65, 1997.

G.R. Halliwell. Simulation of North Atlantic decadal/multidecadal winter SST anomalies driven by basin-scale atmospheric circulation anomalies. *J. Phys. Oceanogr.*, 28:5–21, 1998.

G.R. Halliwell. Evaluation of vertical coordinate and vertical mixing algorithms in the HYbrid Coordinate Ocean Model (HYCOM). *Ocean Mod.*, 7:285–322, 2004.

L.D.D. Harvey. Characterizing and comparing the control run variability of eight coupled AOGCMs and observations. *Clim. Dyn.*, 21:647–658, 2003.

K. Hasselmann. Stochastic climate models. Part I, theory. *Tellus*, 28:473–485, 1976.

H. Hasumi. Sensitivity of the global thermohaline circulation to interbasin freshwater transport by the atmosphere and the Bering Strait throughflow. *J. Climate*, 15:2516–2526, 2002.

E. Hawkins, J. Robson, R.T. Sutton, D. Smith, and N. Keenlyside. Evaluating the potential for statistical decadal predictions of sea surface temperatures with a perfect model approach. *Clim. Dyn.*, 37(11-12):2495–2509, 2011. doi: 10.1007/s00382-011-1023-3.

E. Hawkins and R.T. Sutton. Variability of the Atlantic thermohaline circulation described by three-dimensional empirical orthogonal functions. *Clim. Dyn.*, 29:745–762, 2007.

E. Hawkins and R.T. Sutton. Potential predictability of rapid changes in the Atlantic meridional overturning circulation. *Geophys. Res. Lett.*, 35(L11603), 2008. doi: 10.1029/2008GL034059.

E. Hawkins and R.T. Sutton. Decadal predictability of the Atlantic Ocean in a coupled GCM: forecast skill and optimal perturbations using linear inverse modelling. *J. Climate*, 22(14):3960–3978, 2009. doi: 10.1175/2009JCLI2720.1.

H. Heinrich. Origin and consequences of cyclic ice rafting in the Northeast Atlantic Ocean during the past 130000 years. *Quat. Res.*, 29:143–152, 1988.

L. Hermanson and R.T. Sutton. Climate predictability in the second year. *Philos. Trans. R. Soc. A.*, 367:913–916, 2009.

C. Herweijer, R. Seager, M. Winton, and A. Clement. Why the ocean heat tranport warms the global mean climate? *Tellus*, 57A:662–675, 2005.

W.D. Hibler. A dynamic-thermodynamic sea ice model. *J. Phys. Oceanogr.*, 9:817–846, 1979.

M.P. Hoerling, J.W. Hurrell, and T. Xu. Tropical origins for recent North Atlantic climate change. *Science*, 292:90–92, 2001.

F. Hourdin, M.A. Foujols, F. Codron, V. Guemas, J.L. Dufresne, S. Bony, S. Denvil, L. Guez, F. Lott, J. Ghattas, P. Braconnot, O. Marti, Y. Meurdesoif, and L. Bopp. Climate and sensitivity of the IPSL-CM5A coupled model: impact of the LMDZ atmospheric grid configuration. *Clim. Dyn.*, 2012. In revision.

F. Hourdin, I. Musat, S. Bony, P. Braconnot, F. Codron, J-L. Dufresne, L. Fairhead, M.-A. Filiberti, P. Friedlingstein, J.-Y. Grandpeix, G. Krinner, P. LeVan, Z.-X. Li, and F. Lott. The LMDZ4 general circulation model: climate performance and sensitivity to parametrized physics with emphasis on tropical convection. *Clim. Dyn.*, 27(7-8): 787–813, 2006. doi: 10.1007/s00 382-006-0158-0.

B. Huang, P.S. Schopf, and Z. Pan. The ENSO effect on the tropical Atlantic variability: A regionally coupled model study. *Geophys. Res. Lett.*, 29(21), 2002. doi: 10.1029/2002GL014872.

G.J. Huffman, R.F. Adler, M. Morrissey, D.T. Bolvin, S. Curtis, R. Joyce, B McGavock, and J. Susskind. Global Precipitation at One-Degree Daily Resolution from Multi-Satellite Observations. *J. Hydrometeor.*, 2:36–50, 2001.

J.W. Hurrell. Decadal trends in the North Atlantic Oscillation, regional temperatures and precipitation. *Science*, 269:676–679, 1995a.

J.W. Hurrell. NAO Index Data provided by the Climate Analysis Section, NCAR, Boulder, USAl. 1995b. Updated regularly.

J.W. Hurrell and R.R. Dickson. *Marine Ecosystems and Climate Variation: The North Atlantic*. Climate variability over the North Atlantic. pages 15–31. Oxford University Press, 2004.

J.W. Hurrell, M. Latif, M. Visbeck, T. L. Delworth, G. Danabasoglu, D. Dommenget, H. Drange, K. Drinkwater, S. Griffies, W. Hazeleger, N.J. Holbrook, B. Kirtman, N. Keenlyside, J. Marotzke, J. Murphy, G.A. Meehl, T. Palmer, H. Pohlmann, T. Rosati, R. Seager, D. Smith, R. Sutton, A. Timmermann, K. E. Trenberth, and J. Tribbia. Decadal climate variability, predictability and prediction: Opportunities and challenges. *Rev. Geophys.*, 2012. Submitted.

J.W. Hurrell, G. Meehl, D. Bader, T. Delworth, B. Kirtman, and B. Wielicki. A unified modeling approach to climate system prediction. *Bull. Amer. Meteor. Soc.*, 90:1819–1832, 2009. doi: 10.1175/2009BAMS2752.1.

IPCC. Climate change (1996). the IPCC second scientific assessment. pages 407–444. Cambridge University Press, Cambridge University Press, Cambridge, 1996.

IPCC. Climate change (2001) The Scientific Basis. Contributions of Working Group I to the Third Assessment Report of the Intergovernmental Panel on Climate Change. Cambridge University Press, Cambridge University Press, Cambridge, 2001.

IPCC. Climate change (2007) The physical Science Basis. Contribution of Working Group I to the Fourth Assessment Report of the Intergovernmental Panel on Climate Change. Cambridge University Press, Cambridge University Press, Cambridge, 2007.

W.E. Johns, M.O. Baringer, L.M. Beal, S.A. Cunningham, T. Kanzow, H.L. Bryden, J.J.M. Hirschi, J. Marotzke, C.S. Meinen, B. Shaw, and R. Curry. Continuous, array-based estimates of Atlantic Ocean heat transport at 26.5°n. *J. Climate*, 24(10):2429–2449, 2011.

W.E. Johns, T.J. Shay, J.M. Bane, and D.R. Watts. Gulf Stream structure, transport, and recirculation near 68°W. *J. Geophys. Res.*, 100C:817–838, 1995.

H. Johnson and D. Marshal. Global teleconnections of meridional overturning circulation anomalies. *J. Phys. Oceanogr.*, 34:1702–1722, 2004.

P.D. Jones, M. New, D.E. Parker, S. Martin, and I.G. Rigor. Surface air temperature and its changes over the past 150 years. *Rev. Geophys.*, 37(2):173–199, 1999.

S.A. Josey, E.C. Kent, and P.K. Taylor. *The Southampton Oceanography Centre (SOC) Ocean-Atmosphere Heat, Momentum and Freshwater Flux Atlas*, volume 6. Southampton Oceanography Centre Rep., 1998. 30 pp.

J.H. Jungclaus, H. Haak, M. Latif, and U. Mikolajewicz. Arctic North Atlantic interactions and multidecadal variability of the meridional overturning circulation. *J. Climate*, 18:4013–4031, 2005.

A.B. Kara, A.J. Wallcraft, P.J. Martin, and E.P. Chassignet. Performance of mixed layer models in simulating SST in the Equatorial Pacific Ocean. *J. Geophys. Res.*, 113(C02020), 2008. doi: 10.l029/2O07JCO04250.

N.S. Keenlyside, M. Latif, J. Jungclaus, L. Kornblueh, and E. Roeckner. Advancing decadal-scale climate prediction in the North Atlantic sector. *Nature*, 453:84–88, 2008.

L.D. Keigwin and E. Boyle. Detecting Holocene changes in thermohaline circulation. *Proc. Natl. Acad. Sci. U.S.A.*, 97:1343–1346, 2000.

L.D. Keigwin, W.B. Curry, S.J. Lehman, and S. Johnsen. The role of the deep ocean in North Atlantic climate change between 70 and 130 kyr ago. *Nature*, 371:323–326, 1994.

R.A. Kerr. A North Atlantic climate pacemaker for the centuries. *Science*, 288(5473): 1984–1985, 2000.

J.R. Knight. The Atlantic Multidecadal Oscillation as inferred from the forced climate response in coupled general circulation models. *J. Climate*, 22:1610–1625, 2009.

J.T. Knight, R.J. Allan, C.K. Folland, M. Vellinga, and M.E. Mann. A signature of persistent natural thermohaline circulation cycles in observed climate. *Geophys. Res. Lett.*, 32(L20708), 2005. doi: 1029/ 2005GL024233.

J.T. Knight, C.K. Folland, and A.A. Scaife. Climate impacts of the Atlantic Multidecadal Oscillation. *Geophys. Res. Lett.*, 33(L17706), 2006. doi: 10.1029/2006GL026242.

G.N. Krinner, N. Viovy, N. de Noblet-Ducoudré, J. Ogée, J. Polcher, P. Friedlingstein, P. Ciais, S. Sitch, and I.C. Prentice. A dynamic global vegetation model for studies of the coupled atmosphere-biosphere system. *Glob. Biogeochem. Cyc.*, 19, 2005. doi: 10.1029/2003GB002199.

Y. Kushnir. Interdecadal variations in North Atlantic sea surface temperature and associated atmospheric conditions. *J. Climate*, 7(1):142–157, 1994.

Y-O. Kwon and F. Frankignoul. Stochastically-driven multidecadal variability of the Atlantic meridional overturning circulation in CCSM3. *Clim. Dyn.*, 38:859–876, 2011. doi: 10.1007/s00382-011-1040-2.

W.G. Large, J.C. McWilliams, and S.C. Doney. Oceanic vertical mixing: A review and a model with a non-local boundary layer parameterization. *Rev. Geophys.*, 32:363–403, 1994.

M. Latif, E.R.M. Botset, M. Esch, H.Haak, S. Hagemann, J. Jungclaus, S. Legutke, S. Marsland, and U. Mikolajewicz. Reconstructing, monitoring and predicting multidecadal-scale changes in the North Atlantic thermohaline circulation with sea surface temperature. *J. Climate*, 17:1605–1614, 2004.

M. Latif, M. Collins, H. Pohlmann, and N. Keenlyside. A review of predictability studies of Atlantic sector climate on decadal timescales. *J. Climate*, 19:5971–5987, 2006.

C. Le Quéré, M.R. Raupach, J.G. Canadell, and G. Marland et al. Trends in the sources and sinks of carbon dioxide. *Nat. Geosci.*, 2:831–836, 2009.

J. Le Sommer, T. Penduff, S. Theetten, G. Madec, and B. Barnier. How momentum advection schemes influence current-topography interactions at eddy permitting resolution. *Ocean Model.*, 29(1):1–14, 2009. doi: 10.1016/j.ocemod.2008.11.007.

S. Levitus, J. Antonov, Z. Zhou, H. Dooley, V. Tereschenkov, K. Selemenov, and A.F. Michaels. *Natural Climate Variability on Decade-to-Century Time Scales*. Decadal-scale variability of the North Atlantic Ocean. pages 318–324. Natl. Acad. Sci. Press, Washingthon DC, USA, 1995.

S. Levitus, T.P. Boyer, M.E. Conkright, T. O'Brien, J. Antonov, C. Stephens, L. Stathoplos, D. Johnson, and R. Gelfeld. *World Ocean Database 1998*. Introduction. volume 1. NOAA Atlas NESDIS 18, U.S. Gov. Printing Office, Washington, D.C, 1998. 346 pp.

M. Lévy, A. Estublier, and G. Madec. Choice of an advection scheme for biogeochemical models. *Geophys. Res. Lett.*, 28(19):3725–3728, 2001. doi: 10.1029/2001GL012947.

J.L. Lin. The double-ITCZ problem in IPCC AR4 coupled GCMs: Ocean-atmosphere feedback analysis. *J. Climate*, 20:4497–4525, 2007.

Z. Liu. Dynamics of Interdecadal Climate Variability: A Historical Perspective. *J. Climate*, 25:1963–1995, 2012. doi: http://dx.doi.org/10.1175/2011JCLI3980.1.

Z. Liu, L. Wu, R. Gallimore, and R. Jacob. Search for the origins of pacific decadal climate variability. *Geophys. Res. Lett.*, 29(10), 2002. doi: 10.1029/2001GL013735.

R.A. Madden. Estimates of the natural variability of time-averaged sea-level pressure. *Mon. Weather Rev.*, 104:942–952, 1976.

G. Madec. NEMO ocean engine, note du Pole de modelisation. Technical report, Institut Pierre-Simon Laplace (IPSL), 2008.

G. Madec and M. Imbard. A global ocean mesh to overcome the North Pole singularity. *Clim. Dyn.*, 12(6):381–388, 1996. doi: 10.1007/BF00211684.

S. Manabe and R.J. Stouffer. Multiple-century response of a coupled ocean-atmosphere model to an increase of atmospheric carbon dioxide. *J. Climate*, 7:5–23, 1994.

S. Manabe and R.J. Stouffer. The role of thermohaline circulation in climate. *Tellus*, 51:91–109, 1999.

R. Marsh, M.J. Roberts, R.A. Wood, and A.L. New. An intercomparison of a Bryan-Cox type ocean model and an isopycnic ocean model. Part II: The subtropical gyre and meridional heat transport. *J. Phys. Oceanogr.*, 26:1528–1551, 1996.

J. Marshall, Y. Kushnir, D. Battisti, P. Chang, A. Czaja, R. Dickson, J.W. Hurrell, M. McCartney, R. Saravanan, and M. Visbeck. North Atlantic climate variability: phenomena, impacts and mechanisms. *Int. J. Climatol.*, 21:1863–1898, 2001.

J. Marshall and F. Schott. Open-ocean convection: observations, theory and models. *Rev. Geophys.*, 37:1–64, 1999.

O. Marti, P. Braconnot, J.-L. Dufresne, J. Bellier, R. Benshila, S. Bony, P. Brockmann, P. Cadule, A. Caubel, F. Codron, N. de Noblet, S. Denvil, L. Fairhead, T. Fichefet, M.-A. Foujols, P. Friedlingstein, H. Goosse, J.-Y. Grandpeix, E. Guilyardi, F. Hourdin, A. Idelkadi, M. Kageyama, G. Krinner, C. Lévy, G. Madec, J. Mignot, I. Musat, D. Swingedouw, and C. Talandier. Key features of the IPSL ocean atmosphere model and its sensitivity to atmospheric resolution. *Clim. Dyn.*, 34:1–26, 2010. doi: 10.1007/s00382-009-0640-6.

T.J. McDougall, D.R. Jackett, D.G. Wright, and R. Feistel. Accurate and computationally efficient algorithms for potential temperature and density of seawater. *J. Atmos. Oceanic Technol.*, 20:730–741, 2003.

I. Medhaug and T. Furevik. North Atlantic 20^{th} century multidecadal variability in coupled climate models: Sea surface temperature and ocean overturning circulation. *Ocean Sci. Discuss.*, 8:353–396, 2011. doi: 10.5194/osd-8-353-2011.

I. Medhaug, H.R. Langehaug, T. Eldevik, T. Furevik, and M. Bentsen. Mechanisms for decadal scale variability in a simulated Atlantic meridional overturning circulation. *Clim. dyn.*, 2011. doi: 10.1007/s00382-011-1124-z.

G.A. Meehl, L. Goddard, B. Kirtman, G. Branstator, G. Danabasoglu, E. Hawkins, A. Kumar, T. Rosati, D. Smith, R. Sutton, G. Boer, R. Burgman, C. Cassou, S. Corti, A. Karspeck, N. Keenlyside, M. Kimoto, D. Matei, J. Mignot, R. Msadek, A. Navarra, H. Pohlmann, M. Rienecker, E. Schneider, C. Tebaldi, H. Teng, G.J. van Oldenborgh, G. Vecchi, and S. Yeager. Decadal climate prediction: An update from the trenches. *Bull. Amer. Meteor. Soc.*, 2012. Submitted.

G.A. Meehl, L. Goddard, J. Murphy, R.J. Stouffer, G. Boer G, G. Danabasoglu, K. Dixon, M.A. Giorgetta, A. Greene A, E. Hawkins, G. Hegerl, D. Karoly, N. Keenlyside, M. Kimoto, B. Kirtman, A. Navarra, R. Pulwarty, D. Smith, D. Stammer, and T. Stockdale T. Decadal prediction: Can it be skillful? *Bull. Amer. Meteor. Soc.*, 90: 1467–1485, 2009.

A.P. Megann, A.L. New, and A.T. Blaker. The effect of interannual-timescale salinity anomalies on the stability of the Atlantic meridional overturning circulation. *Clim. Dyn.*, 2012. Submitted.

A.P. Megann, A.P. New, A.T. Blaker, and B. Sinha. The sensitivity of a coupled climate model to its ocean component. *J Climate*, 23:5126–5150, 2010.

U. Merkel and M. Latif. A high resolution AOGCM study of the El-Niño impact on the North Atlantic/European sector. *Geophys. Res. Lett.*, 29(9):1291, 2002. doi: 10.1029/2001GL013726.

J. Mignot and C. Frankignoul. The variability of the Atlantic meridional overturning circulation, the North Atlantic Oscillation, and the El-Niño Southern Oscillation in the Bergen Climate Model. *J. Climate*, 18:2361–2375, 2005.

J. Mignot and C. Frankignoul. Local and remote impacts of a Tropical Atlantic salinity anomaly. *Clim. Dyn.*, 35(7-8):1133–1147, 2010. doi: 10.1007/s00382-009-0621-9.

R. Msadek, K.W. Dixon, T.L. Delworth, and W. Hurlin. Assessing the predictability of the Atlantic meridional overturning circulation and associated fingerprints. *Geophys. Res. Lett.*, 37(L19608), 2010. doi: 10.1029/2010GL044517.

R. Msadek and C. Frankignoul. Atlantic multidecadal oceanic variability and its influence on the atmosphere in a climate model. *Clim. Dyn.*, 2009. doi: 10.1007/s00382-008-0452-0.

R.G. Najjar, X. Jin, F. Louanchi, O. Aumont, K. Caldeira, S.C. Doney, J.-C. Dutay, M. Follows, N. Gruber, F. Joos, K. Lindsay, E. Maier-Reimer, R.J. Matear, K. Matsumoto, P. Monfray, A. Mouchet, J.C. Orr, G.-K. Plattner, J.L. Sarmiento, R. Schlitzer, R.D. Slater, M.-F. Weirig, Y. Yamanaka, and A. Yool. Impact of circulation on export production, dissolved organic matter, and dissolved oxygen in the ocean: Results from Phase II of the Ocean Carbon-cycle Model Intercomparison Project (OCMIP-2). *Global Biogeochem. Cy.*, 21(3):GB3007, 2007. doi: 10.1029/2006GB002857.

A.L. New, Y. Jia, R. Marsh, M. Huddleston, and S. Barnard. An isopycnic model study of the North Atlantic. Part I: Model experiment. *J. Phys. Oceanogr.*, 25:2667–2699, 1995.

M. Newman, P.D. Sardeshmukh, C.R. Winkler, and J.S. Whitaker. A study of subseasonal predictability. *Mon. Weather Rev.*, 131:1715–1732, 2003.

R.J. Nicholls and A. Cazenave. Sea-level rise and its impact on coastal zones. *Science*, 328(5985):1517–1520, 2010. doi: 10.1126/science.1185782.

National Research Council (NRC). *Assessment of Intraseasonal to Interannual Climate Prediction and Predictability.* National Academy of Science, Washingthon DC, USA, 2010. 192 pp.

J.M. Oberhuber. Simulation of the Atlantic circulation with a coupled sea ice-mixed layer isopycnal general circulation model. Part I: model description. *J. Phys. Oceanogr.*, 23:808–829, 1993.

Y. Okumura, S.P. Xie, A. Numaguti, and Y. Tanimoto. Tropical Atlantic air-sea interaction and its influence on the NAO. *Geophys. Res. Lett.*, 28:1507–1510, 2001.

B.C. O'Neill and M. Oppenheimer. Dangerous climate impacts and the Kyoto protocol. *Science*, 296:1971–1972, 2002.

N. Oreskes, K. Shrader-Frechette, and K. Belitz. Verification, validation, and confirmation of numerical models in the earth sciences. *Science*, 263:641–646, 1994. doi:10.1126/science.263.5147.641.

R.C. Pacanowski. MOM 2 Documentation, Users Guide and Reference Manual. gfdl ocean tech. rep. (3), 1995. 232 pp.

A.M. Paiva, E.P. Chassignet, and A.J. Mariano. Numerical simulation of the North Atlantic subtropical gyre: sensitivity to boundary conditions. *Dyn. Atmos. Oceans*, 32(3-4):209–237, 2000.

A.K. Pardaens, H.T. Banks, J.M. Gregory, and P.R. Rowntree. Freshwater transports in HadCM3. *Clim. Dyn.*, 21:177–195, 2003. doi: 10.1007/s0038200303246.

V. Pavan and F.G. Doblas-Reyes. Multi-model seasonal hindcasts over the Euro-Atlantic: Skill scores and dynamical features. *Clim. Dyn.*, 16:611–625, 2000.

S. Peng, W.A. Robinson, and S. Li. Mechanisms for the NAO responses to the North Atlantic SST tripole. *J. Climate*, 15:1987–2004, 2003.

A. Persechino, R. Marsh, B. Sinha, A.P. Megann, A.T. Blaker, and A.L. New. Decadal-timescale changes of the Atlantic overturning circulation and climate in a coupled climate model with a hybrid-coordinate ocean component. *Clim. Dyn.*, 39(3):1021–1042, 2012a. doi: 10.1007/s00382-012-1432-y.

A. Persechino, J. Mignot, D. Swingedouw, and E. Guilyardi. Decadal predictability of the Atlantic Meridional Overturning Circulation and Climate in the IPSL-CM5A-LR model. *Clim. Dyn.*, 2012b. doi: 10.1007/s00382-012-1466-1.

R.S. Pickart, M.A. Spall, M.H. Ribergaard, G.W.K. Moore, and R.F. Milliff. Deep convection in the Irminger Sea forced by the Greenland tip jet. *Nature*, 424:152–156, 2003.

H. Pohlmann, M. Botzet, M. Latif, A. Roesch, M. Wild, and P. Tschuck. Estimating the decadal predictability of a coupled AOGCM. *J. Climate*, 17:4463–4472, 2004.

H. Pohlmann, F. Sienz, and M. Latif. Influence of the multidecadal Atlantic meridional overturning circulation variability on European climate. *J. Climate*, 19:6062–6068, 2006.

V.D. Pope, M.L. Gallani, P.R. Rowntree, and R.A. Stratton. The impact of new physical parametrizations in the Hadley Centre climate model: HadAM3. *Clim. Dyn.*, 16:123–146, 2000. doi: 10.1007/s003820050009.

T. Qu, H. Mitsudera, and B. Qiu. A climatological view of the Kuroshio/Oyashio system east of Japan. *J. Phys. Oceanogr.*, 31:2575–2589, 2001. doi: 10.1007/s003820050009.

M.H. Quenouille. *Associated measurements*. Butterworths, 1952. 242 pp.

S. Rahmstorf. Risk of sea-change in the Atlantic. *Nature*, 388:825–826, 1997.

S. Rahmstorf. Shifting seas in the greenhouse? *Nature*, 399:523–524, 1999.

S. Rahmstorf. Ocean circulation and climate during the past 120,000 years. *Nature*, 419:207–214, 2002.

S. Rahmstorf and A. Ganapolski. Long-term global warming scenarios computed with an Efficient coupled climate model. *Clim. Change*, 43:353–367, 1999.

B. Rajagopalan, Y. Kushnir, and Y.M. Tourre. Observed mid-latitude and Tropical Atlantic climate variability. *Geophys. Res. Lett.*, 25:3967–3970, 1998.

D. Rayner, J.J.-M. Hirschi, T. Kanzow, W.E. Johns, P.G. Wright, E. Frajka-Williams, H.L. Bryden, C.S. Meinen, M.O. Baringer, J. Marotzke, L.M. Beal, and S.A. Cunningham. Monitoring the Atlantic meridional overturning circulation. *Deep-Sea Res. Pt II*, 58:1744–1753, 2011.

N.A. Rayner, D.E. Parker, E.B. Horton, C.K. Folland, L.V. Alexander, D.P. Rowell, E.C. Kent, and A. Kaplan. Global analyses of sea surface temperature, sea ice, and night marine air temperature since the late nineteenth century. *J. Geophys. Res.*, 108 (D14), 2003. doi: 10.1029/2002JD002670.

C.J.C. Reason and S.B. Power. The influence of the Bering Strait on the circulation in a coarse resolution global ocean model. *Clim. Dyn.*, 9:363–369, 1994.

J.L. Reid. On the total geostrophic circulation of the South Atlantic Ocean: flow patterns, tracers, and transports. *Prog. Oceanogr.*, 23:149–244, 1989.

R.W. Reynolds. Improved global sea surface temperature analyses using optimum interpolation. *J. Climate*, 7(6):929–948, 1994.

A.T. Roach, K. Aagaard, C.H. Pease, S.A. Salo, T. Weingartner, V. Pavlov, and M. Kulakov. Direct measurements of transport and water properties through the Bering Strait. *J. Geophys. Res.*, 100C:18443–18457, 1995.

M.J. Roberts, R. Marsh, A.L. New, and R.A. Wood. An intercomparison of a Bryan-Cox type ocean model and an isopycnic ocean model. Part I: the subpolar gyre and high latitude processes. *J. Phys. Oceanogr.*, 26:1495–1527, 1996.

M.J. Rodwell, D.P. Rowell, and C.K. Folland. Oceanic forcing of the wintertime North Atlantic Oscillation and European climate. *Nature*, 398:320–333, 1999.

D.P. Rowell. Assessing potential seasonal predictability with an ensemble of multidecadal GCM simulations. *J. Climate*, 11:109–120, 1998.

D.P. Rowell, C.K. Folland, K. Maskell, and M.N. Ward. Variability of summer rainfall over Tropical North-Africa (1906-92) observations and modeling. *Q. J. R. Meteorol. Soc.*, 121:669–704, 1995.

R. Sadourny and K. Laval. *New Perspectives in Climate Modelling*. January and July performance of the LMD General Circulation Model. pages 173–198. Elsevier Science Publishers, Amsterdam, 1984.

D.T. Sandwell and W.H.F. Smith. Marine gravity anomaly from Geosat and ERS-1 satellite altimetry. *J. Geophys. Res.*, 102:10039–10050, 1997.

R. Saravanan and P. Chang. Interaction between Tropical Atlantic variability and El-niño Southern Oscillation. *J. Climate*, 13:2177–2194, 2000.

M.E. Schlesinger and N. Ramankutty. An oscillation in the global climate system of period 65-70 years. *Nature*, 367:723–726, 1994. doi: 10.1038/367723a0.

W.J.Jr Schmitz and P.L. Richardson. On the sources of the Florida Current. *Deep-Sea Res.*, 38(1):S389–S409, 1991. doi: 10.1038/367723a0.

E.K. Schneider. Understanding differences between the equatorial Pacific as simulated by two coupled GCMs. *J. Climate*, 15:449–469, 2002.

E.K. Schneider and M. Fan. Weather noise forcing of surface climate variability. *J. Atmos. Sci.*, 64:3265–3280, 2007.

P.S. Schopf and A. Loughe. A reduced-gravity isopycnal ocean model: Hindcasts of El Niño. *Mon. Wea. Rev.*, 123:2839–2863, 1995.

F. Schott, J. Carton, W. Hazeleger, W. Johns, Y. Kushnir, C. Reason, and S.-P. Xie. A White Paper on Tropical Atlantic Climate Experiment (TACE). 2004. Available from http://ioc-goos-oopc.org.

A.J. Semtner. A model for the thermodynamic growth of sea ice in numerical investigations of climate. *J. Phys. Oceanog.*, 6:379–389, 1986.

U. Send, M. Lankhorst, and T. Kanzow. Observation of decadal change in the Atlantic meridional overturning circulation using 10 years of continuous transport data. *Geophys. Res. Lett.*, 38(L24606), 2011.

C. Senior and J.F.B Mitchell. CO_2 and climate: the impact of cloud parametrization. *J. Climate*, 6:393–418, 1993.

J. Servain, A.J. Busalacchi, M.J. McPhaden, A.D. Moura, G. Reverdin, M. Vianna, and S.E. Zebiak. A Pilot Research Moored Array in the Tropical Atlantic (PIRATA). *Bull. Amer. Meteor. Soc.*, 79:2019–2031, 1998.

J.P. Severinghaus, A. Grachev, B. Luz, and N. Caillon. A method for precise measurement of argon 40/36 and krypton/argon ratios in trapped air in polar ice with applications to past firn thickness and abrupt climate change in Greenland and at Siple Dome, Antarctica. *Geochim. Cosmochim. Acta.*, 67:325–343, 2003.

B. Sinha, A.T. Blaker, J.J.-M. Hirschi, S. Bonham, M. Brand, S. Josey, R.S. Smith, and J. Marotzke. Mountain ranges favour vigorous Atlantic meridional overturning. *Geophys. Res. Lett.*, 39(L02705), 2012. doi: 10.1029/2011GL050485.

S. Sitch, B. Smith, I.C. Prentice, A. Arneth, A. Bondeau, W. Cramer, J.O. Kaplan, S. Levis, W. Lucht, M.T. Sykes, K. Thonicke, and S. Venevsky. Evaluation of ecosystem dynamics, plant geography and terrestrial carbon cycling in the LPJ dynamic

global vegetation model. *Glob. Change Biol.*, 9:161–185, 2003. doi: 10.1046/j.1365-2486.2003.00569.x.

D.M. Smith, S. Cusack, A.W. Colman, C.K. Folland, G.R. Harris, and J.M. Murphy. Improved surface temperature prediction for the coming decade from a global climate model. *Science*, 317:796–799, 2007.

D.M. Smith, R. Eade, N.J. Dunstone, D. Fereday, J.M. Murphy, H. Pohlmann, and A.A. Scaife. Skillful multi-year predictions of Atlantic hurricane frequency. *Nat. Geosci.*, 2010. doi: 10.1038/NGEO1004.

R.N.B. Smith. A scheme for predicting layer clouds and their water content in a general circulation model. *Q. J. R. Met. Soc. Lond.*, 116:435–460, 1990.

R.N.B. Smith. Experience and developments with the layer cloud and boundary layer mixing schemes in the UK Meteorological Office United Model. Reading, England, 1993.

Y.T. Song and D.B. Haidvogel. A semi-implicit ocean circulation model using topography-following coordinate. *J. Comput. Phys.*, 115:228–244, 1994.

Y.T. Song and T.Y. Hou. Parametric vertical coordinate formulation for multiscale, Boussinesq, and non-Boussinesq ocean modeling. *Ocean Model.*, 11:298–332, 2006.

D.A. Stainforth, M.R. Allen, E.R. Tredger, and L.A. Smith. Confidence, uncertainty and decision-support relevance in climate predictions. *Phil. Trans. R. Soc. A*, 365: 2145–2161, 2007.

H. Stommel and A.B. Arons. On the abyssal circulation of the world ocean - II. An idealized model of the circulation pattern and amplitude in oceanic basins. *Deep-Sea Res.*, 6:219–233, 1960. doi: 10.1016/0146-6313(59)90075-9.

R.J. Stouffer, J. Yin, J.M. Gregory, K.W. Dixon, M.J. Spelman, W. Hurlin, A.J. Weaver, M. Eby, G.M. Flato, H. Hasumi, A. Hu, J.H. Jungclaus, I.V. Kamenkovich, A. Levermann, M. Montoya, S. Murakami, S. Nawrath, A. Oka, W.R. Peltier, D.Y. Robitaille, A. Sokolov, G. Vettoretti, and S.L. Weber. Investigating the causes of the response of the thermohaline circulation to past and future climate changes. *J. climate*, 19: 1365–1387, 2006.

S. Sun and R. Bleck. Thermohaline circulation studies with an isopycnic coordinate ocean model. *J. Phys. Oceanogr.*, 31:2761–2782, 2001.

S. Sun and R. Bleck. Multi-century simulations with the coupled GISS-HYCOM climate model: Control experiments. *Clim. Dyn.*, 26:407–428, 2006. doi: 10.1007/s00382-005-0091-7.

S. Sun, R. Bleck, C. Rooth, J. Dukowicz, E.P. Chassignet, and P. Killworth. Inclusion of thermobaricity in isopycnic-coordinate ocean models. *J. Phys. Oceanogr.*, 29:2719–2729, 1999.

R.T. Sutton. PREDICATE final report. 2003. http://ugamp.nerc.ac.uk/predicate/.

R.T. Sutton and D.L.R. Hodson. Atlantic Ocean forcing of North American and European summer climate. *Science*, 309:115–118, 2005.

R.T. Sutton, W.A. Norton, and S.P. Jewson. The North Atlantic Oscillation - what role for the ocean? *Atmos. Sci. Lett.*, 1(2):89–100, 2001. doi: 10.1006/asle.2000.0018.

D. Swingedouw, P. Braconnot, P. Delecluse, E. Guilyardi, and O. Marti. The impact of global freshwater forcing on the thermohaline circulation: adjustment of North Atlantic convection sites in a CGCM. *Clim. Dyn.*, 28:291–305, 2007.

D. Swingedouw, J. Mignot, P. Braconnot, E. Mosquet, M. Kageyama, and R. Alkama. Impact of freshwater release in the North Atlantic under different climate conditions in an OAGCM. *J. Climate*, 22:6377–6403, 2009.

D. Swingedouw, J. Mignot, S. Labetoule, E. Guilyardi, and G. Madec. Initialisation and predictability of the AMOC over the last 50 years in a climate model. *Clim. Dyn.*, 2012. In revision.

L.D. Talley. Shallow, intermediate, and deep overturning components of the global heat budget. *J. Phys. Oceanogr.*, 6333:530–560, 2003.

K.E. Taylor, R.J. Stouffer, and G.E. Meehl. *A summary of the CMIP5 experiment design.* Lawrence Livermore National Laboratory Rep, 2009. 32 pp.

L.A. te Raa and H.A. Dijkstra. Instability of the thermohaline circulation on interdecadal timescales. *J. Phys. Oceanogr.*, 32:138–160, 2002.

L.A. te Raa, J. Gerrits, and H.A. Dijkstra. Identification of the Mechanism of Interdecadal Variability in the North Atlantic Ocean. *J. Phys. Oceanogr.*, 34:2792–2807, 2004.

H. Teng, G. Branstator, and G.A. Meehl. Predictability of the Atlantic Overturning Circulation and associated surface patterns in two CCSM3 climate change ensemble experiments. *J. Climate*, 24:6054–6076, 2011.

L. Terray and C. Cassou. Tropical Atlantic sea surface temperature forcing of the quasi-decadal climate variability over the North Atlantic-Europe region. *J. Climate*, 15: 3170–3187, 2002.

A. Timmerman, M. Latif, R. Voss, and A. Grötzner. Northern Hemispheric interdecadal variability: A coupled air-sea mode. *J. Climate*, 11:1906–1931, 1998.

M. Ting, Y. Kushnir, R. Seager, and C. Li. Forced and internal twentieth century SST trends in the North Atlantic. *J. Climate*, 22:1469–1481, 2009.

Y.M. Tourre, B. Rajagopalan, and Y. Kushnir. Dominant patterns of climate variability in the atlantic ocean region during the last 136 years. *J. Climate*, 12:2285–2299, 1999.

K.E. Trenberth. Observational needs for climate prediction and adaptation. *WMO Bulletin*, 57(1):17–21, 2008.

K.E. Trenberth and J.M. Caron. Estimates of meridional atmosphere and ocean heat transports. *J. Climate*, 14:3433–3443, 2001.

S. Valcke. OASIS3 User Guide (prism2-5), Technical Report TR/CMGC/06/73, PRISM Report. Technical Report 2, CERFACS, Toulouse, France, 2006. 60 pp.

S. Valcke, L. Terray, and A. Piacentini. OASIS 2.4 user's guide. Technical report, European Centre for Research and Advanced Training in Scientic Computing, 2000. 68 pp.

M. Vellinga and R.A. Wood. Global climatic impacts of a collapse of the Atlantic thermohaline circulation. *Clim. Change*, 54:251–267, 2002.

M. Vellinga and R.A. Wood. Impacts of thermohaline circulation shutdown in the twenty-first century. *Clim. Change*, 91(1-2):43–63, 2008. doi:10.1007/s10584-006-9146-y.

M. Vellinga and P. Wu. Low-latitude freshwater influence on centennial variability of the Atlantic thermohaline circulation. *J. Climate*, 17:4498–4511, 2004.

M.H. Visbeck, J.W. Hurrell, L. Polvani, and H.M. Cullen. The North Atlantic Oscillation: Past, present, and future. *Proc. Natl. Acad. Sci. USA*, 98:12876–12877, 2001.

H. Von Storch and F.W. Zwiers. *Statistical analysis in climate research*. Cambridge University Press, 1999.

A.J. Wallcraft, A.B. Kara, H.E. Hurlburt, and P.A. Rochford. NRL Layered Ocean Model (NLOM) with an embedded mixed layer sub-model: formulation and tuning. *J. Atmos. Oceanic Technol.*, 20:1601–1615, 2003.

R. Wanninkhof. Relationship between wind-speed and gas-exchange over the ocean. *J. Geophys. Res.*, 97(C5):7373–7382, 1992. doi: 10.1029/92JC00188.

P.D. Welch. The use of Fast Fourier Transform for the estimation of power spectra: A method based on time averaging over short, modified periodograms. *IEEE Trans. on Audio Electroacoustics*, 15:70–73, 1967.

J. Willebrand, B. Barnier, C. Böning, C. Dieterich, P.D. Killworth, C. LeProvost, Y. Jia, J.M. Molines, and A.L. New. Circulation characteristics in three eddy-permitting models of the North Atlantic. *Prog. Oceanogr.*, 48:123–161, 2001.

J.K. Willis. Can in situ floats and satellite altimeters detect long-term changes in Atlantic Ocean overturning? *Geophys. Res. Lett.*, 37(L06602), 2010. doi: 10.1029/2010GL042372.

M. Winton. On the climatic impact of ocean circulation. *J. Climate*, 16:2875–2889, 2003.

B. Wu, J. Wang, and J. Walsh. Possible feedback of winter sea ice in the Greenland and the Barents Seas on the local atmosphere. *Mon. Wea. Rev.*, 32:1868–1876, 2004.

C. Wunsch and P. Heimbach. Two decades of the Atlantic Meridional Overturning Circulation: Anatomy, variations, extremes, prediction, and overcoming its limitation. *J. Climate*, 2012. Submitted.

S.P. Xie, Y. Okumura, T. Miyama, and A. Timmermann. Influences of Atlantic climate change on the Tropical Pacific via the Central American Isthmus. *J. Climate*, 21: 3914–3928, 2008.

S.T. Zalesak. Fully multidimensional flux-corrected transport algorithms for fluids. *J. Comput. Phys.*, 31:335–362, 1979.

L. Zanna, P. Heimbach, A.M. Moore, and E. Tziperman. Upper ocean singular vectors of the North Atlantic Climate with Implications for Linear Predictability and Variability. *Q. J. R. Meteorol. Soc.*, 138(663):500–513, 2012.

R. Zhang and T.L. Delworth. Simulated tropical response to a substantial weakening of the Atlantic thermohaline circulation. *J. Climate*, 18:1853–1860, 2005.

R. Zhang and T.L. Delworth. Impact of Atlantic multidecadal oscillations on India/Sahel rainfall and Atlantic hurricanes. *Geophys. Res. Lett.*, 33(L17712), 2006. doi: 10.1029/2006GL026267.

K. Zickfeld, A. Levermann, H.M. Granger, S. Rahmstorf, T. Kuhlbrodt, and D.W. Keith. Expert judgements on the response of the Atlantic meridional overturning circulation to climate change. *Clim. Change*, 82:235–265, 2007.